Phosphonium Containing UV-Curable Antimicrobials for the Coating and Fabrication of Common Touch Plastics

by

Joseph P. Bedard

Bachelor of Science, Honours

Ryerson University, Toronto, Ontario, Canada 2017

A thesis presented to Ryerson University

in partial fulfillment of the

requirements for the degree of

Master of Science

in the program of Molecular Science

Toronto, Ontario, Canada, 2020

AUTHOR'S DECLARATION

I hereby declare that I am the sole author of this thesis. This is a true copy of the thesis including any required final revisions, as accepted by my examiners.

I authorize Ryerson University to lend this thesis to other institutions or individuals for the purpose of scholarly research.

I further authorize Ryerson University to reproduce this thesis by photocopying or by other means, in total or in part, at the request of other institutions or individuals for the purpose of scholarly research.

I understand that my thesis may be made electronically available to the public.

Phosphonium Containing UV-Curable Antimicrobials for the Coating and Fabrication of Common Touch Plastics

Joseph P. Bedard

Master of Science – Molecular Science, Ryerson University, 2020

ABSTRACT

The attachment and proliferation of antibiotic resistant, biofilm-forming bacteria to oft-handled material surfaces has emerged as a growing concern, particularly in the biomedical, healthcare and food packaging industries. The development of both biocide-releasing and tethered, immobilized biocide surface coatings has risen to meet this demand. While these surface coatings have demonstrated excellent antimicrobial efficacy, there are few examples of antimicrobial surfaces with long-term durability and efficacy. To that end, UV-curable phosphoniums bearing benzophenone anchors were synthesized with a variety of alkyl, aryl, and fluoroalkyl functional groups at phosphorus to probe their efficacy as thermally stable antimicrobial additives in plastics or as surface coatings. The surface topology and characteristics of these materials were studied to gain insight into the mechanism of antimicrobial activity of these materials. Additionally, general design principals for tailoring phosphoniums to function as both additives during injection molding processes and as UV-curable coatings are described, and evaluation against both Gram-negative and Gram-positive bacteria in both applications were carried out. Crucially, polypropylene (PP) materials containing phosphonium with a perfluoroalkyl substituent maintained the ability to kill biofilm-forming bacteria even after being subject to abrasion processes, demonstrating the potential to serve as a long-term antimicrobial material.

ACKNOWLEDGMENTS

DEDICATION

For my parents, Phil Bedard and Mary Delli Colli,

my brother Mike, and my grandmother Lucy.

Thank you for shaping me into the person I am today.

TABLE OF CONTENTS

LIST OF TABLES

LIST OF FIGURES

LIST OF SCHEMES

LIST OF APPENDICES

LIST OF ABBREVIATIONS

Å – angstroms

AIBN - azobisisobutyronitrile

Ar (g) – argon gas

ASTM – American Society for Testing and Materials International

ATRP – atom transfer radical polymerization

Aq – aqueous

BAC – benzalkonium chloride

BPB – bromophenol blue

n-BuLi – n-butyllithium

C – Celsius

C_6D_6 – deuterated benzene

$CDCl_3$ – deuterated chloroform

COSY – homonuclear correlation spectroscopy

CFU – colony forming unit

CRP – controlled radical polymerization

CTAB – cetyltrimethylammonium bromide

d – days

DART – direct analysis in real time

DCM – dichloromethane

DMF – N,N-dimethylformamide

EPS – exopolysaccharide

eq – equivalents

Et_2O – diethyl ether

EtOAc – ethyl acetate

EtOH – ethanol

ESI – electrospray ionization

F - fluorine

g – grams

h – hours

HCAI – healthcare associated infection

HCl – hydrochloric acid

H_2O – water

HRMS – high resolution mass spectrometry

HSQC – heteronuclear single quantum correlation spectroscopy

Hz – hertz

IAI-3 – indoor air isolate 3

IL – ionic liquid

ISO – International Organization for Standardization

J – joules

K_2CO_3 – potassium carbonate

kDa – kilodaltons

kPa – kilopascals

L – litre

LDI – large droplet inoculation

Li (s) – lithium metal

M – molar

M_n – molecular weight

MeCN – acetonitrile

Mg (s) – magnesium metal

$MgSO_4$ – magnesium sulfate

MHz – megahertz

min – minutes

mL – millilitres

mmol – millimoles

mol – moles

Mp – melting point

N_2 (g) – nitrogen gas

NEt_3 – triethylamine

nm – nanometers

NMR – nuclear magnetic resonance

ON – overnight

P – phosphorus

P^+ – phosphonium

PBS – phosphate buffered saline

P(n-Bu)$_3$ – tri(n-butyl)phosphine

PC – polycarbonate

PCl$_3$ – phosphorus(III)chloride

PH$_3$ – phosphine gas

Ph$_2$PH – diphenylphosphine

Ph$_2$P(O)H – diphenylphosphine oxide

Ph$_2$PCl – P-chlorodiphenylphosphine

PIL – phosphonium ionic liquid

PLA – (poly)lactic acid

PMe$_3$ – trimethylphosphine

PP – polypropylene

PPh$_3$ – triphenylphosphine

PO – phosphine oxide

polyQAC – polymeric quaternary ammonium compound

iPrOH – iso-propanol

PS – polystyrene

PTFE – polytetrafluoroethylene

PTC – phase transfer catalyst

PVP – n-hexylated(polyvinylpyridine)

QAC – quaternary ammonium compound

QPC – quaternary phosphonium compound

RAFT – reverse addition fragmentation chain transfer

RBF – round bottom flask

ref. – reference

RMS – root mean squared

R.T. – room temperature

SIPN – semi-intepenetrating polymeric network

SiQAC – organosilane-based quaternary ammonium compound

TBAB – tetrabutylammonium bromide

TEMPO - (2,2,6,6-tetramethylpiperidin-1-yl)oxidanyl

THF – tetrahydrofuran

TLC – thin layer chromatography

TOF – time-of-flight

UV – ultraviolet

µm – micron

µW – microwave

W – watts

λ – wavelength

θ_C – advancing water contact angle

1   INTRODUCTION

1.1   Microbial Threats

The attachment and proliferation of antibiotic resistant, biofilm-forming bacteria to oft-handled material surfaces has resulted in increased occurrence of healthcare-associated infections (HCAIs), placing a heavy burden on our healthcare system.[1–4] Patients with HCAIs incur longer hospital stays, and result in costs to the healthcare system estimated at $10 billion USD per annum in the United States alone.[5] The incidence of these HCAIs and their associated costs have risen in part due to the emergence of antibiotic resistant bacterial strains, brought on by the over-prescription of antibiotics and overuse of common disinfectants at sub-lethal concentrations.[6] In response to sub-inhibitory doses of antibiotics, both Gram-negative and Gram-positive bacteria can produce biofilms (Figure 1): these multi-microbial colonies existing in a matrix of exopolysaccharide (EPS) help foster antibiotic resistance. When compared to planktonic cells, biofilm-ensconced bacteria are 100 to 1000 times less susceptible to antibiotics.[7–11] Within the biofilm, bacteria have shown remarkable persistence when challenged with antibiotics. This may be due to poor penetration of the active agent, adaptive stress responses expressed by some cells,
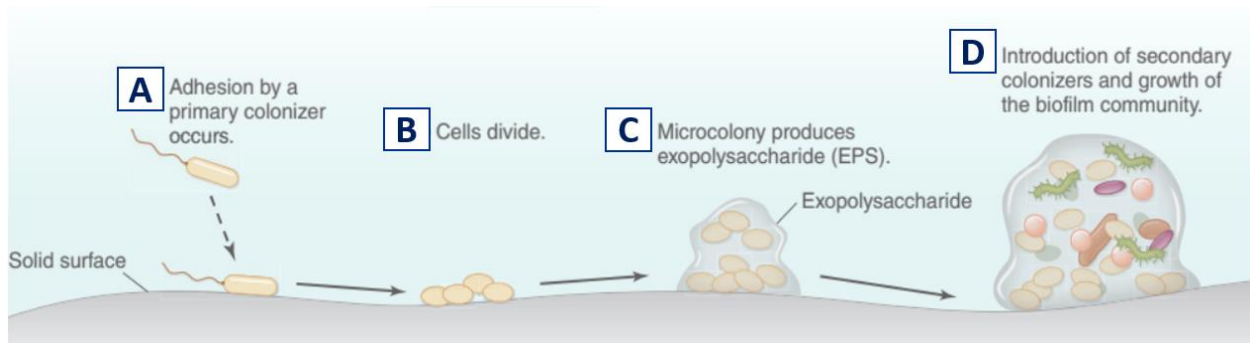
Figure 1.1 General representation of biofilm growth and maturation on a material surface.
Biofilm formation is illustrated by (A) initial adhesion by primary colonizing cells, (B) cell division, (C) subsequent secretion of EPS matrix, and (D) maturation of the biofilm with inclusion of secondary microbial species. Upon maturation, portions of the biofilm can detach and colonize other surface area (Adapted from ref.[14]).

and accelerated horizontal gene transfer of resistant genes.[12–14] The resistance to conventional antibiotics and antibacterial agents afforded to microbial threats by biofilms has necessitated a new approach to combat HCAIs.

1.2 Antimicrobial Solutions

A drug discovery void in the development of conventional antibiotics to combat antimicrobial resistance has led researchers to seek out alternative approaches. Coating touch-surfaces with an effective antimicrobial agent has emerged as an attractive solution to deterring biofilm formation and thus the proliferation of antibiotic resistant bacteria (Figure 1.1).[15–19] This approach has largely focused on deterring microbial attachment, thus preventing biofilm formation (Figure 1.1A). The application of antimicrobial coatings to surfaces, including metals, textiles, and plastics has become ubiquitous as a research approach due to ease of application, lower costs, and antibacterial efficacy,[20,21] although the long term efficacy and real-world applicability of these coatings has proven challenging. Antimicrobial surface coatings function as either antifouling or bactericidal agents. Antifouling agents are non-lethal and repel microbes through ionic or
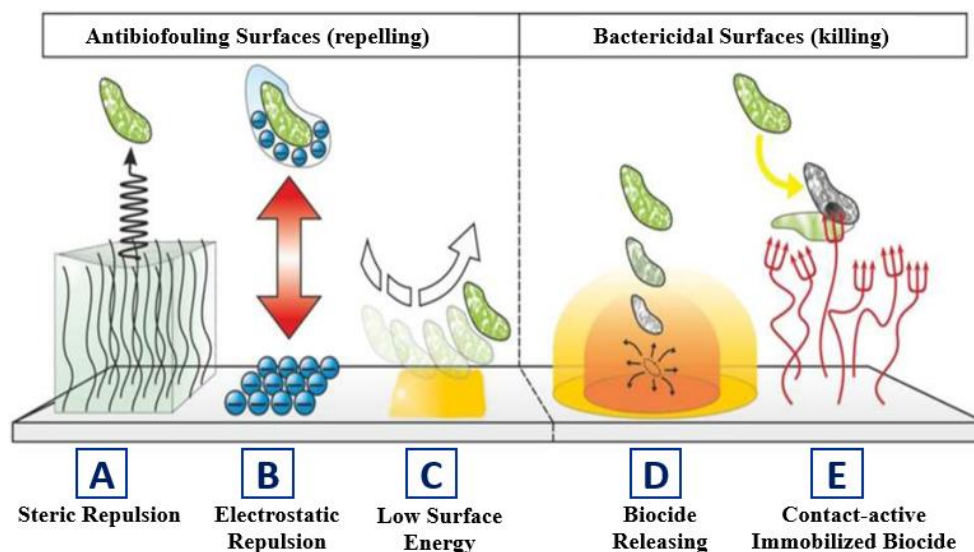
Figure 1.2 Antimicrobial modes of action. Illustrated examples of antimicrobial surfaces and various mechanisms of antimicrobial activity (adapted from ref.[18]).

hydrophobic forces that reduce microbial ability to adhere and proliferate on surfaces (Figure 1.2A-C). Bactericidal surfaces kill microbes either by releasing a biocide that interferes with the microbe's metabolism upon intake (Figure 1.2D), or via a surface-mediated disruption of the microbial membrane (Figure 1.2E).[22] Earlier iterations of antimicrobial surfaces used the biocide-release mechanism to deter biofilm formation, but these techniques were proven to be short-term solutions that can cause cumulative toxicity and encourage microbial resistance.[23,24] Inorganic nanoparticles have been employed commercially in fabrics as effective antimicrobial agents, although their frequent use has raised concern about bioaccumulation and toxicity in aquatic environments.[25–27] The quaternary ammonium compound (QAC), a class of chemicals containing cationic nitrogen, has proven to be an effective antimicrobial, and some of the simplest derivatives
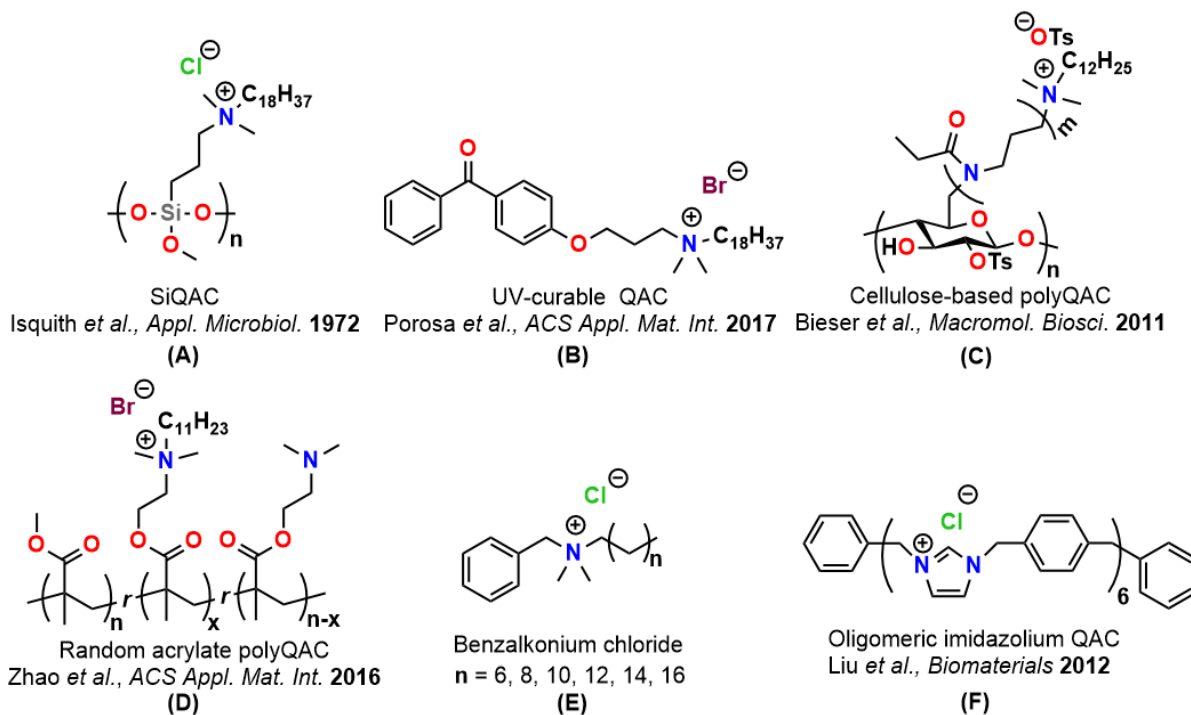
Figure 1.3 Literature and commercial examples of quaternary ammonium compounds. Compounds include (A) the trimethoxysilane QAC (SiQAC),[36] (B) a UV-curable small molecule with a C18 chain,[17] (C) cellulose polymer functionalized with flexible oligomeric spacer,[34] (D) a random acrylate-based copolymer with varying degrees of quaternization,[35] (E) benzalkonium chloride (BAC), commonly used in household and industrial disinfectants, and (F) a imidazolium oligomer with reported activity against antibiotic resistant bacterial strains in solution.[33]

have seen widespread use as the active component in disinfectant solutions (Figure 1.3).[28] This motif has been extended into polymeric QACs (polyQACs) (Figure 1.3B,C), which have been thoroughly researched and highlighted in recent reviews.[29,30] QACs in their small molecule and macromolecular form have been among the most promising class of antimicrobials, as they have shown broad spectrum antimicrobial activity against challenging, antibiotic resistant and biofilm-forming strains.[17,31–35]

1.2.1   Surface-Immobilized Antimicrobials

The development of ammonium-based antimicrobials as surface-immobilized coatings has been crucial to the advancement of antimicrobial surfaces. In the late 1960s, the Dow Corning corporation discovered a trimethoxysilane-based QAC originally designed for control of algal growth had also demonstrated impressive antibacterial effects. Studies on their activity and binding to glass and cellulose through a sol-gel condensation method were published in 1972.[36] This initial report established a new paradigm in antibiofilm technologies and chemistries, as most current research efforts to combat the spread of biofilms and antibiotic resistant bacteria involve either using well-defined attachment chemistries to tether novel biocides to surfaces, or developing novel surface attachment chemistries for proven antimicrobials. In some cases, it has been demonstrated that a surface with a strong affinity for the active antimicrobial can facilitate physisorption of the compound though favourable electrostatic or hydrophobic forces. Park *et al*. showed hydrophobic polycations could be physically deposited onto a similarly hydrophobic polyethylene surface and retain antimicrobial properties without leaching.[37] Covalent attachment (chemisorption) to a surface has less substrate-specificity, and as such it is required for many antimicrobial-surface motifs to ensure surface confinement and non-leaching.[38] QACs can be immobilized to surfaces either as small, monolayer-forming molecules, or as polymers.

1.2.1.1 "Grafting To" and "Grafting From" Material Surfaces

Graft polymerization is used to functionalize both surfaces and the polymers themselves for antimicrobial application. This approach includes "grafting from," where initiating sites on the substrates polymerize the monomer,[39] and the "grafting to" approach, where pre-prepared polymer chains react with the substrate surface.[40] The "grafting from" approach uses initiating sites on the material surface. The most widely used "grafting from" techniques involve in situ controlled radical polymerization (CRP), namely surface-initiated atom transfer radical polymerization
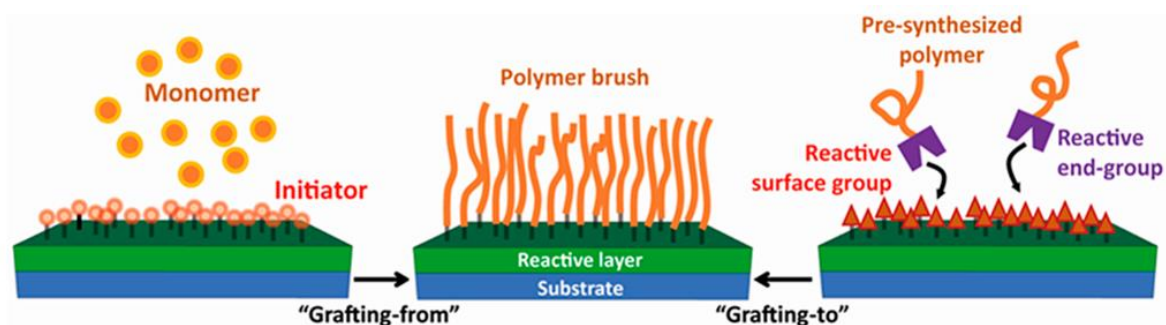
Figure 1.4. Grafting methodologies. Schematic rendering of the grafting-from approach (left), where monomers are grown from initiation sites at the surface, and the grafting-to approach (right), where pre-synthesized polymers are attached via reaction of an end group with reactive surface groups (adapted from ref.[41]).

(ATRP), and reversible addition-fragmentation chain transfer (RAFT). These techniques are two-step processes, generally involving the attachment of an ATRP or RAFT initiator to the surface followed by addition of the monomer, resulting in growth of a so-called polymer brush (Figure 1.4).[41] "Grafting to" surfaces is a powerful method as it allows for a more robust range of attachment chemistries: reactive end groups can be tailored to their targeted substrate, and installed as groups on telechelic polymers through facile synthetic methodologies. While this approach is especially effective for monolayers, steric hinderance can lead to lower grafting densities when extended to polymer brushes.[42] Matyjaszewski *et al.* reported the synthesis of a block copolymer comprised of a poly 2-(dimethylamino)ethyl methacrylate (polyDMAEMA) block, and a poly(3-

5

(trimethoxysilyl)propyl methacrylate) (polyTMSPMA) anchoring block.[43] The block copolymers were grafted to glass slides using the sol-gel method (Figure 1.5A). The polymer coating was then quaternized post-graft with ethyl bromide to yield the QAC functionality. The coated surfaces had predictably lower charge densities and thus lower antimicrobial activity when compared to surfaces prepared using the same polymer via a "grafting from" method. However, after controlling for the density of QAC produced via the "grafting to" and "grafting from" methods, surfaces produced by the "grafting to" method actually showed enhanced biocidal activity, suggesting the local density of biocidal centres plays a role in antimicrobial activity.[43] A two-step "grafting to" method was reported by Su and coworkers, where reactive surface groups are
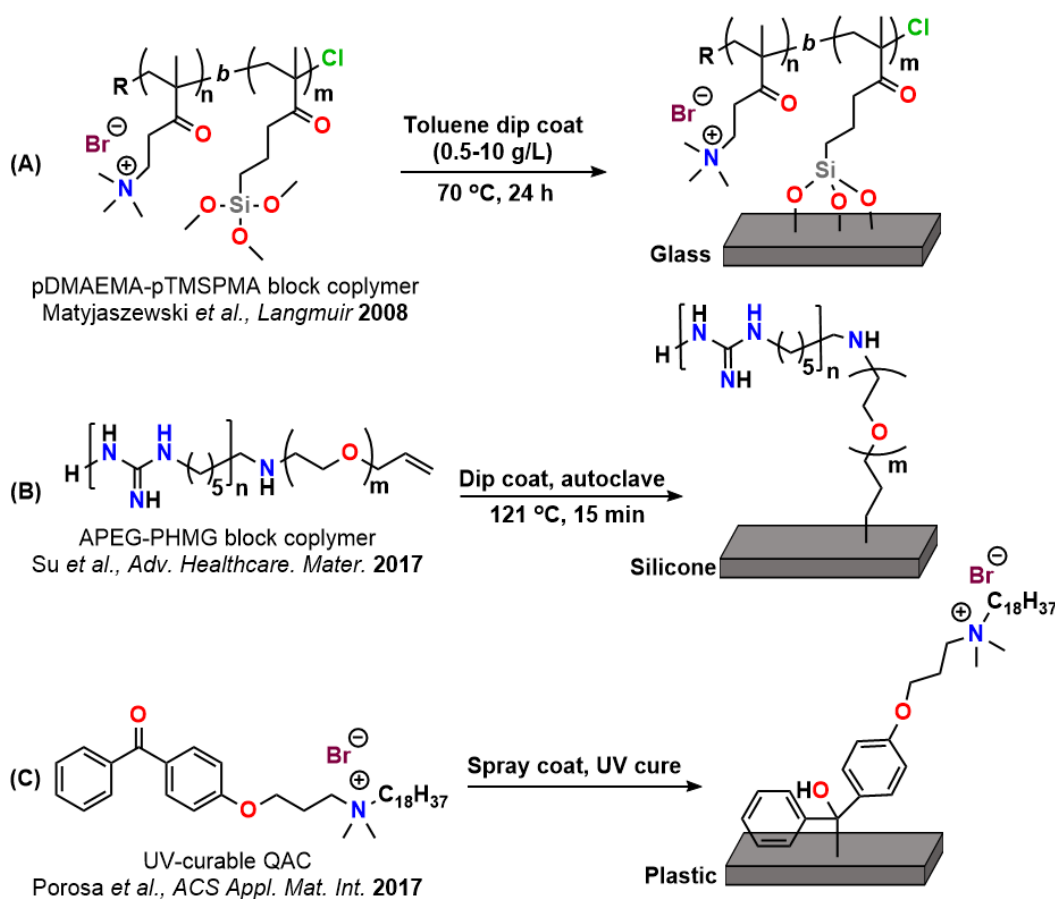
Figure 1.5. "Grafting to" surfaces. Examples of antimicrobials grafting onto (A) glass slides using a sol-gel method,[43] (B) silicone rubber after plasma pre-treatment and autoclaving,[44] and (C) plastics after UV curing.[17]

6

generated via plasma treatment of the silicone surface (Figure 1.5B).[44] The silicone substrates were then dip-coated in a solution containing an allyl-terminated polyethylene glycol-polyhexamethylene guanidine (APEG-PHMG) block copolymer, and the pieces were autoclaved to facilitate reaction of the surface with the olefinic moieties on the polymer.[44] The Foucher group and the Locklin groups have both independently reported benzophenone-containing small molecule QACs that could be grafted to several plastic substrates via a UV-curing step.[17,45] Upon irradiation of UV light, an electron from the carbonyl group in benzophenone subunit undergoes a n-π* transition to form a biradical triplet state. The electron deficient oxygen abstracts hydrogen from the substrate, forming a surface radical that recombines with the carbon radical on the benzophenone to form a covalent C-C bond (Figure 1.5C).[46] This attachment strategy is widely applicable in industry due to the straightforward nature of the UV-curing step. The surfaces prepared by Porosa and coworkers were measured by Atomic Force Microscopy (AFM) to have a thickness of *ca.* 366 $\pm$ 144 nm, corresponding to ~80 molecules in height and substantial surface roughness.[17] These surfaces were bactericidal against *Pseudomonas aeruginosa* (PAO1), *Listeria monocytogenes* (Scott A), and *Arthrobacter* sp. (IAI-3).

1.3   Antimicrobial Additives for Materials

While a dominant commercial strategy in the 20th century, using antimicrobial additives in materials to fabricate antifouling and bactericidal materials has been largely eschewed in favour of applying surface coatings due to environmental concerns.[47] On the other hand, the application of antimicrobials as additives remains a powerful approach as costs can be lower in comparison to some expensive surface modification techniques. Biocides well dispersed throughout a substrate can give rise to materials that can retain antimicrobial properties despite weathering and abrasion.[48]

The development of legitimately robust, yet effective antimicrobial coatings has not yet been realized commercially. To capitalize on these benefits, there has been recent interest in the development of safer biocidal additives, in particular non-leaching additives that are still immobilized to the material matrix, with the potential to maintain long-term efficacy. Harney and coworkers incorporated QACs containing various ratios of oxyethylene and *n*-alkyl chain length into polyurethane materials, and found that longer *n*-alkyl chains led to increased migration of the QAC to the polyurethane-air interface, as well as enhanced antimicrobial activity against Gram-negative and Gram-positive species (Figure 1.6A).[48] No evidence of leaching from the polyurethane films was found after 7 d submerged in aqueous solution.
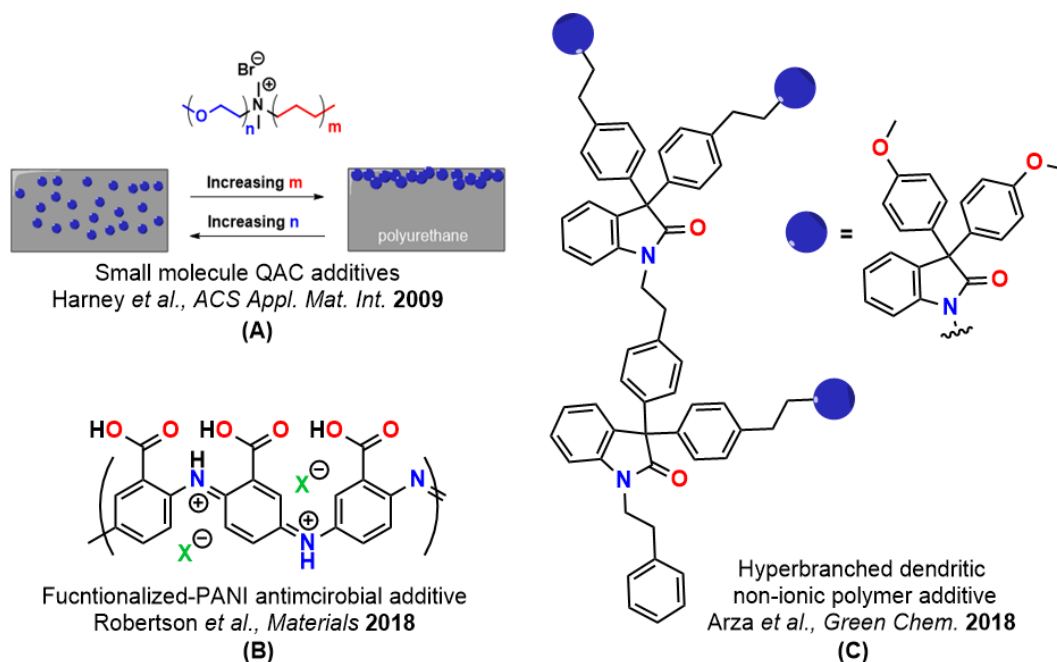
Figure 1.6. Non-leaching additives. Antimicrobials employed as non-leaching additives in plastics and resins, including (A) a small molecule, self surface enriching QAC for polyurethane films,[48] (B) carboxylic acid functionalized oxidized polyaniline polymers compression molded into styrenic films,[49] and (C) a dendritic polymer with antimicrobial anisole functionalities used as an additive in cellulose films.[50]

Recently, Robertson and coworkers reported antimicrobial compression molded styrene ethylene butylene styrene (SEBS) films with 3 % (w/w) loadings of a carboxylic acid functionalized oxidized polyaniline (fPANI) (Figure 1.6B). These surfaces were able to reduce the

number of viable *Escherichia coli* (*E. coli*) by *ca.* log 2 colony forming units (CFUs), however, under the same conditions reduction of *Staphylococcus aureus* (*S. aureus*) was not achieved.[49] Efforts by Arza *et al.* to prepare a non-leaching antimicrobial additive led to the design of a hyperbranched dendrimer with anisole moieties (Figure 1.6C).[50] When added to cellulose film, the dendrimers exhibited inhibition of several Gram-positive strains, and were more active against Gram-negative strains. UV-Vis analysis did not find any leaching of the dendrimer into aqueous solutions after 5 days.[50]

1.4 Mechanism of Antimicrobial Action

The mechanism of antimicrobial activity of cationic antimicrobials has been studied extensively, as the elucidation of the mode of action could lead to more focused and effective efforts in combatting antibiotic resistant bacteria. In solution, factors such as alkyl chain length, molecular weight, and number of positive charges all play a role in determining the effectiveness of cationic antimicrobials.[51] Solution-based cationic antimicrobials kill bacteria by destroying the bacterial cell walls and membranes via a two-step mechanism: cationics are attracted to the net-negatively charged membrane and diffuse to the inner cellular membrane, where they form ion pairs with the negatively charged phospholipids.[51,52] Once installed in the cell membrane, the nonpolar region of the antimicrobial begins to denature membrane proteins and as the antimicrobials attached to the membrane begin to reach a critical concentration, the cell begins to lose function and the ability to repair membrane damage.[52] The membrane concentration of cationic compound increases to the point where the phospholipids contained in the membrane are solubilized by the amphiphilic antimicrobial, and begin to leave as vesicles, irreversibly destroying the cell.[53] This mechanism has been well studied, and as such there have been reports detailing the manner in which bacteria can acquire resistance to solution-based cationic surfactant-type

molecules.[54,55] The mechanism of action for surface immobilized cationic antimicrobials has also been well studied, although a unified model of killing has not been established, and the precise nature of antimicrobial activity by tethered cationics is still debated in the literature. There are two dominant theories: the "polymeric spacer effect" and the "phospholipid sponge effect."

1.4.1   The Polymeric Spacer Effect

The polymeric spacer effect, first put forth by Klibanov in 2001, represents the first attempt to describe the killing action of antimicrobial surfaces (Figure 1.7A).[56] *N*-alkylated poly(4-vinylpyridine) (PVP) was grafted onto glass slides, and the surfaces were tested against *S. aureus* and PAO1. Polymers with *n*-hexyl chains were the most effective when challenged with the bacteria (Figure 1.7B), and the authors proposed that the alkyl chains decorating the vinylpyridinium polymer were responsible for balancing the hydrophobic-hydrophilic interactions
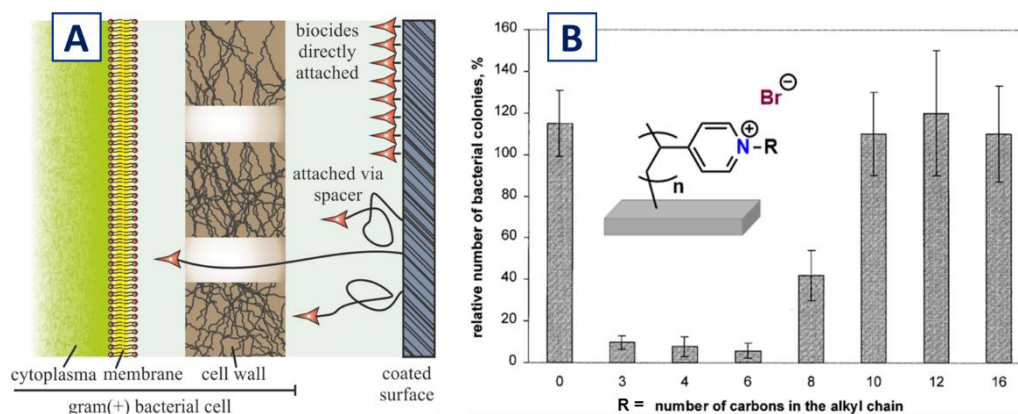
Figure 1.7. Evidence for the polymeric spacer effect. (A) depiction of the polymeric spacer effect, and (B) evidence of a requirement for alkyl chain length (adapted from refs.[18,56]).

between the QAC and the membrane, facilitating polymer chain insertion.[56] Crucially, it was observed that molecular weight (M_n) corresponded to activity against bacteria species: 60 kDa PVP grafts killed $62 \pm 8\%$ of bacteria inoculated on surface, while the larger $M_n = 160$ kDa polymer gave reductions up to 97%. Interestingly, when the polymeric QACs were in solution, they did

10

not display any efficacy against the bacterial species, suggesting a mode of action unique to the surface-bound antimicrobials.

1.4.2   The Phospholipid Sponge Effect

While the polymer spacer effect describes the action of long cationic polymer brushes against bacteria, there are several examples of surfaces with other structural motifs that kill bacteria upon contact.[57] In 2011, Li *et al.* described the synthesis of a hydrogel comprised of a QAC-chitosan-*graft*-PEG methacrylate. It was reported that larger pore sizes and higher degrees of quaternization (i.e. higher surface charge) led to better antimicrobial activity.[58] To rationalize this phenomenon, Bieser and Tiller proposed in 2011 that strong electrostatic interactions between the positively charged substrate and the anionic phospholipid were responsible for the observed activity of these highly charged "porous" surfaces (Figure 1.8A).[59]

Bacterial cell membranes contain polar groups with functionalities that are either zwitterionic, as is the case with phosphatidylcholine, or negatively charged, such as phosphatidylglycerol and phosphatidyserine.[60] The phospholipid sponge effect mechanism suggests strong electrostatic interactions between the positively charged substrate and the anionic phospholipid results in a diffusion of the phospholipid components of the cell membrane to the polycationic polymeric surface.[61] In the report describing the membrane-suctioning hydrogel, Li and coworkers reported computer simulations showing on a nanosecond timescale the diffusion of these lipopolysaccharides (LPS) into a sufficiently porous and charged membrane (Figure 1.8B).[58] Additional evidence for this mechanism was provided by Busscher *et al.*, when the interaction between *Staphylococcus epidermis* (*S. epidermis*) and a hyperbranched polyurea-polyethylene imine (PU-PEI) coating on glass was measured by AFM to have adhesive forces of approximately 100 nN, a 100-fold increase over control surfaces.[62] Recently, Gao and coworkers provided
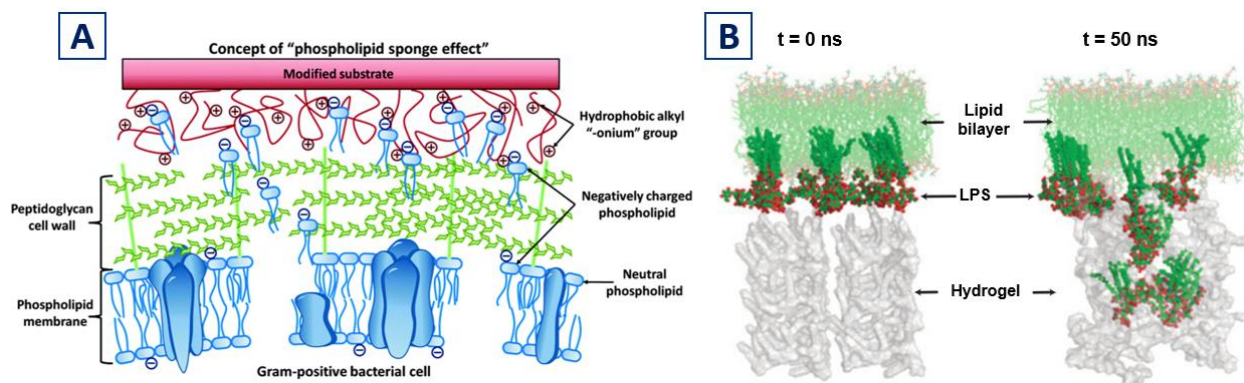
Figure 1.8. The phospholipid sponge effect. (A) A schematic of the phospholipid sponge effect in action. Negatively charged phospholipids are drawn to the highly cationic surface, creating holes and facilitating leakage of cell components. (B) Computer simulation of LPS leaving the cell membrane as molecular aggregates (reproduced with permission from refs.[58,61]).

evidence for this mechanism, with grafted UV-curable benzophenone-containing PEI and PVP polymers to plastic substrates.[63] Crosslinking density of the coatings was controlled by UV-curing time, with longer cure times producing more densely crosslinked coatings. The more "loosely" crosslinked coatings were significantly more active against *S. aureus* and *E. coli*., adhering to the basic proposed tenets of the lipid sponge effect: larger pore size is required for the "suctioning" of phospholipids from the cell membrane, and to allow a higher density of "accessible" charge.[59,63]

1.5   Phosphonium-Containing Antimicrobials
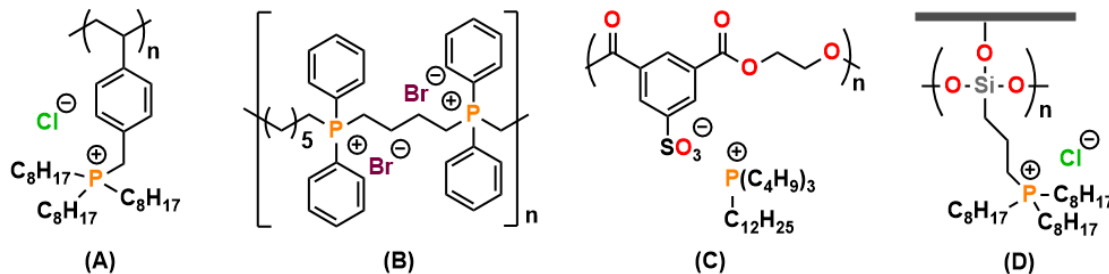
Figure 1.9. Phosphonium-containing polymers. Select examples of phosphoniums reported by Kanazawa *et al.* include (A) styrenic polymers with pendant trialkyl phosphonium groups,[68] (B) polymers with phosphonium in the polymer backbone,[70] (C) polyester-based materials that release phosphonium counterions as biocides,[72] and (D) trimethoxysilane functionalized phosphoniums that can bind to cellulose fibres.[73]

Most research efforts have involved the development of QACs as either solution-based disinfectants or surface-immobilized coatings, while less attention has been paid to their

phosphorous-containing congeners, the quaternary phosphonium compound (QPC). These materials contain formally positively charged phosphorus atoms, which have been reported to have greater thermal stability,[64] low cytotoxicity,[65] and excellent antimicrobial selectivity.[66] The dearth in literature examples of phosphonium antimicrobials is likely due to challenges associated with their synthesis, especially relative to the commercially available and air stable tertiary amine precursors used in QACs. Precursors to QPCs are typically air sensitive, electron-rich phosphine species,[67] and due to their reactivity, wide libraries of precursors to phosphoniums are either prohibitively expensive, or not readily available. Despite these challenges, the promise and novelty of these phosphonium-containing antimicrobials has led to some significant breakthroughs in the field of antimicrobial and polymer chemistry. Kanazawa and coworkers presented the first examples of phosphonium-containing polymers for use as antimicrobials in a series of reports (Figure 1.9),[68–74] demonstrating the wide breadth of applicability and versatility of these groups. Styrenic polymers with pendant *n*-trioctyl phosphonium groups were tested against *E. coli* and *S. aureus* were bactericidal in solution at low concentrations (10 µg/mL) after just 30 min.[68]

The first example of a surface immobilized phosphonium antimicrobial was reported in 1982 by Speier and Malek while working at Dow Corning.[75] Along with several QAC-type compounds, a triphenyl(3-(trimethoxysilyl)propyl)phosphonium iodide was drop cast from water onto cellulosic substrates, and showed full reductions of viable *E. coli* and *S. aureus* cells. In 2002, Kenawy reported a poly(glycidyl methacrylate-co-2-hydroxyethyl methacrylate) random copolymer that was functionalized with tributyl- and triphenylphosphonium reagents (Figure 1.10A).[76] The phosphonium-containing copolymers were not immobilized to any substrate, but rather deposited as powders on nutrient agar and inoculated with bacteria. This does not approximate a surface-immobilized biocide but represents a departure from some solution-based

13

tests. When tested against both Gram-positive and Gram-negative species, it was found that the tributylphosphonium-containing polymer outperformed both the triphenyl derivative and the ammonium-containing analogue, positioning these trialkyl phosphonium functionalities as powerful antimicrobial agents.[76]

Seddon and coworkers synthesized several variants of phosphorus-based ionic liquids (ILs), salts that exist as liquids at room temperature (Figure 1.10B).[77] The phosphonium-ILs (PILs) consisted of a quaternary phosphonium group, three *n*-hexyl alkyl substituents, and an alkyl group of varied length. The anion of the PILs were also varied along with the alkyl chain length. These were challenged with a tube dilution test (a solution-based antimicrobial test method[78]), and PILs of each alkyl chain length demonstrated excellent antimicrobial efficacy. While counterion effects were not observed for nitrogen-based imidazolium ILs,[79] the counterion showed an effect on bactericidal, as well as electrostatic activity of the PIL. In the case of $[(C_6H_{13})_3P^+(C_{14}H_{29})][PF_6^-]$ derivative there was a complete lack of antimicrobial activity against either Gram-positive or Gram-negative strains. Furthermore, in the case of imidazolium based ILs, shorter chain

(A)
R = Ph, *n*-Bu
Phosphonium-functionalized methacrylate copolymer
Kenawy *et al., J. Polym. Sci. Part A Polym. Chem.* **2002**

(B)
n = 2-4, 6-8, 10, 12, 14, 16
X = Br, Cl, OTf, NTf₂, N(CN)₂, PF₆, BF₄
Phosphonium-based ionic liquid (PIL) antimicrobials
Seddon *et al., Green Chem.* **2005**

(C)
X = Br, NTf₂,
Fluorinated PILs
Tindale & Ragogna, *Chem. Commun.* **2009**

(D)
Polymerizable fluoroalkyl phosphoniums
Guterman *et al.,J. Polym. Sci. Part A Polym. Chem.* **2013**

Figure 1.10. Phosphonium polyelectrolytes and ionic liquids. Developments in phosphonium-based molecules since initial the Kanazawa reports include (A) an antimicrobial phosphonium functionalized methacrylate copolymer,[76] (B) the first report of antimicrobial phosphonium-based ionic liquids (PILs),[77] (C) highly fluorinated PILs,[80] and (D) fluorinated PILs with polymerizable functionality.[64]

14

substituents (n < 5) were unable to kill bacteria and fungi, highlighting another key difference between ammonium and phosphoniums in solution, where the shorter chain PILs were bactericidal.[77,79]

Work carried out by Tindale and Ragogna introduced several fluorinated PILs (Figure 1.10C) derived from the simplest phosphine, phosphine gas (PH$_3$).[80] These salts were developed to act as media for superhydrophobic and antibiofouling surfaces. The Ragogna group further advanced this principle in 2013 with the development of fluorinated PILs with photopolymerizable groups (Figure 1.10D) and cast polymeric films with excellent thermal stability from these monomers.[64] The antimicrobial activity of these films were not tested.

In 2015, Ragogna and Gillies reported a series of acrylate-based non-adhering UV-curable coatings where the phosphonium was a component in a photocurable resin (Figure 1.11A).[81] A liquid phosphonium with an acrylate substituent was deposited on a silicon wafer along with two other liquid components: a crosslinking agent (tricyclodecanedimethanol diacrylate), and an
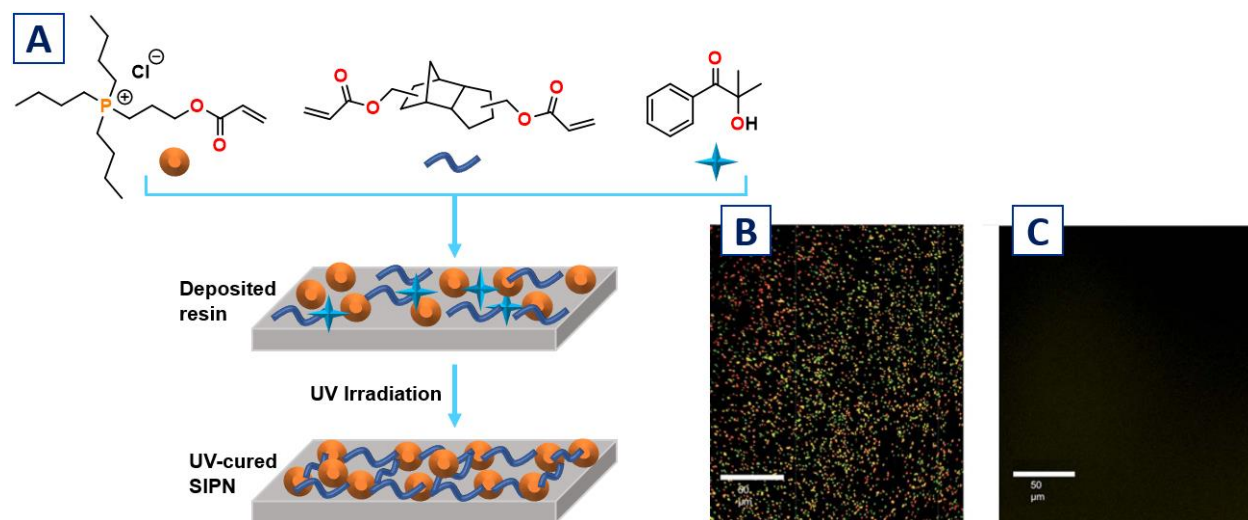
Figure 1.11. UV-cured polyphosphonium networks. The network was comprised of: (A) a phosphonium acrylate monomer, a crosslinker, and an initiator, and was UV cured to a silicon wafer. When a LIVE/DEAD[TM] assay was performed, (B) a control surface showed no significant kill, while (C) the coated surface showed no bacterial adhesion to the surface (Adapted from ref.[81])

initiator (2-hydroxy-2-methyl-1-phenylpropanone) (Figure 1.11A). After UV-curing under an atmosphere of nitrogen (N_2), the resins were cured into networks and their antibacterial efficacy challenged by depositing *ca.* 10^7 colony forming units/cm^2 (CFUs cm^{-2}) of *S. aureus* and *E. coli* on the cured networks, and assessing their efficacy using a LIVE/DEAD^{TM} assay. If bacteria are dead, the propidium iodide component in the LIVE/DEAD^{TM} stain will permeate the destroyed membranes and fluoresce red under a fluorescence microscope, while live cells will uptake the dye SYTO 9, which fluoresces green.[81] The control surface (Figure 1.11B) showed live bacteria and no significant reduction viable cells, while the surfaces with the polyphosphonium network cured under N_2 showed no adhered bacteria, demonstrating phosphoniums networks could be effective antimicrobials. It should be noted that the LIVE/DEAD^{TM} assay is not a quantitative method, which is typically required for robust testing of antimicrobial properties.

Ragogna and Gillies extended the concept of non-adhered coatings to styrenic phosphonium-containing polymers at various molecular weights.[65] Polyphosphoniums were synthesized through reversible addition-fragmentation chain-transfer (RAFT) polymerization, yielding polyphosphoniums of various molecular weights. These trialkyl groups at the phosphonium were also varied, with ethyl, *n*-butyl, and *n*-octyl derivatives all synthesized (Figure 1.12). The polyphosphoniums were then mixed with a tetraethylene glycol diacrylate (TEGDA)
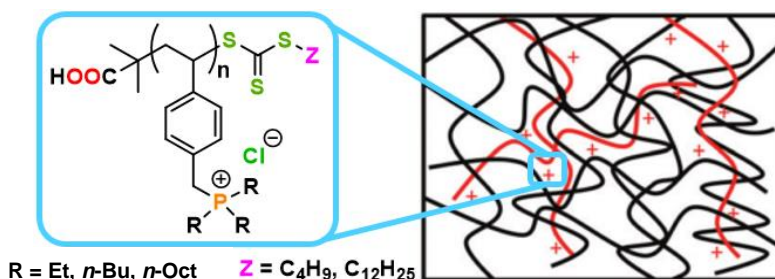
Figure 1.12. Semi-interpenetrating polymer networks. A semi-interpenetrating polymer network (SIPN) consisting of crosslinked TEGDA networks and a phosphonium-containing styrenic polymer prepared by Cuthbert and coworkers.[65]

16

crosslinker, and a photoinitiator, 2,2-dimethoxy-2-phenylacetophenone (DMPA, λ_{max} = 325 nm), and cast as films using either methanol (MeOH) or *N,N*-dimethylformamide (DMF). Once cast, the films were irradiated with UV light to form semi-interpenetrating polymer networks (SIPNs) (Figure 1.12). It was hypothesized that the polyphosphonium network was either physically entwined with the TEGDA network, or that UV-initiated fragmentation of the terminal RAFT agent could result in covalent linkage to the TEGDA monomers and thus the resulting polymers.[65] There was no observable phase separation of the polyphosphonium from the TEGDA network. The SIPNs were ground into powders and tested against Gram-negative (*E. coli*) and Gram-positive (*S. aureus*) bacteria in solution, and with one exception, the networks inhibited >90% of bacterial growth. Networks comprised of the polymer (M_n = 40 kDa) containing tri(*n*-octyl) phosphonium groups were not bactericidal; this was attributed to charge burial of the antimicrobially active phosphonium within the network.[65]

Recently, Ragogna and Gillies demonstrated surprising antibacterial activity from trishydroxypropyl-polyphosphoniums, which were more active than trialkyl-polyphosphoniums
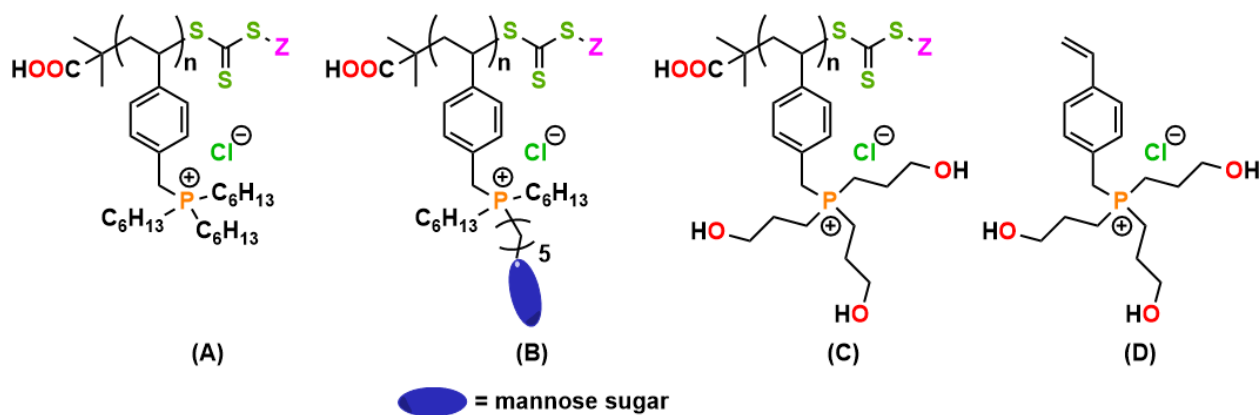
Figure 1.13. Phosphoniums tested for selectivity against bacteria. Phosphoniums examined for antimicrobial efficacy and hemolytic potential include (A) the tri(*n*-hexyl)phosphonium polymer, (B) a mannose sugar functionalized phosphonium polymer, (C) a tris(hydroxypropyl)-phosphonium containing polymer, and (D) the tris(3-hydroxypropyl)(4-vinylbenzyl)phosphonium chloride monomer.[66]

and a sugar-functionalized polyphosphonium synthesized in the same report. (Figure 1.13A).[66] Crucially, the hydroxyl polyphosphoniums exhibited the greatest selectivity for bacteria over red blood cells, with very low toxicity compared to other antibacterials. When the tris(3-hydroxypropyl)(4-vinylbenzyl)phosphonium chloride (Figure 1.13D) monomer was subjected to the same bacterial and hemolysis assays, the opposite behaviour was observed: the monomer was hemolytic and had low activity against the bacteria. This suggests the polymeric form was crucial for the observed selectivity.[66] Despite these advances in polyphosphonium coatings, there is a scarcity of tethered, robust phosphonium coatings represented in the literature. Abrasion resistance, coating hardness, and chemical resistance testing is yet unknown for phosphonium systems.

1.6   Chemistry of Quaternary Phosphonium Groups

One likely reason phosphonium-based antimicrobials are less prevalent than their ammonium-based counterparts is the relative stability of intermediates and precursors to the stable phosphonium products. Phosphine gas, PH_3, is a flammable and highly toxic reagent that can ignite spontaneously at 150 °C and decomposes in air to give phosphoric acid.[82] Despite this, it has the potential to be an incredibly useful synthon for the production of primary, secondary, and tertiary phosphines.[64] Tertiary phosphines, the immediate precursors to phosphonium salts, are typically sensitive to oxidation in ambient conditions and require handling in inert atmospheres, or alternative preparatory procedures.[82] Compounding this, most precursors to tertiary phosphines are even more susceptible to oxidation.[67] There has been significant interest in the development of facile synthetic routes to tertiary phosphines as a result of their usefulness in coordination chemistry and catalysis,[83–86] as well as emerging interest in their use in materials science.[87,88] In

18

accordance with the scope of this thesis, only synthesis involving the formation of carbon-phosphorus (C-P) bonds will be discussed herein.

1.6.1   Synthesis of Tertiary Phosphine Precursors

The formation of C(sp^3)-P bonds is well established, and one of the simplest routes involves the reaction of organometallic synthons such as Grignard reagents or alkyllithiums with halophosphines (Scheme 1.1A).[89] This transformation involves stoichiometric amounts of the organometallic reagent for the preparation of trialkylphosphines.[90] While seemingly straightforward, the use of these reagents has limitations: the formation of a carbanion precludes

(A) PCl_3 $\xrightarrow[\text{- 3MgBrCl}]{\text{3(RMgBr)}}$ PR_3

(B) PCl_3 $\xrightarrow[\text{- N(}^iPr_2)Cl_2]{\text{2(}^iPr_2NH)}$ $Cl-P(N(^iPr_2)_2$ $\xrightarrow[\text{- MgBrCl}]{\text{ArMgBr}}$ $Ar-P(N(^iPr_2)_2$ $\xrightarrow[\text{- 2(HN(}^iPr_2)Cl)]{\text{2HCl}}$ $Ar-PCl_2$

R = alkyl, Ar = aryl

Scheme 1.1 Grignard reagents in the preparation of P-C bonds. Schematic for the preparation of (A) trialkylphosphines from phosphorus(III) chloride (PCl_3) using a Grignard reagent, and (B) triarylphosphines from PCl_3 using Grignard reagents and diisopropylamino protecting groups to direct the metalating reagent.[95]

the use of Grignard or alkyllithium reagents for phosphine substrates with electrophilic functional groups (*i.e.* carboxylic acids).[91,92] Moreover, in the case of bulkier arylphosphines, a straightforward stoichiometric reaction of the Grignard does not efficiently yield the triarylphosphine, and a stepwise, synthetic route with poor atom-economy involving protection with bulky amines and deprotection with hydrochloric acid (HCl) must be employed (Scheme 1.1B).[89,93–95]

Another, more atom-economical method of C-P bond formation is the hydrophosphination reaction. Hydrophosphination involves the reaction of a phosphorus-hydrogen (P-H) bond and a carbon-carbon (C-C) double bond (Scheme 1.2).[96] A versatile reaction with broad scope of applicability, hydrophosphination can proceed under thermal conditions (Scheme 1.2B),[97,98] by base catalysis (Scheme 1.2B),[99] acid catalysis (Scheme 1.2C),[100] and by radical initiation (Scheme 1.2D)[101] typically give anti-Markovnikov products. In 2012, Alonso and coworkers reported an example of solvent and catalyst-free hydrophosphination of several olefins with diphenylphosphine.[102] Crucially, although the reaction proceeded quickly with heating (1 h, 70 °C), the authors found the hydrophosphination was facile at room temperature after 7 h. Alsono *et al.* proposed in a subsequent report[103] that the mechanism for this transformation was not a radical pathway after addition of common radical traps (cumene, TEMPO) did not inhibit reactivity, and
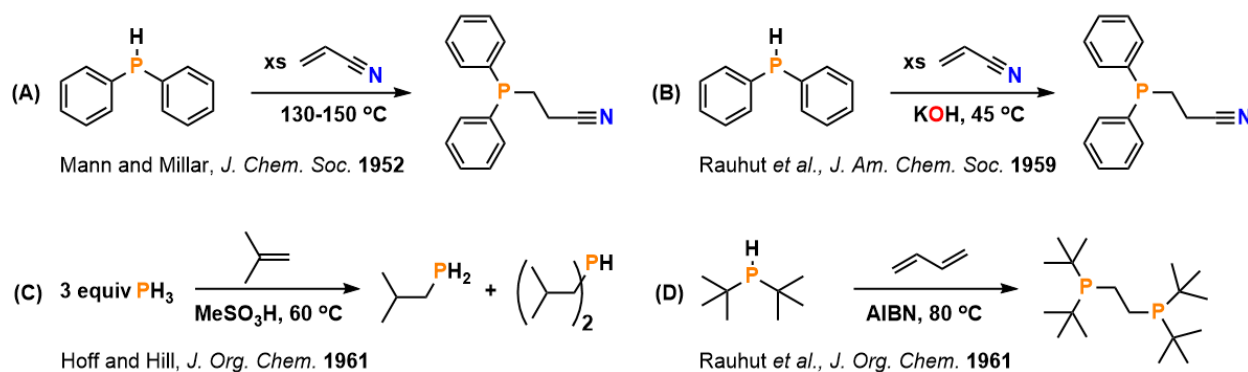
Scheme 1.2. Early advances in hydrophosphination. The initial reports of P-H addition to olefins include (A) thermally initiated hydrophosphination of diphenylphosphine and acrylonitrile,[97] (B) base-catalyzed hydrophosphination of diphenylphosphine and acrylonitrile in the presence of KOH, (C) acid-catalyzed hydrophosphination of phosphine gas and isobutene in the presence of methanesulfonic acid, and (D) the radical initiation of di-tertbutylphosphine and 1,3-butadiene in the presence of azobisisobutyronitrile (AIBN).

products derived from the radical traps were not observed. A concerted hydrophosphination mechanism where the P-H bond is added to the alkene through a four-membered ring intermediate was also excluded as the observed solvent-free hydrophosphination gave *anti* products and hydroboration gives the *syn* isomer.[103] The authors proposed an ionic pathway involving two

different phosphine molecules, citing known examples of phosphines acting as nucleophilic

catalysts in alkene additions.[104]

The Ragogna group has also developed facile synthesis of tertiary phosphines in service of

developing phosphonium materials. Starting from PH_3, fluoroalkyl phosphines were synthesized

using AIBN as a radical initiator for the hydrophosphination (Scheme 1.3).[64] This result provided

a simple route to expanding the library of tertiary phosphines available for phosphonium synthesis.
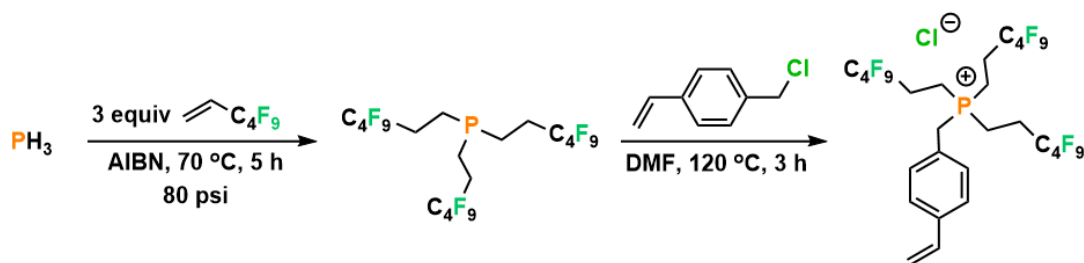
Scheme 1.3. Hydrophosphination of fluoroalkenes. Phosphine gas is reacted with stoichiometric fluoroalkene to yield the trisubstituted tertiary fluoroalkyl phosphine. This can be further reacted with 4-vinylbenzyl chloride to yield the phosphonium salt.[64]

1.6.2   Synthesis of Phosphoniums

The facile synthesis of phosphonium salts is analogous to the synthesis of their ammonium

counterparts, QACs. QACs are synthesized *via* the Menshutkin quaternization reaction, which

involves alkylation of a tertiary amine to yield the desired QAC (Scheme 1.4A).[105] The reaction

occurs between two neutral molecules, where the tertiary amine undergoes nucleophilic attack on

an electrophilic alkyl halide, displacing the halide and forming an ion pair. The reaction proceeds

through an S_N2 pathway, and as such, reactant concentration, nucleophilicity of the amine, solvent,
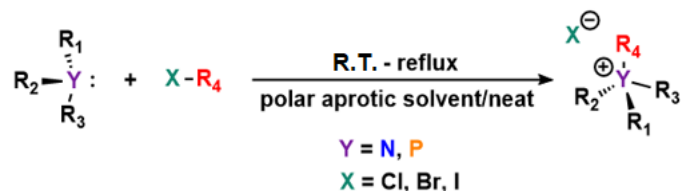
Scheme 1.4. Quaternization of amines and phosphines. General conditions for the Menshutkin quaternization of tertiary amines and Menshutkin-like quaternization of tertiary phosphines.

and temperature and pressure all affect the kinetics of the reaction.[106] In particular, solvent choice has been demonstrated to have significant effect on reaction rate, with highly polar solvents stabilizing both the charged transition state and the ionic final product, giving higher yields with shorter reaction times.[107] The quaternization of phosphoniums is "Menshutkin-like," proceeding through an S_N2 pathway where nucleophilic tertiary phosphines attack the electrophilic sp^3 carbon of an alkyl halide (Scheme 1.4B).[108]

1.7 Detection of Phosphonium on Surfaces

Once phosphoniums are coated and firmly attached onto surfaces, it becomes important to quantify that coating, particularly with respect to accessible phosphonium. One effective, qualitative method is the use of bromophenol blue (BPB) anionic dye to stain the surface. The anionic dye, purple in aqueous solution, turns blue when it forms an ion pair complex with a quaternary -onium functionality.[109] As a result, it is an effective qualitative method for quick visualization of phosphoniums tethered to a substrate: the colourless substrate is stained blue upon complexation with the BPB dye (Figure 1.14).[17]
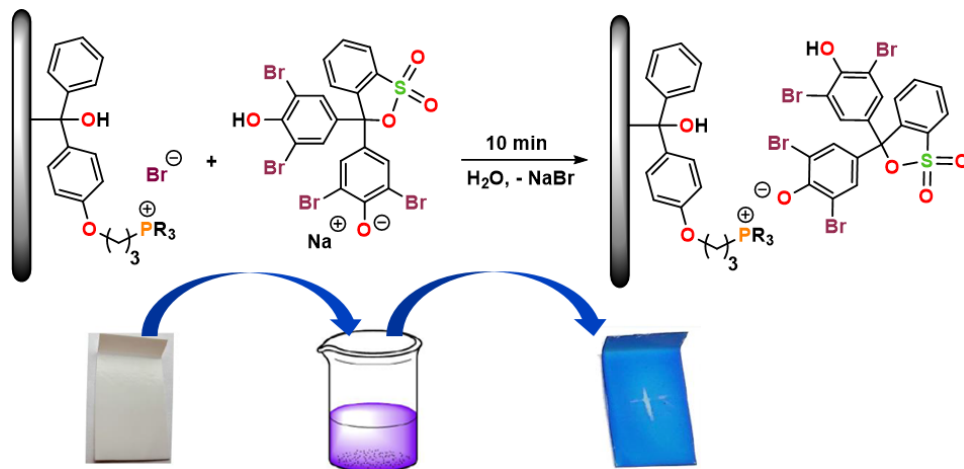
Figure 1.14. BPB staining of coated surfaces. A coated substrate is submerged in an aqueous solution containing bromophenol blue (40-400 ppm), where the dye undergoes anionic exchange with the phosphonium, staining the surface blue.

In 2007, Murata and coworkers utilized a different anionic dye, fluorescein, to quantify accessible surface charge.[110] Coated surfaces were placed in a test tube containing 1 % (w/v) of fluorescein sodium salt overnight on an orbital shaker, to adsorb the dye to the surface. After exhaustive rinsing with water, the pieces were then placed into a 0.1% cetyltrimethylammonium bromide (CTAB) solution containing 10% phosphate buffered saline (PBS) and sonicated to desorb the dye from the substrate. UV-Vis measurements (λ_{max} = 501 nm) were then taken to quantify the concentration of desorbed fluorescein dye (ε = 77 000 $M^{-1}cm^{-1}$).[110]

1.8 Testing Methods for Antimicrobial Efficacy

In the literature, there are two methods commonly applied to examine the antimicrobial efficacy of surfaces: ASTM E2149 (dynamic shake flask assay)[111] and ISO 22196 (cover slip test).[112] The dynamic shake flask assay (DSF) involves submerging a coated surface in a bacterial inoculum, and inducing contact with the surface by shaking the flask. This method simulates bacterial contact with an antimicrobial surface in an aqueous environment (solid-liquid interface), but does not accurately simulate bacterial and biofilm growth on "dry" surfaces.[111] The cover slip test involves the deposition of a droplet containing a known quantity of bacteria on an antimicrobial surface, which is then covered with a glass cover slip to ensure intimate contact with the surface.[112] This method is advantageous in that it assesses killing at a solid-air interface, however it fails to account for the real-world phenomenon of desiccation. In 2016, Campos and coworkers demonstrated that the application of different testing methods for antimicrobial surfaces could yield different results, suggesting a need for a standardized test.[113] The large drop inoculum (LDI) method, a modification of ISO 22196, was first reported by the Wolfaardt lab where after the droplet is deposited, it is allowed to dry on the surface, after which unbound cells are removed

and enumerated.[114] This method accounts for desiccation, which is a stressor believed to incite biofilm formation.[114]

1.9   Research Objectives

Despite some notable recent advances in the synthesis, coating and characterization of antimicrobial phosphoniums, there is little to no precedent for phosphonium materials that maintain antimicrobial activity over extended periods of time. The aims of this thesis are to explore the straightforward synthesis of a new class of phosphoniums capable of UV-curing to plastic materials, and to explore the use of these phosphoniums as additives in plastics. The phosphoniums will be synthesized with a variety of alkyl, aryl, and fluoroalkyl functional groups at phosphorus to probe their efficacy as thermally stable antimicrobial additives in plastics or as surface coatings.

To gain insight into the mechanism of antimicrobial activity of these materials, the surface topology and characteristics of these materials will also be evaluated. Additionally, this thesis aims to establish general design principals for tailoring phosphoniums to function as both additives during injection molding processes and as UV-curable coating. It is hypothesized that the incorporation of fluoroalkyl groups at the phosphonium will lead to improved migration to the solid-air interface. Finally, the evaluation of these coatings and materials against both Gram-negative and Gram-positive bacteria in both applications with a variety of plastics will be carried out. Finally, the capacity for these materials to maintain the ability to kill biofilm-forming bacteria even after being subjected to abrasion processes will be assessed, establishing whether they are suitable as long-term antimicrobial solutions.

2   RESULTS AND DISCUSSION

2.1   Synthesis of Quaternary Phosphonium Antimicrobials
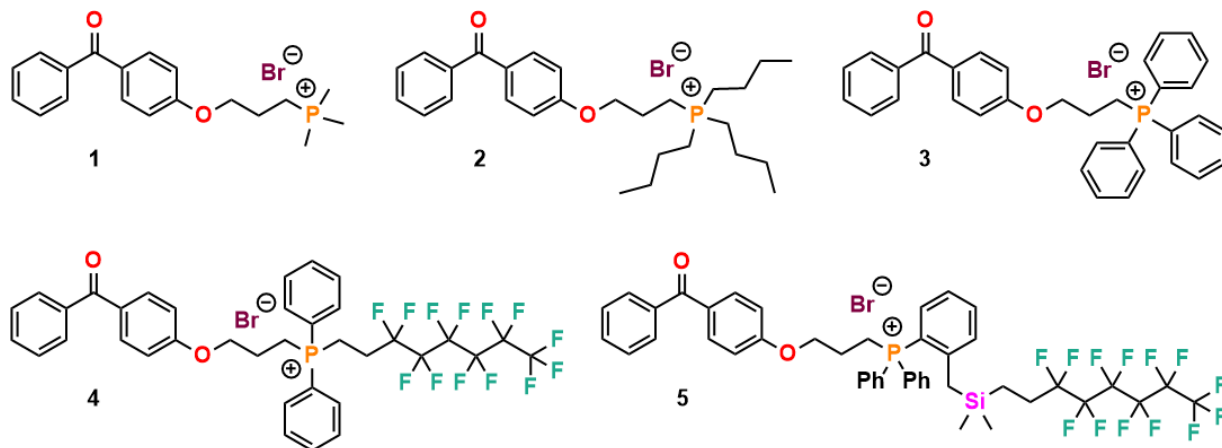
Figure 2.1 Target UV-curable phosphoniums. The proposed phosphonium materials for use as antimicrobial materials.

To establish trends and structure property relationships relating to antimicrobial efficacy, five novel, UV-curable phosphonium-containing compounds were synthesized (Figure 2.1). These phosphoniums represent varying degrees of hydrophobicity and oleophobicity.

2.1.1   Preparation of Benzophenone Anchor Precursor (i)

Incorporated into the proposed phosphonium compounds is a UV-active benzophenone functionality: this allows the molecules to be surface-cured to various substrates. A key intermediate can be prepared from the Williamson-ether reaction of alkyl halides with 4-hydroxybenzophenone. According to literature procedures, the synthesis of the linker molecule 4-
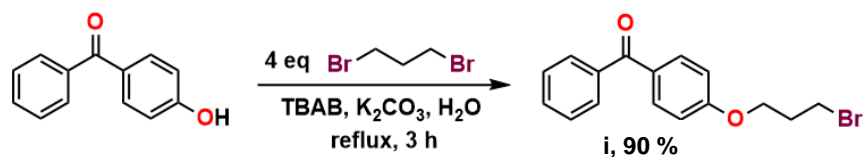
Scheme 2.1. Synthesis of 4-(3-bromopropoxy)benzophenone (i). In this work, **i** is synthesized *via* an efficient phase transfer catalyst route.

(3-bromopropoxy)benzophenone (**i**) typically results in poor yields due to the formation of a benzophenone dimer, 4-((3-bromopropoxy)benzoylphenoxy)benzophenone.[115] Additionally, published procedures involve the use of organic solvents and long reaction times, making them less suitable for scale-up due to environmental and cost concerns.[115,116] It is therefore desirable to use an alternative procedure for the synthesis of **i**. Previous work in the Foucher group led to the preparation of **i** using a phase transfer catalyst (PTC) (Scheme 2.2).[117] Phase transfer catalysis is synthetically advantageous, as it allows for the transfer of a molecule or ion between two reaction phases.[118] Importantly, utilizes an aqueous solvent system, often with the use of a QAC as the catalyst.[118] Landini *et al.* first described a general mechanism for phase transfer catalysis in 1977.[119] With respect to the formation of **i**, the mechanism proceeds as per Scheme 2.2. In the aqueous phase, the PTC undergoes ion exchange to form a complex with the base, shuttling the base into the organic phase, where it is free to deprotonate the orangosoluble 4-
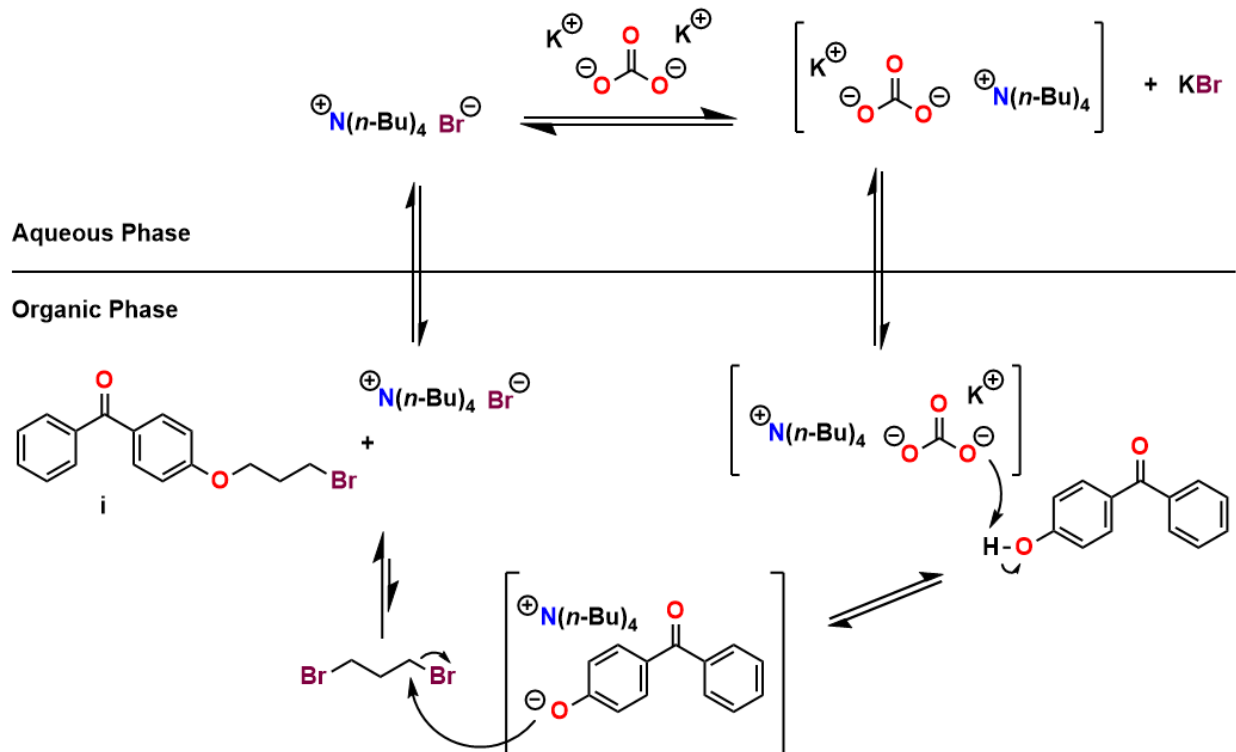
Scheme 2.2. Mechanism of phase transfer catalysis for the formation of i.

26

hydroxybenzophenone. Therefore, a requirement of any PTC is high organophilicty.[119,120] The PTC conjugate base complex is free to attack the electrophilic reagents present in the organic phase and form the ether. Stirring 4-hydroxybenzophenone in water with 1,3-dibromopropane, K_2CO_3, and 0.5 mol % tetra(n-butyl)ammonium bromide (TBAB) as a PTC for 3 h at 110 °C afforded the product **i** in high yield (90 %) (Scheme 2.1).

2.1.2 Synthesis of Quaternary Phosphoniums with Methyl, *n*-Butyl, and Phenyl Substituents
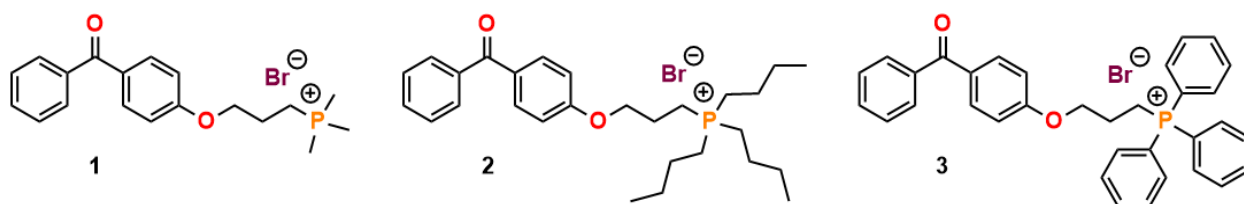
Figure 2.2. Phosphoniums prepared from commercially available tertiary phosphines.

The quaternization of tertiary phosphines is similar to the Menschutkin quaternization of amines: a nucleophilic tertiary phosphine attacks an electrophilic carbon, leading to alkylation at the phosphorus. This reaction proceeds in S_N2 fashion, and as such the concentration of reactants, temperature, quality of the leaving group, and polarity of the solvent all play a role in the rate of the reaction. Three UV-curable phosphoniums that could be synthesized in one step from readily available tertiary phosphine starting materials were envisioned: 4-(propoxybenzophenone)trimethylphosphonium bromide (**1**) 4-(propoxybenzophenone)tri(*n*-butyl)phosphonium bromide (**2**), and 4-(propoxybenzophenone)triphenylphosphonium bromide (**3**) (Figure 2.2).

2.1.2.1 Synthesis of (4-propoxybenzophenone)trimethylphosphonium bromide (1)
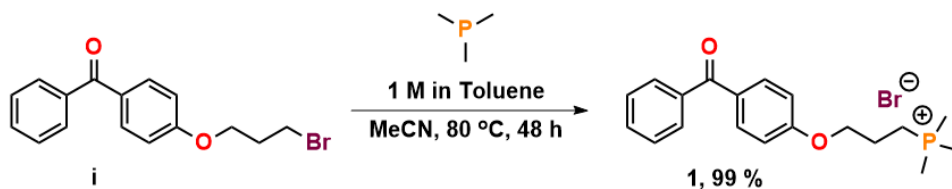
Scheme 2.3. Synthetic route to 1.

Phosphonium compound **1** was synthesized from the reaction of **i** and trimethylphosphine (PMe$_3$) in acetonitrile (MeCN) (Scheme 2.8). The PMe$_3$ starting material was purchased as a 1 M solution in toluene; as such, neat conditions were not attempted for the reaction. The reaction mixture was heated to 80 °C under an atmosphere of N$_2$ (g) in a sealed tube for 48 h, cooled to R. T., and was triturated from cold ether (Et$_2$O), yielding the phosphonium product as a white powder
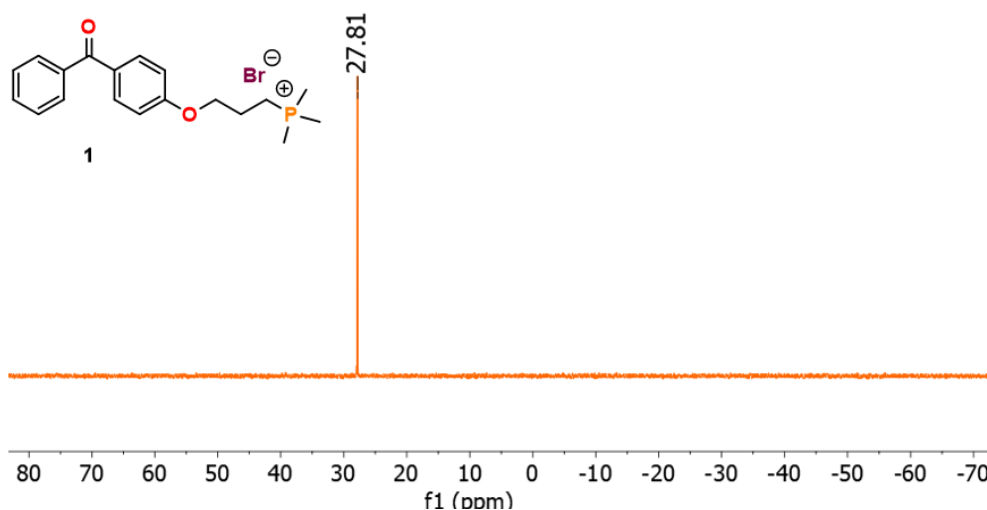
Figure 2.3. ^{31}P {^{1}H} NMR (CDCl$_3$) of 1. The signal is the only visible one in the spectrum and appears significantly upfield of the PMe$_3$ starting material.

in a 99.1% yield. The longer reaction time necessary for complete conversion to the phosphonium is likely a result of both a non-ideal solvent mixture for quaternization reactions and a more dilute mixture.[121] Proton-decoupled ^{31}P NMR spectroscopy (^{31}P {^{1}H} NMR) (CDCl$_3$) showed a new phosphorus environment at δ = 27.8 ppm (Figure 2.3) a significant downfield shift from the PMe$_3$

starting material (δ = -62 ppm). The downfield shift is expected of alkylated phosphoniums, as the electron poor phosphonium is more deshielded relative to the electron-rich trialkyl phosphine.

2.1.2.2 Synthesis of (4-propoxybenzophenone)tri(*n*-butyl)phosphonium bromide (2)
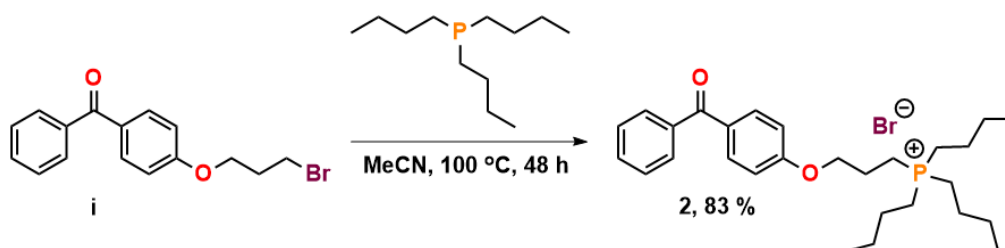
Scheme 2.4. Synthetic route to 2.

Phosphonium **2** was synthesized *via* quaternization of the commercially available tri(*n*-butyl)phosphine P(*n*-Bu)$_3$ with **i** in MeCN (Scheme 2.9). The reaction proceeded in similar fashion to the synthesis of **1**, at 100 °C for 48 h furnishing the product in an 83 % yield as a greasy, off-white coloured solid after trituration from cold Et$_2$O. ^{31}P {^{1}H} NMR (CDCl$_3$) analysis of the solid showed a major signal at δ = 33.6 ppm, and a low intensity signal at δ = 37.3 ppm (Figure 2.8). The larger peak was attributed to the phosphonium product **2** after high resolution mass spectrometry (HRMS) (Figure B 2). The signal with low relative intensity (1:0.03) is likely a small
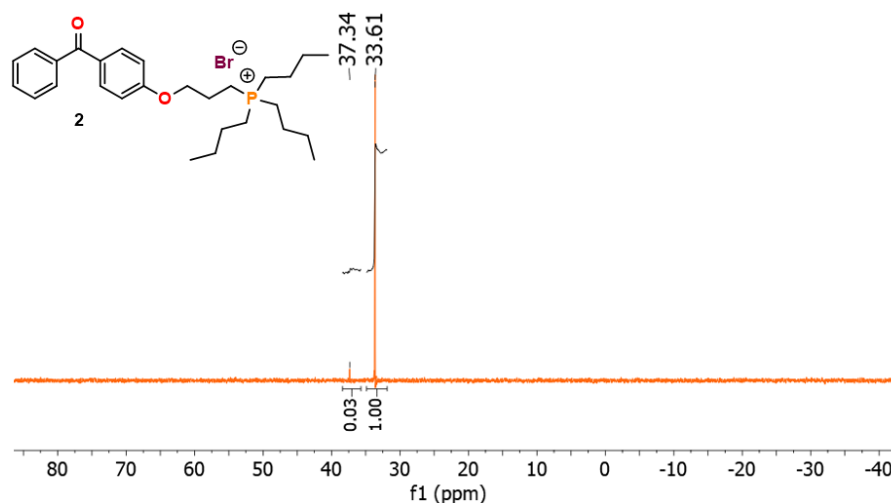
Figure 2.4. ^{31}P {^{1}H} NMR (CDCl$_3$) of 2. The signal at δ = 33.6 ppm corresponds to the phosphonium environment, while the signal upfield at δ = 37.3 ppm likely corresponds to oxidized starting material.

amount of oxidized P(*n*-Bu)₃ starting material, as the P(V) phosphine oxide (PO) which is expected

to appear downfield due to a higher oxidation state. The oxide was removed by additional washing

with Et₂O. Analysis by ¹H NMR (CDCl₃) further established the purity of the product (Figure 2.9).

Assignments were made with the aid of 2D NMR spectroscopy (CDCl₃). The integration of the

area under the signals totalled 43 (with proton environment H8 as a standard), while the molecule

has 42 protons; this discrepancy is consistent with the signal at $\delta = 37.3$ ppm in the ^{31}P {^{1}H} NMR
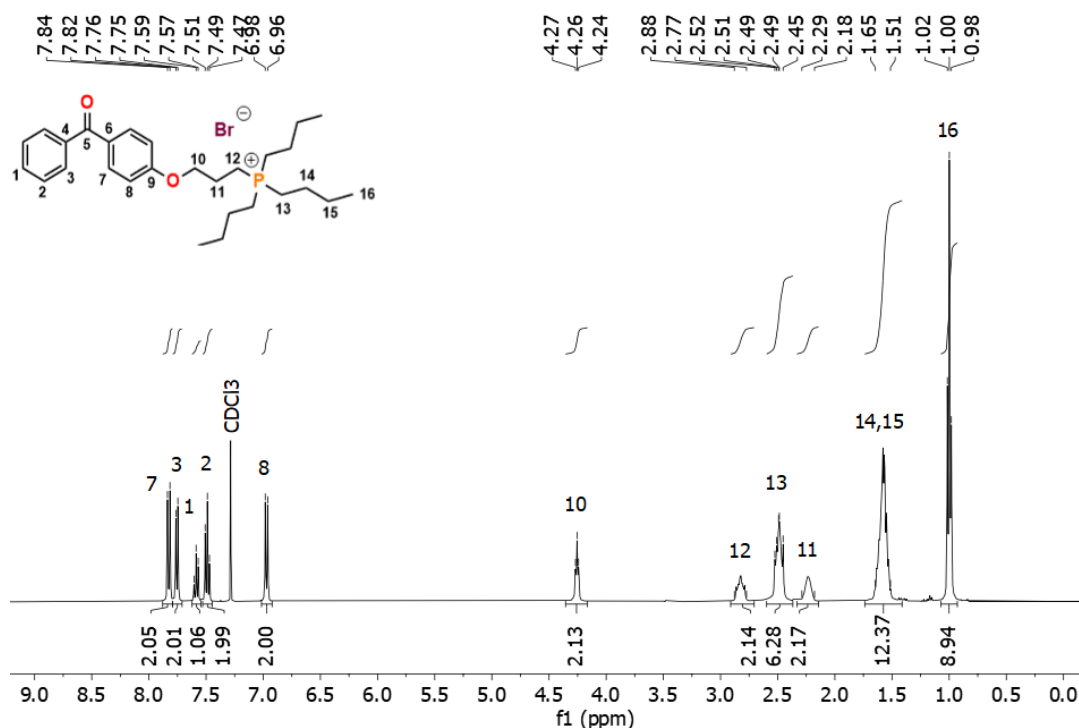
Figure 2.5. ¹H NMR (CDCl₃) spectrum of 2.

spectrum of **2** integrating with a ratio of 1:0.03. The benzophenone moiety appears in the aromatic

region with signals appearing in the same relative intensity and chemical shift as the starting

material **i**.[122] The ¹H environment at $\delta = 4.26$ ppm was labelled as H10, due to the electron

withdrawing nature of the benzoylphenoxy group. The ¹H environment labelled H12 shifted

upfield relative to the same proton on the starting material (Figure A 1), from $\delta = 3.62$ ppm to $\delta =$

2.77–2.88 ppm, providing more evidence of phosphonium formation. The ¹H environments at $\delta =$

2.77–2.88, 2.45–2.52, 2.18-2.29, and 1.51-1.65 (labelled H12, H13, H11, and H14 + H15) all

30

experienced signal broadening and as such were labelled multiplets. This broadening is likely the result of coupling with the spin active phosphonium, as well as the presence of butyl isomers: the starting P(n-Bu)$_3$ was 95 % pure, with isomers comprising the remainder of the material. Attribution of the overlapping signals at δ = 1.51–1.65 ppm to the chemically similar ^{1}H environments labelled H14 and H15 was supported by the integration for *ca.* 12 protons. Lastly, the triplet at δ = 1.00 ppm was attributed to the ^{1}H environment H16.

2.1.2.3   Synthesis of (4-propoxybenzophenone)triphenylphosphonium bromide (3)
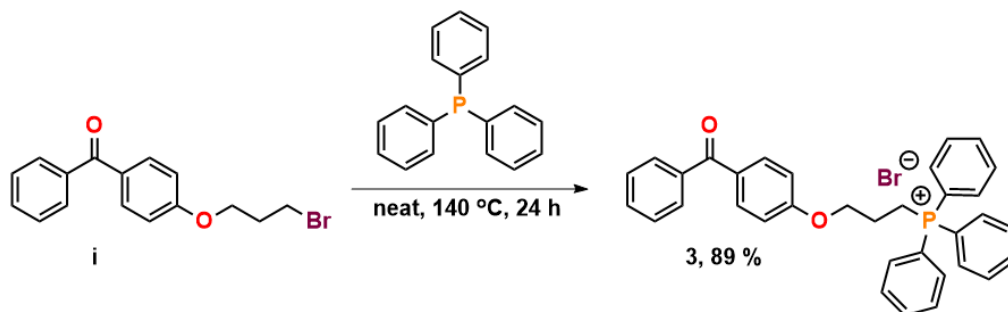
Scheme 2.5. Synthetic route to 3.

Phosphonium compound **3** was synthesized by reaction of triphenylphosphine (PPh$_3$) and **i** at 140 °C (Scheme 2.10). The neat reaction maximizes the concentration of reactants, favouring product formation in the reaction equilibrium. Additionally, exclusion of a solvent allowed for higher reaction temperatures. A higher reaction temperature is necessary, as the melting point of the phosphonium product was measured to be 191 °C, and a reaction temperature lower than 120 °C resulted in unreacted starting material becoming trapped in the solid matrix of the product, lowering reaction yield (72 %, 24 h). After 24 h stirring at 140 °C, the mixture was cooled and
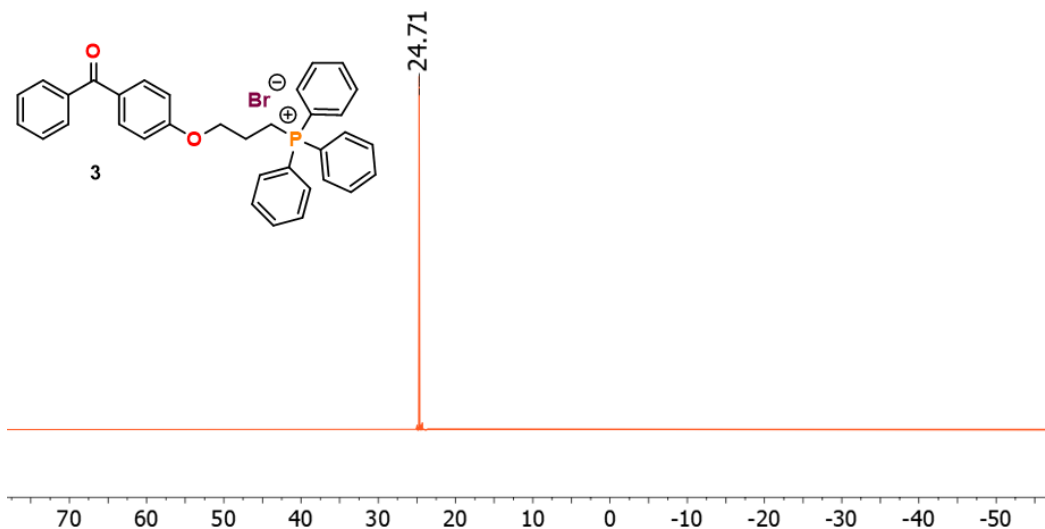
Figure 2.6. ^{31}P {^{1}H} NMR (CDCl$_3$) of 3.

dissolved in MeCN, then triturated from cold Et$_2$O, yielding the product as an off-white coloured

powder in an 89 % yield. An inert atmosphere of N$_2$ (g) was used during the reaction to ensure

minimal oxidation of the PPh$_3$ starting material at high temperatures.
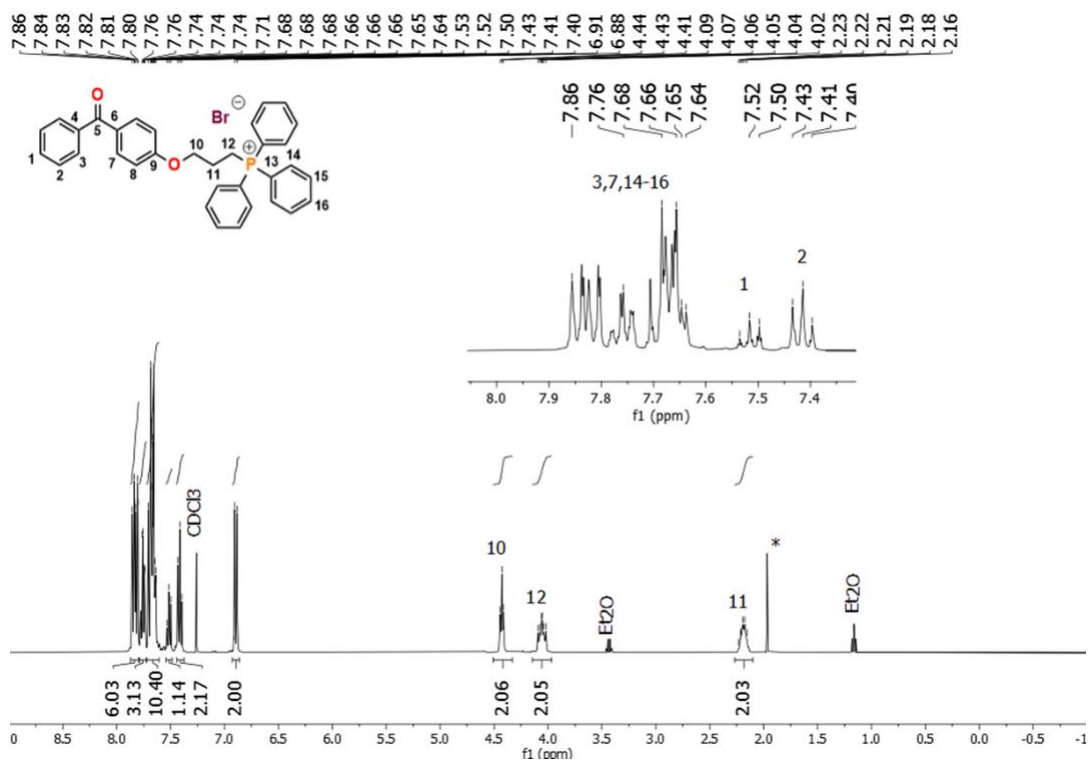
Figure 2.7. ^{1}H NMR (CDCl$_3$) spectrum of 3.

^{31}P {^{1}H} NMR (CDCl$_3$) analysis on the product (Figure 2.6) confirmed a new phosphorus environment was formed, with a signal appearing at δ = 24.7 ppm, a significant downfield shift from PPh$_3$ starting material. ^{1}H NMR (CDCl$_3$) of the phosphonium product (Figure 2.12) showed a significant downfield shift to δ = 4.09-4.22 from δ = 3.62 ppm for the ^{1}H environment neighboring the phosphonium (H12) relative to the starting material **i**, indicating formation of a new bond to the PPh$_3$. The aromatic proton environments on the triphenylphosphonium (H14, H15, H16) moiety overlapped with the aromatic signals from the benzophenone moiety, making individual assignments difficult.

2.1.3 Synthesis and Characterization of Tertiary Fluorinated Phosphine Precursors

Of the molecules synthesized, two required preparation of tertiary phosphine precursors, diphenyl((perfluorohexyl(ethyl)phosphine (**iv**), and ((dimethyl(perfluorohexylethyl)silyl)o-tolyl)diphenylphosphine (**vii**) (Figure 2.8), for **4** and **5**, respectively.
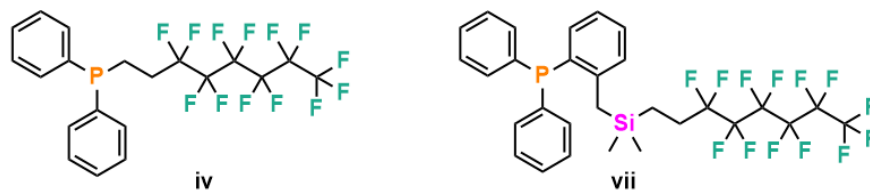
Figure 2.8. Tertiary phosphine precursors to phosphoniums 4 and 5.

2.1.3.1 Preparation of diphenyl(perfluorohexylethyl)phosphine (iv)
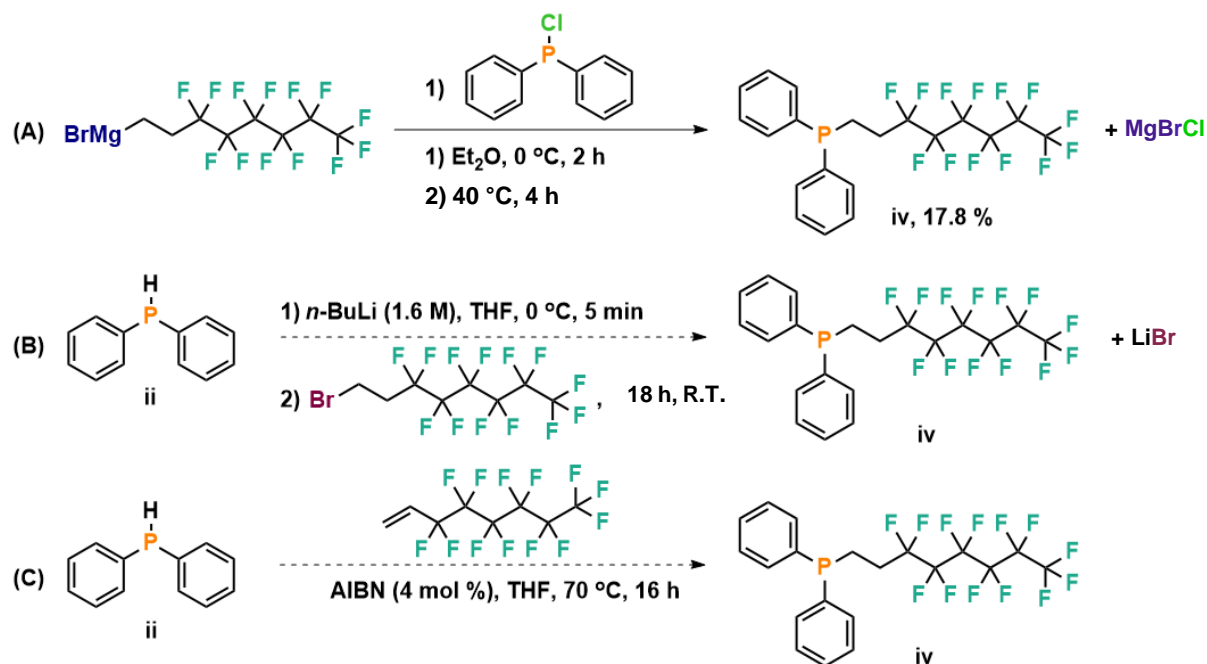
Scheme 2.6. Synthetic routes to diphenyl(perfluorohexylethyl)phosphine (iv). Proposed routes to yield **iv** include (A) alkylation of *P*-chlorodiphenylphosphine with a Grignard reagent, (B) lithiation of diphenylphosphine (**ii**) and addition to (perfluorohexylethyl)bromide, and (C) hydrophosphination of perfluorohexylethylene.

The first route attempted was *via* alkylation of *P*-chlorodiphenylphosphine (Ph$_2$PCl) by a

prepared Grignard reagent (Scheme 2.6A). In dry Et$_2$O, (perfluorohexylethyl)bromide was
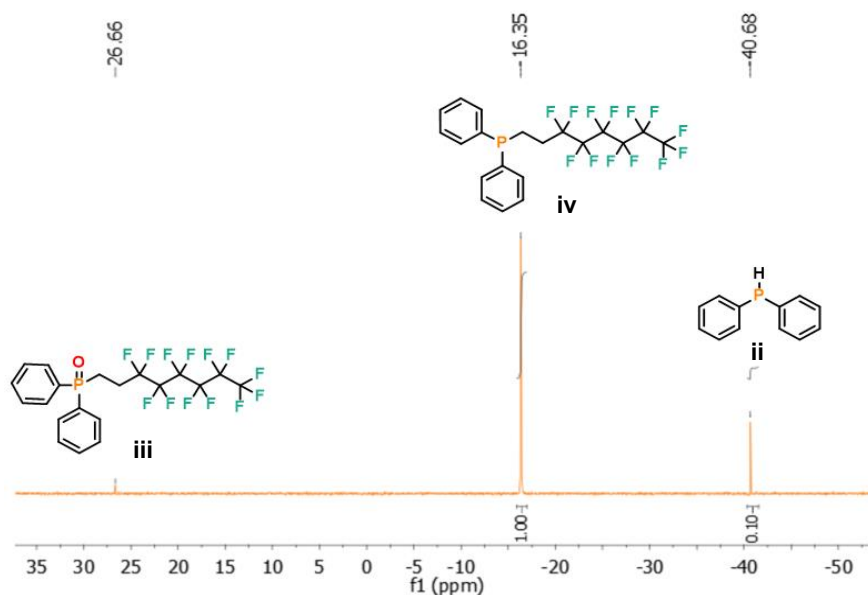
Figure 2.9. ^{31}P {^{1}H} NMR (C$_6$D$_6$) of the product mixture resulting from the alkylation of Ph$_2$PCl.

refluxed with a large excess of ground Mg (s) to produce the Grignard reagent, which was then added to a solution of Ph_2PCl over ice. The resulting product was isolated after workup in a low yield (18 %) and analyzed by $^{31}P\{^1H\}$ NMR (C_6D_6) (Figure 2.9). The spectrum shows a small amount of the oxidized product (26.7 ppm), the desired phosphine (-16.4 ppm) and a quantity of Ph_2PH, likely a product of the reduction of Ph_2PCl by the Mg metal. $^{31}P\{^1H\}$ and ^1H NMR (C_6D_6) analysis of the crude product before purification showed the major product of the reaction was diphenylphosphine oxide $(Ph_2P(O)H)$, suggesting the desired reaction of the Grignard reagent and Ph_2PCl was not occurring efficiently.

Another attempted route to yield the desired phosphine was the lithiation of Ph_2PH (Scheme 2.6B), which was reported in 2018 to undergo nucleophilic addition to perfluoroalkyl bromides.[123] Despite the literature reporting that this reaction proceeded to the tertiary phosphine product at room temperature, the reaction mixture instantly turned black with no evidence of product formation observed by NMR spectroscopy. The reaction was attempted at -78 °C for 8 h, however, upon warming to R.T. during the workup, the solution turned black and no product was formed. Reaction at -40 °C gave a similar result.

The hydrophosphination of perfluorohexylethylene (Scheme 2.6C) is the most atom economical route to the desired precursor, and as such, was the focus of the synthetic efforts to yield this product. The Ph_2PH starting material is commercially available but is costly, and thus was prepared according to a literature procedure[124] from the reduction of PPh_3 with metallic Li
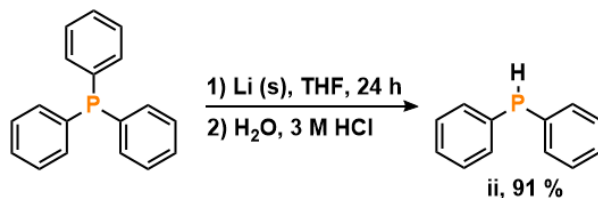
Scheme 2.7. Preparation of diphenylphosphine (ii). The reduction of triphenylphosphine in the presence of lithium metal under argon, followed by protonation by HCl yields **ii** (adapted from ref.[124]).

35

and subsequent protonation by 3 M HCl (Scheme 2.7). Vacuum distillation furnished the product **ii** in good yield (91 %).

The reaction of **ii** with alkenes to produce tertiary phosphines has been reported to proceed without the use of any solvent or initiator,[103] but the lack of miscibility between perfluorohexylethylene and diphenylphosphine **ii** precluded solvent-free conditions. AIBN was used as the radical initiator at low loading (4 mol %) and was sequentially added every 2 h for 8
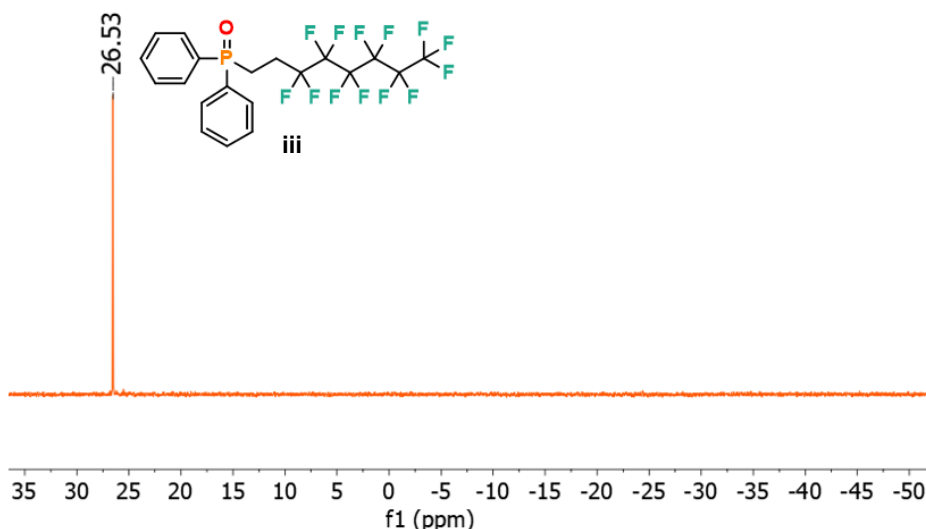
Figure 2.10. ^{31}P {^{1}H} NMR (C$_6$D$_6$) spectrum of the isolated product (iii) of the hydrophosphination reaction.

h. Stirring overnight with heating under an atmosphere of Ar (g) did not yield the desired product, instead proceeding to the oxidized, non-nucleophilic P(V) anti-Markovnikov addition product **iii** (Scheme 2.8). Susceptibility to oxidation in air has been observed for fluoroalkyl phosphines with (CH$_2$)$_x$ spacers,[125] and dominant oxidation products of hydrophosphination reactions have been observed for simple alkene systems, with the source of oxygen not identified.[103] The oxide **iii** was
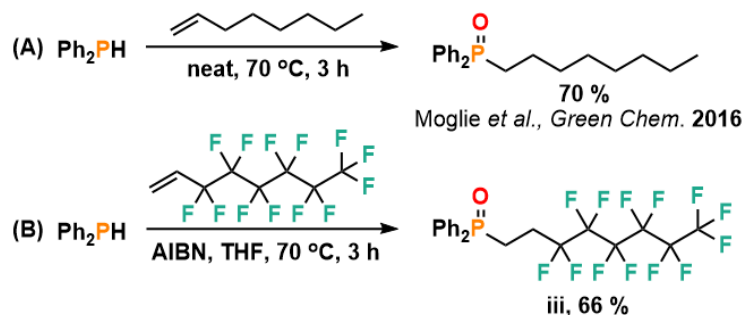
Scheme 2.8. Oxidation product of hydrophosphination. The product of the hydrophosphination of alkenes (A) 1-octene,[103] and (B) perfluorohexylethylene by **ii**.

isolated after sublimation (140 °C, 5 mmHg), and ^{31}P {^{1}H} NMR (C_6D_6) analysis revealed a new

peak at $\delta = 26.5$ ppm (Figure 2.10). Despite several attempts, the P(III) species **iv** was not obtained

from this reaction, with oxidation occurring each time. The oxidation likely occurs after the P-H

addition to the alkene takes place, as formation of the anti-Markovnikov phosphine product is

observed, while the $Ph_2P(O)H$ peak ($\delta = 18.0$ ppm) is much less prominent in ^{31}P {^{1}H} NMR

spectra of the crude mixture.

Reduction of **iii** could be achieved by reflux with a large excess (11.6 eq) of trichlorosilane

($HSiCl_3$) in toluene (Scheme 2.9). This reaction yielded the desired air sensitive product **iv** in

moderate yield (70 %) after a basic workup to neutralize the excess $HSiCl_3$, and purification by

sublimation (60 °C, 5 mmHg). ^{31}P {^{1}H} NMR (C_6D_6) analysis confirmed the formation of a new
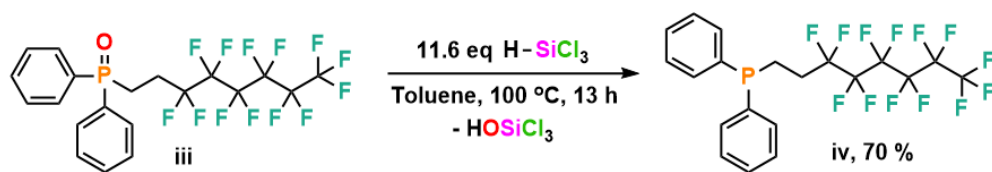
Scheme 2.9. Reduction of oxidized phosphine species iii. The reduction of **iii** with excess $HSiCl_3$ to yield **iv.**
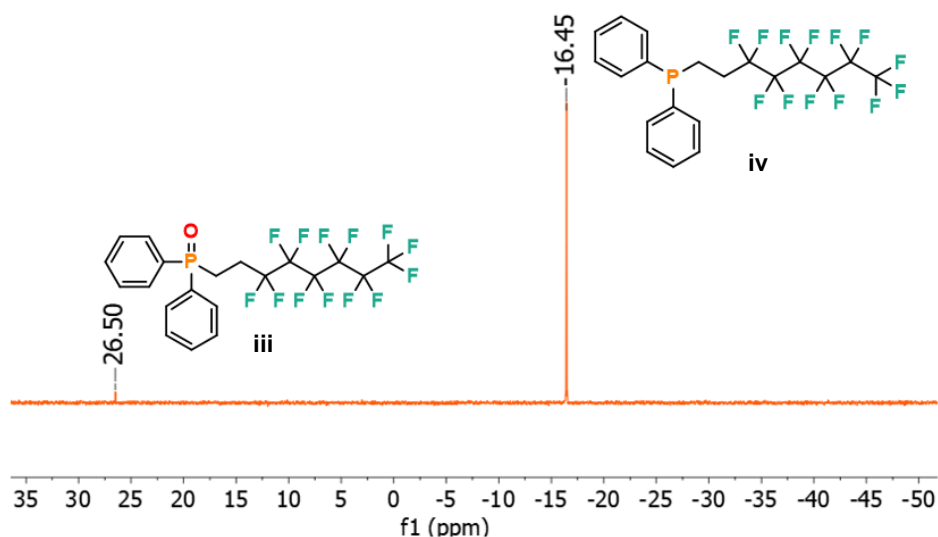
Figure 2.11. $^{31}P\{^{1}H\}$ NMR (C_6D_6) spectrum of iv.

phosphorus environment, with a signal at $\delta = -16.5$ ppm dominating the spectrum (Figure 2.11). A generalized mechanism for this reduction has been proposed from density functional theory (DFT) analysis.[126] In the proposed mechanism (Figure 2.12), the silane coordinates to the oxide, and a four-membered ring transition state is formed as the hydride coordinates to the electron poor
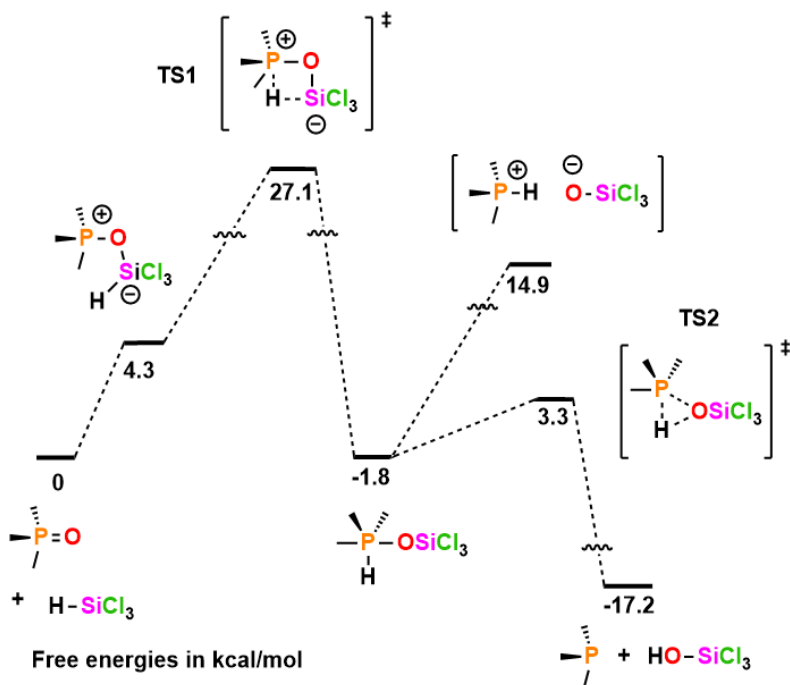
Figure 2.12. Proposed mechanism for the reduction of phosphine oxides to P(III) species by HSiCl₃. The mechanism was proposed from DFT after calculating the lowest energy (local minima) transition states for the reactants.[126]

38

phosphonium. The formation of this ring is the rate determining step in the reaction (27.1 kcal mol^{-1}), and the formation of a phosphorane intermediate where the oxygen is apical and the hydride equatorial is an energetically downhill process.[126] The extrusion of the phosphine is proposed to occur through a three membered ring transition state with a low activation barrier (3.3 kcal mol^{-1}), producing both the target phosphine and a trichlorosilanol byproduct.[126]

2.1.3.2 Preparation of ((dimethyl(perfluorohexylethyl)silyl)o-tolyl)diphenylphosphine (vii)

Scheme 2.10. Synthetic route to ((dimethyl(perfluorohexylethyl)silyl)o-tolyl)diphenyl-phosphine (vii). (A) The alkylation of Ph₂PCl by a prepared Grignard reagent, and subsequent lateral lithiation, (B) the hydrosilylation of perfluorohexylethylene in the presence of Wilkinson's catalyst, (C) and reaction of each synthon at 0 °C to yield **vii**.

The tertiary phosphine ((dimethyl(perfluorohexylethyl)silyl)o-tolyl)diphenylphosphine (**vii**) was prepared by the reaction of two synthons, (2-(diphenylphosphine)benzyl)lithium, and chlorodimethyl(ethyl(perfluorohexylethyl))silane (**vi**). Diphenyl(o-tolyl)phosphine (**v**) was synthesized according to an adapted literature procedure *via* alkylation of Ph₂PCl by a prepared Grignard reagent,[127] and hydrosilylation of perfluorohexylethylene in the presence of Wilkinson's catalyst furnished **vi** in good yield (Scheme 2.10A,B).[128] The precursor was prepared *via* lateral lithiation of **v** with *n*-butyllithium (*n*-BuLi) in the presence of TMEDA, and subsequent

39

Figure 2.13. ^{31}P {^{1}H} **NMR (C$_6$D$_6$) signals from a ((dimethyl(perfluorohexylethyl)silyl)o-tolyl)diphenylphosphine reaction mixture.** ^{31}P {^{1}H} NMR analysis was performed on (A) the reaction of lithiated **v** and **vi** after workup, (B) the starting material **v**, and (C) the desired product **vii** after sublimation. Diphenyl(*o*-tolyl)phosphine sublimed out as white crystals.

addition of the **vi** at 0 °C (Scheme 2.10C). ^{31}P {^{1}H} NMR (C$_6$D$_6$) analysis of the resulting product

after an aqueous workup showed two unique phosphorus environments at δ = -13.25 ppm and -

13.38 ppm (Figure 2.13A) with the downfield signal at δ = -13.25 ppm corresponding to the shift

for starting material **v** in C$_6$D$_6$ (Figure 2.13B), suggesting the lithiation was not efficient at the *o*-

methyl position. Despite several attempts, the reaction did not fully proceed to the desired silyl

phosphine. However, separation of the reaction mixture was achieved by sublimation under

reduced pressure (Figure 2.13C) (120 °C, 5 mmHg) affording the product **vii** as an orange oil in a

50 % yield. The purity was confirmed by HRMS (Figure B 7).

2.1.4   Synthesis of Quaternary Phosphonium Antimicrobials with Fluoroalkyl Substituents

2.1.4.1   Synthesis of (4-propoxybenzophenone)diphenyl(perfluorohexyl)ethyl)phosphonium bromide (4)
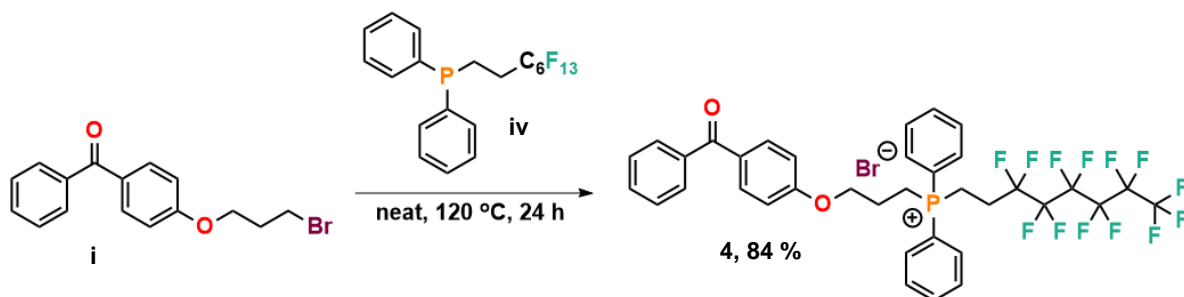
Scheme 2.11. Synthetic route to 4.

The synthesis of phosphonium **4** followed the quaternization protocol used for **3**, with the prepared starting material **iv** stirred with the anchor group **i** at 120 °C for 24 h. After cooling to R.T., the solidified product was dissolved in MeCN, and subsequent trituration from cold Et$_2$O gave **4** in an 84% yield (Scheme 2.11).

The loss of electron density about the phosphorus upon alkylation was reflected in the ^{31}P {^{1}H} NMR (CDCl$_3$) spectrum by a downfield shift to δ = 29.8 ppm (Figure 2.14) from the signal
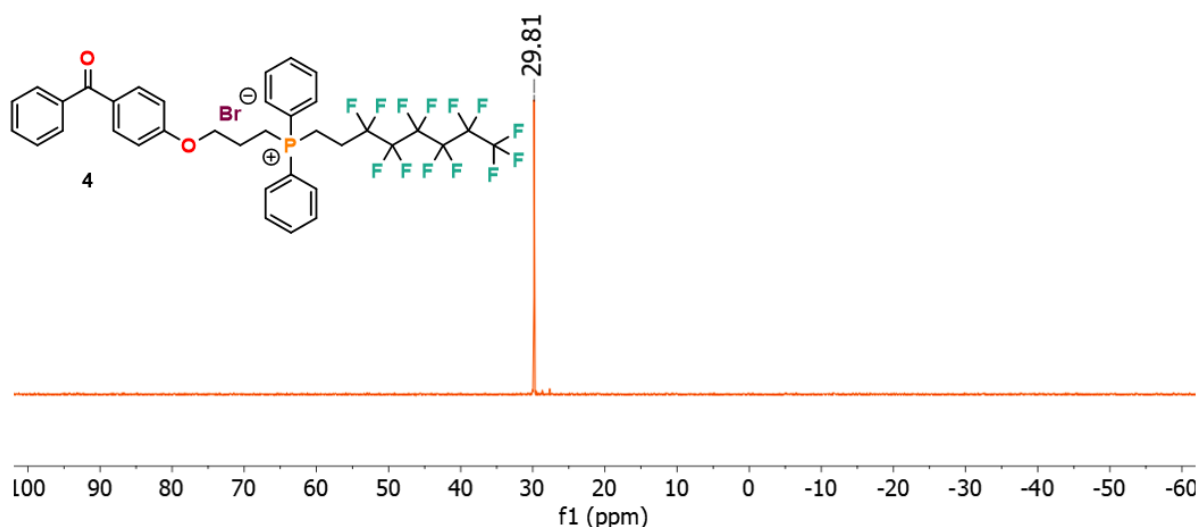
Figure 2.14. ^{31}P {^{1}H} NMR (CDCl$_3$) spectrum of 4.

at δ = -16.5 ppm for the phosphine starting material **iv**. No amount of PO species **iii**, which produces a signal in the spectrum at δ = 26.5 ppm, was detected. ^{1}H NMR analysis (CDCl$_3$) of the product (Figure 2.15) showed an upfield shift for ^{1}H environment H12 to δ = 3.95 ppm from δ = 3.62 ppm for the starting material **i**, further confirming formation of the product.
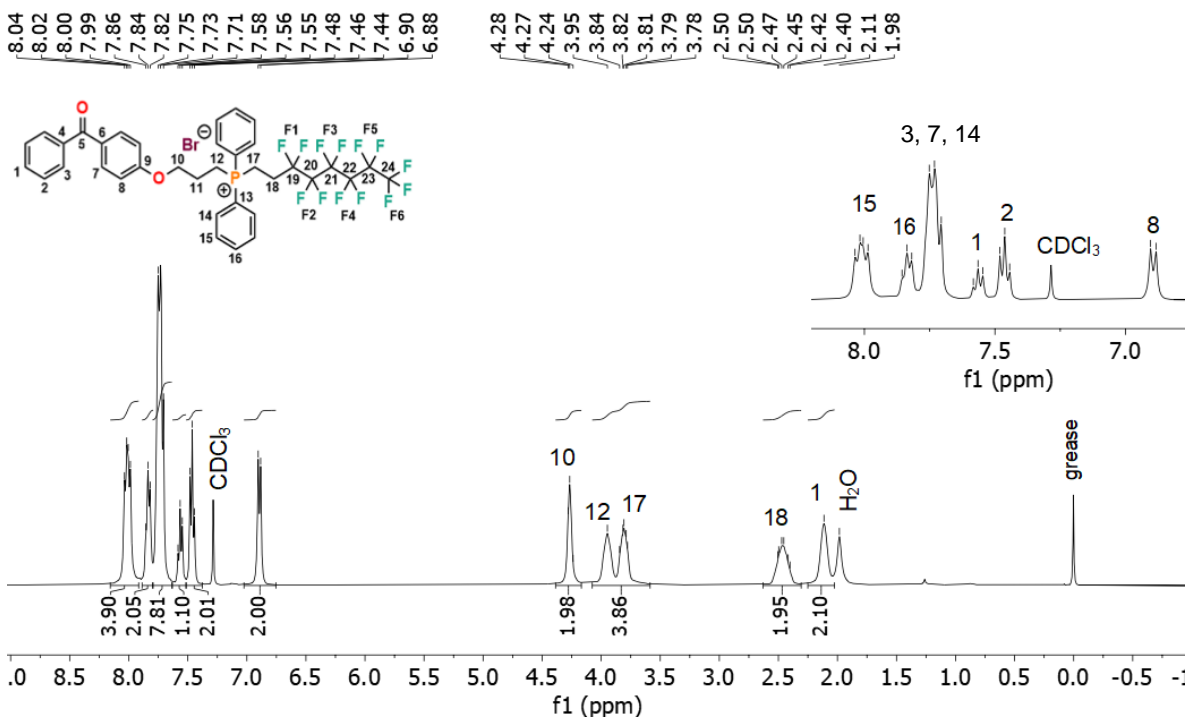
Figure 2.15. ^{1}H NMR (CDCl$_3$) spectrum of 4.

2.1.5 Synthesis of (3-(4-benzoylphenoxy)propyl)(2-((dimethyl(perfluorohexyl)ethyl)silyl)methyl)phenyl)diphenylphosphonium bromide (5)
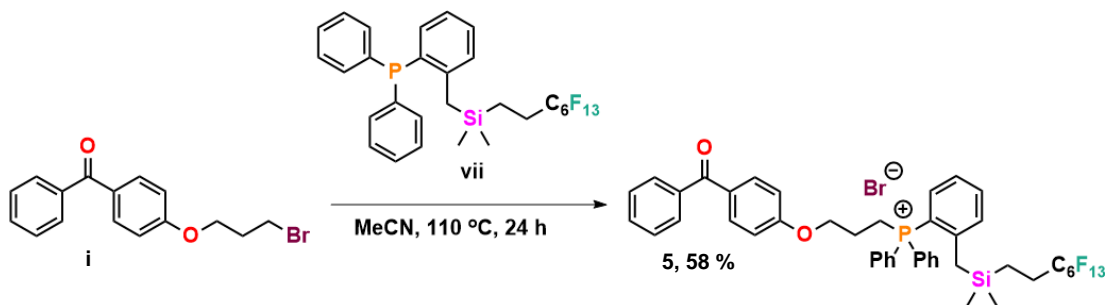
Scheme 2.12. Synthetic route to 5.

The synthesis of **5** followed the quaternization procedure used for phosphoniums **1** and **2**. The tertiary phosphine **vii** was dissolved in dry MeCN and added to a stirring solution of **i** under Ar (g), and refluxed for 24 h. After cooling to R.T., the product was triturated from cold Et$_2$O to furnish the product as a sticky off-white solid in a 58 % yield (Scheme 2.12). The lower yield (relative to **4**) is potentially due to the added bulk of the perfluoroalkyl silane coupled to the *o*-tolyl group of the phosphine starting material, which may hinder the rate of formation. ^{31}P {^{1}H} NMR (CDCl$_3$) analysis of the material (Figure 2.16) showed a new ^{31}P environment at δ = 24.5 ppm; a signal at -13.8 ppm was indicative of the starting material **v** in CDCl$_3$, shifted upfield relative to that same resonance in C$_6$D$_6$ (δ = -13.3 ppm, Figure 2.13B). The presence of some starting material after washing with cold Et$_2$O suggests incomplete reaction of **vii**. Another signal,
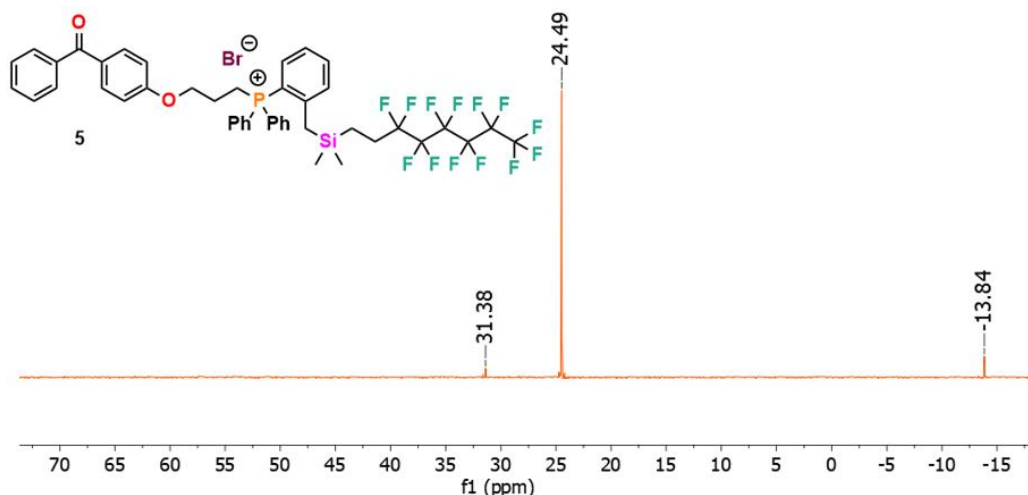
Figure 2.16. ^{31}P {^{1}H} NMR (CDCl$_3$) spectrum of 5.

at δ = 31.4 ppm, was attributed to oxidized starting material **vii**. A signal in this region was observed in the ^{31}P {^{1}H} NMR (C$_6$D$_6$) spectrum for **vii** (Figure A 42). Qualitative observation has suggested that the starting material oxidizes slowly in the presence of air, and the elevated temperature used for the reaction may be allowing small amounts of oxygen present in the mixture to consume the starting material. ^{1}H NMR (CDCl$_3$) analysis of the material showed that while new
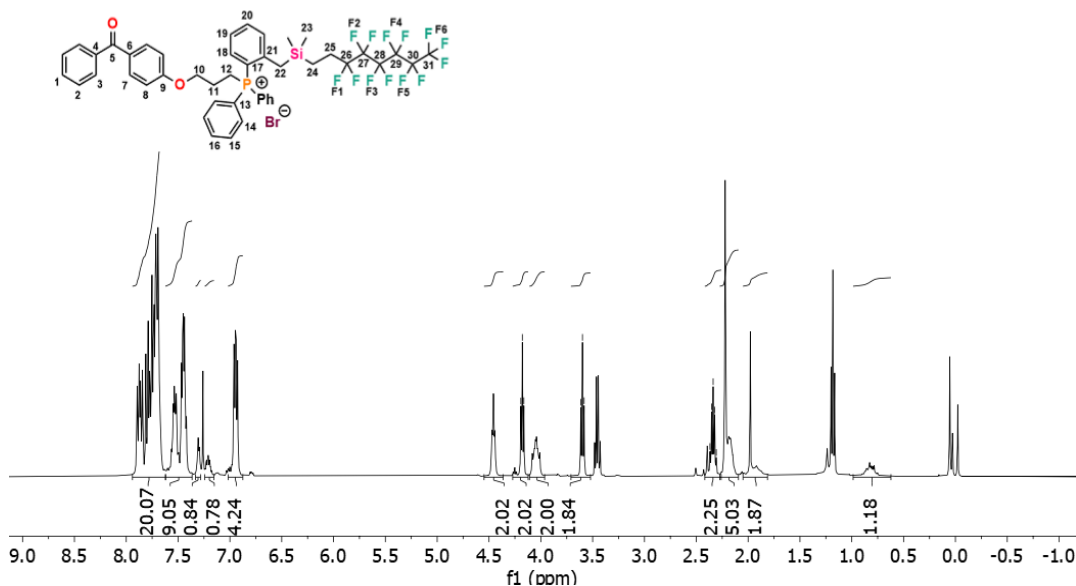
Figure 2.17. ^{1}H NMR (CDCl$_3$) spectrum of **5**. Peak labels are omitted for clarity.
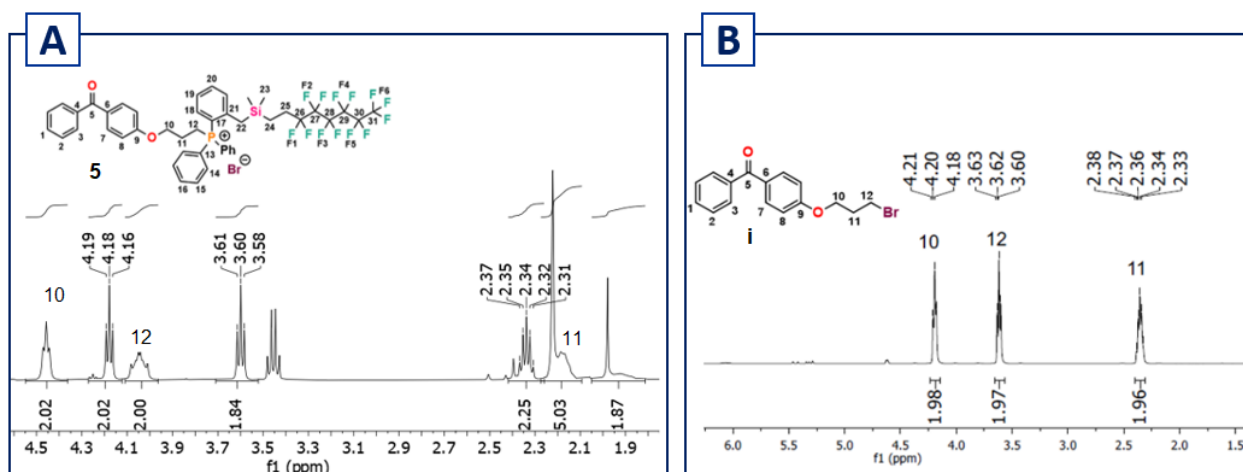
Figure 2.18. ^{1}H NMR (CDCl$_3$) **spectral windows for 5 and i.** (A) The so-called alkyl region of **5**, and (B) the alkyl region for **i**.

^{1}H environments were present, the total integration gave 54 protons, 9 protons more than expected for the material (Figure 2.17). Signals from the Et$_2$O solvent used for washing were also evident in the spectrum. In addition, resonances at $\delta = 4.18$, 3.60, and 2.34 ppm were attributed to starting material **i** (Figure 2.18B). In the ^{1}H NMR (CDCl$_3$) spectrum for **5**, the relative peak intensity for the signals corresponding to **i** and the signals labelled H10, H11, and H12 are 1:1 (Figure 2.18A), suggesting a roughly 1:1 mixture of the starting material **i** and the product **5** in the sample. This

44

supports the hypothesis that **vii** is less reactive in comparison to **iv**. Longer reaction times and neat conditions may be necessary to yield the desired product in larger quantities.

2.2 UV-Initiated Grafting of Phosphoniums to Plastic Substrates

2.2.1 Detection of Available Phosphonium Charge on Coated Plastic Substrates

The incorporation of the UV-active benzophenone functionality allows for this class of phosphoniums to be applied both as UV-immobilized surface-active additives, and as non-leaching, tethered coatings. Immobilized phosphonium-containing coatings on polymer plastic substrates were prepared by dissolving phosphoniums **1**, **2**, **3**, or **4** at 1% (w/v) in a solution of 95% EtOH. The solutions were spray coated onto plastic and cured using UVA (~360 nm) light with a measured dosage strength of 0.16 W/cm^2 for 1 min. These parameters were established after spray coating triphenyl phosphonium **3** on polystyrene (PS) plastic coupons using UV light to cure the coating to the surface. Dosage strength was controlled by cure time. A light blue coloration at
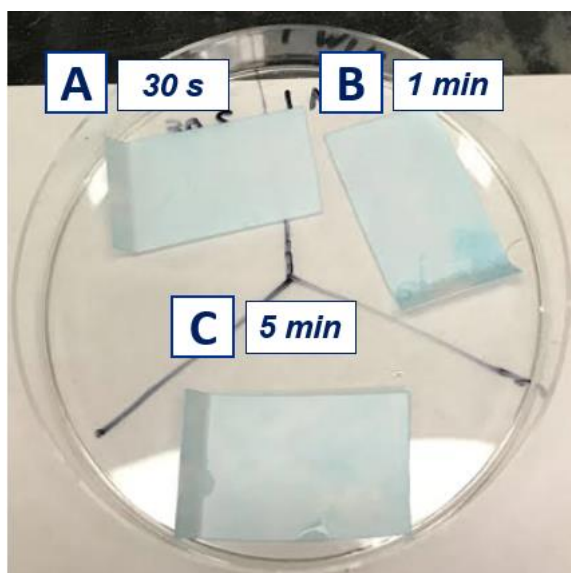
Figure 2.19. Optimizing curing conditions. Pieces were cured for (A) 30 s (5.85 J cm^{-2}), (B) 1 min (10.53 J cm^{-2}), and (C) 5 min (30.44 J cm^{-2}). Coating quality was visualized by staining with BPB.

the plastic surface after rinsing off unbound BPB was indicative of covalently tethered phosphonium, as the anionic dye can undergo counterion exchange with the phosphonium salt to form a blue complex. After two spray coating and curing cycles, coatings comprised of **3** were exhaustively washed with water and submerged in a 40 ppm BPB solution for 10 min. The pieces were removed and rinsed with water, and stain results were analyzed qualitatively (Figure 2.19). Cure times of 30 s, 1 min, and 5 min were tested, corresponding to dosage strengths of 5.85 J cm^{-2}, 10.53 J cm^{-2}, and 30.44 J cm^{-2} respectively. Coatings of **3** cured for 1 and 5 min had similar results in terms of coloration by the BPB stain. This suggests that after 1 min, *ca.* 10 J cm^{-2} was suitable to activate all available benzophenone moieties, as 5 mins of cure time resulted in a three-fold increase in dosage (*ca.* 30 J cm^{-2}) but no noticeable difference in curing quality. Thus, 1 min cure times were used throughout this work.

To quantify the amount of phosphonium present in the coating, charge density measurements were performed on the coated PS substrates.[17,65,110] Pieces with 4 cm^2 of coated surface were submerged in 1% (w/v) aqueous fluorescein solutions. As is the case for the BPB stain test, it is assumed that the relation of dye molecules to phosphonium molecules is 1:1, and that the dye molecules undergo counterion exchange and form complexes at the surface with available phosphoniums. After being submerged overnight in the solution, the coated pieces were rinsed with water until the rinse solution was clear, and then sonicated for 20 min in 9 mL of CTAB and 1 mL of 0.1 M PBS to liberate bound fluorescein into solution. UV-Vis was performed on the solutions at $\lambda = 501$ nm to quantify the number of fluorescein molecules in solution, and thus the number of phosphonium charges available on the coated substrate. Surface charge density results (Table 2.1) were calculated using the Beer-Lambert law with a path length of 1 cm and an extinction coefficient (ε_{501}) of 77 000 M^{-1} cm^{-1} (Equation 1,2).

$$(1) \quad C_{Fluorescein}(mol \ L^{-1}) = A_{501} \ / \ \varepsilon_{501} \ (M^{-1} \ cm^{-1}) \times L \ (cm)$$

$$(2) \quad [P^+] = \frac{C_{Fluorescein} \ (mol \ L^{-1}) \times V \ (L) \times N}{A \ (cm^2)}$$

Table 2.1. Charge density and θ_C measurements for UV-cured phosphonium coatings

Material	Surface charge density^a ([P$^+$] cm^{-2})	$\theta_C{}^a$ (deg)
PS control	N/A	92.2 ± 1.0
PS coated with **1**	$(1.60 \pm 0.03) \times 10^{15}$	71.9 ± 5.1
PS coated with **2**	$(3.89 \pm 0.5) \times 10^{15}$	36.4 ± 11.0
PS coated with **3**	$(2.90 \pm 0.2) \times 10^{15}$	63.5 ± 5.8
PS coated with **4**	$(2.95 \pm 0.05) \times 10^{15}$	68.0 ± 2.0

^{a}*Surface charge and θ_C measurements for each sample were performed in triplicate.*

Analysis of the surface charge results indicated each of the phosphonium-based coatings on the PS substrate had a measured surface charge density on the order of 10^{15} [P$^+$] cm^{-2}, within the same magnitude of charge densities measured for analogous small molecule ammonium-based coatings.[110,122] Charge measurements for coatings comprising **2** and **3** were within the charge density threshold (3.89×10^{15} and 2.90×10^{15} [P$^+$] cm^{-2}, respectively) proposed by both Murata and Kugler as necessary for antimicrobial efficacy against biofilm forming bacteria.[110,129] Interestingly, despite deploying identical coating and curing conditions to other phosphonium small molecules, the surface charge measurement for PMe$_3$ analogue **1** was 1.60×10^{15} [P$^+$] cm^{-2}, outside of the established range. PS coated with **4** possessed significant surface charge density (2.95×10^{15} [P$^+$] cm^{-2}), indicating phosphonium charges were still accessible despite the incorporation of a large fluoroalkyl group. Advancing water contact angle (θ_c) measurements were performed on the coated pieces to further probe the relationship between the structure of the phosphonium small molecules coated on the substrate and their macroscopic properties as coatings (Table 2.1).

Contact angle measurements for each treated surface trend with charge density results (Table 2.1). The relatively low density of accessible charge and high θ_C of **1** is surprising, as networks formed upon UV-curing the PMe$_3$ derivative **1** could be expected to exhibit similar or higher hydrophilicity than networks with *n*-butyl (**2**) and phenyl (**3**) structures that have larger hydrophobic cross sections, as has been observed in similar systems. It is proposed that the methyl
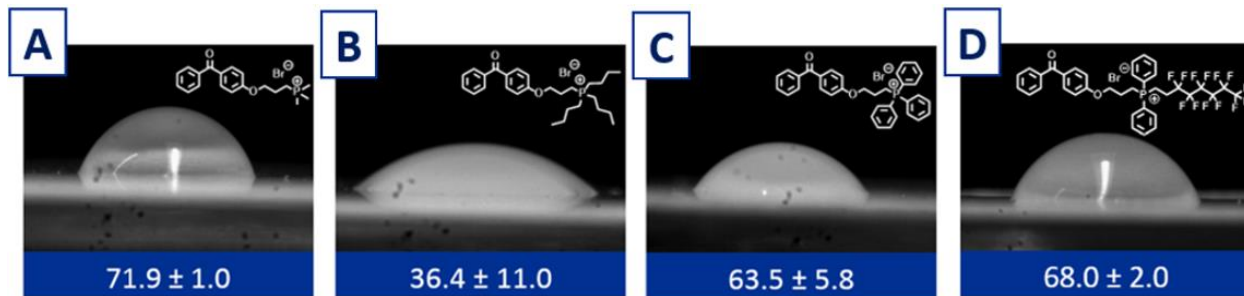
Figure 2.20. Water contact angle images for coated PS plastics. θ_C images for PS plastics coated and with UV cured coatings of (A) **1**, (B) **2**, (C) **3**, and (D) **4**.

groups decorating the phosphonium small molecule may limit the grafting capabilities and thus the charge density of surfaces. It follows that alkyl substituent length is a necessity not just for the increased hydrophobicity imparted by the chains, but also for the availability of sites for hydrogen abstraction and thus supramolecular network growth by the UV-grafting antimicrobial molecule. More dramatic decreases in θ_C were observed for PS coated with **2** and **3**, in correlation with their higher surface charge densities, exhibiting θ_C of $36.4 \pm 11.0°$ and $63.5 \pm 5.8°$ respectively. Coatings of fluoroalkyl-containing phosphonium **4** had slightly increased hydrophobicity relative to known phosphonium and ammonium coatings,[65,110] however, the coating maintained a hydrophilic contact angle ($\theta_C = 68.0 \pm 2.0°$). The incorporation of a fluoroalkyl group about the charged phosphonium did not significantly alter the hydrophilicity of the coating, a property thought to be a factor in mechanism of kill for antimicrobial coatings.[130,131] With respect to one another, nonpolar *n*-butyl (**2**) and phenyl (**3**) substituents can be expected to have similar effects on coating hydrophilicity. Thus, the increased hydrophilicity imparted by coatings of **2** may be a consequence of a higher

degree of surface roughness formed by these coatings, as roughness is known to increase the wettability of surfaces if they are fabricated with hydrophilic materials.[132–134]

2.2.2   Determination of Coating Microstructure

The effect on surface topography of the observed properties of the phosphonium coatings was examined using atomic force microscopy (AFM) (Figure 2.21). Polycarbonate (PC) plastic was used as a model substrate due to the material's relative smoothness when compared to the PS samples available, allowing for greater clarity in accessing the coating properties.
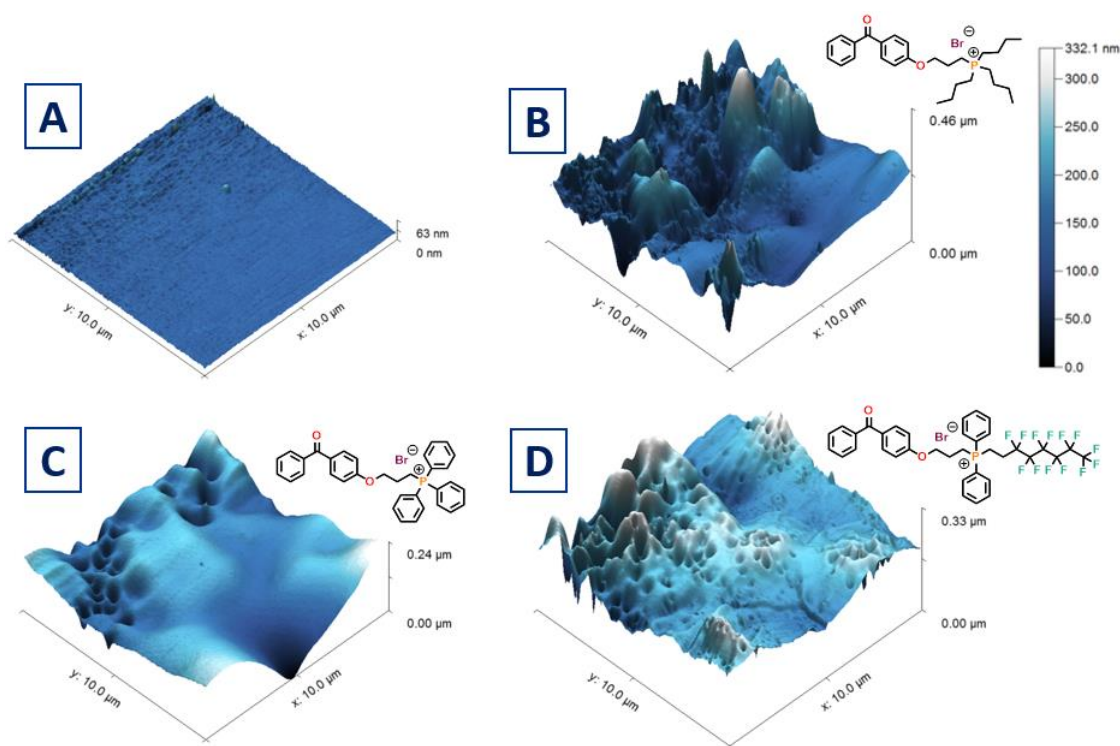
Figure 2.21. AFM images of phosphonium coatings. A) Untreated PC plastic; B) PC coated with **2**; C) PC treated with **3**, and D) PC treated with **4**.

Table 2.2. Thickness and roughness of phosphonium-containing coatings on PC.

Material	Thickness (nm)[a]	RMS roughness (nm)
PC control	N/A	2.58
PC coated with **2**	47.45 ± 11.34	55.5
PC coated with **3**	94.64 ± 38.38	32.1
PC coated with **4**	105.8 ± 13.52	35.5

[a]Thickness measurements were taken at three points along the separation line of the half-coated sample.

Previous studies have shown that the antimicrobial activity of UV-curable benzophenone-anchored coatings is independent of the plastic substrate.[17] Coating height and roughness data is tabulated in Table 2.2. Plastic substrates coated with **2** had an average coating thickness of 47.45 nm (± 11.34 nm) with a root mean square (RMS) roughness value of 55.50 nm, a 42% increase over the roughness value measured for UV-cured spray coatings of **3**. Despite identical spray coating parameters, substrates coated with **3** had nearly double the average thickness (94.64 ± 38.38 nm) compared to **2**, suggesting the morphology of the coating is highly dependent on the phosphonium "tail" groups. Increased roughness may also be linked to the higher surface charge measurements observed for coatings of **2**; surface area accessible to the AFM instrument can be thought of analogous to surface area accessible to the fluorescein dye, as both tests probe the surface at the molecular level. The thicker, but smoother, coatings of **3** may have fewer phosphonium molecules accessible to the fluorescein dye due to lower roughness.

Surfaces coated with **4** had an average thickness (105. 83 ± 13.52 nm) and roughness value similar (35.45 nm) to **3**. Interestingly, both coatings possessed pore-like microstructures (Figure 2.21C, D) with the indentations ranging in size between 290 and 180 nm in diameter and depths between 80 and 44 nm. This is a unique observation in the literature for small molecule-based coatings. The similarities between the two coatings indicate that the introduction of the fluoroalkyl

moiety about phosphonium **4** does not yield significant differences in coating thickness and roughness, and suggests that the phenyl substituents are dominant in governing these properties for the UV-cured coatings prepared. The roughness values align with the observed differences in θ_C, with the rougher surface of **2** also displaying a lower contact angle compared to the relatively smoother surfaces comprising coatings of **3** and **4**.

2.3   Antimicrobial Efficacy of UV-Cured Phosphonium Coatings

To establish the antimicrobial efficacy of the novel small molecule phosphonium-based coatings, treated plastic pieces were subjected to the large drop inoculum (LDI) test method previously reported by Ronan *et al*.[135] This method has been shown to be critical for determining how antimicrobial coatings function in simulated solid-air interface environments that more closely resemble the real-world phenomenon of desiccation, to which biofilm-forming bacteria are commonly subjected.[17,122,135] A large droplet with a known quantity of viable bacterial cells was deposited on the test surfaces, allowing for desiccation of the cells on the test surface, providing biofilm-forming conditions at the solid/air interface.[136] To guarantee all inoculated cells enter into contact with the test surface, the samples with the droplet are subjected to a standardized 3 or 24 h drying period. The cells are then recovered, serially diluted, plated out onto tryptic soy agar, and enumerated to assess the extent of cell survival and thus antimicrobial efficacy of the test surfaces. *Arthrobacter* sp. (IAI-3) and *E. coli* (ATCC strain 11229) were chosen as representative Gram-positive and Gram-negative bacterial strains. *Arthrobacter* sp. was used as a representative member of the indoor airborne flora continuously deposited on surfaces; they have been shown to

be vital for the survival and proliferation of multi-bacterial biofilms as a result of their high tolerance for dessication.[135,136]
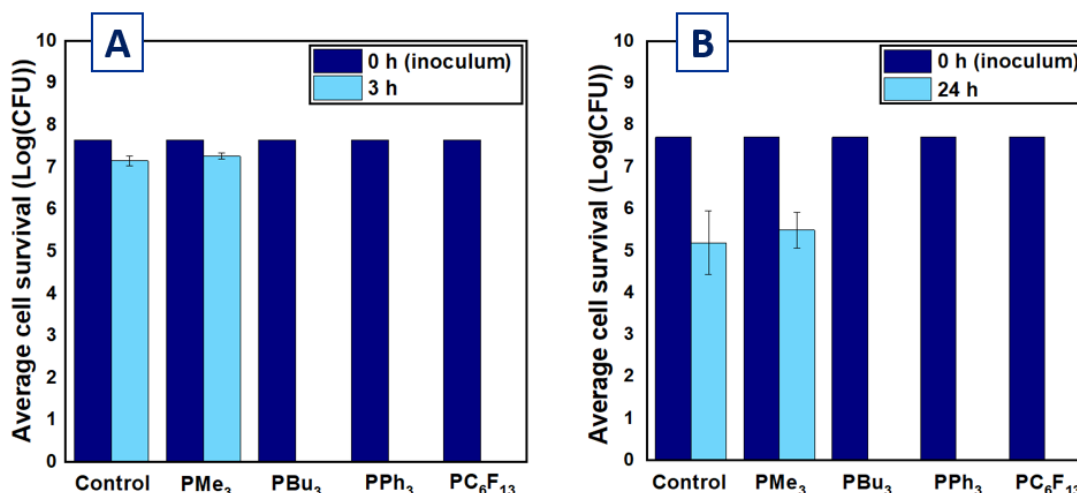
Figure 2.22. Average cell survivability of: A) *Arthrobacter sp.* (IAI-3) and B) *E. coli* (ATCC strain 11229) against (from left) uncoated PS, (PMe$_3$) **1**, (P(*n*-Bu)$_3$) **2**, (PPh$_3$) **3**, and (PC$_6$F$_{13}$) **4**. All testing was performed in triplicate. The measurement at 0 h was the initial bacterial load placed on the sample.

Polystyrene plastic coated with **1** exhibited no antimicrobial activity against Gram-positive or Gram-negative bacteria. This result further supports evidence for a charge density threshold, as these coatings had lower quantity of accessible charge as well as a lower contact angle (Table 2.1). Coatings consisting of phosphoniums **2**, **3**, and **4** each exhibited full reductions of viable Gram-positive *Arthrobacter* sp. (Figure 2.22A) and Gram-negative *E. coli* cells (Figure 2.22B) and after 3 and 24 h contact with the surface, respectively. A 24 h time point was used for the *E. coli* species due to their intolerance to desiccation in the laminar flow hood, an apparatus used to prevent contamination from other microbial species. The inoculated plastics were kept covered, increasing drying times. Despite these efforts, cell survivability for *E. coli* on control surfaces was reduced when compared to the inoculum.

These coatings possess significant densities of charged phosphonium, and as such, efficacy against both bacterial cell membrane types is predicted by the phospholipid sponge theory, which

requires surface charge density to incite deterioration of the membrane.[63] From these results, no threshold for the roughness and thickness of these phosphonium coatings at which antimicrobial efficacy begins to diminish was established, with all coatings exhibiting full kill of both strains.

2.4 Co-Extrusion of Phosphonium-Containing Polypropylene
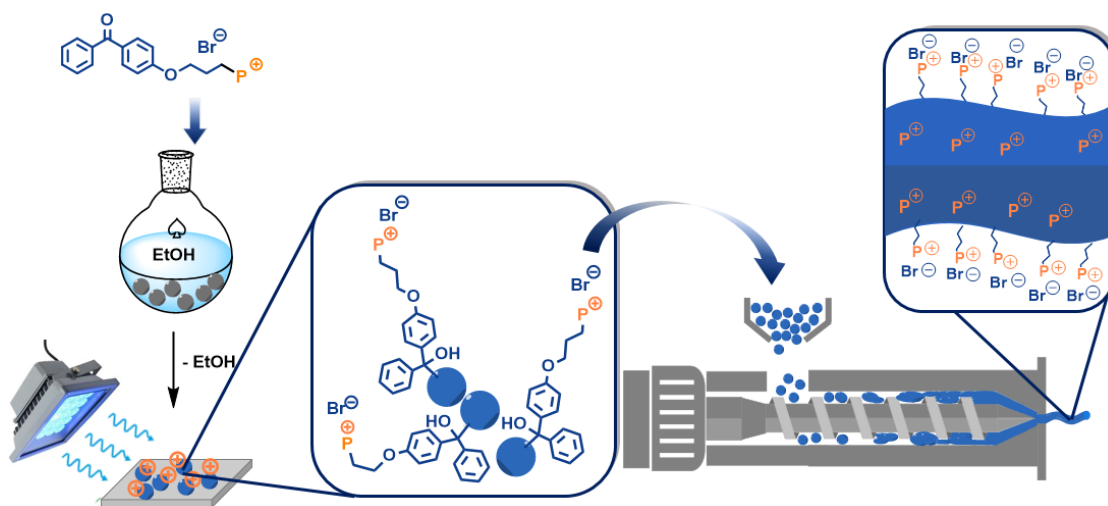
Figure 2.23. Co-extrusion of phosphonium-containing plastics. A schematic representation of the experimental concept for the co-extrusion of PP with phosphoniums **1**, **2**, **3**, and **4** to yield plastics with antimicrobial-enriched surfaces.

While standard antimicrobial coatings are susceptible to abrasion and deactivation by bacterial debris,[137] it was hypothesized that the incorporation of phosphoniums **2**, **3**, and **4** into the bulk polypropylene (PP) plastic would provide subsurface concentration of active antimicrobial tethered to the substrate, endowing the materials with antimicrobial longevity. Due to a lack of observed antimicrobial activity from LDI testing on **1**, further experiments using the molecule were not pursued. The antimicrobials were fabricated by co-extrusion of the phosphoniums with PP. Of interest was the relative ability of each phosphonium to self-concentrate at the solid-air interface, effectively forming a concentration gradient of the active antimicrobial at the surface (Figure 2.23).

Phosphoniums **2**, **3**, and **4** were dissolved at 1 % (w/w) in minimal EtOH, and PP beads were added to the solution. Rotary evaporation of the solvent gave an even coating of the phosphoniums on the plastic. Initial attempts to fabricate plastics with immobilized antimicrobials used a post-extrusion UV-cure step to covalently link the benzophenone-containing phosphonium to the plastic
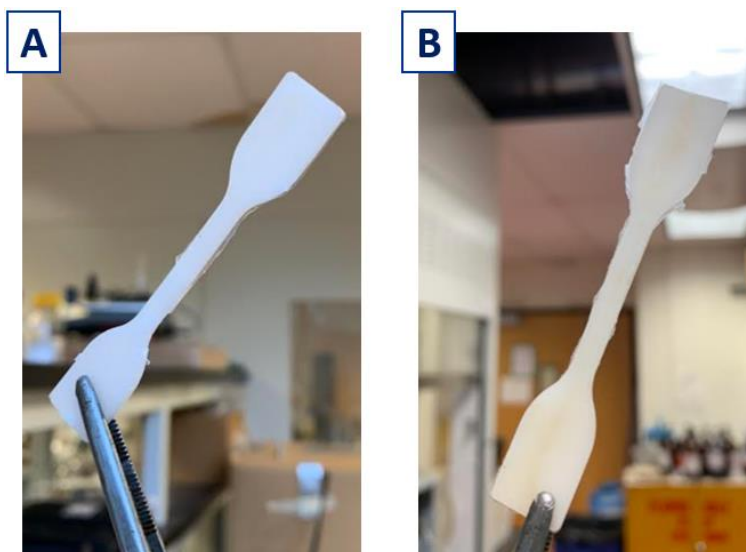
Figure 2.24. Molded polypropylene "dogbones." Two examples of molded PP pieces, containing (A) virgin polypropylene beads, (B) pre-UV cured PP with 1.5 (w/w) % **3** (**PP-3**). The off-white coloration is evident with **PP-3.**

polymer network. Despite this, when placed in an aqueous solution, a small concentration of phosphonium was visible in the solution by UV-leachate analysis. Thus, after the coating step, a pre-extrusion UV-cure process was introduced to ensure immobilization of the phosphoniums to the plastic bead surface. Extrusion of these pre-cured beads at 220 °C into a mold pre-heated to 100 °C yielded the tributylphosphonium-containing plastic **PP-2**, triphenylphosphonium-containing **PP-3,** and perfluoroalkylphosphonium-containing **PP-4** as off-white coloured "dogbone" pieces. (Figure 2.24) The discoloration was due to the amber or off-white coloring of the added phosphonium in the melt, and not due to UV or heat exposure.

2.4.1 Surface Properties of Polypropylene Co-Extruded with Phosphonium Antimicrobials

The effect of incorporating each phosphonium at 1% (w/w) was quantified by θ_C (Table 2.3). Relative to virgin molded PP pieces, pieces containing phosphoniums **2-4** exhibited more modest decreases in θ_C (Table 2.3), indicating that while present at the plastic-air interface, there was a lower density of accessible phosphonium charge at the extruded plastic surface in comparison to the UV-cured surface coatings, as the distribution of phosphonium small molecules were likely subsurface or in the bulk thermoplastic scaffold. A larger difference was observed in **PP-2** (Figure 2.25), consistent with the θ_C results for the UV-cured coatings on the PS substrates (Table 2.1). Fluoroalkyl phosphonium-containing **PP-4** had the most significant decrease in θ_C relative to the control, a strong indicator that the surfaces containing this phosphonium had a larger active concentration of positively charge P, thus lowering the contact angle.

Table 2.3. θ_C for injection molded PP dogbones.

Material[a]	$\theta_C{}^a$ (deg)
Molded PP control (**PP**)	96.7 ± 3.1
Molded PP co-extruded with **2** (**PP-2**)	82.4 ± 3.7
Molded PP co-extruded with **3** (**PP-3**)	90.7 ± 5.6
Molded PP co-extruded with **4** (**PP-4**)	78.8 ± 5.0

[a]Phosphonium compounds incorporated in non-control samples at 1 % (w/w). [b]θ_C measurements for each sample were performed in triplicate.
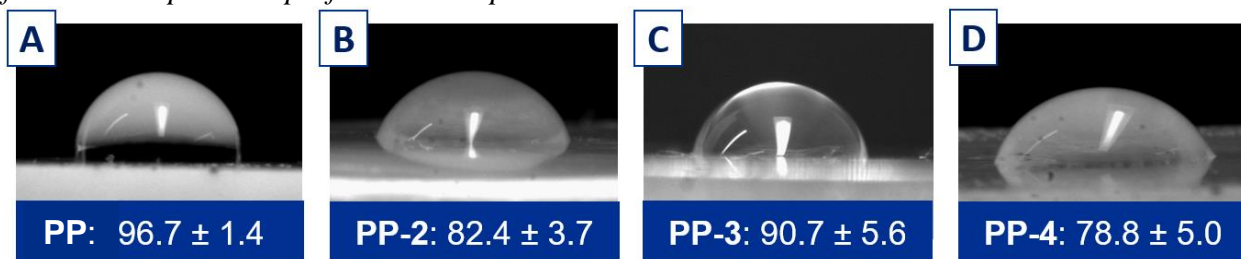
Figure 2.25. θ_C images for the molded phosphonium-containing PP pieces. (A) Control molded PP, (B) PP molded with **2**, (C) PP molded with **3**, and (D) PP molded with **4**. Values below the images are averages (in °) of triplicate measurements for that substrate.

AFM analysis was carried out on the molded plastics to examine whether incorporation of the phosphonium antimicrobial resulted in changes to the surface microstructure. A control molded sample (Figure 2.26A) and **PP-2** (Figure 2.26B) were selected for analysis to obtain representative structural data on the phosphonium containing plastics. The phosphonium-containing surface did not have significant structural differences on the micron scale, as both extruded surfaces had much

RMS roughness = 63.14 nm   **RMS roughness = 91.24 nm**
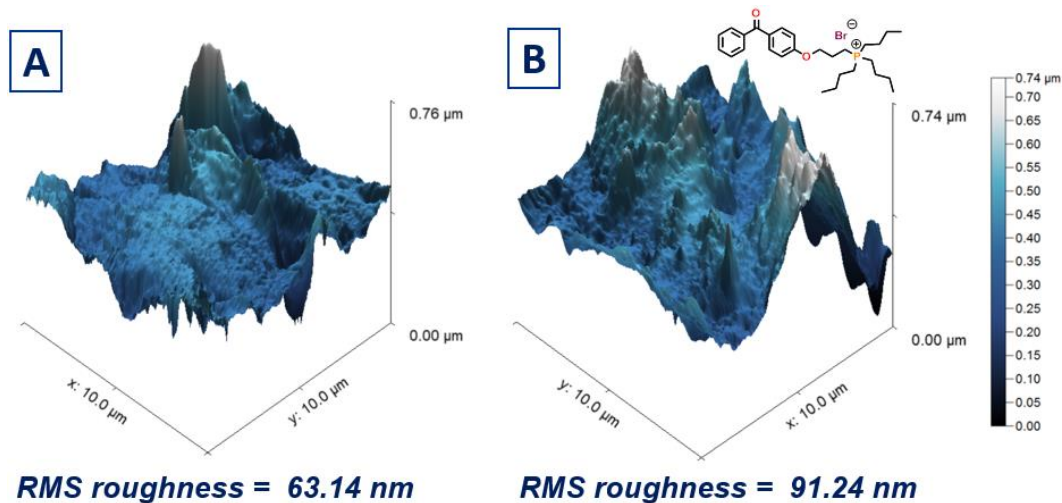
Figure 2.26. AFM images of molded PP pieces. (A) Virgin molded PP, and (B) **PP-2.**

larger peaks and valleys than the coated PC substrates (Figure 2.21). Roughness values were also much higher, while the **PP-2** plastic had a substantial increase in roughness (91.24 nm) relative to the control surface (63.24 nm). Due to the nature of the extrusion process and the removal of the piece from the stainless-steel mold, higher roughness values could be expected.

2.4.2 Evaluation of Phosphonium Content in Co-Extruded Polypropylene

A key aim of this work is to develop plastic materials with a concentration of active phosphonium antimicrobial in the bulk, so when abrasion occurs, a new antimicrobial surface will be generated, rather than deactivating existing ones. X-ray photoelectron spectroscopy (XPS) was employed to probe the phosphonium content at and below the surface of materials co-extruded with phosphoniums **2** and **4**, providing a representative depth profile of phosphonium content within the molded plastic. For **PP-2**, small slices (surface, 100 µm, 300 µm, and 500 µm) of the material were taken, and XPS measurements were carried out at each depth (Figure 2.27).
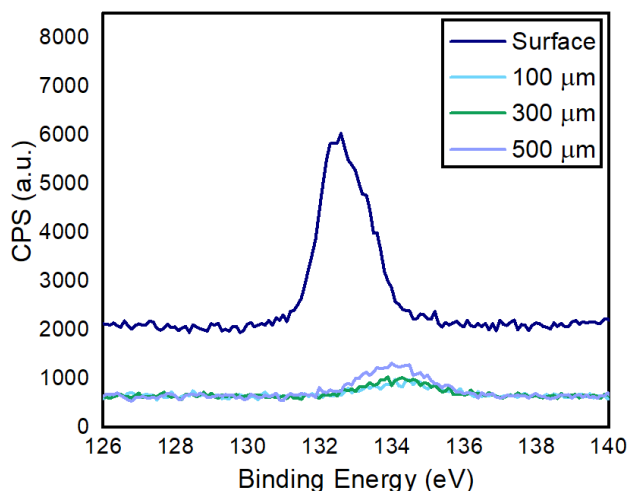
Figure 2.27. XPS analysis of PP-2. The spectrum highlights the P 2p peak corresponding to the phosphorus atom present in the phosphonium **2**.

At the plastic-air interface there was a prominent peak at a binding energy of 132.9 eV, corresponding to the P 2p peak found in similar cationic phosphonium systems.[138] Elemental analysis *via* XPS (Table 2.4) for **PP-2** showed 1.31 % P at the surface, corresponding closely with the ratio of P in the chemical composition of **2** (1.37 %), and indicating these co-extruded materials had significant accessible phosphonium charge. Of interest was the subsurface concentration of

Table 2.4. Elemental analysis of PP-2 by XPS at different depths.

Depth (µm)	0 (Surface)	100	300	500
Element	Atomic %			
C	81.43	99.02	98.69	97.87
O	12.55	0.82	1.03	1.70
P	**1.31**	**0.15**	**0.18**	**0.26**
Ca	0.73	0.00	0.00	0.00
N	0.60	0.00	0.09	0.16
Si	2.39	0.00	0.00	0.00
Br	0.99	0.00	0.00	0.00

phosphonium in the molded pieces, as an active layer of phosphonium tethered to the thermoplastic scaffold can allow access to long-term antimicrobial plastics. Elemental analysis of the characteristic P 2p signal was obtained from XPS measurements taken 100 µm from the surface of **PP-2**, and showed a dramatic decrease in phosphorus to 0.15 %. The low loading of phosphonium at this depth indicates tributylphosphonium **2** preferentially migrates to the plastic-air interface rather than remain in the bulk plastic. Further analysis at 300 µm and 500 µm showed similar phosphorus content (0.18 % and 0.26 %, respectively), thus with respect to depth, a consistent gradient was not observed for the material. Slices for the depth profile analysis were taken at different locations horizontally across the molded plastic piece (Figure 2.28), and the

observed differences in atomic P % across the sample between the 300 and 500 µm slices may be a result of non-uniformity in phosphorus content laterally across the sample.
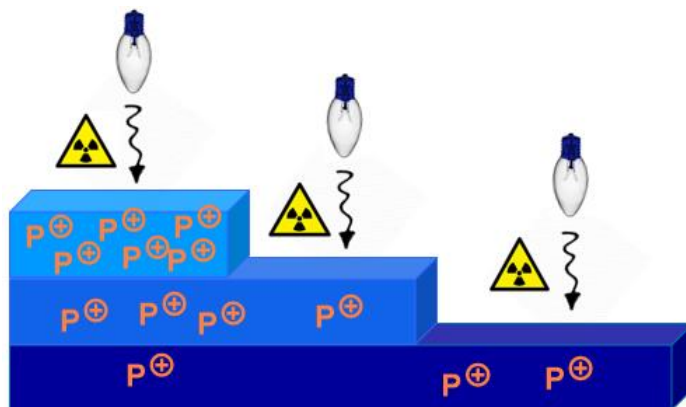
Figure 2.28. Schematic of XPS depth profiling experiment. Molded PP pieces were abraded with a microtome to create "steps" and XPS analysis was performed on each step height.

Due to the lack of an observed concentration gradient in **PP-2**, XPS analysis measurements for P % in **PP-4** were taken at shallower step heights (surface, 5 µm, 10 µm, 20 µm and 50 µm). A control sample was also prepared and analyzed. Peak analysis was done on the P 2p signal in each XPS spectrum (Figure 2.29). The peak intensity was sustained from the surface to the 5 µm step height, while at 10 µm there was a significant drop off. At 20 µm however, an increased response was observed; providing further evidence for non-uniformity across the sample.
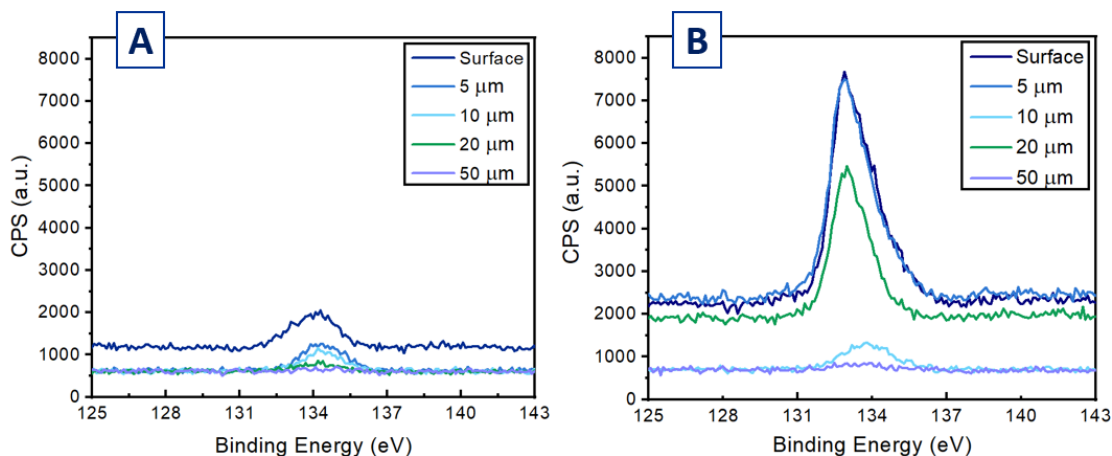
Figure 2.29. XPS peak analysis on molded plastics. Analysis was performed on (A) control extruded PP and (B) **PP-4**, at step heights of 0, 5, 10, 20, and 50 µm.

59

Table 2.5 Elemental analysis of PP-4 by XPS at different depths.

Depth (µm)	0 (Surface)	5	10	20	50
Element			Atomic %		
C	71.01	75.82	97.3	82.21	98.79
O	7.63	6.53	1.54	3.79	0.47
F	16.95	14.09	0.44	11.63	0.33
P	**2.01**	**1.83**	**0.32**	**1.16**	**0.12**
N	0.47	0.41	0.31	0.27	0.19
S	0.07	0.00	0.09	0.00	0.00
Si	0.71	0.32	0.05	0.18	0.07
Br	1.55	1.01	0.04	0.77	0.03

Elemental analysis performed on the XPS data (Table 2.5) showed significant P present at the surface (2.01%), a significant increase over the amounts present at the surface of **PP-2**, and a atomic % of P greater than than a single molecule of **4** (1.22%). This suggests the quantities of phosphonium **4** migrating to the surface is greater than one molecule per area unit surveyed in the XPS scan. A large quantity of F (16.95% atomic composition) at the surface was also indicative of surface migration of **4**. Crucially, the subsurface levels of P at 5 µm were also substantial (1.83 %), with a decrease of only 0.18 % compared to the surface. Phosphonium content was diminished greatly at 10 µm, but at 20 µm the atomic % of P was nearly equal to the ratio of P in the molecule, representing a quantity similar to that of a monolayer.[139,140]

2.5 Antimicrobial Efficacy of Polypropylene Co-Extruded with Phosphonium

A significant challenge to the plastics co-extruded with the phosphonium antimicrobials is having a sufficient concentration of the active phosphonium at the surface-air interface to

effectively kill bacteria. As mentioned above, XPS analysis of **PP-2** and **PP-4** showed the bound phosphoniums could self-segregate to the plastic-air interface. The LDI test method was performed for **PP-2**, **PP-3** and **PP-4** against *Arthrobacter* sp. and *E. coli* (ATCC 11229). After extrusion and exhaustive washing of the surface with distilled water, the molded pieces were subjected to the test, with one side of the piece consistently used throughout the test.
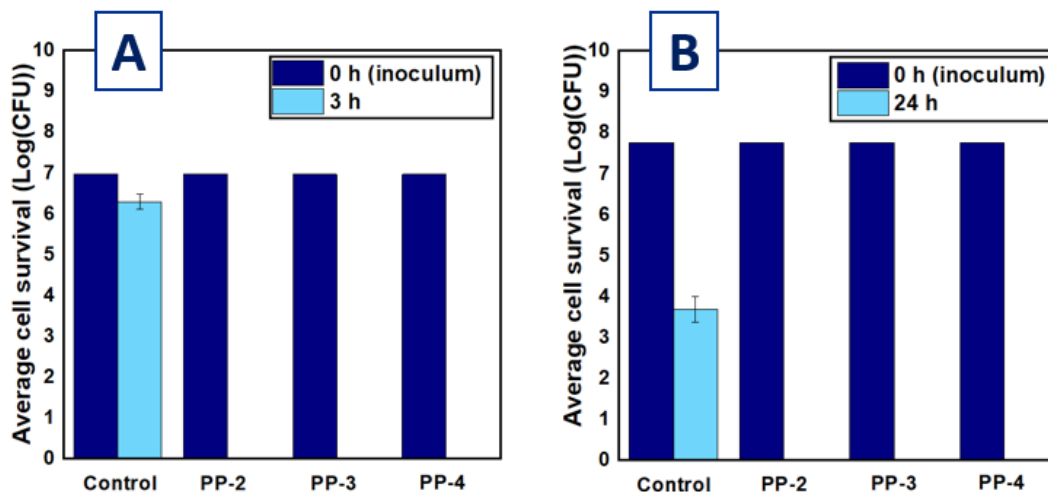
Figure 2.30. Antimicrobial efficacy of co-extruded plastics. The antimicrobial activity was measured for **PP-2**, **PP-3**, and **PP-4** against (A) *Arthrobacter sp.*, and (B) *E. coli* using the LDI test method.

Despite possessing higher contact angles relative to their UV-cured coating counterparts, all phosphonium-containing molded pieces exhibited full log reductions of Gram-positive *Arthrobacter* sp. (Figure 2.30A) and Gram-negative *E. coli* (Figure 2.30B) after 3 and 24 h, respectively. In this instance of **PP-2**, these results indicate a surface P content of 1.31 % (as measured by XPS, Table 2.5) is a high enough concentration of phosphonium to render that surface bactericidal. The *E. coli* subjected to control PP samples extruded without phosphonium did experience some die off after 24 h; this reduction is likely due to desiccation-related cell death, a phenomenon observed for *E. coli* used during the LDI protocol.[122] The antimicrobial activity of the co-extruded plastics also indicates that the phosphonium molecules did not decompose to yield

inactive molecular components at the high temperatures necessary for injection molding (180-220 °C).

2.6 Abrasion Resistance of Plastics Co-Extruded with Antimicrobial Phosphonium

The efficacy of these materials against the representative strains of Gram-negative and Gram-positive bacteria lead us to probe the antimicrobial capability of these materials after being subject to abrasive processes. The ability to withstand abrasion and retain antimicrobial efficacy is critical for any potential long-term antimicrobial material. Abrasion testing on antimicrobial coatings and materials has been limited,[141,142] and when applied, criteria for resistance to abrasion are varied. Locklin and coworkers reported high abrasion resistance for UV-cured benzophenone-containing antimicrobial coatings,[45] however their testing deviated from the internationally
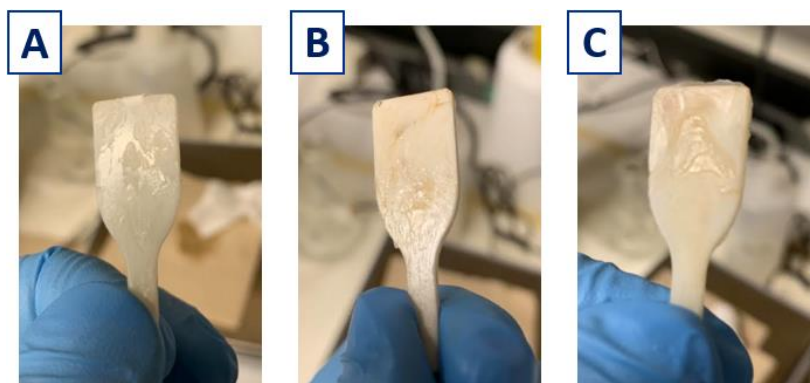
Figure 2.31. Abraded plastics. The abraded surfaces of (A) control PP, (B) **PP-2**, and (C) **PP-4** after 100 solvent double rubs.

recognized ASTM D5402 solvent double rub test,[143] and a surface demonstrating antimicrobial activity after 15 rubbing cycles were performed was deemed "highly" abrasion-resistant.[45] In addition, the post-abrasion evaluation of antimicrobial efficacy often rely on indirect measurements of antimicrobial potential such as surface charge, or anionic dye stain assays.[45]

In this work, ASTM D5402 solvent double rub test was used to assess the capability of co-extruded plastics to maintain antimicrobial activity after abrasion (Figure 2.31). Water was chosen

as the solvent due to its ubiquity in cleaning solutions. Of interest was whether the subsurface concentration of phosphonium observed in the XPS experiments could translate to bactericidal concentrations after abrasion. **PP-2** and **PP-4** were initially selected as candidates to compare the XPS results with the abrasion and antimicrobial efficacy testing. **PP-2** and **PP-4** fabricated with a 1 % (w/w) concentration of the active phosphonium were subjected to the LDI test under standard conditions (no abrasion). Only Gram-positive *Arthrobacter* sp. was initially tested.
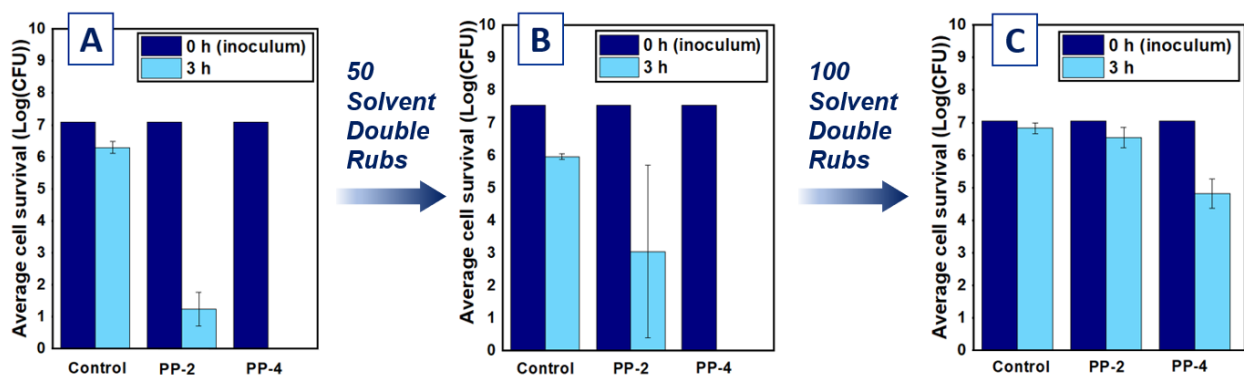
Figure 2.32. Antimicrobial efficacy of 1 % (w/w) PP-2 and PP-4 after abrasion. The LDI procedure was performed on the materials after (A) no abrasion (B) 50 cycles of the solvent double rub, and (C) 100 cycles of the solvent double rub.

When subjected to the LDI test without abrasion, **PP-2** reduced the number of viable cells by an average of log 4.67 CFU (Figure 2.32A). While a significant reduction, there was not complete kill of *Arthrobacter* sp., potentially due to suboptimal loading of phosphonium. **PP-4** killed all of the bacteria (Figure 2.32A), resulting in a full log reduction relative to the 5.90 CFU of *Arthrobacter* sp. growing on the control surface. After the test, the pieces were washed exhaustively with saline solution, then distilled water, and lastly sterilized using UV light. Once dry, the pieces were rubbed with a piece of cotton saturated in water for 50 cycles using a pressure resulting in a reading between 1.0 and 1.6 kg on a top loading balance on which the rubs were performed.

Testing after the 50 cycles of abrasion (Figure 2.32B) showed that **PP-2** samples had an average reduction of log 3.04 CFU, suggesting they were significantly less active against the *Arthrobacter* sp. relative to the unabraded sample, while **PP-4** maintained its ability to fully prevent the survival of viable cell colonies. XPS analysis of **PP-4** showed that the material had a greater proportion of P at the surface in comparison to **PP-2**, and that increase seems to be related to increased ability to maintain antibacterial properties after abrasion. After the cleaning and abrasion process was repeated for another 50 cycles (Figure 2.32C), both **PP-2** and **PP-4** had reduced viability as antimicrobial surfaces; **PP-2** showed no significant reduction of the bacteria deposited on the surface, while **PP-4** killed an average of log 2.01 CFU. This may represent the limit of antimicrobial efficacy for surface with 1% loading of phosphonium antimicrobials, as XPS analysis of **PP-2** and **PP-4** showed significant decreases in P % at depths of 50 and 100 µm, respectively. Importantly, the average cell survival on the control PP samples tested remained high each time; indicating the pieces undergoing solvent double rub procedure had no effect on the survivability of cells inoculated on the surface. To extend the durability of these materials, samples of **PP-2**, **PP-3**, and **PP-4** were prepared at loadings of 1.5 % (w/w) of the active phosphonium. These materials had similar visual properties to the pieces co-extruded with 1 % (w/w) phosphonium and were subjected to the LDI test against both Gram-positive *Arthrobacter* sp. and Gram-negative *E. coli* (Figure 2.33). All of the surfaces co-extruded with phosphonium antimicrobials exhibited full log reductions of viable bacteria for both species (Figure 2.33A,C), indicating that at the higher loadings, the phosphonium molecules were still concentrating at the surface. After cleaning, the pieces were subjected to 100 solvent double rubs, and re-tested against both bacterial strains. For plastics tested against *Arthrobacter* sp., there was large deviation in killing abilities for the triplicate samples of **PP-2** and **PP-3** (Figure 2.33B). After 100 solvent rubs,
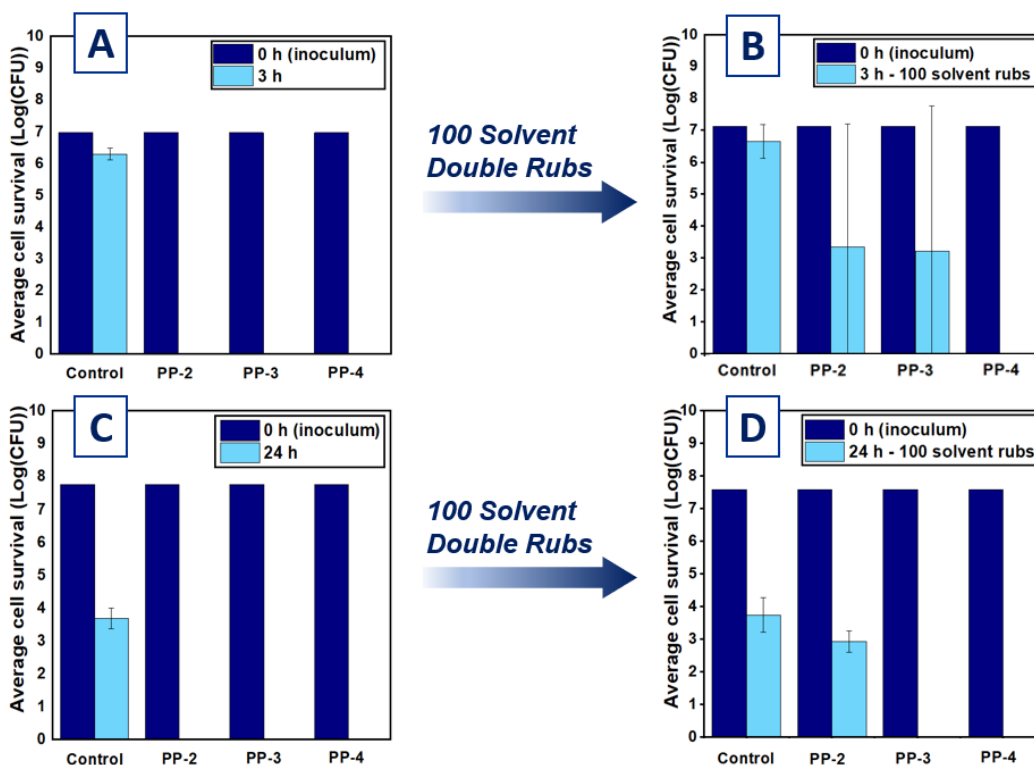
Figure 2.33. Antimicrobial testing of 1.5 % (w/w) PP-2, PP-3 and PP-4. The average cell survivability (log CFU) on **PP-2**, **PP-3**, and **PP-4** of A) *Arthrobacter* sp. without abrasion, B) *Arthrobacter* sp. after 100 cycles of solvent rub abrasion, C) *E. coli* without abrasion, and D) *E. coli* on the PP pieces after 100 cycles of solvent rub abrasion.

two out of three **PP-2** samples tested did not reduce the cell viability, while one sample killed all bacteria deposited on the surface. This same phenomenon was observed for **PP-3**. The lack of homogeneity in P % laterally across the sample observed by XPS may explain this result: the samples may have a greater concentration of phosphonium at other points on the surface that were not abraded or inoculated with the bacteria. **PP-4** was effective in maintaining complete antimicrobial efficacy after 100 rubs (Figure 2.33B), far surpassing the durability and abrasion resistance of other antimicrobial surfaces reported in the literature.[45,141,142]

Plastics tested against *E. coli* were successful in inhibiting all bacterial cell growth initially and were subjected to the solvent double rub test for 100 cycles. Results of this test had much less deviation between triplicates, and abraded **PP-2** exhibited low average reductions of log 0.81 CFU,

while abraded **PP-3** killed all the Gram-negative species inoculated onto the surface (Figure 2.33D). The reduced efficacy of **PP-2** after the abrasive cycles suggests that even at higher loadings, the observed decrease in P % for **PP-2** relative to **PP-4** still holds. Abraded **PP-4** pieces exhibited full log reductions relative to the control (Figure 2.33 D), and as such the materials exhibit broad spectrum antimicrobial efficacy even after abrasion. The efficacy of **PP-3** relative to **PP-2** suggests that the aryl moiety structures contribute to the kill of the Gram-negative species; this difference has not been reported or commented on in literature reports of antimicrobial phosphonium surfaces.

2.7 Co-Extrusion of Phosphonium-Containing Polystyrene
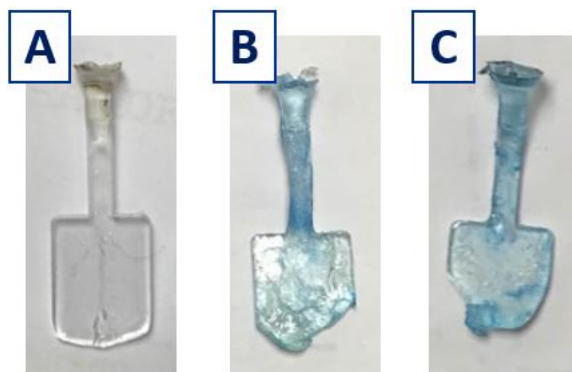
Figure 2.34. PS co-extruded with phosphoniums 2 and 3. Subjected to the BPB dye assay were (A) a control extruded PS piece, (B) **PS-2**, and (C) **PS-3**. The extruded dogbones were significantly smaller than PP-based pieces.

To expand the scope of application for extrudable phosphoniums, preliminary studies were performed using a different plastic. Phosphoniums **2** and **3** were co-extruded with PS pellets (**PS-2**, **PS-3**), using the same pre-coating and curing procedure employed for the PP pieces. The nature of the materials that resulted suggested that PS was not an ideal candidate for this process; the pieces that resulted were brittle, and often the extrusion of the plastic did not fill the mold, resulting in "half-dogbones" (Figure 2.34). This is likely due to the mold temperature being below the melt temperature for the plastic. A mold with controllable temperature settings may allow for these

materials to be more viable. Due to time and cost restraints, phosphonium **4** was not tested in this material.

Despite these challenges, PS materials containing 1% (w/w) **2** and **3** were fabricated. Preliminary visualization of **PS-2** and **PS-3** using a qualitative BPB stain assay (Figure 2.34B,C) showed evidence of available phosphonium charge at the surface. Analysis by θ_C revealed drops in θ_C relative to the control plastic (Table 2.6). Water droplets on virgin molded PS gave contact angles similar to those measured in (92.2° ± 1.0, Table 2.1), although the deviation in θ_C between

Table 2.6 θ_C for injection molded PS dogbones.

Material[a]	θ_C[a] (deg)
Molded PS control (**PS**)	87.8 ± 5.1
Molded PS co-extruded with **2** (**PS-2**)	74.1 ± 2.1
Molded PS co-extruded with **3** (**PS-3**)	80.5 ± 0.5

[a]Phosphonium compounds incorporated in non-control samples at 1 % (w/w). [b]θ_C measurements for each sample were performed in triplicate.

triplicate extruded samples were larger (87.8 ± 5.1); likely a result of the induced roughness due to the molding process. Drops in θ_C for **PS-2** and **PS-3** showed a similar trend to the PP samples (Figure 2.35), with average decreases for **PS-2** (13.7°) and **PS-3** (7.3°) similar to those decreases observed for **PP-2** (14.3°) and **PP-3** (6.0°). This suggests similar concentrations of phosphonium are present at the surface of **PS-2** and **PS-3** in comparison to their PP counterparts.

Figure 2.35. θ_C images for PS co-extruded with phosphonium. Water droplets on (A) virgin molded PS, (B) **PS-2**, and (C) **PS-3**. Values below the images are averages (in °) of triplicate measurements for that substrate.

2.7.1 Antimicrobial Efficacy of Polystyrene Co-Extruded with Phosphonium
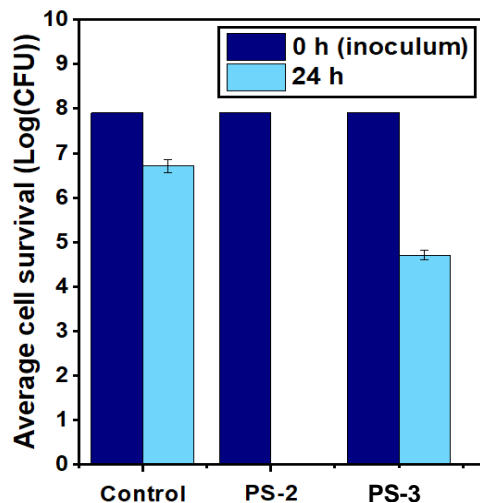
Figure 2.36. Antimicrobial activity of coextruded PS against *E. coli*. The antimicrobial activity of control samples, **PS-2**, and **PS-3**.

The activity of **PS-2** and **PS-3** against *E. coli* (ATCC 11229) was evaluated using the LDI method. Due to time and availability constraints, *E. coli* was chosen over *Arthrobacter* sp. The bacteria showed above average growth on the control when compared to *E. coli* ATCC 11229 survival on other surfaces tested in this work, while **PS-2** showed a full log reduction of the inoculated bacteria (Figure 2.36). On the other hand, **PS-3** had modest log reductions (average reduction of log 1.94 CFUs). This may be a result of the three phenyl moieties present in **3**, which are potentially more miscible in the styrenic bulk polymer compared to alkyl or fluoroalkyl groups.[144] As such, the rate of migration to the plastic-air interface for the phosphonium may be reduced for **PS-3**, affording a less antimicrobially active surface.

3   CONCLUSIONS

3.1   Conclusion and Summary

In this work, five novel phosphonium compounds were synthesized to assess the antimicrobial efficacy of UV-curable small molecule phosphonium against Gram-negative and Gram-positive bacteria. Phosphoniums **1**-**4** were applied as UV-curable spray coatings, and their properties as coatings were examined *via* several surface and material characterization techniques. Phosphoniums **2**-**4** were used as additives in melt extrusion processing of PP and PS. The properties of these materials were quantified, and the antimicrobial efficacy was tested. Each phosphonium was able to kill both Gram-negative and Gram-positive bacteria, and PP samples with **4** maintained their killing capacity after abrasion.

Phosphoniums **1**-**3** were synthesized using commercially available and accessible tertiary phosphines using Menshutkin-like quaternization procedures in high yield. Two novel tertiary phosphine species were synthesized, and further reacted to furnish phosphoniums **4** and **5**. The reaction of precursors **i** and **vii** to yield **5** did not proceed efficiently relative to other quaternizations in this work, and this was attributed to poorer nucleophilicity for the bulkier **vii**. Consequently, the synthetically impure **5** was not used in further testing.

Coatings comprised of **1**, **2**, **3**, and **4** were prepared after UV-curing spray coated solutions of the phosphoniums on PS coupons. P^+ content of coatings **1**-**4** were analyzed by θ_C, surface charge density analysis calculated from UV-Vis values, and **2**-**4** were probed by AFM to determine coating thickness and surface roughness. Coatings of phosphonium **1** did not show evidence of significant phosphonium charge.

LDI testing, which can simulate real-world desiccation conditions, against *E. coli* (ATCC strain 11229) and *Arthrobacter* sp. (IAI-3) was employed to test antimicrobial efficacy of the coatings. Phosphoniums **2**-**4** showed full log reductions of the inoculated bacteria, while **1** did not significantly reduce either bacterial strain to which it was subjected. This was attributed to the lack of charge density measured on the coatings.

Phosphinium **2**-**4** were shown to be suitable additives in injection molding processes. The phosphoniums were UV-cured to PP beads and subsequently extruded into a dogbone mold to give plastics **PP-2**, **PP-3**, and **PP-4**. The P^+ content of resulting pieces was analyzed by θ_C and XPS. XPS analysis was able to quantify the P content of **PP-2** and **PP-4** at both the surface (1.31 and 2.01 %, respectively) and throughout the material. **PP-4** showed a significant concentration of P up to a depth of 20 µm. AFM analysis on **PP-2** revealed a rougher surface than virgin PP pieces.

Antimicrobial testing against *E. coli* (ATCC 11229) and *Arthrobacter* sp. (IAI-3) using the LDI protocol showed **PP-2**, **PP-3**, and **PP-4** all exhibit full log reductions of both strains, confirming the phosphoniums are effective antimicrobials when used as additives in the injection molding process. Abrading the surfaces of **PP-2**, **PP-3**, and **PP-4** for 100 solvent double-rub cycles showed a loss in antimicrobial activity for plastics impregnated with 1 % (w/w) phosphonium. A loading of 1.5 % (w/w) allowed **PP-4** to maintain full log reductions of Gram-positive and Gram-negative species after 100 abrasion cycles, while **PP-2** and **PP-3** had reduced efficacies. This positions **4** as an effective antimicrobial that can be used as both a coating and an additive; when used as the latter, long-lasting abrasion-resistant antimicrobial surfaces can be generated.

Lastly, preliminary work demonstrating the compatibility of the phosphoniums with other plastic was carried out. Incorporated at 1% (w/w) into PS were phosphoniums **2** and **3**, yielding **PS-2** and **PS-3**. These materials were examined using θ_C, and subjected to the LDI using *E. coli*

(ATCC 11229). **PS-3** exhibited modest antimicrobial activity, while **PS-2** showed a full log reduction of the inoculated *E. coli*. The reduced efficacy of **PS-3** was attributed to slower rate of migration of the phosphonium additive to the surface-air interface in the PS plastic relative **to PP-2**.

3.2 Future Work

   This work was able to produce antimicrobial materials with the ability to retain antimicrobial properties after abrasion. Of the five phosphoniums synthesized to realize this goal, only four were tested in any capacity. Phosphonium **5** was formed, but analysis of the ^{1}H NMR (CDCl$_3$) spectrum showed the reaction was incomplete after a 24 h reflux. Further attempts to obtain this product in good yield and purity could utilize longer reaction times, more concentrated reactants, and higher temperatures (Scheme 3.1).
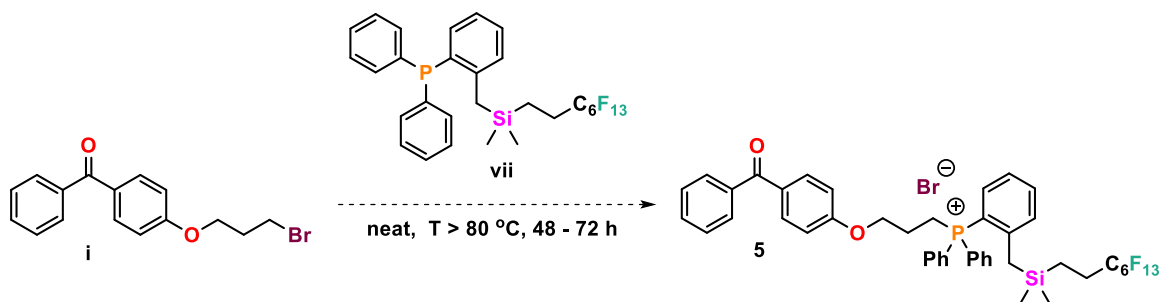
Scheme 3.1. Preparation of 5 using alternate reaction conditions.

   Another advancement of the synthetic work done would be the oxidation-free P-H addition of Ph$_2$PH across (perfluorohexyl)ethylene (Scheme 3.2). In this work, the reaction of the two starting materials in the presence of 4 mol % AIBN yielded only the oxidized adduct; further efforts to have this reaction cleanly yield the desired phosphine **iv** should be explored. Silanizing glassware to remove any free hydroxyl groups, using higher vacuum to remove oxygen from the

glass, and perhaps using different reaction apparatus entirely may be necessary to preclude the formation of the oxide, **iii**.
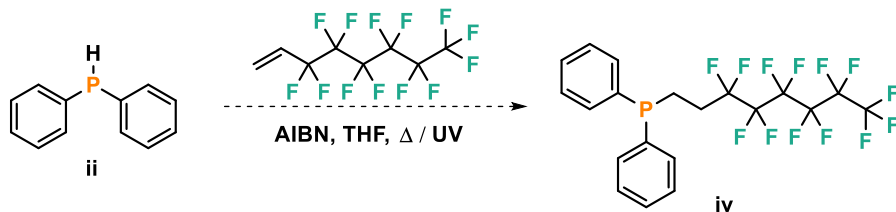
Scheme 3.2. Proposed oxidation-free synthesis of iv.

Additionally, this work established differences in the properties of coatings and co-extruded plastics with **2**, **3**, and **4**. A significant amount of insight on the differences between alkyl, aryl, and perfluoroalkyl groups as they pertain to use in these materials, however three materials is likely insufficient to establish a trend. Due to the success of **4** in antimicrobial and abrasion trials, architectures with varying degrees of fluorinated groups should be explored (Figure 3.1).
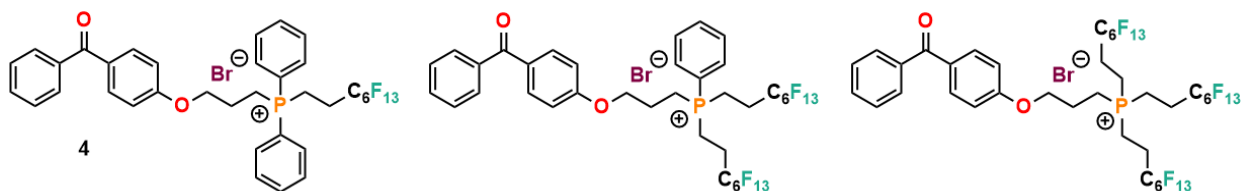
Figure 3.1. Proposed phosphoniums with varying amounts of fluoroalkyl substituents.

Additionally, this work has introduced a new class of small molecule phosphoniums with antimicrobial efficacy. Due to the prevalence of QAC-containing antimicrobial polymers in the literature, it is logical to extend the phosphonium motif into polymeric form (Figure 3.2). The phosphoniums can be tailored to include polymerizable groups, and block copolymers of these phosphoniums can be synthesized and grafted to various substrates.
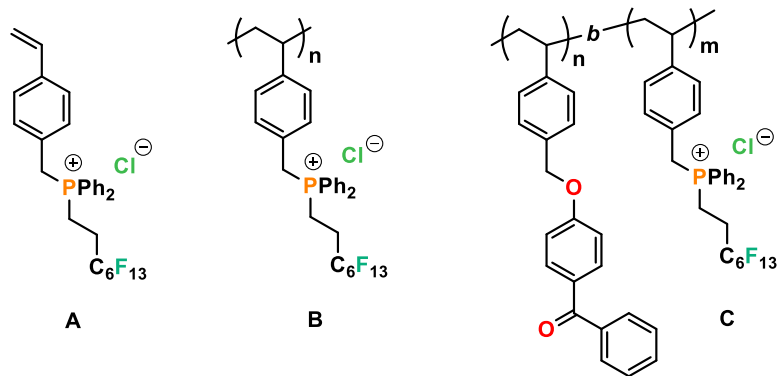
Figure 3.2. Proposed phosphonium-containing polymers. (A) A monomer with a polymerizable group, (B) a homopolymer, and (C) a block copolymer containing a small portion of a UV-curable benzophenone block.

The preliminary testing of **2** and **3** in PS is promising, and a full gamut of testing, including: the incorporation of **4** into PS, AFM analysis on the pieces relative to a control, XPS analysis at different depths on the extruded materials, LDI testing with Gram-positive bacteria, and abrasion testing should be carried out. If these results are promising, co-extrusion with other plastics, especially those relevant to 3D printing and additive manufacturing processes, such as PLA, should be tested.

4   EXPERIMENTAL METHODS

4.1   General Methodology

4.1.1   General Synthetic Methods

All syntheses, unless otherwise stated, were carried using standard Schlenk and glovebox protocols. Unless otherwise noted, solvents were purified via a solvent purification system (SPS). PS coupons were cut from weigh boats (cat. 89106-754) supplied by VWR International, and PS and PP beads used in extrusion were donated by Electro-Pack Inc. All reagents were purchased from commercial sources and used as received unless otherwise noted. (Perfluorohexyl)ethylene was purchased from Oakwood chemicals and degassed *via* a freeze-pump-thaw (FPT) method (4 cycles). Sodium hydroxide (NaOH, 1 M), 10 % aqueous ammonium chloride (NH_4Cl), and 3 M hydrochloric acid (HCl) were sparged with N_2 (g) for 1 h before use. Acetonitrile (MeCN) was dried over 4 Å molecular sieves for 48 h prior to use. The concentration of *n*-butyllithium purchased from Sigma Aldrich was determined to be 1.4 M in hexanes *via* titration of diphenylacetic acid in anhydrous THF under N_2. 2,2′-Azobis(2-methylpropionitrile) (AIBN) was recrystallized $2 \times$ from MeOH.

Column chromatography was carried out on silica gel (Silica Gel 60, 40-63 μm, EMD). Reactions and chromatographic purifications were monitored by thin layer chromatography (TLC). Silica-coated aluminum plates (Alugram Sil G/UV254, Macherey-Nagel) were used for TLC tests. Plates were visualized by UV light or $KMnO_4$ staining and heated with a heat gun.

4.1.2   Characterization of Compounds

Nuclear magnetic resonance (NMR) experiments were carried out on a 400 MHz Bruker Avance II Spectrometer using $CDCl_3$ or C_6D_6. ^1H NMR (400 MHz) and ^{13}C {^1H} NMR (100.6 MHz) spectra were referenced to the residual proton and central carbon peak of the solvent. ^{31}P {^1H}, ^{19}F {^1H}, and ^{29}Si {^1H} spectra were referenced to external standards 85 % H_3PO_4 (δ (^{31}P) = 0.00 ppm), $CFCl_3$ (δ (^{19}F) = 0.00 ppm) and TMS (δ (^{29}Si) = 0.00 ppm), respectively. All chemical shifts are given in δ (ppm) relative to the solvent and assigned to atoms on basis of available 2D spectra for each compound. High resolution mass spectrometry (HRMS) for novel small molecules was carried out using electrospray ionization time of flight (ESI-TOF) and Direct Analysis in Real Time (DART) at the Advanced Instrumentation for Molecular Structure (AIMS) laboratory at the University of Toronto.

4.1.3   Coated Sample Preparation

Coating of plastic test samples, which consisted of 6.25 cm^2 ± 1 cm^2 coupons of each plastic material, was performed via an ESS AD – LG electrospray apparatus set to 125 kPa that applied the compound uniformly over the test surfaces. UV curing of phosphonium-coated PS and antimicrobial phosphonium-containing plastics was performed using a Novacure spot curing system, supplied from a mercury-arc discharge lamp, at a peak intensity of 5000 mW into a reflective curing chamber 6.5 cm from the light guide source giving a 0.164 W/cm² intensity giving an approximate 10 J cm⁻² total dose as measured using an EIT UV Power Puck 2.

4.1.4 Co-extrusion of Phosphonium Containing Plastics

Antimicrobial plastics were extruded into a stainless-steel mold using a hand press thermal extruder donated by Electro-Pack Inc., with the die temperature set to 220 °C and the mold heated in a vacuum oven at 110 °C. Plastic beads were placed in a 500 mL round bottom flask (RBF) and 1 or 1.5 % (w/w) of the active phosphonium was added. EtOH was added to dissolve the compound and the solvent was removed *via* rotary evaporation, adsorbing the phosphonium to the beads. Once dry, the coated beads were then cured using the Novacure spot curing system under the same parameters utilized for the coated networks.

4.1.5 Surface Characterization of Antimicrobial Materials

Advancing water contact angle θ_C images of treated and untreated surfaces were taken using a Teli CCD camera equipped with a macro lens attached perpendicular to the sample surface. The camera was connected to a monitor using a Sony CMA-D camera adapter. Contact angle measurements were performed using SCA20 contact angle software by Data Physics Corporation. Contact angle experiments performed in accordance with ASTM D7334, and images and measurements were taken 30 s after placing the water droplet on the surface. Atomic force microscopy (AFM) using an Anasys nanoIR2 equipped with Contact Mode NIR2 Probes (Resonance frequency 13 ± 4 kHz, Spring constant 0.07 - 0.4 N m^{-1}) was performed at the Ontario Centre for Characterization of Advanced Materials (OCCAM). PC samples were prepared by putting a piece of 3M Scotch© Tape on one half of the sample, coating and curing the sample, and subsequently removing the tape to create a coated and uncoated side. AFM data was processed using Gwyddion 2.48. The preparation of samples for XPS experiments and the XPS experiments themselves were performed at OCCAM.

4.1.6   Antimicrobial Testing using the Large Drop Inoculum Method

Bacterial test species were grown overnight in 10 mL of 3 g L^{-1} tryptic soy broth (EMD Millipore) at 30 °C within a shaking incubator, and cultures were washed twice via centrifugation at 9000 × g to replace the growth media with sterile water. *Arthrobacter* sp. (IAI-3), a Gram-positive bacterium originally isolated from indoor laboratory air was inoculated onto all treated and control test surfaces as the model organism for bacterial survival on solid surfaces.[39] Lab strains of Gram-negative *Escherichia coli* (ATCC 11229) was also tested on treated materials. These strains were chosen since they are well characterized and are present in biofilms found within high-risk environments. The large drop inoculum (LDI) method was used to assess the antimicrobial efficacy of the antimicrobial treatment at a solid/air interface and is a modification of the ISO 22196/JIS Z 2801 standard procedure. Triplicate treated samples were inoculated with 100 mL bacterial aliquots of subsequently determined concentration, and survival on the sample was determined by spot plating, described as following. For *Arthrobacter* sp., the inoculated droplets were naturally air-dried within a class II, type A2 biosafety cabinet (Model 3440009, Labconco Corp.) to avoid contamination, and surviving cells were enumerated upon drying, which took 3 hours. *E. coli* samples were dried in a petri dish with lid closed, over a period of 24 h. Enumeration was performed by rehydrating and vortexing samples in 5 mL of a 0.9% saline retrieval solution, which was then serially diluted and spot-plated onto 3 g L1 tryptic soy agar. Plates were then incubated at 25 °C for a period of 3–5 d which allowed for visualization of colony forming units (CFU). At each time point, bacterial survival on the treated samples was compared to survival on triplicate untreated control surfaces of the same material.
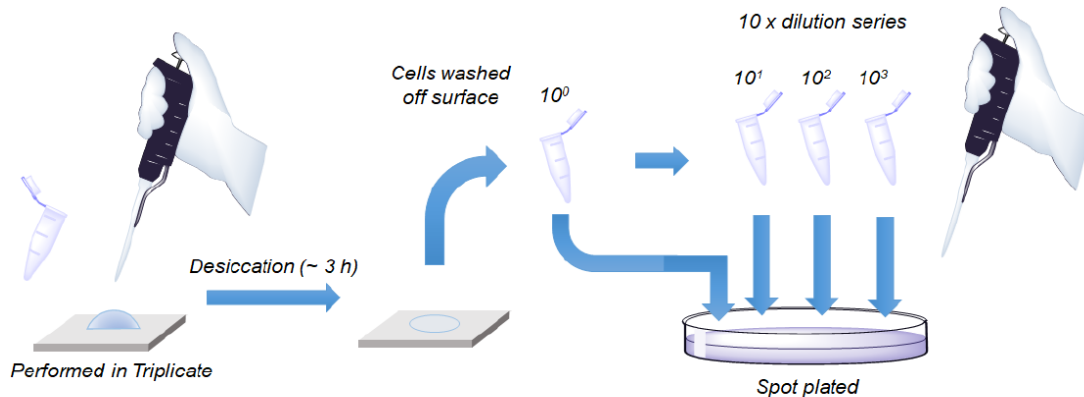
Figure 4.1. Schematic describing the LDI protocol.

4.1.7   Abrasion and Antimicrobial Testing of Extruded Plastics

Abrasion of the extruded PP samples was done according to ASTM D5402-19.[143] After LDI testing, the samples were removed from the 50 mL falcon tubes, rinsed with distilled water, and vortexed again in a 50 mL falcon tube containing 15 mL 0.9% saline solution. The samples were rinsed with distilled water again, dried, placed in the biosafety cabinet and sterilized with UV light for 10 minutes. The sterilized pieces were placed on a scale and rubbed using cotton cloth saturated with distilled water. One rub was counted as a back-and-forth motion with consistently applied pressure resulting in a reading between 1.0 and 1.6 kg on a top loading balance. After rubbing the pieces were once again sterilized in the biosafety cabinet for 10 min, after which they were subject to the LDI protocol.

4.2   Synthesis of Antimicrobial Compounds and Precursors

4.2.1   Synthesis of 4-(3-bromopropoxy)benzophenone (i)
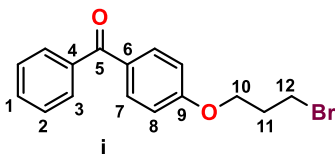
Under ambient conditions, to a 2 L round bottom flask a magnetic stir bar, 4-hydroxybenzophenone (100.0 g, 504 mmol), TBAB (8.13 g, 25.2 mmol), K_2CO_3 (77.0 g, 555 mmol), 1,3-dibromopropane (154.3 mL, 1513 mmol), and H_2O (300 mL) was added. The reaction was heated to 110 °C for 1.5 h and allowed to cool to R.T. The bottom layer in the flask was flash frozen in liquid N_2 and the top aqueous layer was decanted. The frozen solid was further washed with H_2O (200 mL). After warming to R.T., excess 1,3-dibromopropane was removed *via* vacuum distillation (80 °C, 5 mmHg). The reaction mixture was dissolved in EtOAc (300 mL) with heating, and insoluble impurities were filtered out. The contents of the flask were collected, and the volatiles removed *in vacuo* to give a white coloured powder. Yield: 92 % (135 g). Mp = 72 °C. **¹H NMR** (400 MHz, CDCl₃) δ = 7.83 (d, $^3J_{HH}$ = 8.81 Hz, 2H, H7), 7.75 (d, $^3J_{HH}$ = 8.28 Hz, 2H, H3), 7.57 (t, $^3J_{HH}$ = 7.37 Hz, 1H, H1), 7.47 (t, $^3J_{HH}$ = 7.51, 2H, H2), 6.97 (d, $^3J_{HH}$ = 8.79 Hz, 2H, H8), 4.20 (t, $^3J_{HH}$ = 5.72 Hz, 2H, H10), 3.62 (t, $^3J_{HH}$ = 5.87 Hz, 2H, H12), 2.38-2.33 (m, 2H, H11) ppm. **¹³C {¹H} NMR** (101 MHz, CDCl₃) δ: 195.50 (C5), 162.31 (C9), 138.25 (C4), 132.59 (C3), 131.94 (C2), 130.38 (C6), 129.75 (C7), 128.22 (C1), 114.05 (C8), 65.46 (C10), 32.15 (C12), 29.82 (C11) ppm. NMR spectral data agreed well with literature values.[17]

4.2.2   Synthesis of (3-(4-benzoylphenoxy)propyl)trimethylphosphonium bromide (1)
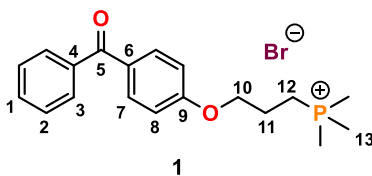
In a sealed 20 mL microwave vial, PMe$_3$ (3.40 mL, 1 M in toluene, 3.40 mmol) was added dropwise to a stirring solution of **i** (1.00 g, 3.10 mmol) in dry MeCN (5 mL) and stirred at R.T. for 1 h. The mixture was heated to 80 °C for 48 h, and after cooling to R.T., was washed with cold dry Et$_2$O (3 × 15 mL). Volatiles were removed *in vacuo*, yielding the desired product as a white coloured powder. Yield: 99% (1.2 g). **^{1}H NMR** (400 MHz, CDCl$_3$) δ: 7.81 (d, $^3J_{HH}$ = 8.9 Hz, 2H, H7), 7.74 (t, $^3J_{HH}$ = 6.9 Hz, 2H, H3), 7.57 (t, $^3J_{HH}$ = 7.4 Hz, 1H, H1), 7.47 (t, $^3J_{HH}$ = 7.4 Hz, 2H, H2), 6.96 (d, $^3J_{HH}$ = 8.9 Hz, 2H, H8), 4.26 (t, $^3J_{HH}$ = 5.5 Hz, 2H, H10), 2.81–2.88 (m, 2H, H12), 2.26 (d, $^2J_{PH}$ = 14.2 Hz, 9H, H13), 2.15-2.21 (m, 2H, H11) ppm; **^{13}C {^{1}H} NMR** (101 MHz, CDCl$_3$) δ: 195.65 (C5), 161.79 (C9), 138.09 (C4), 132.70 (C7), 132.24 (C1), 130.87 (C6), 129.85 (C3), 128.39 (C2), 114.26 (C8), 67.20 (d, $^3J_{C-P}$ = 15.4 Hz, C10), 22.09 (d, $^2J_{C-P}$ = 3.7 Hz, C11), 21.28 (d, $^1J_{C-P}$ = 53.9 Hz, C12), 9.27 (d, $^1J_{C-P}$ = 54.7 Hz, C13) ppm. **^{31}P {^{1}H} NMR** (162 MHz, C$_6$D$_6$) δ: 27.81 ppm. **HRMS (ESI-TOF)** (m/z): [M$^+$ - Br] for C$_{34}$H$_{30}$O$_2$P: calculated 441.2917; found 441.2915.

4.2.3 Synthesis of (3-(4-benzoylphenoxy)propyl)tributylphosphonium bromide (2)

2
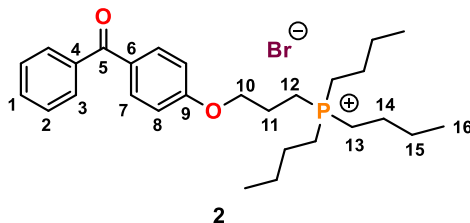
In a 100 mL Schlenk flask, PPh_3 (0.73 mL, 4.45 mmol) was added dropwise to a solution of **i** (1.42 g, 4.45 mmol) were dissolved in dry MeCN (5 mL) in a 100 mL Schlenk and heated at 120 °C for 48 h. The reaction mixture was cooled to R.T. and was washed with dry Et_2O (3 × 30 mL), and then dried *in vacuo*, giving an orange gel. Yield: 83 % (1.92 g). **^{1}H NMR** (400 MHz, CDCl$_3$) δ: 7.83 (d, $^3J_{HH}$ = 8.7 Hz, 2H, H7), 7.76 (t, $^3J_{HH}$ = 7.0 Hz, 2H, H3), 7.59 (t, $^3J_{HH}$ = 7.5 Hz, 1H, H1), 7.49 (t, $^3J_{HH}$ = 7.5 Hz, 2H, H2), 6.97 (d, $^3J_{HH}$ = 8.8 Hz, 2H, H8), 4.26 (t, $^3J_{HH}$ = 5.4 Hz, 2H, H10), 2.77–2.88 (m, 2H, H12), 2.45–2.52 (m, 6H, H13), 2.18-2.29 (m, 2H, H11), 1.51-1.65 (m, 12H, H14 + H15 overlap), (t, $^3J_{HH}$ = 7.0 Hz, 9H, H16) ppm; **^{13}C {^{1}H} NMR** (101 MHz, CDCl$_3$) δ: 195.62 (C5), 161.84 (C9), 138.18 (C4), 132.74 (C7), 132.18 (C1), 130.85 (C6), 129.85 (C3), 128.38 (C2), 114.20 (C8), 67.29 (d, $^4J_{C-P}$ = 15.3 Hz, C10), 24.14 (d, $^4J_{C-P}$ = 15.3 Hz, C15), 23.94 (d, $^3J_{C-P}$ = 4.7 Hz, C14), 22.27 (d, $^3J_{C-P}$ = 3.7 Hz, C11), 19.33 (d, $^2J_{C-P}$ = 47.3 Hz, C13), 16.75 (d, $^2J_{C-P}$ = 49.4 Hz, C12) ppm; **^{31}P {^{1}H} NMR** (162 MHz, C$_6$D$_6$) δ: 33.61 ppm. **HRMS (ESI-TOF)** (m/z): [M$^+$ - Br] for C$_{28}$H$_{42}$O$_2$P: calculated 441.2917; found 441.2915.

4.2.4 Synthesis of (3-(4-benzoylphenoxy)propyl)triphenylphosphonium bromide (3)

3
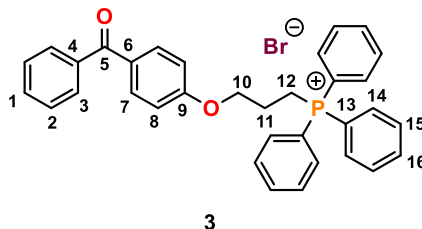
Triphenylphosphine (4.00 g, 15.2 mmol) and **i** (4.85 g, 15.2 mmol) were combined in a 100 mL Schlenk and heated at 130 °C for 24 h. The waxy, solidified mixture was cooled to R.T. and was washed with dry Et$_2$O (3 × 70 mL), and then dried *in vacuo*, giving an off-white coloured powder. Yield: 89 % (7.08 g). mp: 191 °C. **^{1}H NMR** (400 MHz, CDCl$_3$) δ: 7.65-7.86 (m, 19H, H7 + H3 + H14-H16 overlap), 7.52 (t, $^3J_{HH}$ = 7.4 Hz, 1H, H1), 7.41 (t, ^3J = 7.5 Hz, 2H, H2), 6.90 (d, ^3J = 8.9 Hz, 2H, H8), 4.43 (t, $^3J_{HH}$ = 5.7 Hz, 2H, H10), 4.02-4.09 (m, 2H, H12), 2.16-2.23 (m, 2H, H11) ppm; **^{13}C{^{1}H} NMR** (101 MHz, CDCl$_3$) δ: 195.57 (C5), 161.89 (C9), 138.09 (C4), 135.18 (d, $^4J_{C-P}$ = 2.8 Hz, C16), 133.70 (d, $^3J_{C-P}$ = 10.1 Hz, C15), 132.50 (C7), 131.99 (C1), 130.57 (d, $^2J_{C-P}$ = 12.6 Hz, C14), 130.30 (C6), 129.72 (C3), 128.22 (C2), 118.03 (d, $^1J_{C-P}$ = 86.4 Hz, C13), 114.24 (C8), 66.97 (d, $^3J_{C-P}$ = 17.5 Hz, C10), 22.82 (d, $^2J_{C-P}$ = 3.4 Hz, C11), 19.73 (d, $^1J_{C-P}$ = 53.0 Hz, C12) ppm; **^{31}P {^{1}H} NMR** (162 MHz, CDCl$_3$) δ: 24.71 ppm **HRMS (ESI-TOF)** (m/z): [M$^+$ - Br] for C$_{34}$H$_{30}$O$_2$P: calculated 501.1978; found 501.1985.

4.2.5 Synthesis of diphenylphosphine (ii)
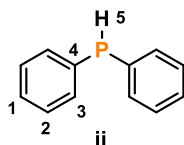
Compound **ii** was prepared according to a literature procedure.[124] Briefly, under Ar (g) at 0 °C, a solution of PPh$_3$ (25.0 g, 95.3 mmol) dissolved in 50 mL of dry THF was transferred *via* cannula in a flame dried 500 mL Schlenk to a suspension of Li (2.65 g, 381 mmol) in dry THF (50 mL), facilitating an immediate colour change from clear to dark red. The reaction mixture was stirred at room temperature for 24 h. The mixture was then cooled to 0 °C, and degassed water (40 mL, sparged with Ar (g)) was added dropwise to the mixture, followed by the addition of degassed 3 M HCl solution (25 mL). Dry hexanes (70 mL) was added and the organic layer was extracted *via* cannula into a clean 500 mL Schlenk. Volatiles were removed *in vacuo* and product was distilled from the reaction mixture at 130 °C under reduced pressure (5 mmHg) to afford the desired air and moisture-sensitive phosphine as a clear, colourless liquid. Yield: 91 % (16.1 g). **^{1}H NMR** (400 MHz, C$_6$D$_6$) δ: 7.35-7.39 (m, 4H, H2), 6.98-7.05 (m, 6H, H1 + H3 overlap), 5.21 (d, $^1J_{P-H}$ = 215.7 Hz, 1H, H5); **^{13}C {^{1}H} NMR** (101 MHz, C$_6$D$_6$) δ: 134.97 (d, $^1J_{C-P}$ = 10.6 Hz, C4), 134.00 (d, $^2J_{C-P}$ = 17.2 Hz, C3), 130.59 (d, $^3J_{C-P}$ = 8.6 Hz, C2), 128.54 (d, $^4J_{C-P}$ = 6.2 Hz, C1); **^{31}P {^{1}H} NMR** (162 MHz, C$_6$D$_6$) δ: -40.73 ppm. NMR spectral data agreed well with literature values.[124]

4.2.6   Synthesis of diphenyl(perfluorohexylethyl)phosphine oxide (iii)
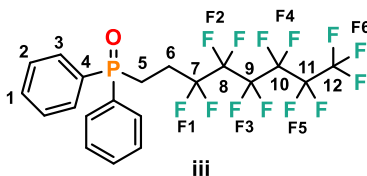
Under Ar (g), (perfluorohexyl)ethylene (1.17 mL, 5.16 mmol), **ii** (0.70 g, 4.03 mmol) and AIBN (0.025 g, 4 mol %, 0.15 mmol) were combined in a 50 mL Schlenk flask and the biphasic mixture was stirred under Ar (g) at 70 °C for 2 h. Subsequent portions of AIBN (0.025 g) were added every 2 h for a total of four additions (0.10 g total), and the reaction was stirred at 70 °C for 14 h. The resulting waxy yellow solid was sublimed (70 °C, 5 mmHg) for 4 h to remove excess (perfluorohexyl)ethylene and tetramethylsuccinonitrile. The leftover crude material was sublimed further (140 °C, 5 mmHg) to yield the compound as a white coloured solid. Analysis by ^{31}P {^{1}H} NMR and ^{1}H NMR spectroscopy, and HRMS indicated the desired material had oxidized. Yield: 66 % (1.46 g). **^{1}H NMR** (400 MHz, C_6D_6) δ: 7.61-7.66 (m, 4H, H3), 6.98-7.06 (m, 6H, H1 + H2 overlap), 2.38-2.53 (m, 2H, H5), 2.21-2.28 (m, 2H, H6) ppm; **^{13}C {^{1}H} NMR** (101 MHz, C_6D_6) δ: 132.95 (d, $^{1}J_{C-P}$ = 99.5 Hz, C4), 131.42 (d, $^{3}J_{C-P}$ = 9.3 Hz, C2), 128.94 (d, $^{2}J_{C-P}$ = 11.7 Hz, C3), 24.80 (t, $^{2}J_{C-F1}$ = 23.00 Hz, C6), 21.33 (d, $^{1}J_{C-P}$ = 71.5 Hz, C5) ppm; **^{31}P {^{1}H} NMR** (162 MHz, C_6D_6) δ: 26.53 ppm; **^{19}F {^{1}H} NMR** (376 MHz, C_6D_6) δ: -81.06, -114.32, -121.89, -122.8, -123.25, -126.19 ppm. **HRMS (DART)** (m/z): [M + H^{+}] for $C_{20}H_{14}F_{13}OP$: calculated 549.0647; found 549.0650.

4.2.7   Synthesis of diphenyl(perfluorohexylethyl)phosphine (iv)

iv
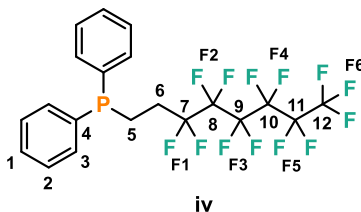
Under Ar (g), **iii** (1.00 g, 1.82 mmol) obtained in the previous hydrophosphination reaction was dissolved in dry toluene (20 mL) in a 250 mL Schlenk flask. $HSiCl_3$ (2.14 mL, 21.2 mmol, 11.6 eq) was added in dropwise, discolouring the solution to a light yellow. The reaction was stirred overnight for 13 h at 100 °C, and upon cooling to R.T., degassed 1 M NaOH solution (80 mL) was added dropwise, facilitating an exothermic formation of white precipitate and vigorous gas evolution. Dry Et_2O (70 mL) was added to the mixture and the organic layer was extracted *via* cannula transfer, filtered over $MgSO_4$, and volatiles removed *in vacuo*, yielding a clear, off-white coloured solid. The crude solid was sublimed (60 °C, 5 mmHg) to yield white, needle-like crystals. Yield: 70 % (0.68 g). **^{1}H NMR** (400 MHz, C_6D_6) δ: 7.26-7.32 (m, 4H, H3), 6.00-7.06 (m, 6H, H1 + H2 overlap), 1.97-2.15 (m, 4H, H5 + H6 overlap) ppm; **^{13}C {^{1}H} NMR** (101 MHz, C_6D_6) δ: 138.05 (d, $^3J_{C\text{-}P}$ = 9.3 Hz, C2) 133.26 (d, $^1J_{C\text{-}P}$ = 99.5 Hz, C4), 129.33 (d, $^3J_{C\text{-}P}$ = 9.3 Hz, C2), 28.64 (d, $^2J_{C\text{-}F}$ = 23.0 Hz, C6), 18.92 (d, $^1J_{C\text{-}P}$ = 71.5 Hz, C5) ppm; **^{31}P {^{1}H} NMR** (162 MHz, C_6D_6) δ: -16.45 ppm; **^{19}F {^{1}H} NMR** (376 MHz, C_6D_6) δ: -81.06, -114.32, -121.89, -122.89, -123.25, -126.19 ppm. **HRMS (DART)** (m/z): [M + H$^+$] for $C_{20}H_{14}F_{13}P$: calculated 533.0698; found 533.0701.

4.2.8   Synthesis of (o-tolyl)diphenylphosphine (v)
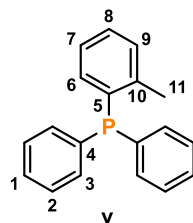
A solution of 2-bromotoluene (8.41 mL, 70.2 mmol) dissolved in dry Et_2O (30 mL) was added to a suspension of Mg (8.53 g, 350 mmol) and I_2 (0.06 g) in dry Et_2O (50 mL) in a 500 mL 3-neck round bottom flask over a 0.5 h period. The mixture was then stirred at 110 °C for 1 h, and the cloudy suspension cooled to -4 °C and was before transferring by syringe to a solution of chlorodiphenylphosphine (12.6 mL, 70.2 mmol) in dry Et_2O (20 mL) in a 250 mL Schlenk at -4 °C, resulting in the formation of white precipitate. The resulting mixture was stirred at reflux temperature for 2.5 h, then quenched by the addition of 10% aqueous NH_4Cl (100 mL). The solution was transferred to a 500 mL separatory funnel, the organic layer extracted and dried over $MgSO_4$, and concentrated *in vacuo*. The resulting yellow coloured gel was recrystallized in EtOH at -30 °C to afford an off-white coloured solid. Yield: 75 % (10.3 g). **^{1}H NMR** (400 MHz, C_6D_6) δ: 7.23-7.40 (m, 12H, H1-H3 + H7 + H9 overlap), 7.13 (t, $^3J_{HH}$ = 7.11, 7.44 Hz, 1H, H8), 6.81-6.84 (m, 2H, H6), 2.44 (s, 3H, H11) ppm; **^{13}C {^{1}H} NMR** (101 MHz, C_6D_6) δ: 142.56 (d, $^1J_{C-P}$ = 25.7 Hz, C5) 137.17 (d, $^3J_{C-P}$ = 11.4 Hz, C4), 136.79 (d, $^3J_{C-P}$ = 12.8 Hz, C10), 134.45 (d, $^1J_{C-P}$ = 19.8 Hz, C7), 133.31 (C1), 130.48 (d, $^2J_{C-F}$ = 4.4 Hz, C6), 128.95 (d, $^3J_{C-F}$ = 15.0 Hz, C2), 128.93 (d, $^2J_{C-F}$ = 1.8 Hz, C3 + C9 overlap), 126.48 (C8), 21.34 (d, $^3J_{C-P}$ = 21.6 Hz, C11) ppm; **^{31}P {^{1}H} NMR** (162 MHz, C_6D_6) δ: -13.26 ppm. NMR spectral data agreed well with literature values.[127]

4.2.9 Synthesis of chlorodimethyl(perfluorohexylethyl)silane (vi)

vi
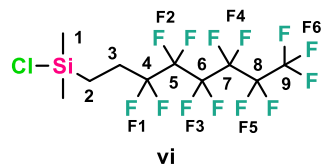
The compound was prepared according to a previously reported literature procedure.[128] Briefly, (perfluorohexyl)ethylene (4.61 mL, 20.2 mmol) and Wilkinson's catalyst (0.118 g, 0.128 mmol, 0.6 mol %) were dissolved in dry C_6H_6 (20 mL) in the dark and after stirring for 15 min, HMe_2SiCl (4.50 mL, 40.5 mmol) was added in dropwise. The stirring yellow solution was refluxed for 2.5 h, and after cooling, the excess HMe_2SiCl and C_6H_6 were distilled at ambient pressure. Flame distillation under reduced pressure (120 °C, 5 mmHg) afforded the air and moisture-sensitive product as a clear colourless liquid. Yield: 90 % (7.98 g). **^{1}H NMR** (400 MHz, C_6D_6) δ: 1.98-2.07 (m, 2H, H3), 0.73-0.77 (m, 2H, H2), 0.06 (s, 6H, H1) ppm; **^{13}C {^{1}H} NMR** (101 MHz, C_6D_6) δ: 25.55 (t, $^2J_{C-F}$ = 23.7 Hz, C3) 8.66 (t, $^3J_{C-F}$ = 3.1 Hz, C2), 0.76 (C1) ppm; **^{29}Si {^{1}H} NMR** (79 MHz, C_6D_6) δ: 30.65 ppm; **^{19}F {^{1}H} NMR** (376 MHz, C_6D_6) δ: -81.31, -115.63, -122.00, -122.99, -123.28, -126.35 ppm. NMR spectral data agreed well with literature values.[145]

4.2.10 Synthesis of 2-(dimethyl(perfluorohexylethyl)silyl)methyl)phenyl) diphenylphosphine (vii)

vii
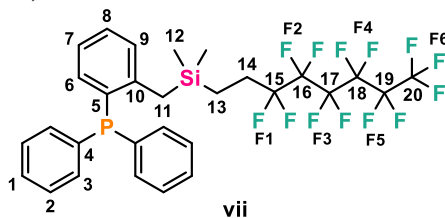
In a 50 mL Schlenk flask, a stirring suspension of **v** (0.99 g, 3.62 mmol) and TMEDA (0.70 mL, 4.71 mmol) in dry hexanes (15 mL) was cooled to 0 °C, and *n*-BuLi (2.58 mL, 1.42 M in hexanes, 3.62 mmol) was added dropwise, the addition of which turned the suspension orange. After stirring at 0 °C for 2 h, a solution of **vi** (1.52 g, 3.62 mmol) in dry hexanes (5 mL) was run in *via* cannula transfer, discharging the orange colour slowly. The mixture was stirred for 18 h, then quenched with the addition of degassed H_2O (20 mL). The organic layer was extracted *via* cannula transfer, and the aqueous layer washed with dry hexanes (2×20 mL). The organic extracts were combined, filtered over $MgSO_4$, and concentrated *in vacuo*. The resulting orange oil was transferred to a sublimation chamber and impurities were sublimed out from the product (120 °C, 5 mmHg), affording the product as a viscous, orange-coloured gel. Yield: 50 % (1.24 g). **^{1}H NMR** (400 MHz, C_6D_6) δ: 7.36 (d, $^3J_{HH}$ = 7.68 Hz, $^4J_{HH}$ = 1.7 Hz, 4H, H7), 6.99-7.09 (m, 9H, H1–H5, H9 overlap), 6.81-6.89 (m, 2H, H6 + H8 overlap), 2.33 (s, 2H, H11), 1.87-2.00 (m, 2H, H14), 0.76-0.81 (m, 2H, H13), 0.09 (s, 6H, H12) ppm; **^{13}C {^{1}H} NMR** (101 MHz, C_6D_6) δ: 142.56 (d, $^1J_{C-P}$ = 25.7 Hz, C5) 137.16 (d, $^3J_{C-P}$ = 11.4 Hz, C4), 136.79 (d, $^3J_{C-P}$ = 12.8 Hz, C10), 134.46 (d, $^1J_{C-P}$ = 19.8 Hz, C7), 133.31 (C1), 130.50 (d, $^2J_{C-F}$ = 4.4 Hz, C6), 128.95 (d, $^3J_{C-F}$ = 15.0 Hz, C2), 128.93 (d, $^2J_{C-F}$ = 1.8 Hz, C3 + C9 overlap), 126.48 (C8), 25.58 (t, $^2J_{C-F}$ = 23.7 Hz, C14) 25.58 (t, $^2J_{C-F}$ = 23.7 Hz, C14), 21.34 (d, $^2J_{C-P}$ = 21.3 Hz, C11), 7.56 (C13), -0.28 (C14) ppm; **^{29}Si {^{1}H} NMR** (79 MHz, C_6D_6) δ: 30.65 ppm. **HRMS (DART)** (m/z): [M + H$^+$] for $C_{29}H_{26}F_{13}SiP$: calculated 681.1407; found 681.1403.

4.2.11 Synthesis of Synthesis of (3-(4-benzoylphenoxy)propyl)diphenyl (tridecafluorohexylethyl))phosphonium bromide (4)
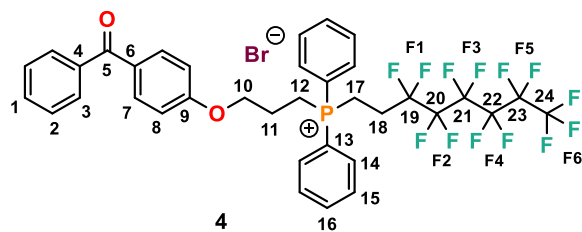
Under Ar (g), to a flame dried 100 mL Schlenk, 0.924 g (2.89 mmol) of **i** and 1.40 g (2.63 mmol) of **ii** were added. The mixture was stirred at 120 °C for 24 h, then cooled to R.T. The solid was dissolved in 5 mL MeCN, and the product precipitated as an oily residue from 80 mL of cold Et$_2$O. The Et$_2$O was decanted, and the product washed again with Et$_2$O (2 × 50 mL). Volatiles were removed *in vacuo*, yielding the product as a fine off-white coloured powder. Yield: 84 % (1.87 g). **^{1}H NMR** (400 MHz, CDCl$_3$) δ: 7.99-8.04 (m, 4H, H15), 7.84 (t, $^3J_{HH}$ = 7.4 Hz, 2H, H16), 7.71- 7.77 (m, 8H, H3 + H7 + H14 overlap), 7.56 (t, $^3J_{HH}$ = 7.3 Hz, 1H, H1), 7.46 (t, $^3J_{HH}$ = 7.5 Hz, 2H, H2), 6.89 (d, $^3J_{HH}$ = 8.3 Hz, 2H, H8), 4.24-4.28 (m, 2H, H10), 3.88-4.03 (m, 2H, H12), 3.78-3.84 (m, 2H, H17), 2.40-2.54 (m, 2H, H18), 2.04-2.19 (m, 2H, H11) ppm; **^{13}C {^{1}H} NMR** (101 MHz, CDCl$_3$) δ: 195.61 (C5), 161.73 (C9), 138.15 (C4), 135.57 (d, $^4J_{C\text{-}P}$ = 3.3 Hz, C16), 133.40 (d, $^3J_{C\text{-}P}$ = 9.9 Hz, C15), 132.59 (C7), 132.12 (C1), 130.84 (d, $^2J_{C\text{-}P}$ = 12.5 Hz, C14), 130.69 (C6), 129.81 (C3), 128.32 (C2), 116.34 (d, $^1J_{C\text{-}P}$ = 83.6 Hz, C13), 114.24 (C8), 66.84 (d, $^3J_{C\text{-}P}$ = 16.9 Hz, C10), 24.80-24.68 (m, C18) 22.55 (d, $^2J_{C\text{-}P}$ = 3.1 Hz, C11), 19.42 (d, $^1J_{C\text{-}P}$ = 51.7 Hz, C12), 15.00 (d, $^1J_{C\text{-}P}$ = 55.4 Hz, C17) ppm; **^{31}P {^{1}H} NMR** (162 MHz, CDCl$_3$) δ: 29.81 ppm; **^{19}F {^{1}H} NMR** (376 MHz, C$_6$D$_6$) δ: -80.82, -113.41, -121.85, -122.71, -122.86, -126.15 ppm. **HRMS (ESI-TOF)** (m/z): [M$^+$ - Br] for C$_{36}$H$_{29}$F$_{13}$O$_2$P: calculated 771.1692; found 771.1688.

4.2.12 (3-(4-benzoylphenoxy)propyl)(2-((dimethyl (tridecafluorohexylethyl))silyl)methyl)phenyl)diphenylphosphonium

5
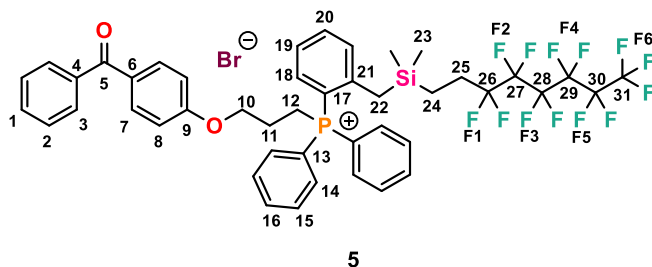
Under Ar (g), to a flame dried 100 mL Schlenk, 0.400 g (1.25 mmol) of **i** and 0.705 g (1.00 mmol) of **vii** were added. The mixture was stirred at 120 °C for 24 h, then cooled to room temperature. The solid was dissolved in 5 mL MeCN, and the product was precipitated as an oily residue with 50 mL of cold Et$_2$O. The Et$_2$O was decanted, and the product was washed again with Et$_2$O (2 × 30 mL). Volatiles were removed *in vacuo*, yielding the product as a sticky, off-white coloured solid. Yield: 58 % (0.72 g). **^{1}H NMR** (400 MHz, CDCl$_3$) δ: 7.72-7.92 (m, 20H), 7.54-7.57 (m, 4H), 7.44- 7.49 (m, 4H), 6.95-6.98 (m, 4H), 4.48 (t, $^3J_{HH}$ = 5.8 Hz, 2H, H10), 3.99-4.11 (m, 2H, H12), 2.16-2.28 (m, 2H, H11) ppm; **^{31}P {^{1}H} NMR** (162 MHz, CDCl$_3$) δ: 24.49 ppm; **^{19}F {^{1}H} NMR** (376 MHz, C$_6$D$_6$) δ: -80.76, -116.00, -121.91, -122.86, -123.27, -126.10 ppm.

Appendix A – NMR spectra for synthesized compounds
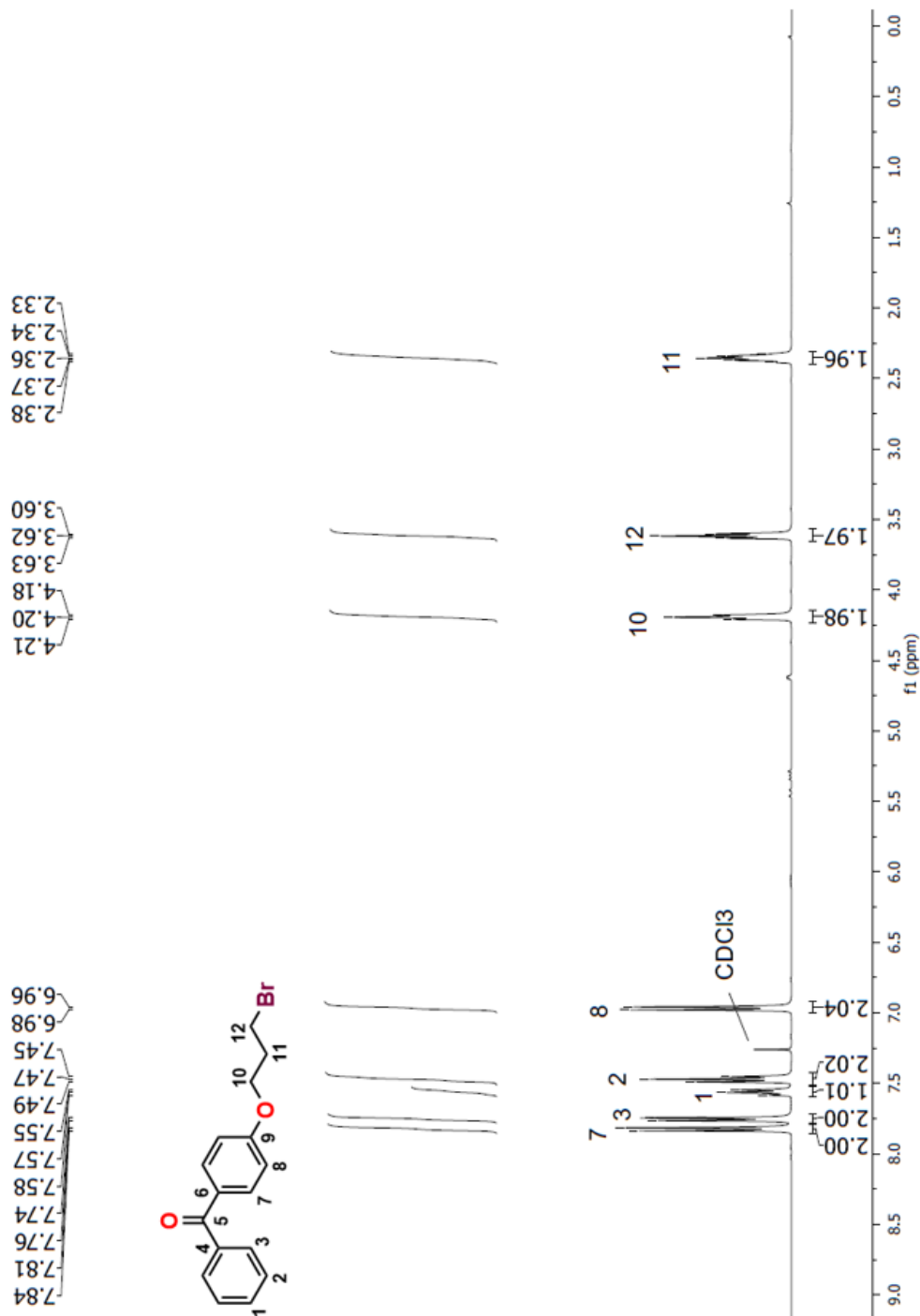
Figure A 1. ^{1}H NMR (CDCl$_3$) spectrum of **i.**
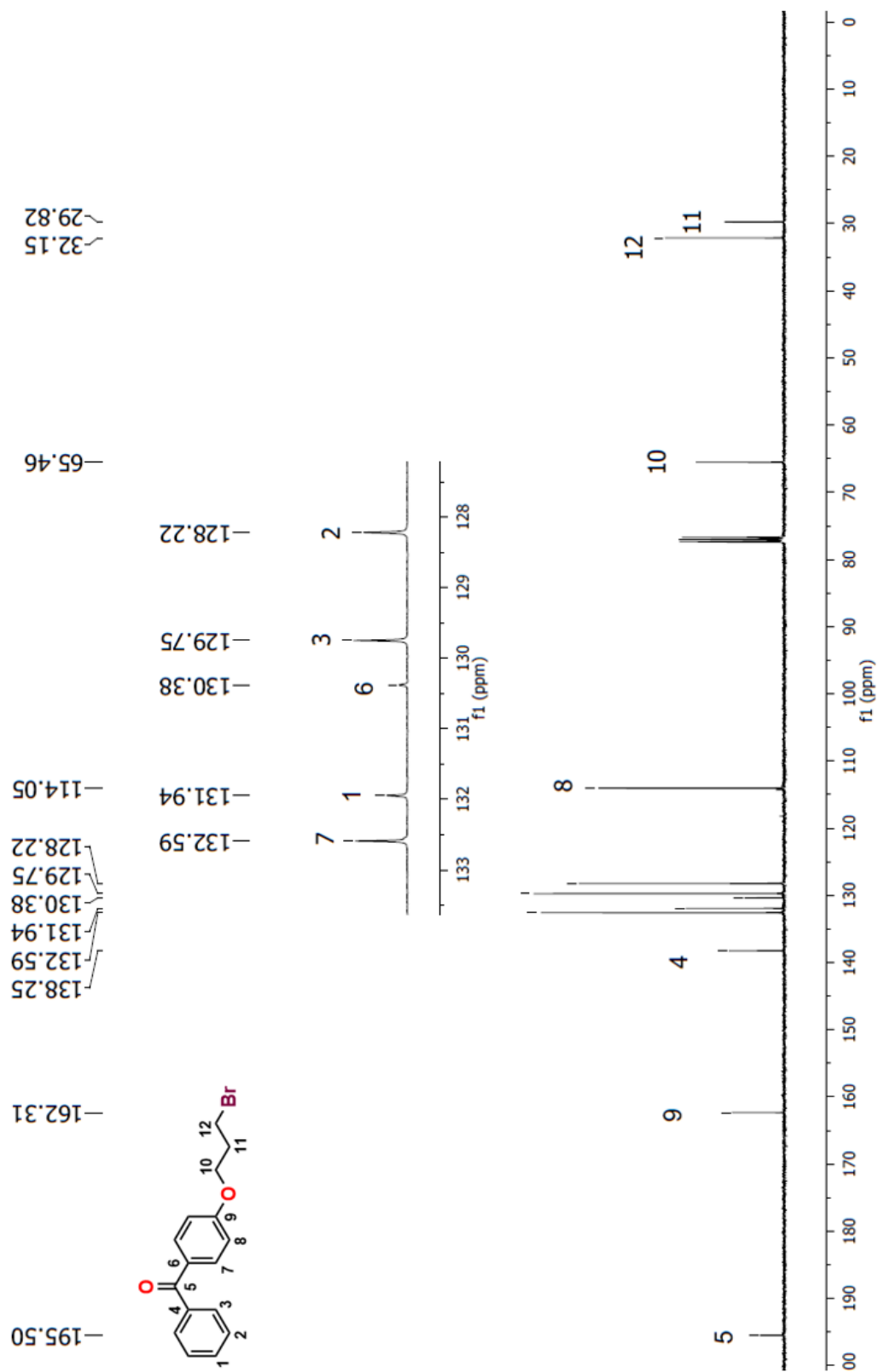
Figure A 2. ^{13}C {^1H} NMR (CDCl$_3$) spectrum of **i.**
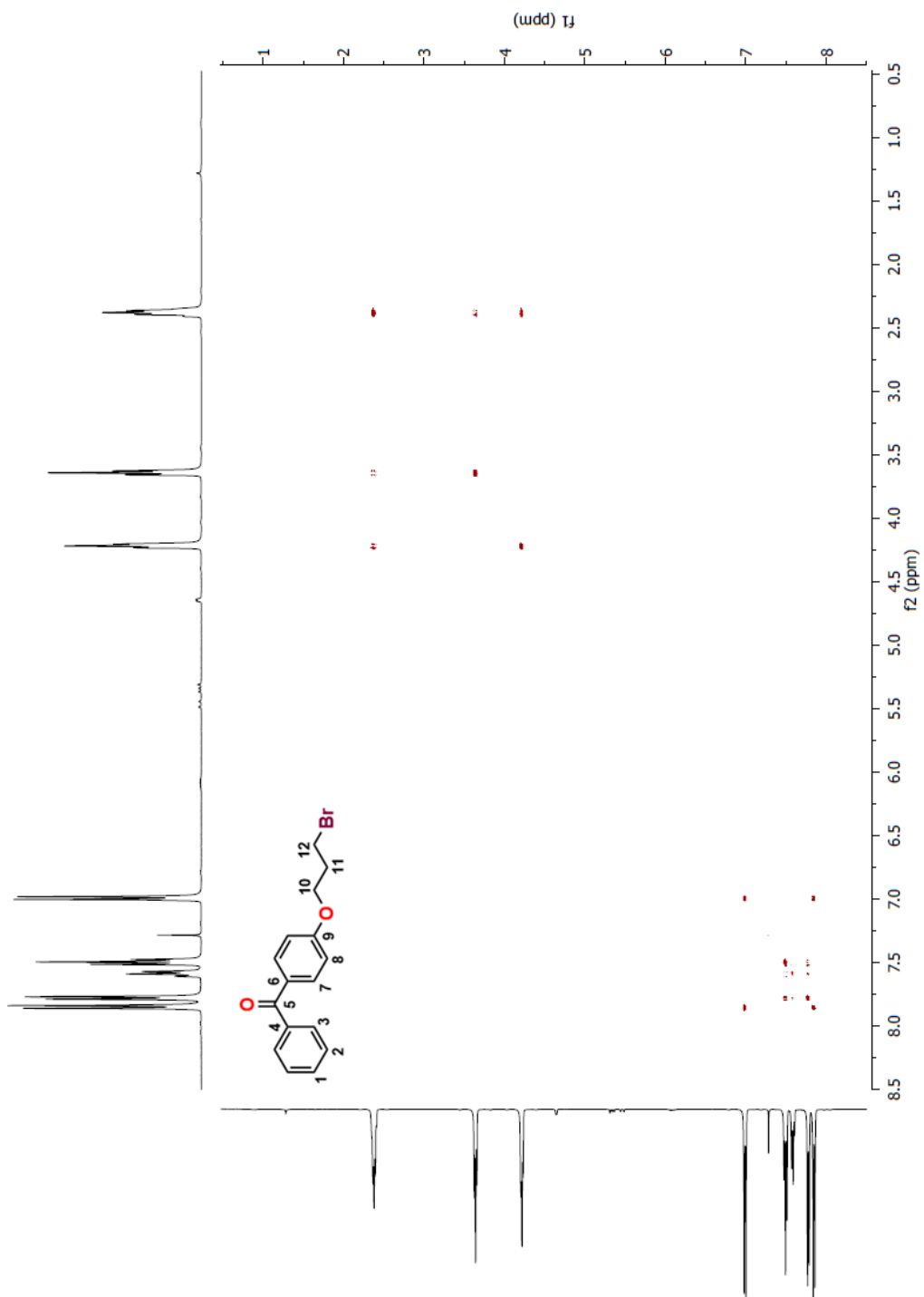
Figure A 3. 2D COSY NMR (CDCl₃) spectrum of **i.**
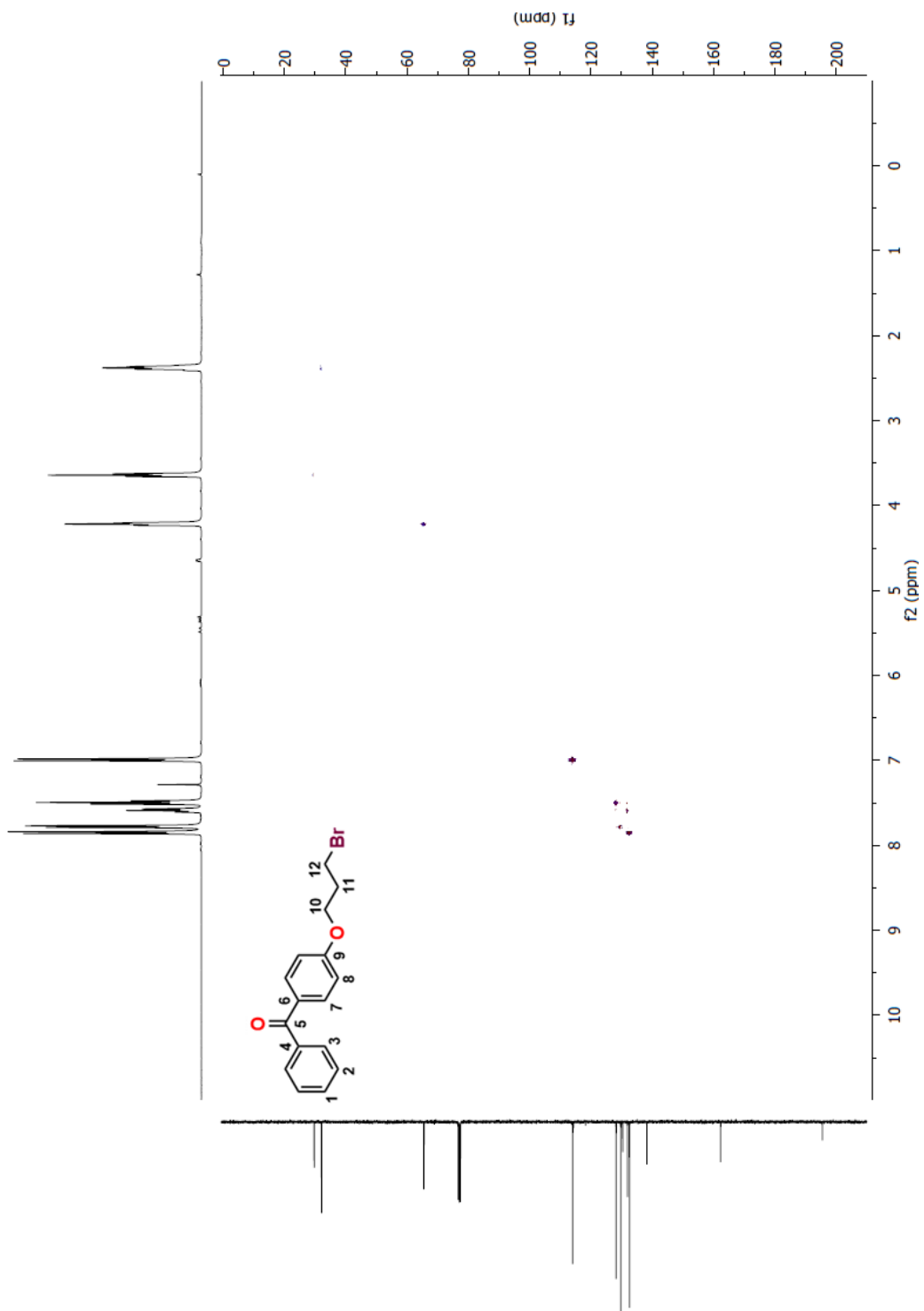
Figure A 4. 2D HSQC NMR (CDCl$_3$) spectrum of **i.**
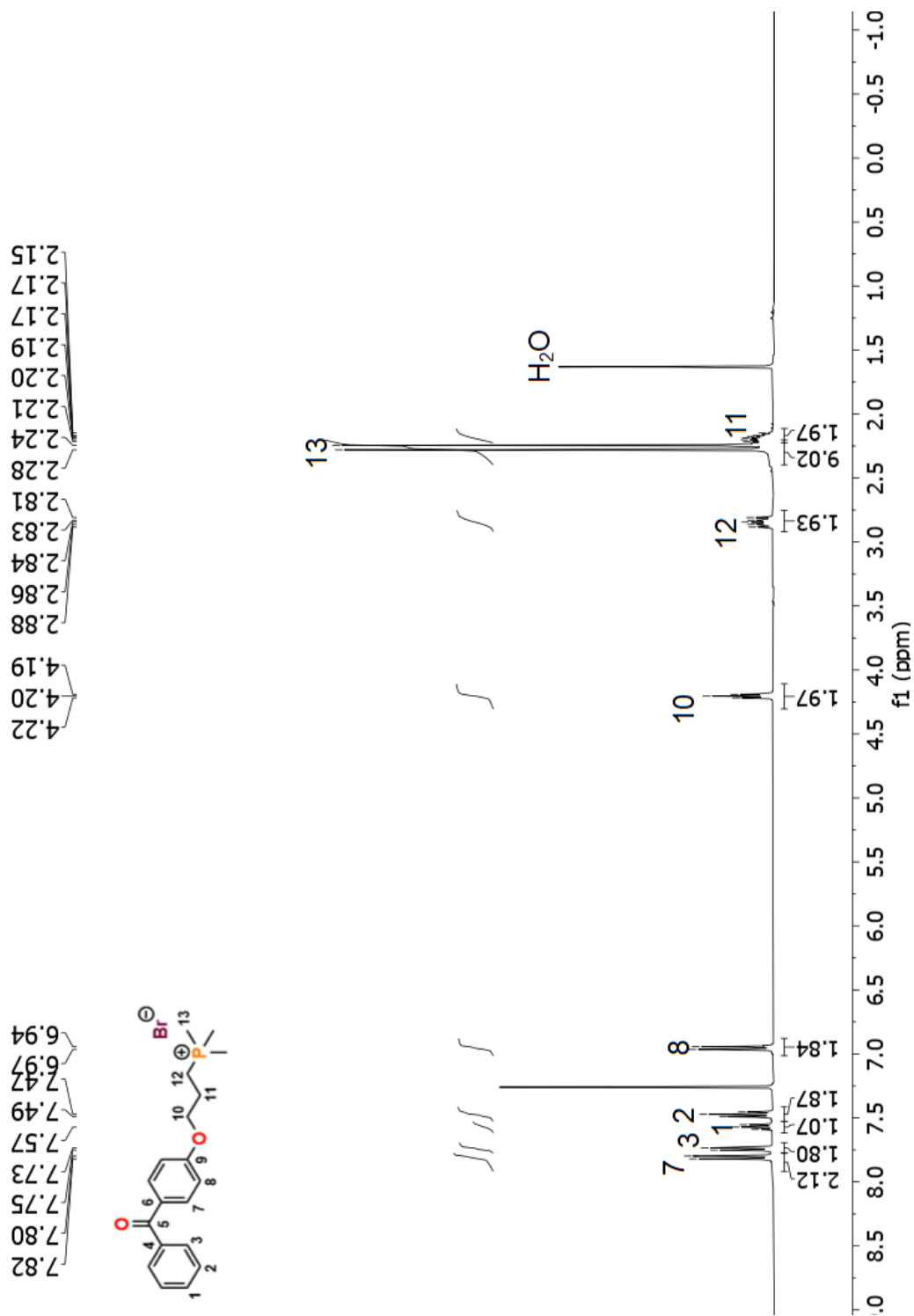
Figure A 5. ^{1}H NMR (CDCl$_3$) spectrum of **1.**
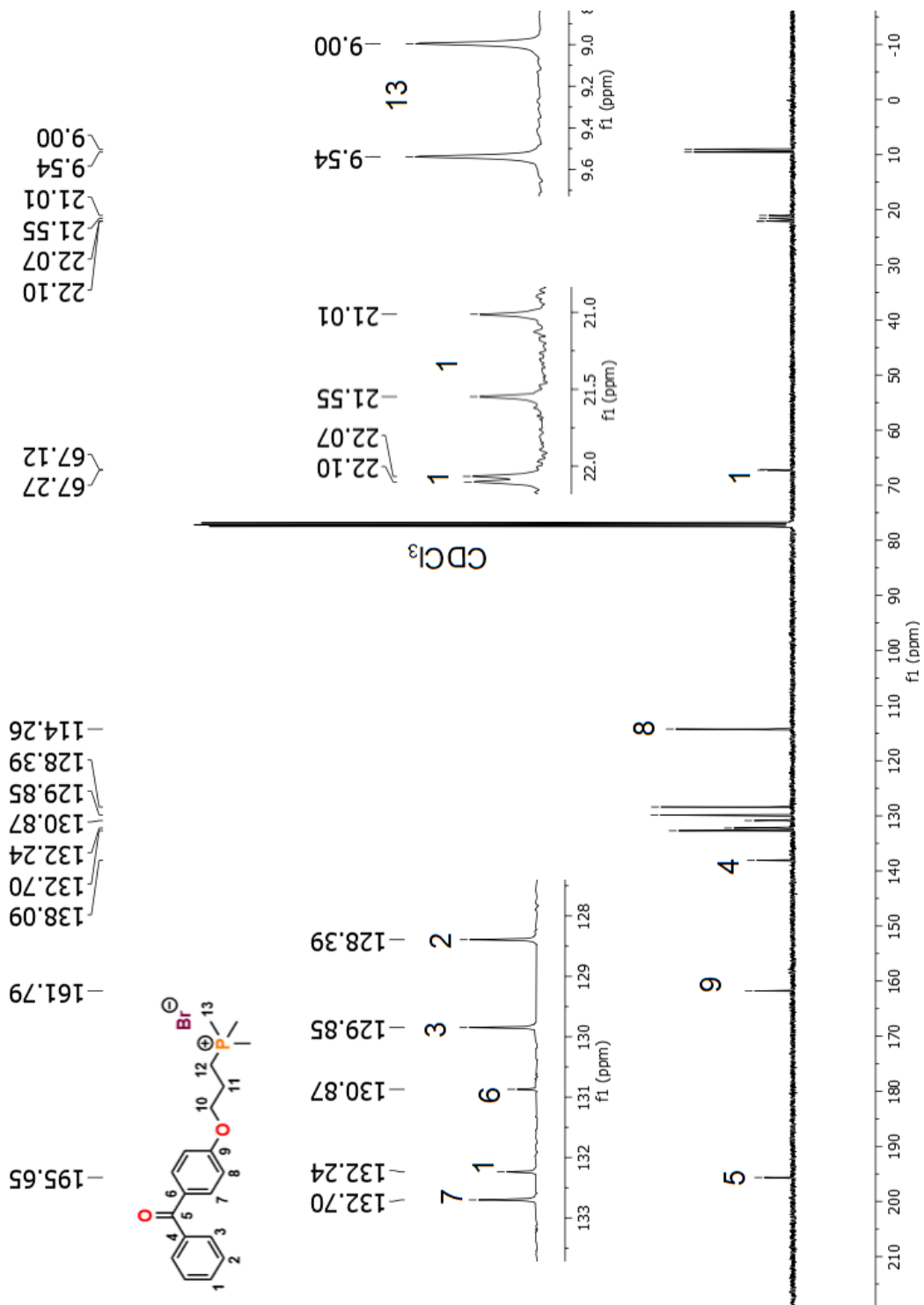
Figure A 6. $^{13}C\{^1H\}$ NMR (CDCl$_3$) spectrum of **1.**

96
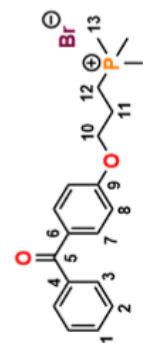
Figure A 7. ^{31}P {^{1}H} NMR (CDCl$_3$) spectrum of **1**.
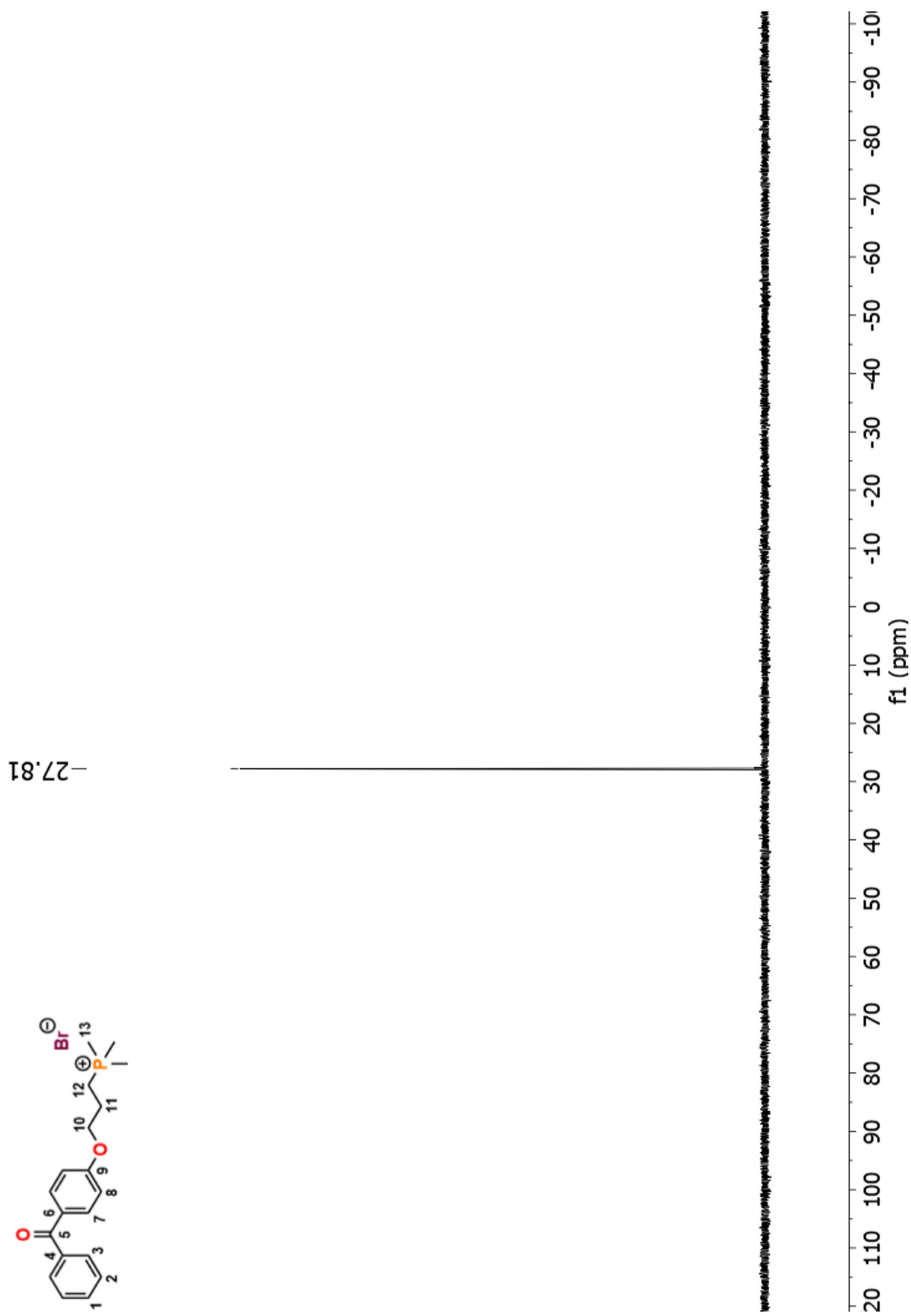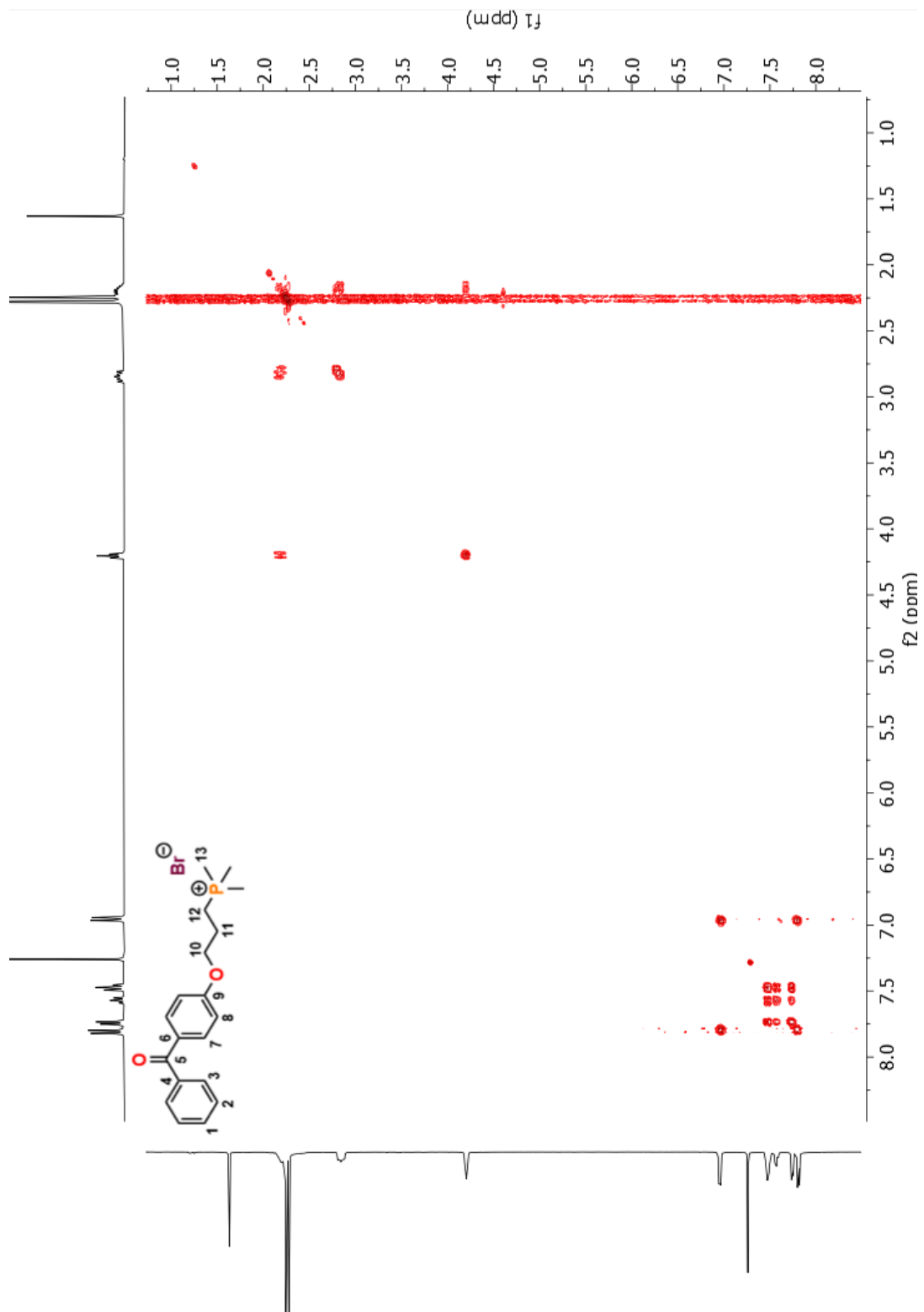
Figure A 8. 2D COSY NMR (CDCl$_3$) spectrum of **1.**
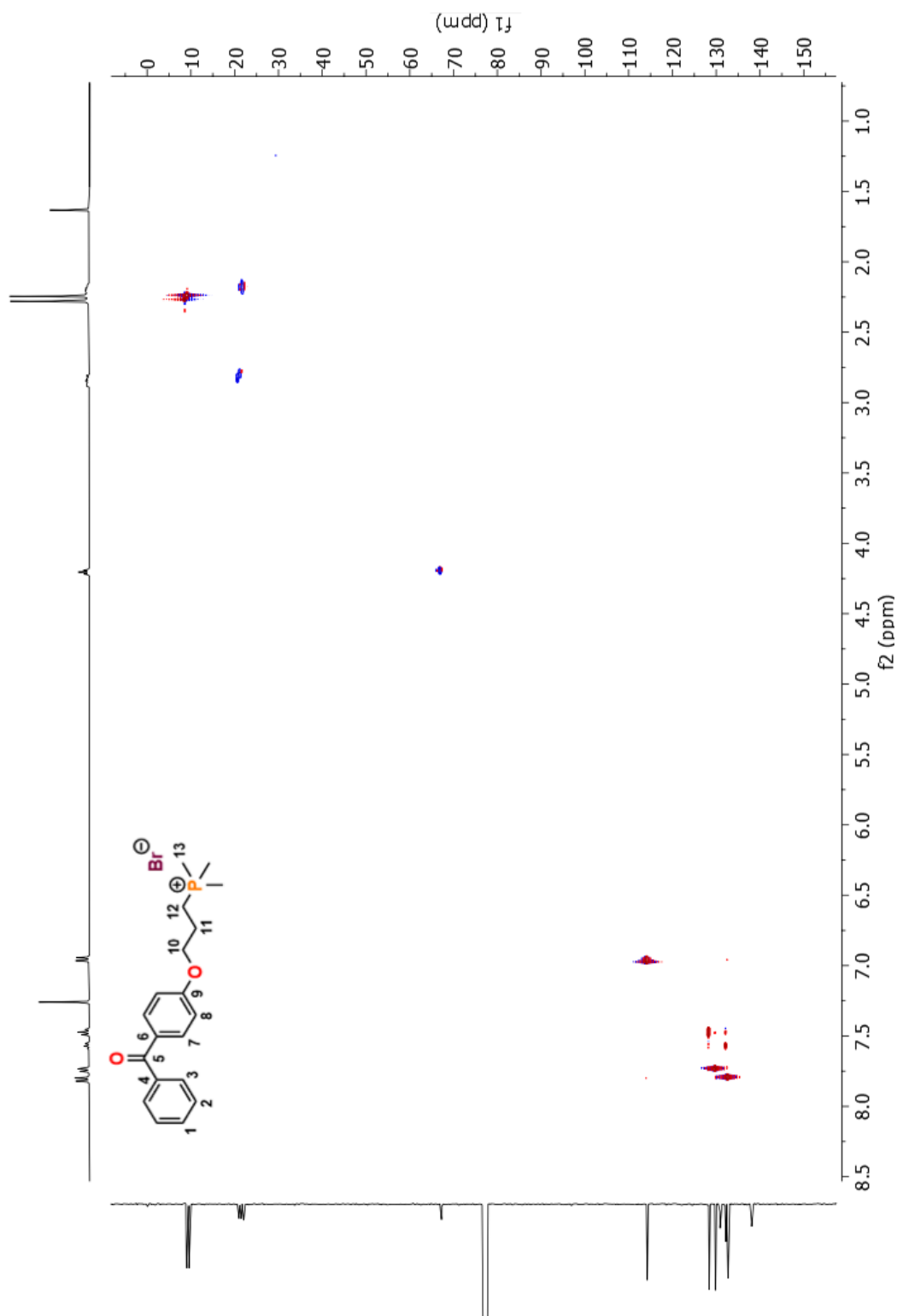
Figure A 9. 2D HSQC NMR (CDCl$_3$) spectrum of **1.**
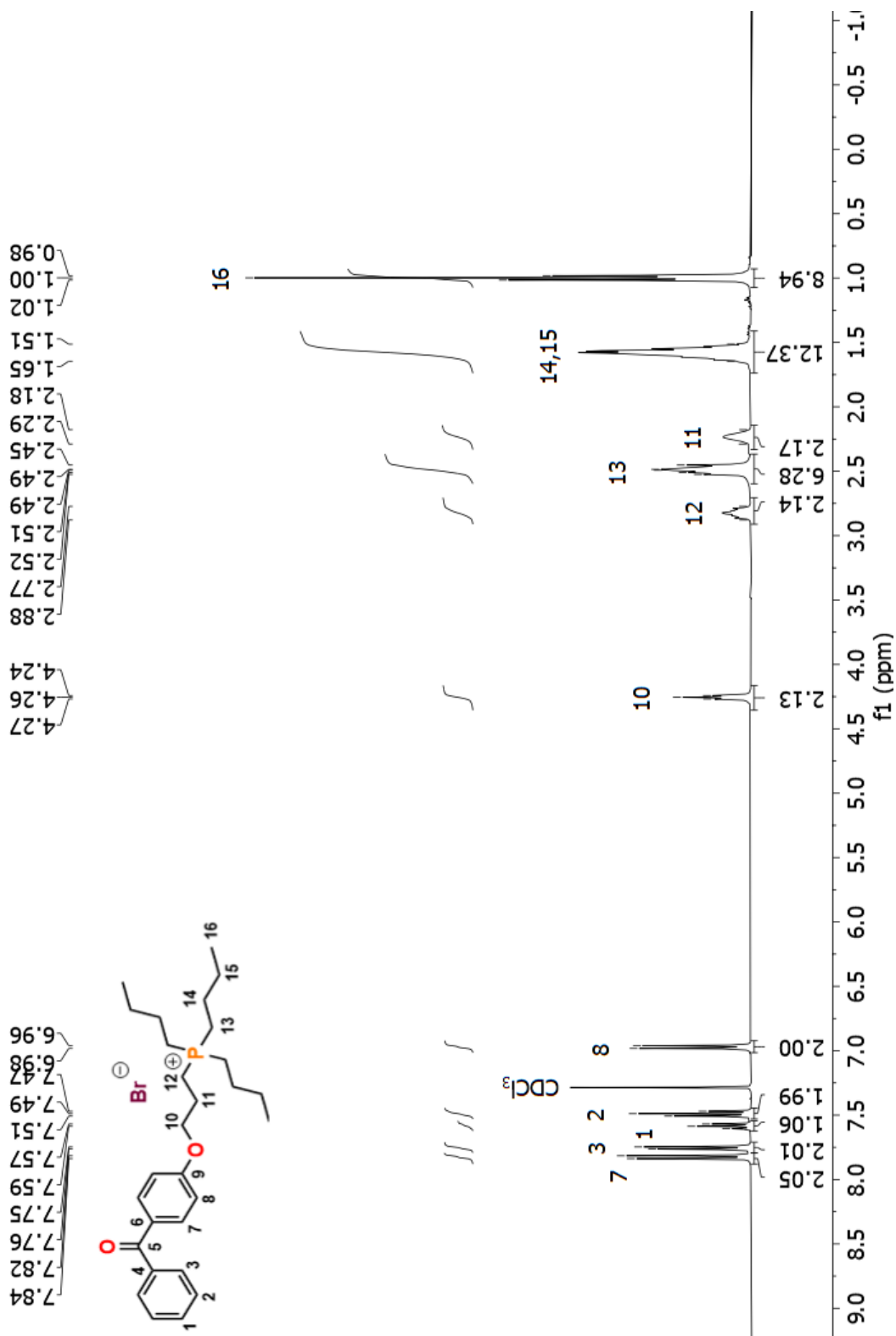
Figure A 10. ^{1}H NMR (CDCl$_3$) spectrum of **2.**
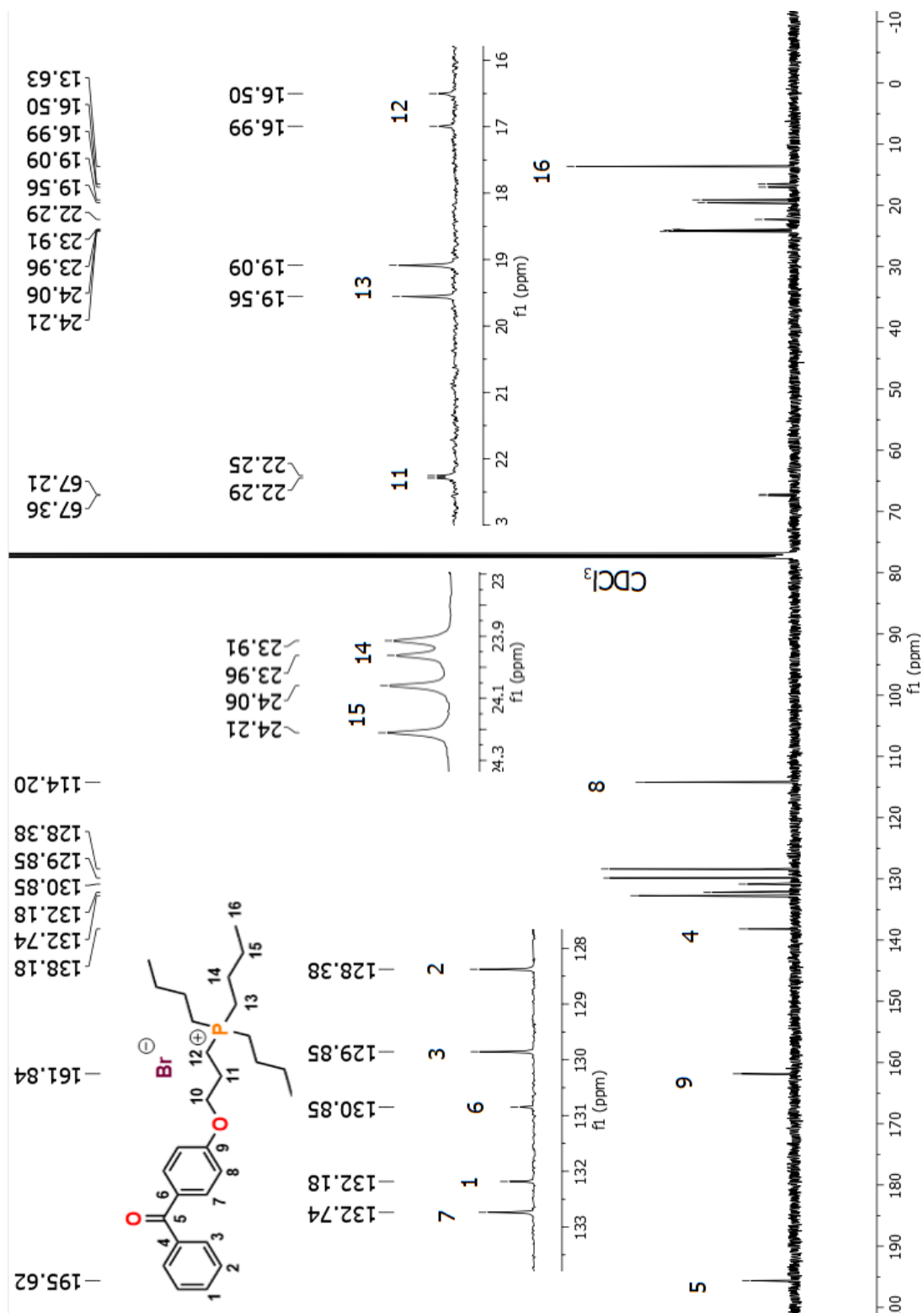
Figure A 11. ^{13}C {^1H} NMR (CDCl$_3$) spectrum of **2.**
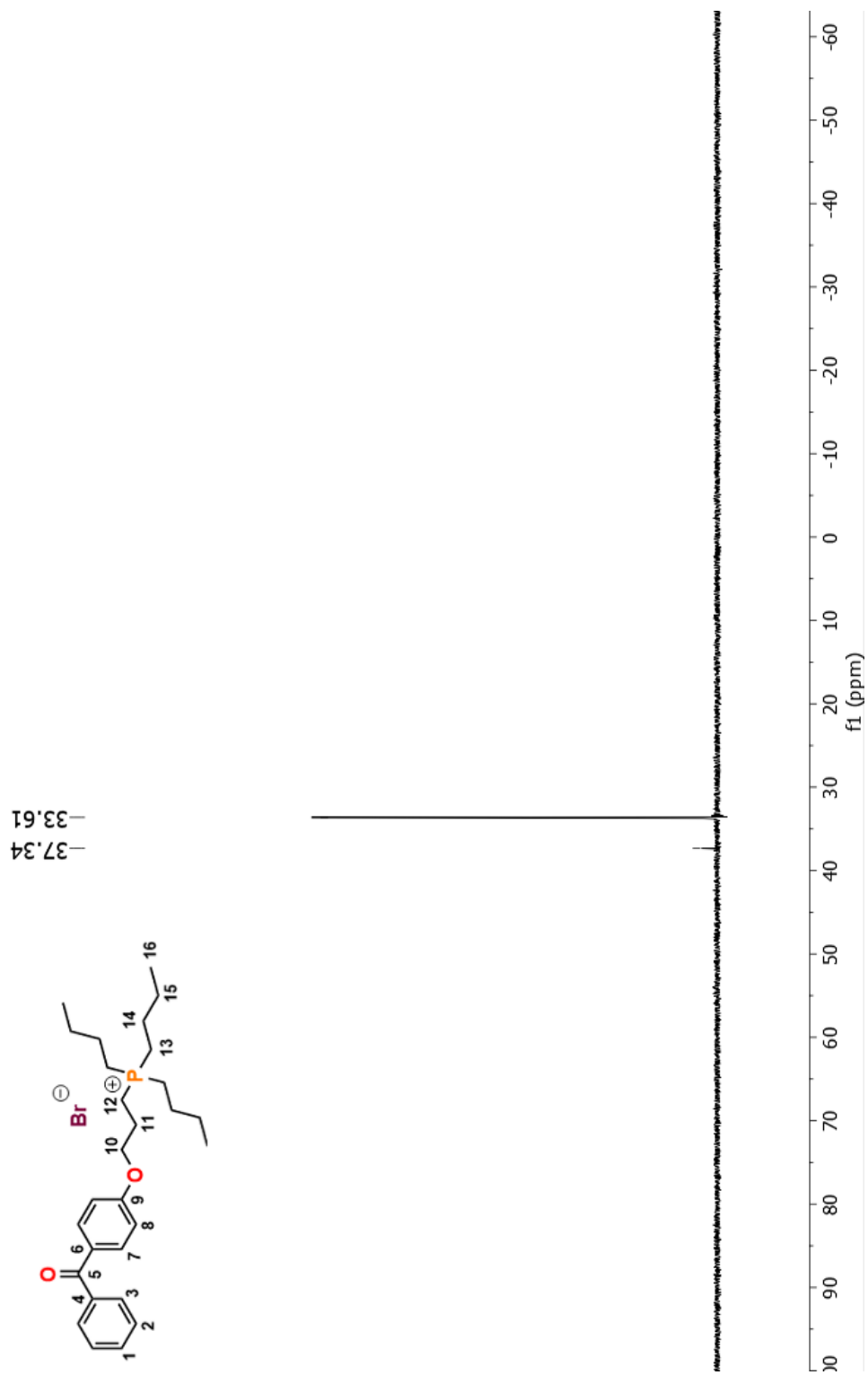
Figure A 12. ^{31}P {^1H} NMR (CDCl$_3$) spectrum of **2**.
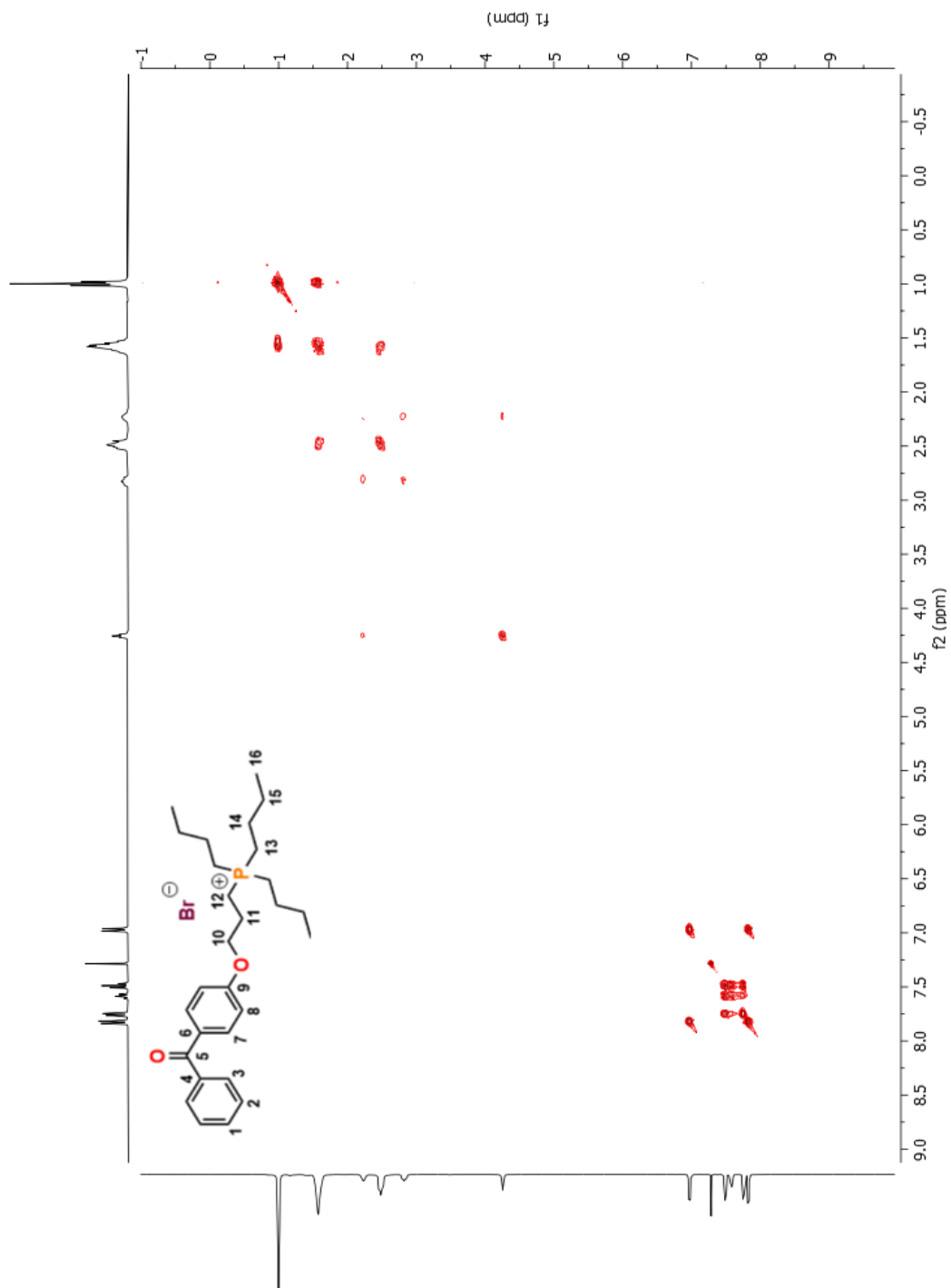
Figure A 13. 2D COSY NMR (CDCl₃) spectrum of **2.**
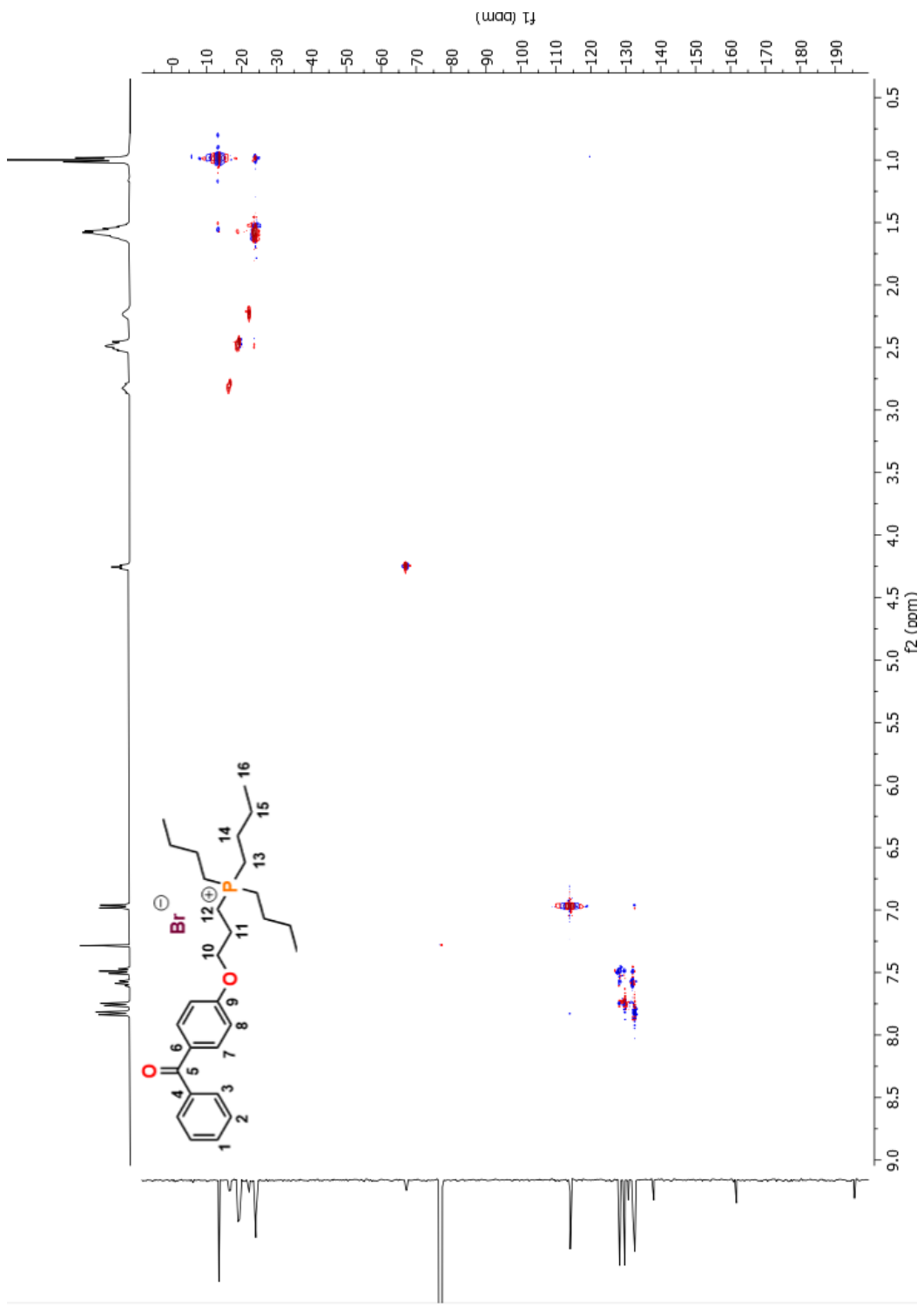
Figure A 14. 2D HSQC NMR (CDCl$_3$) spectrum of **2.**
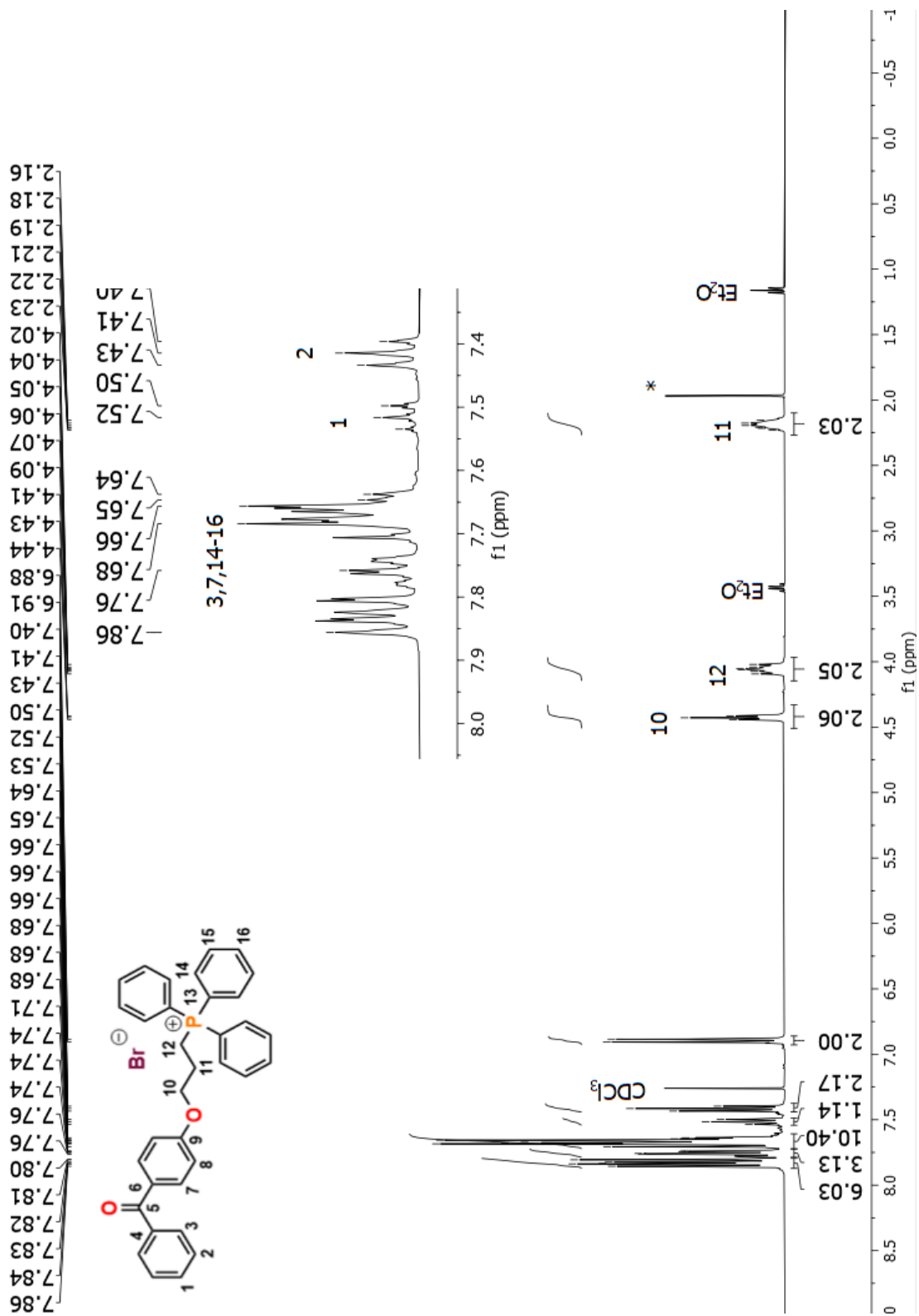
Figure A 15. ^{1}H NMR (CDCl$_3$) spectrum of **3.**
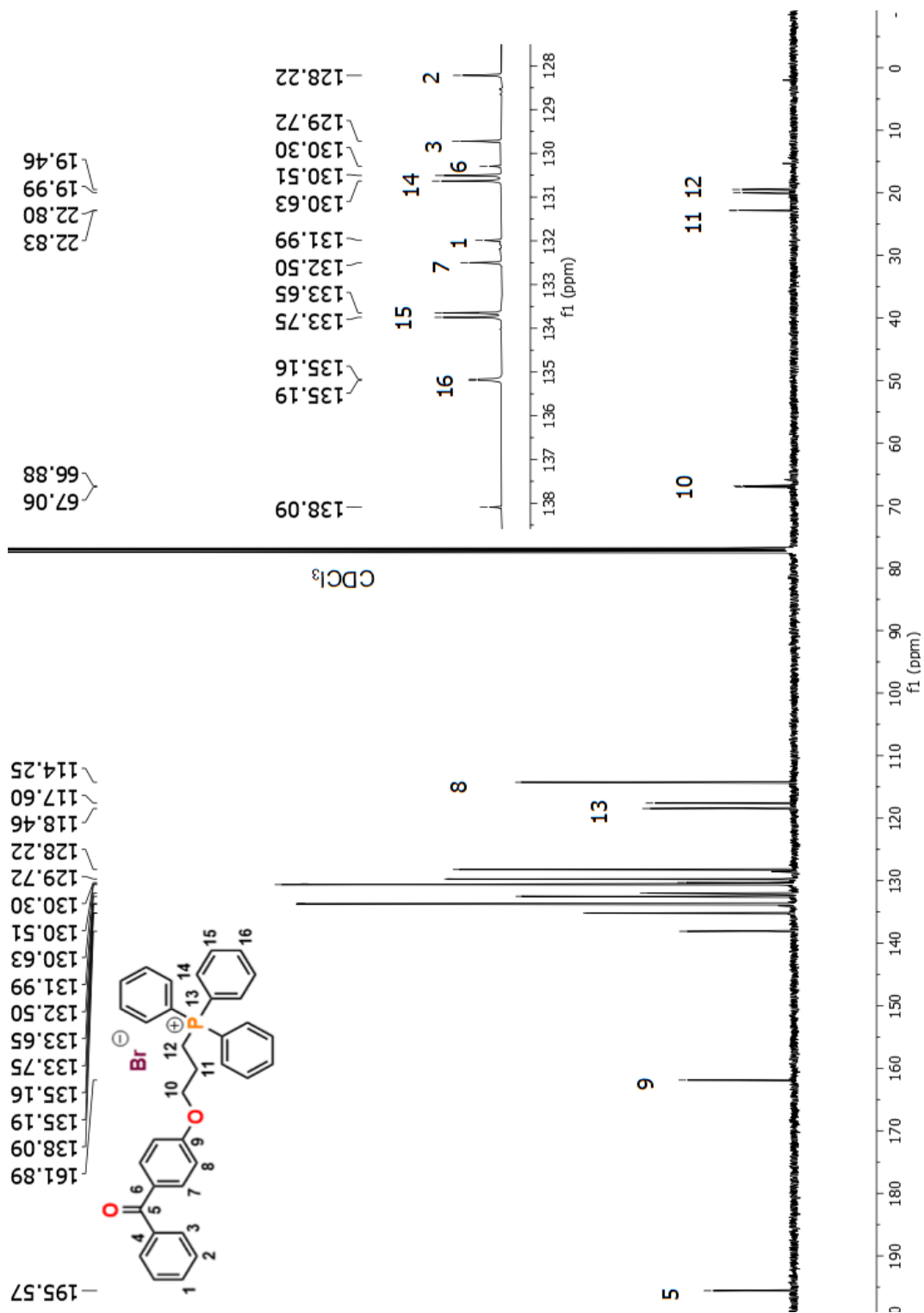
Figure A 16. ^{13}C {^{1}H} NMR (CDCl$_3$) spectrum of **3.**
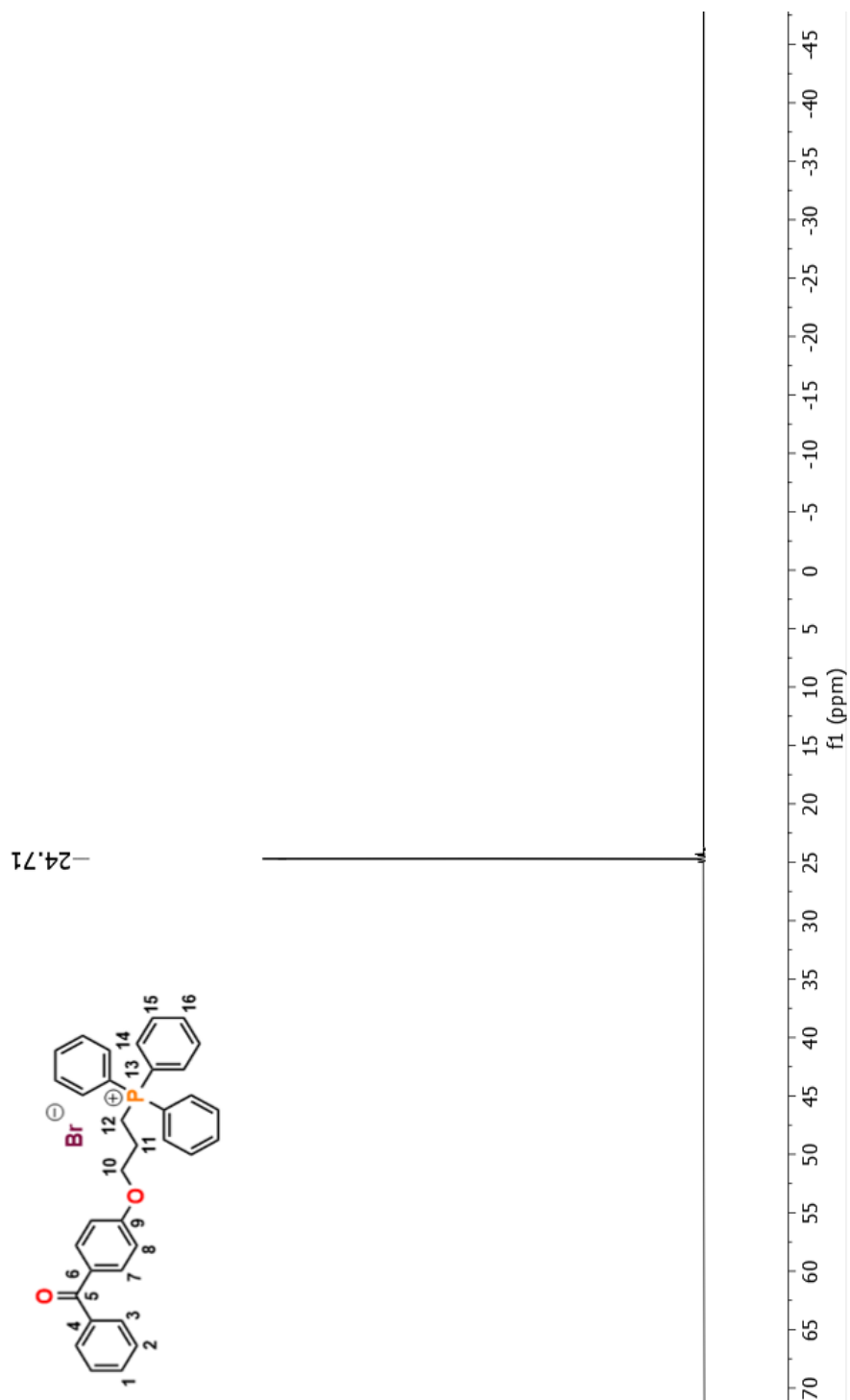
Figure A 17. ^{31}P {^1H} NMR (CDCl$_3$) spectrum of **3**.
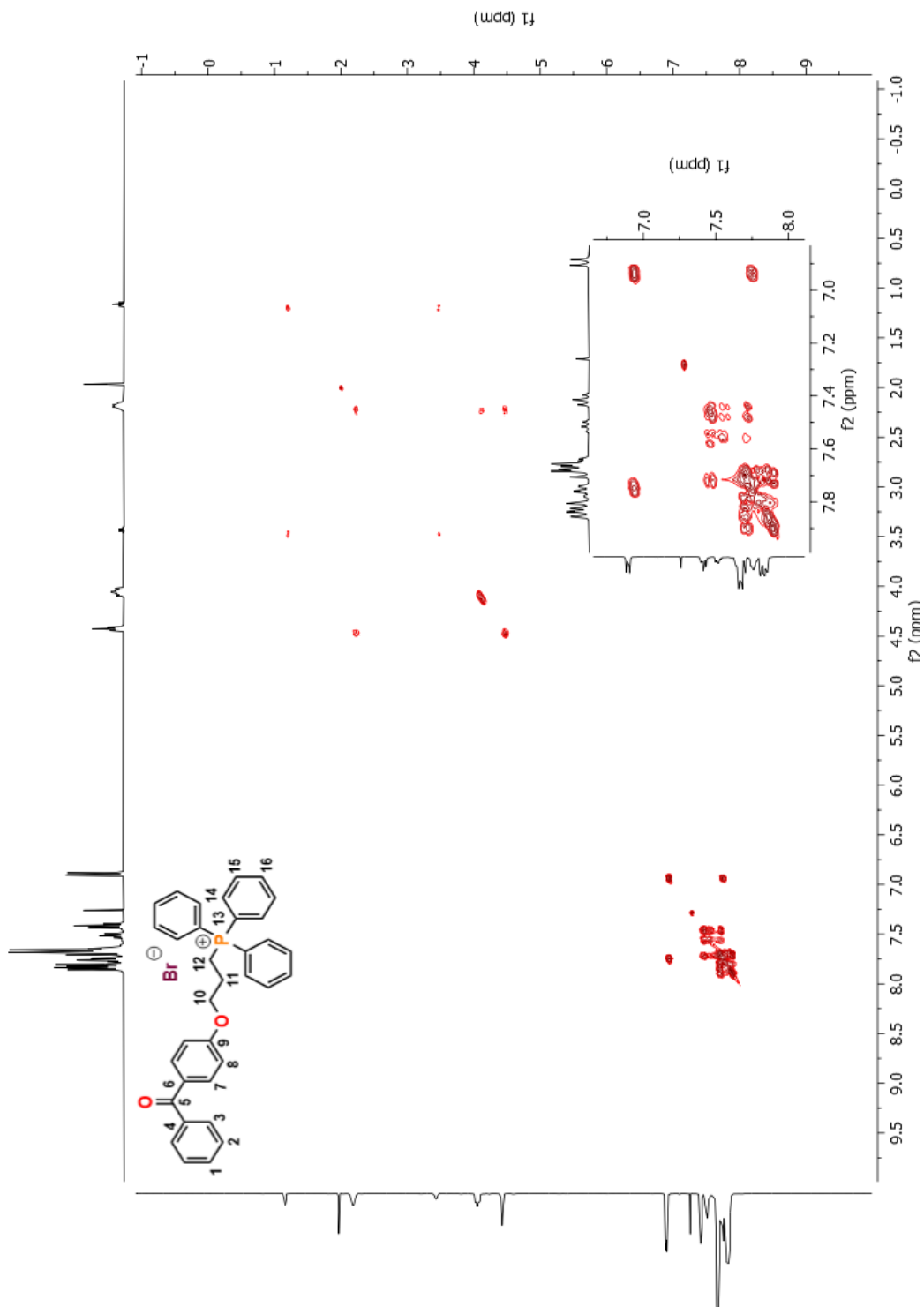
Figure A 18. 2D COSY NMR (CDCl₃) spectrum of **3.**

Figure A 19. 2D HSQC NMR (CDCl₃) spectrum of **3.**
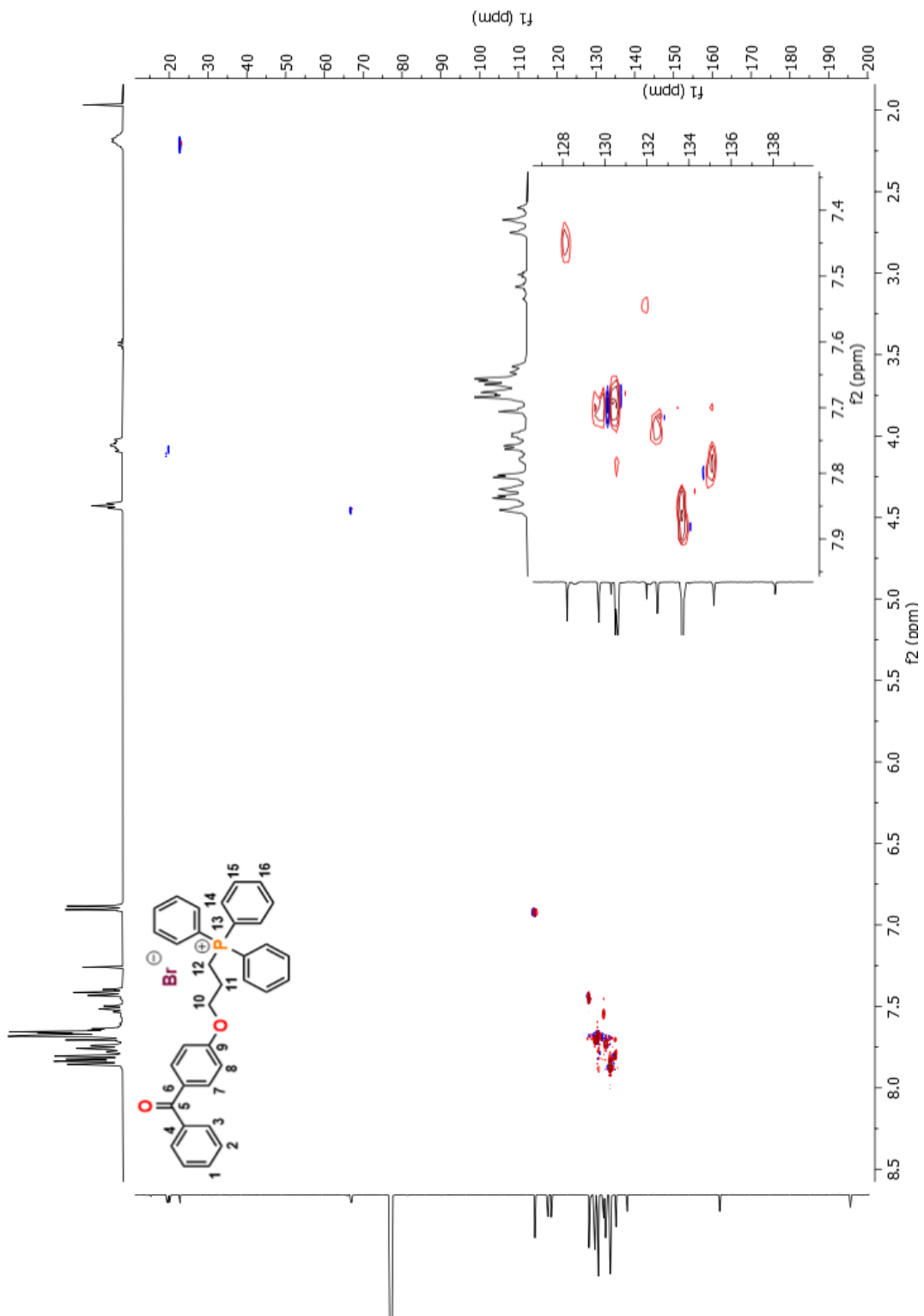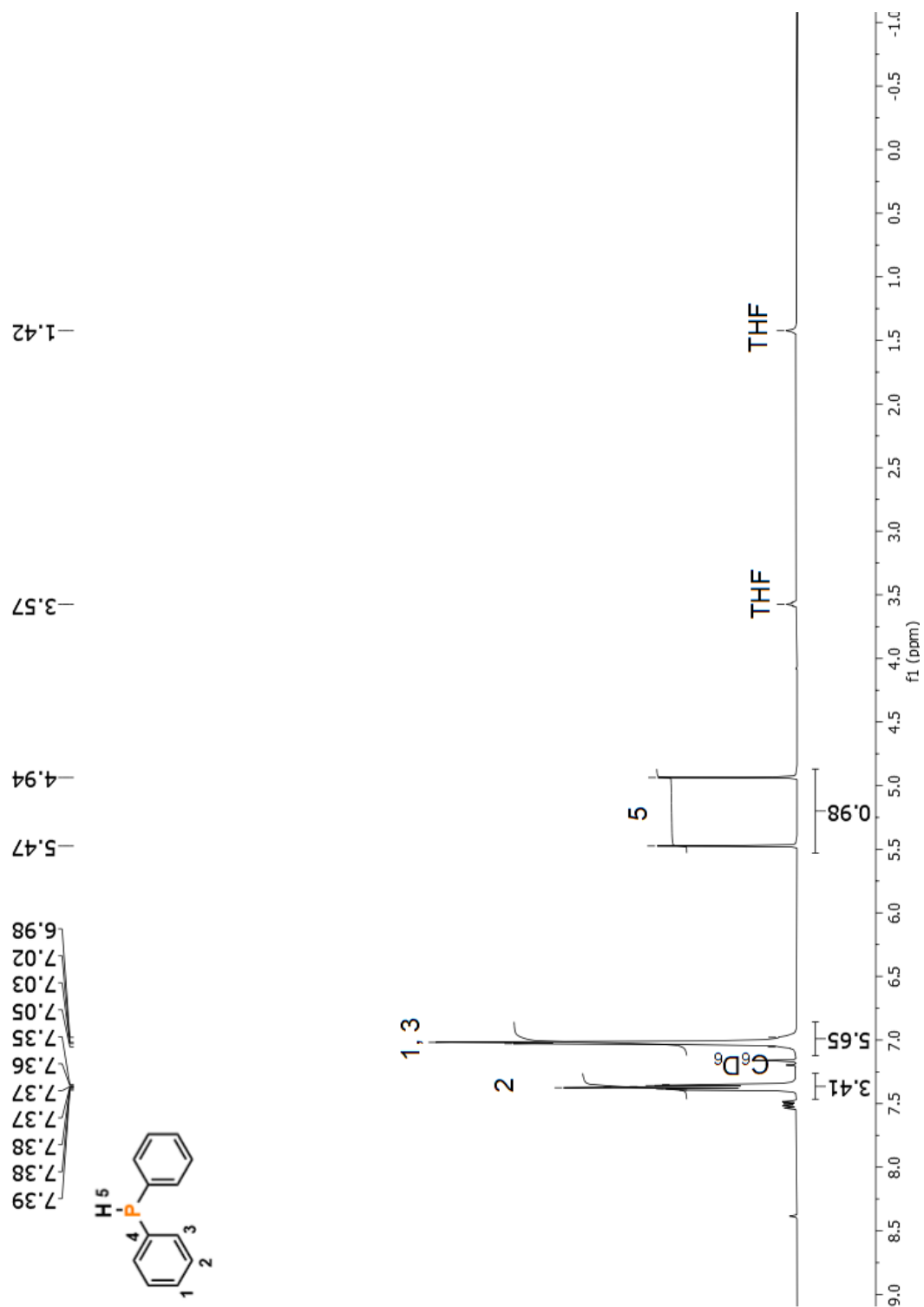
Figure A 20. ^{1}H NMR (C$_6$D$_6$) spectrum of **ii.**
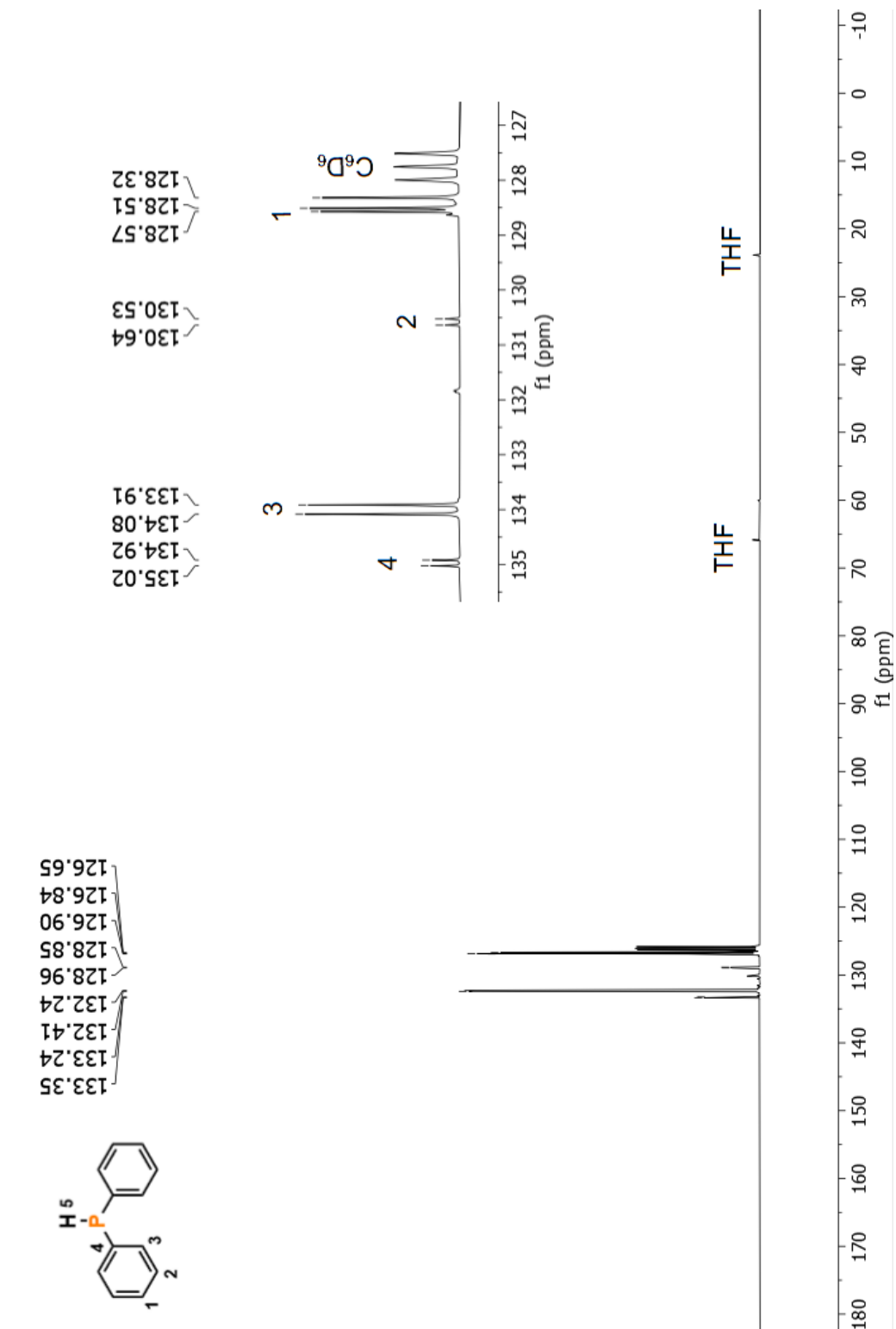
Figure A 21. $^{13}C\ \{^1H\}$ NMR (C_6D_6) spectrum of **ii.**
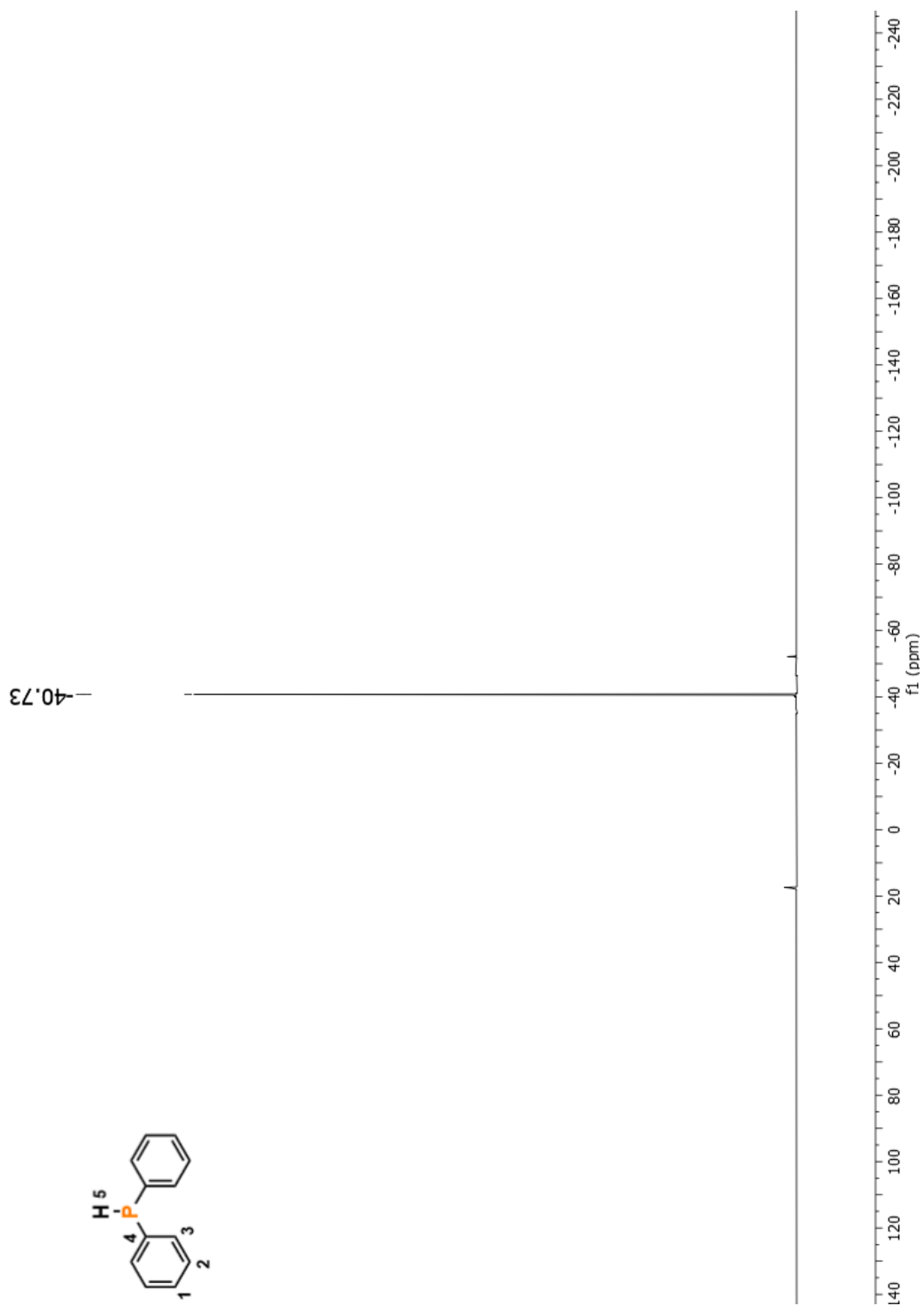
Figure A 22. ^{31}P {^1H} NMR (C$_6$D$_6$) spectrum of **ii**.

−40.73
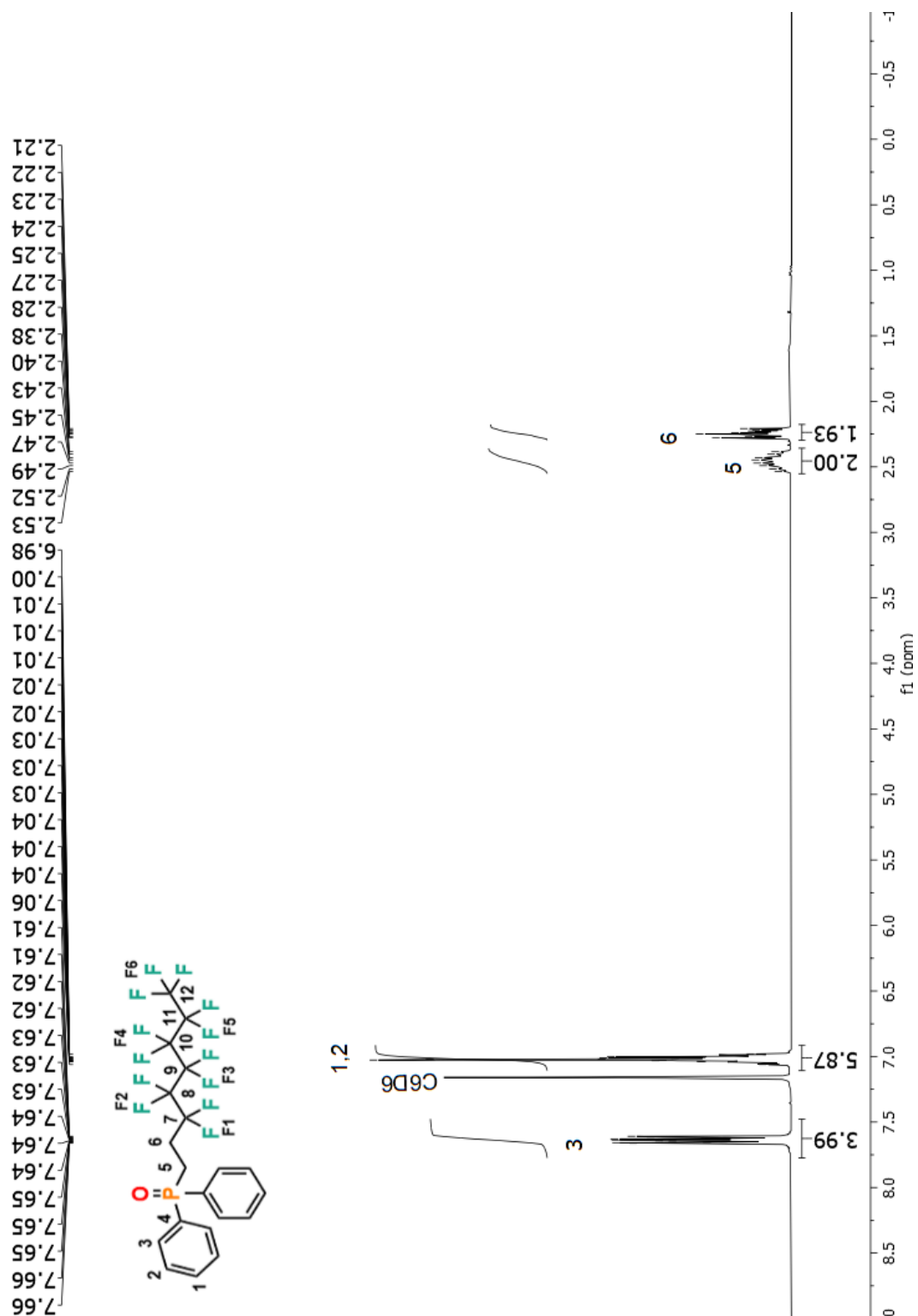
Figure A 23. ^{1}H NMR (C$_6$D$_6$) spectrum of **iii.**
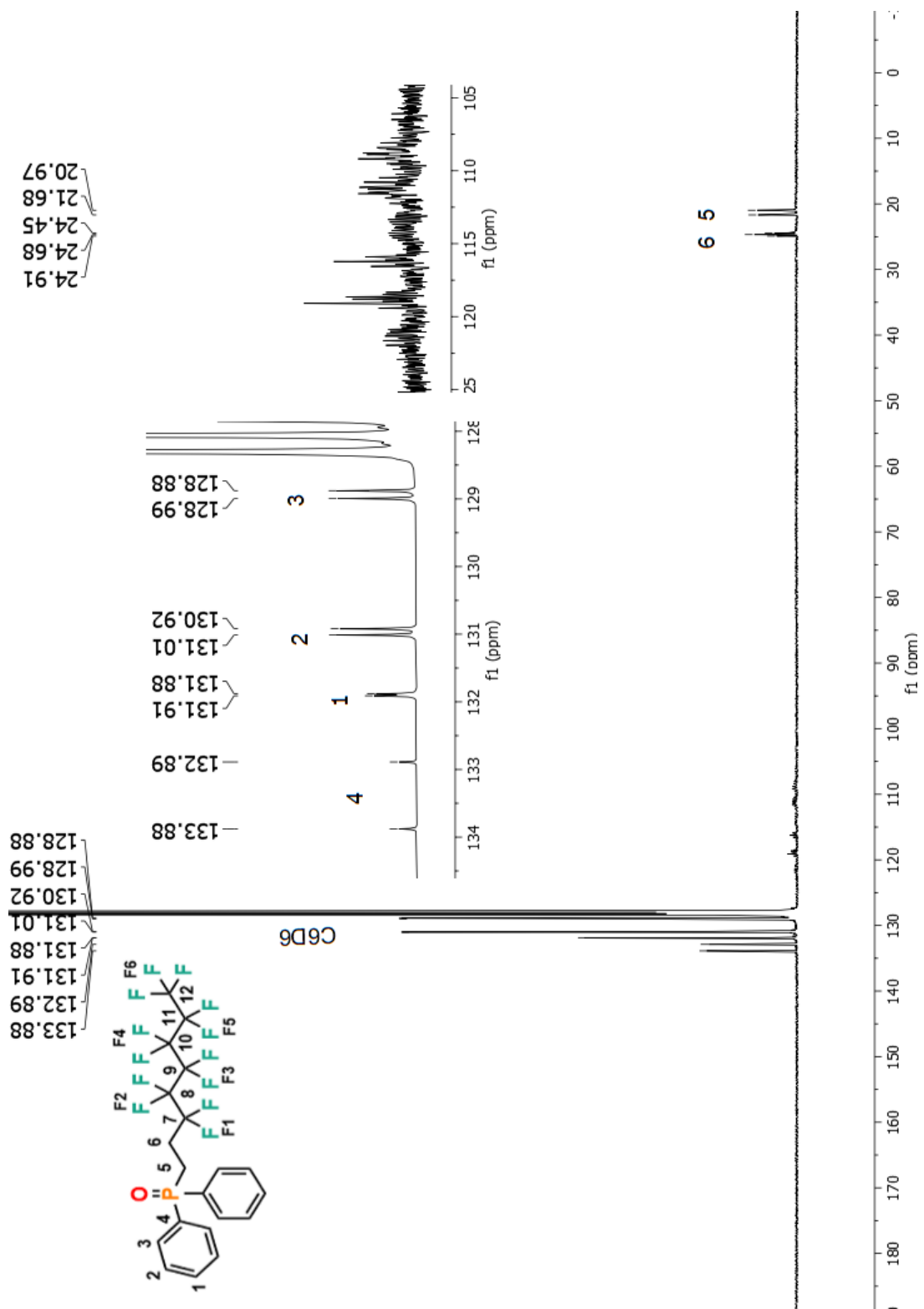
Figure A 24. $^{13}C\{^1H\}$ NMR (C_6D_6) spectrum of **iii.**
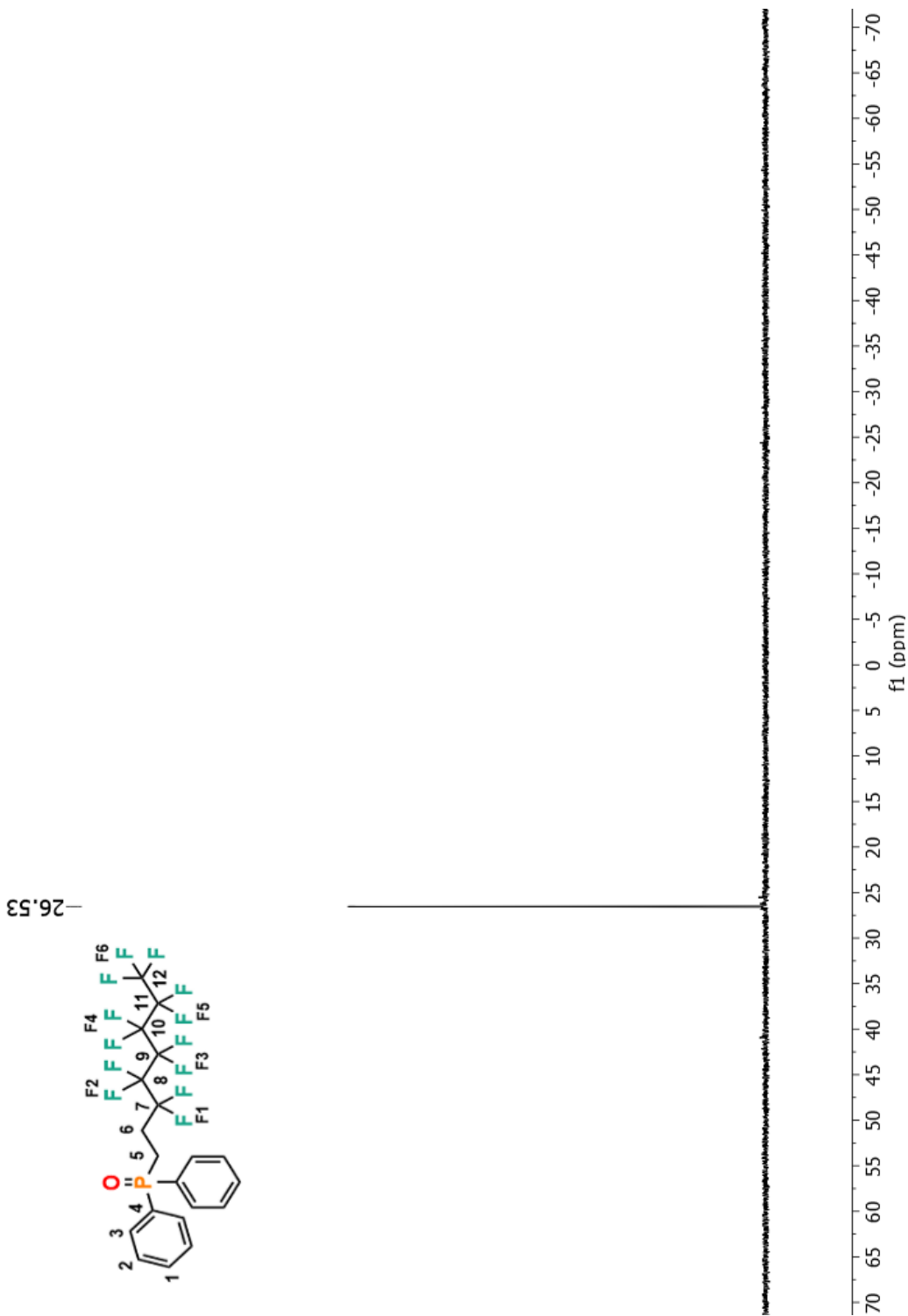
Figure A 25. ^{31}P {^{1}H} NMR (C$_6$D$_6$) spectrum of **iii**.
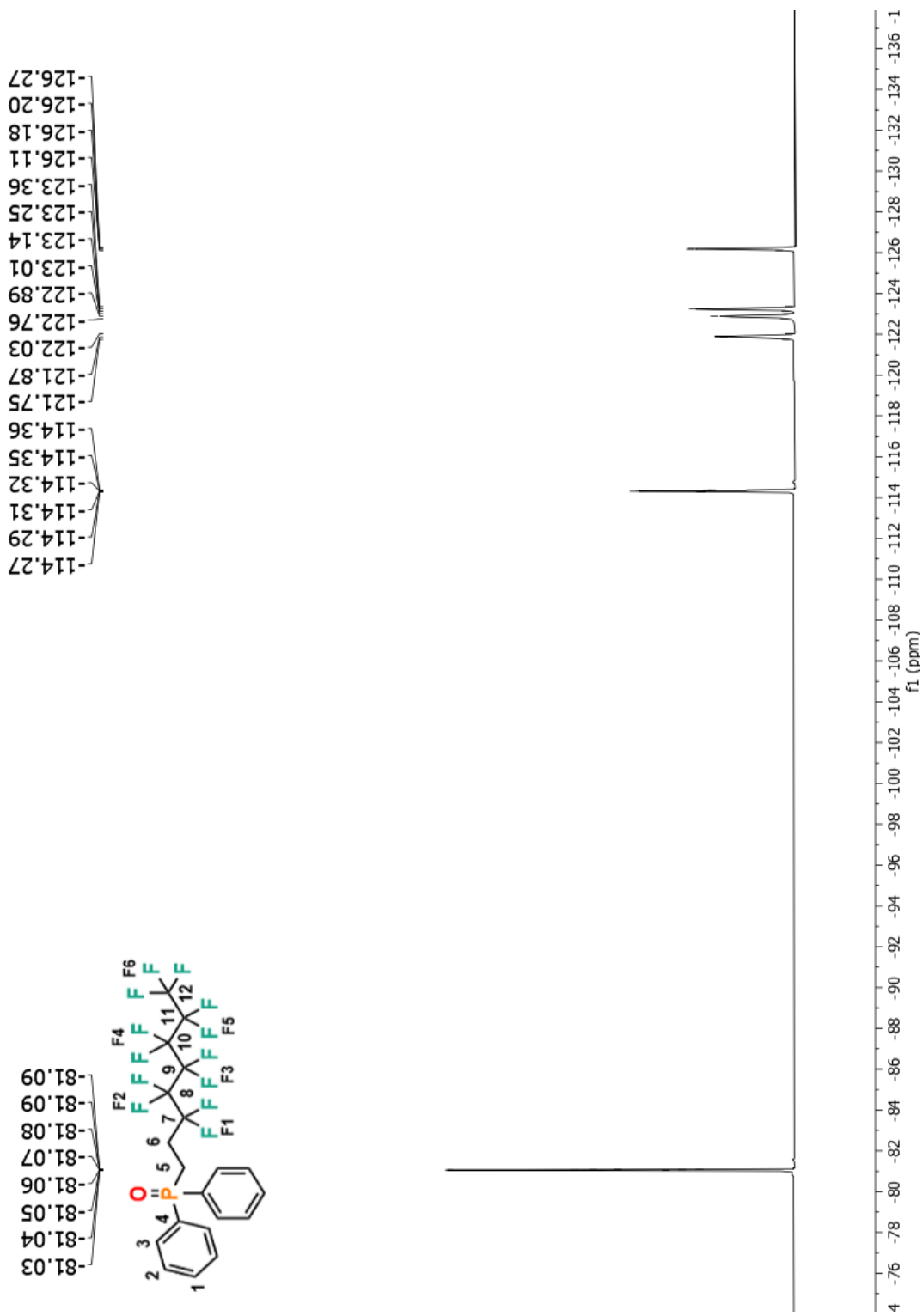
Figure A 26. ^{19}F {^{1}H} NMR (C_6D_6) spectrum of **iii**.
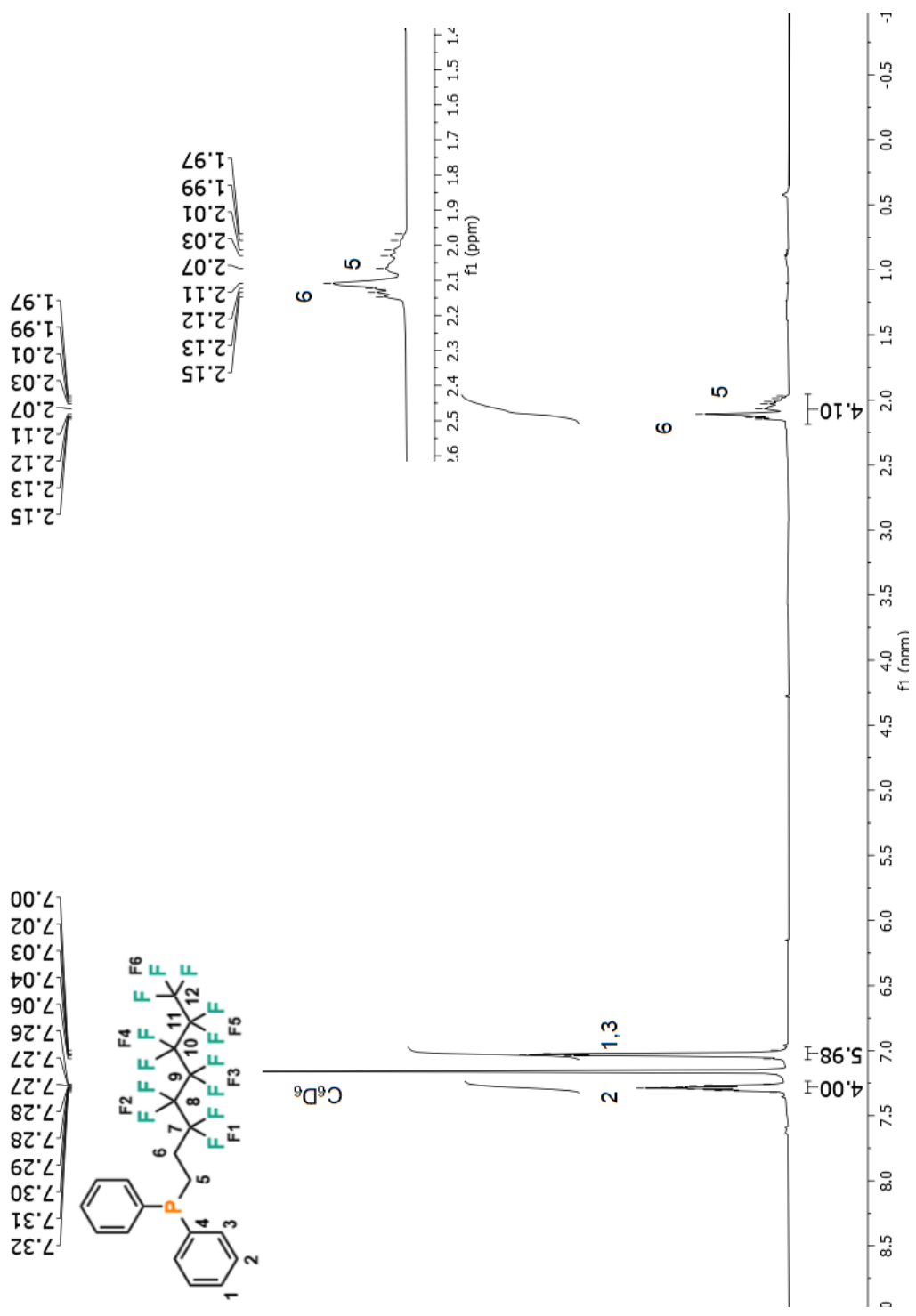
Figure A 27. ^{1}H NMR (C$_6$D$_6$) spectrum of **iv.**
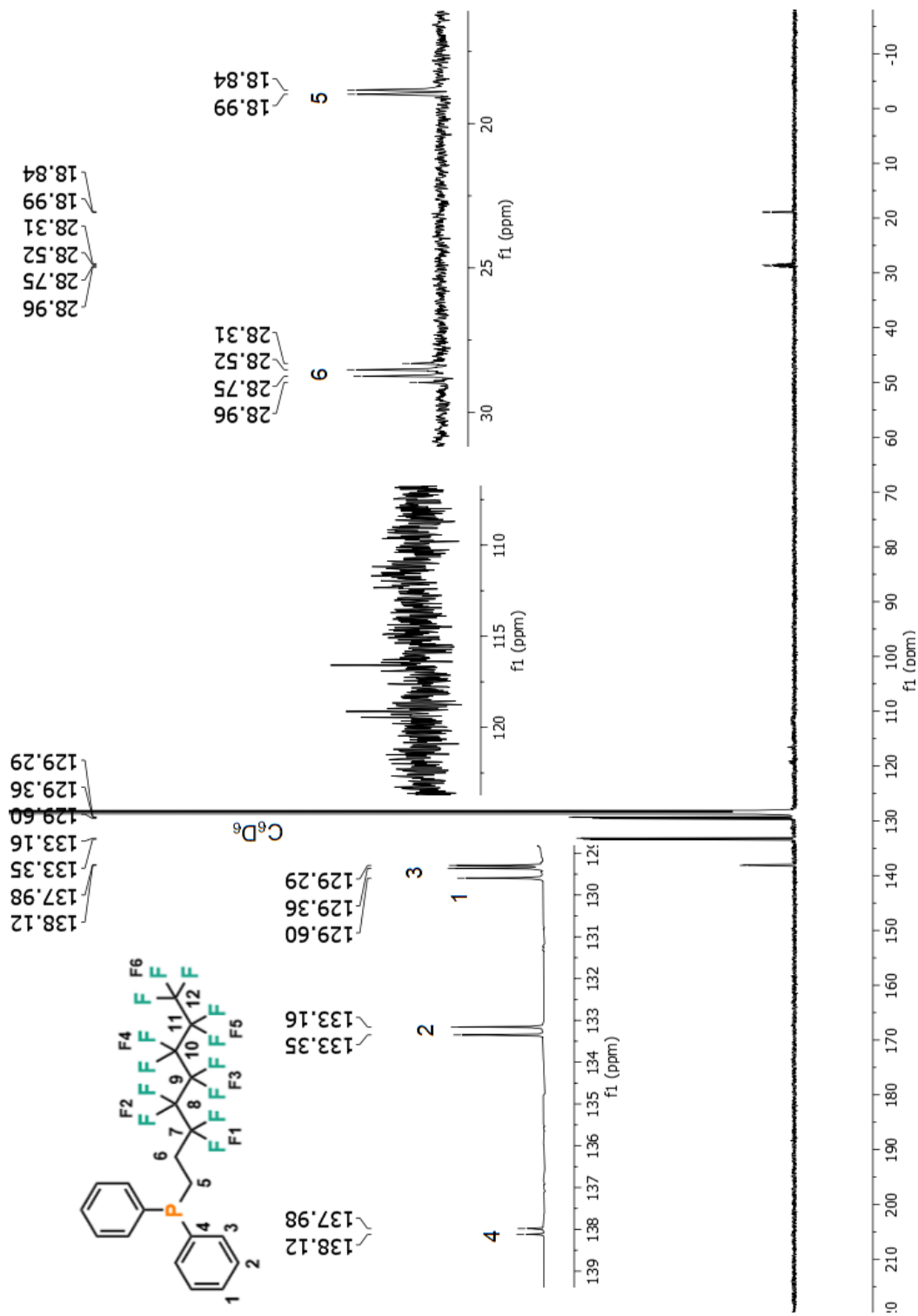
Figure A 28. $^{13}C\{^1H\}$ NMR (C_6D_6) spectrum of **iv.**
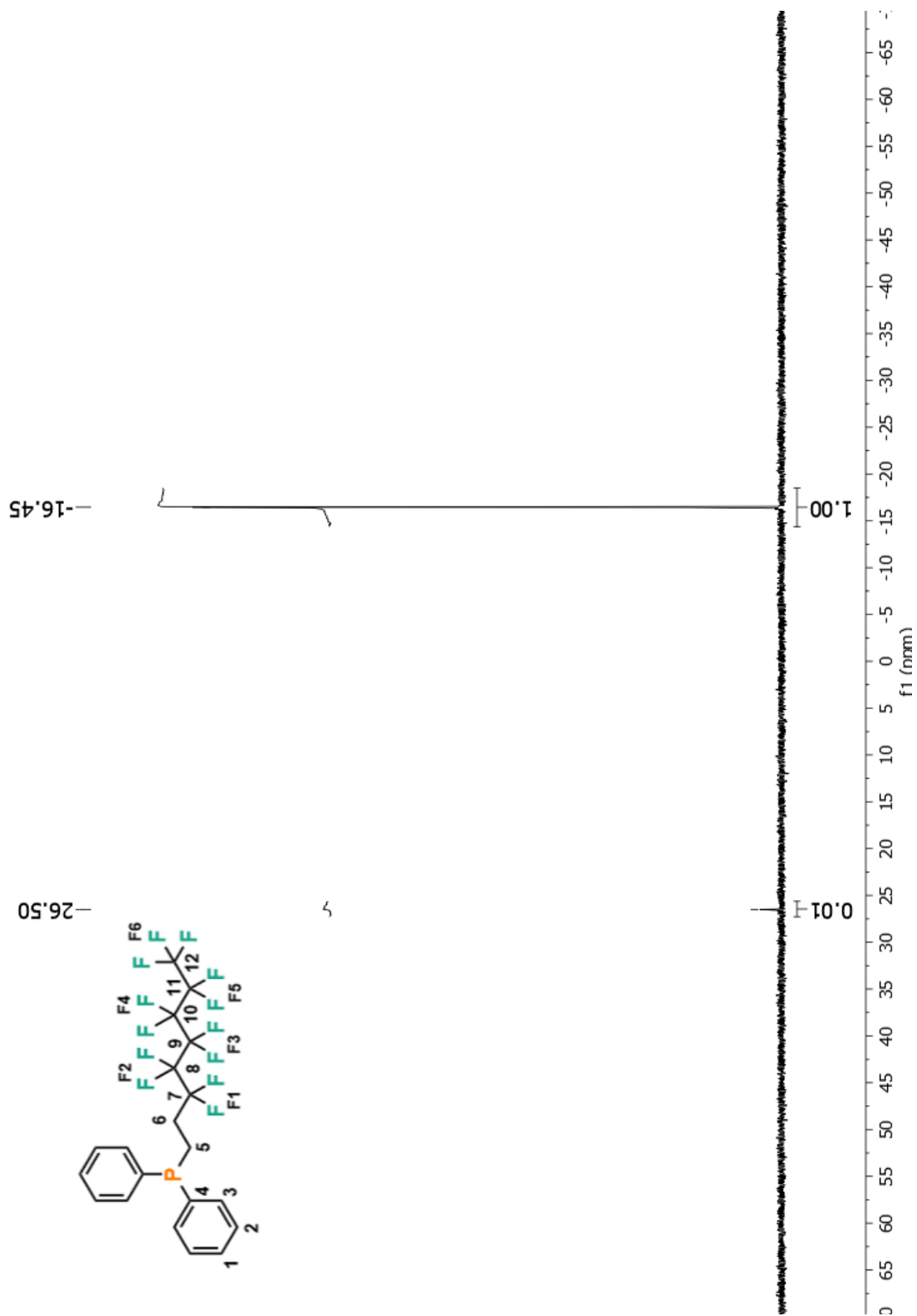
Figure A 29. ^{31}P {^1H} NMR (C_6D_6) spectrum of **iv**.

119
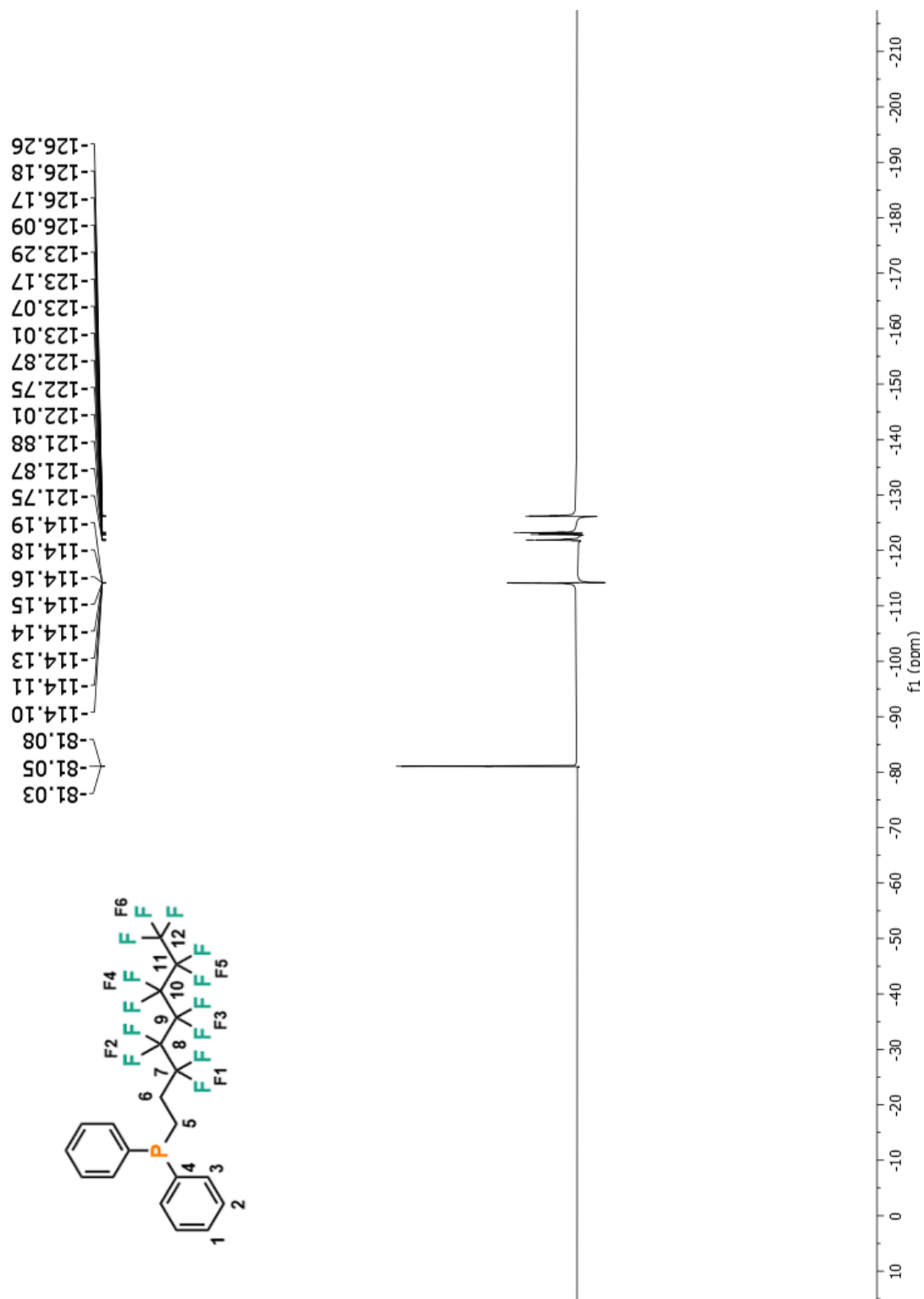
Figure A 30. ^{19}F {^{1}H} NMR (C$_6$D$_6$) spectrum of **iv**.
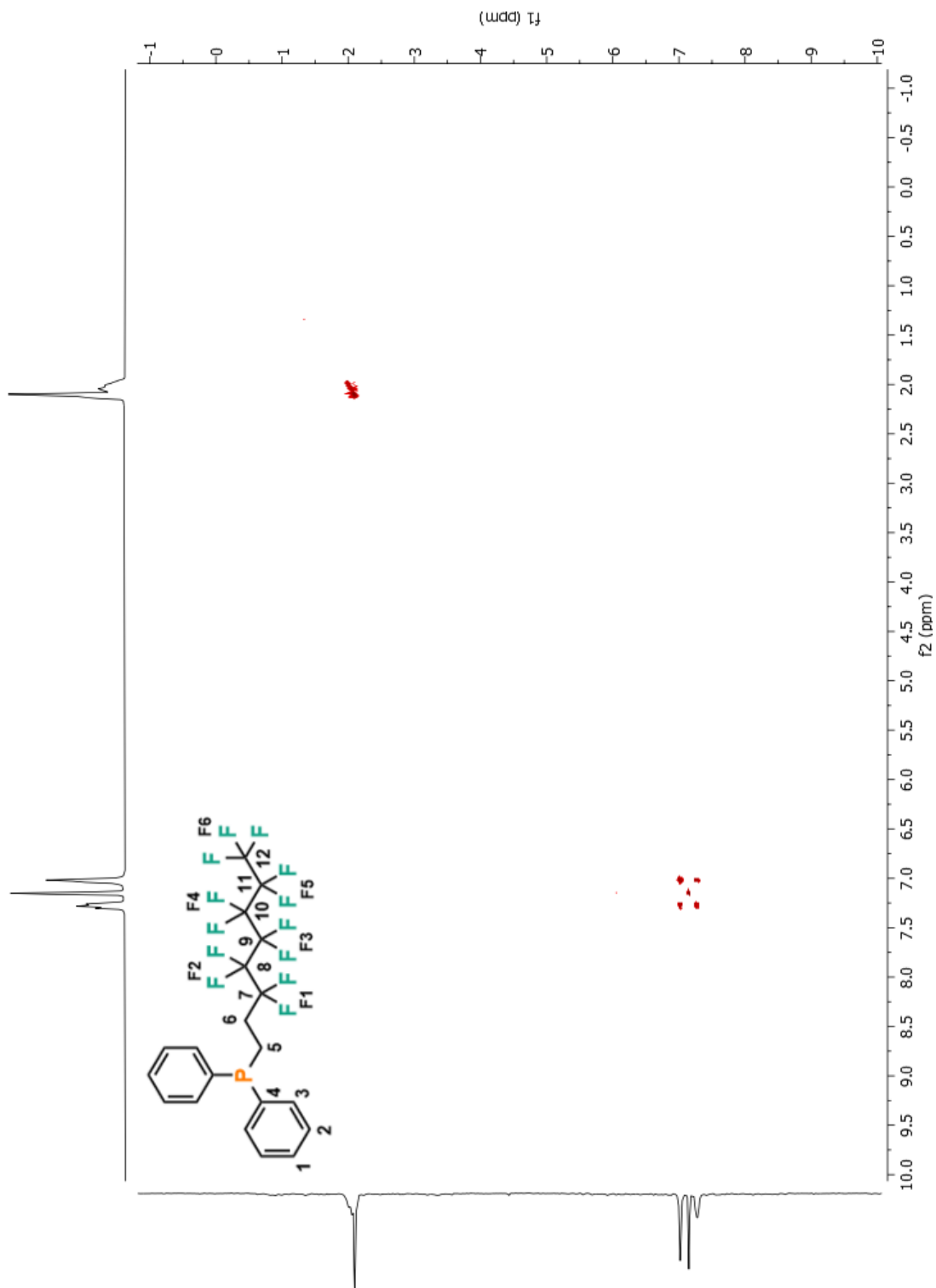
Figure A 31. 2D COSY NMR (C₆D₆) spectrum of **iv.**
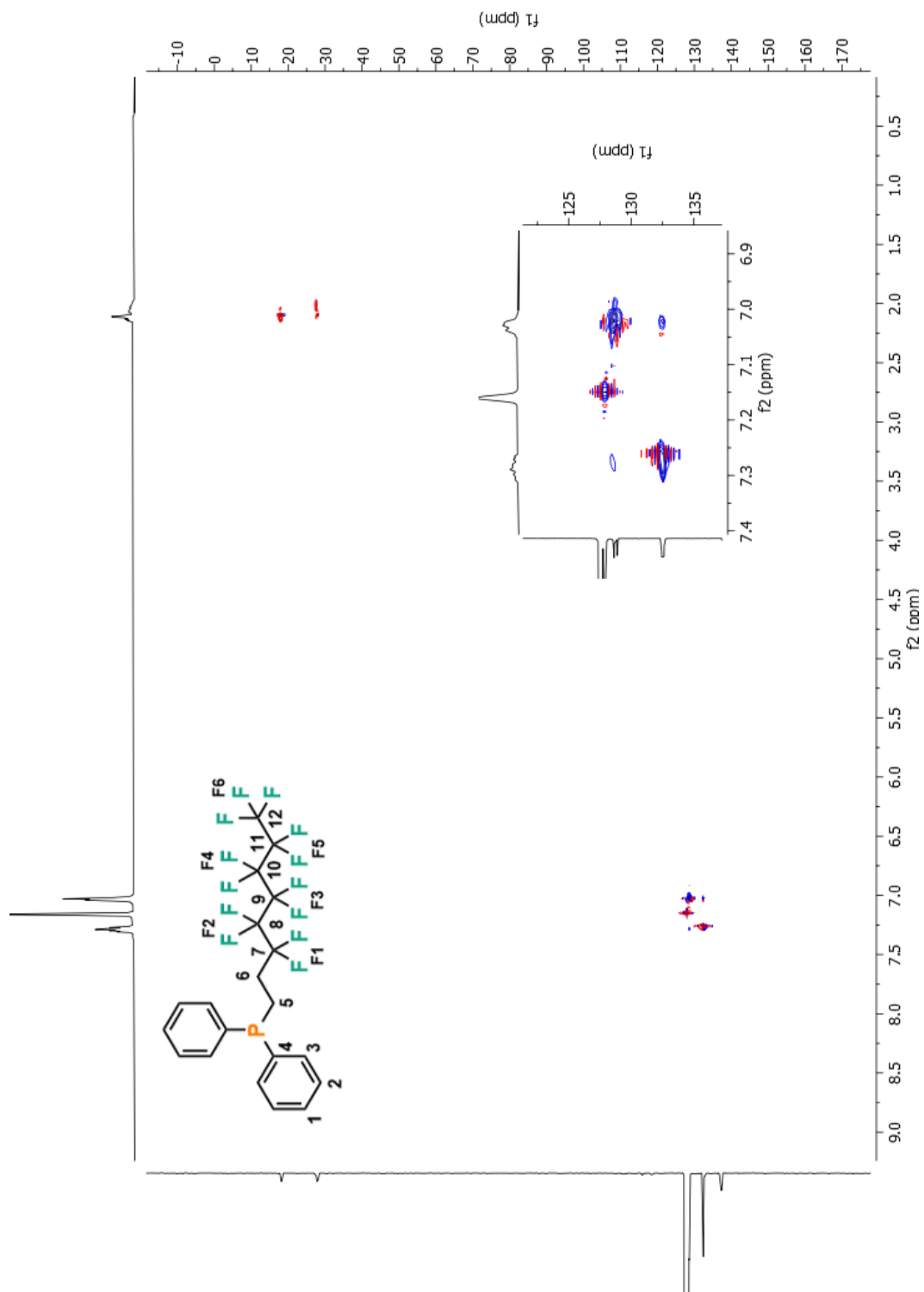
Figure A 32. 2D HSQC NMR (C_6D_6) spectrum of **iv.**
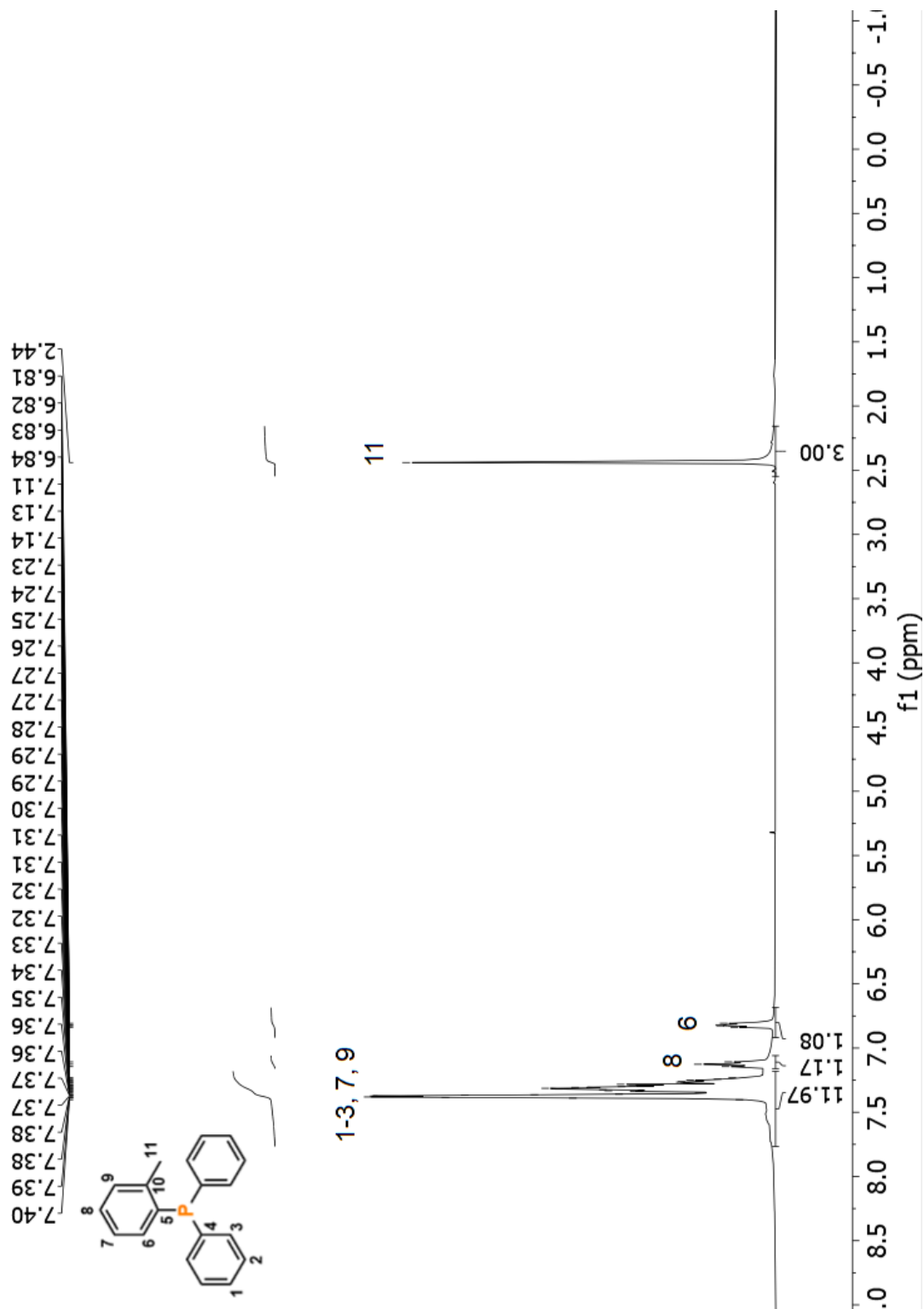
Figure A 33. ^{1}H NMR (C$_6$D$_6$) spectrum of **v.**

124
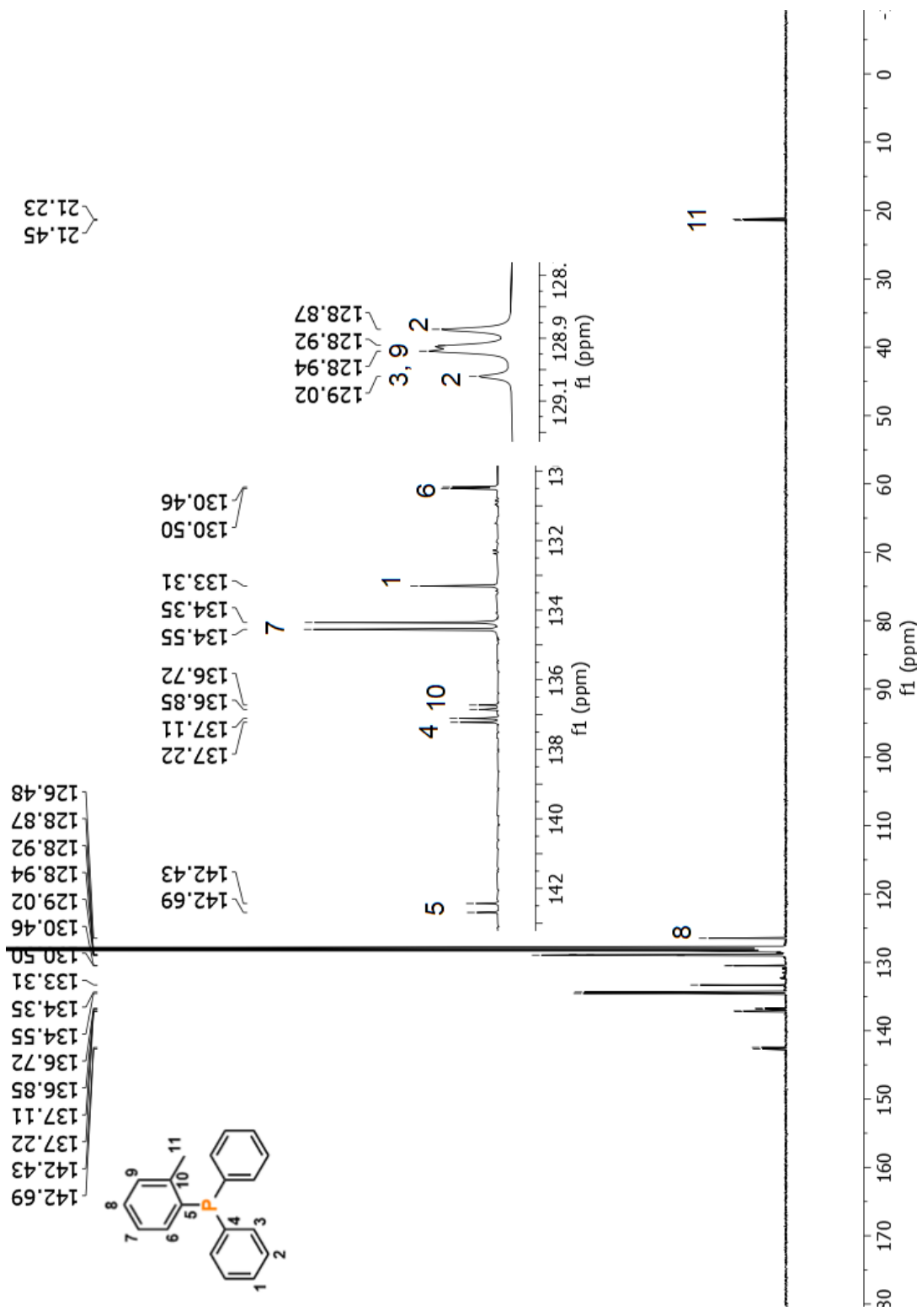
Figure A 35. ^{31}P {^{1}H} NMR (C$_6$D$_6$) spectrum of **v**.
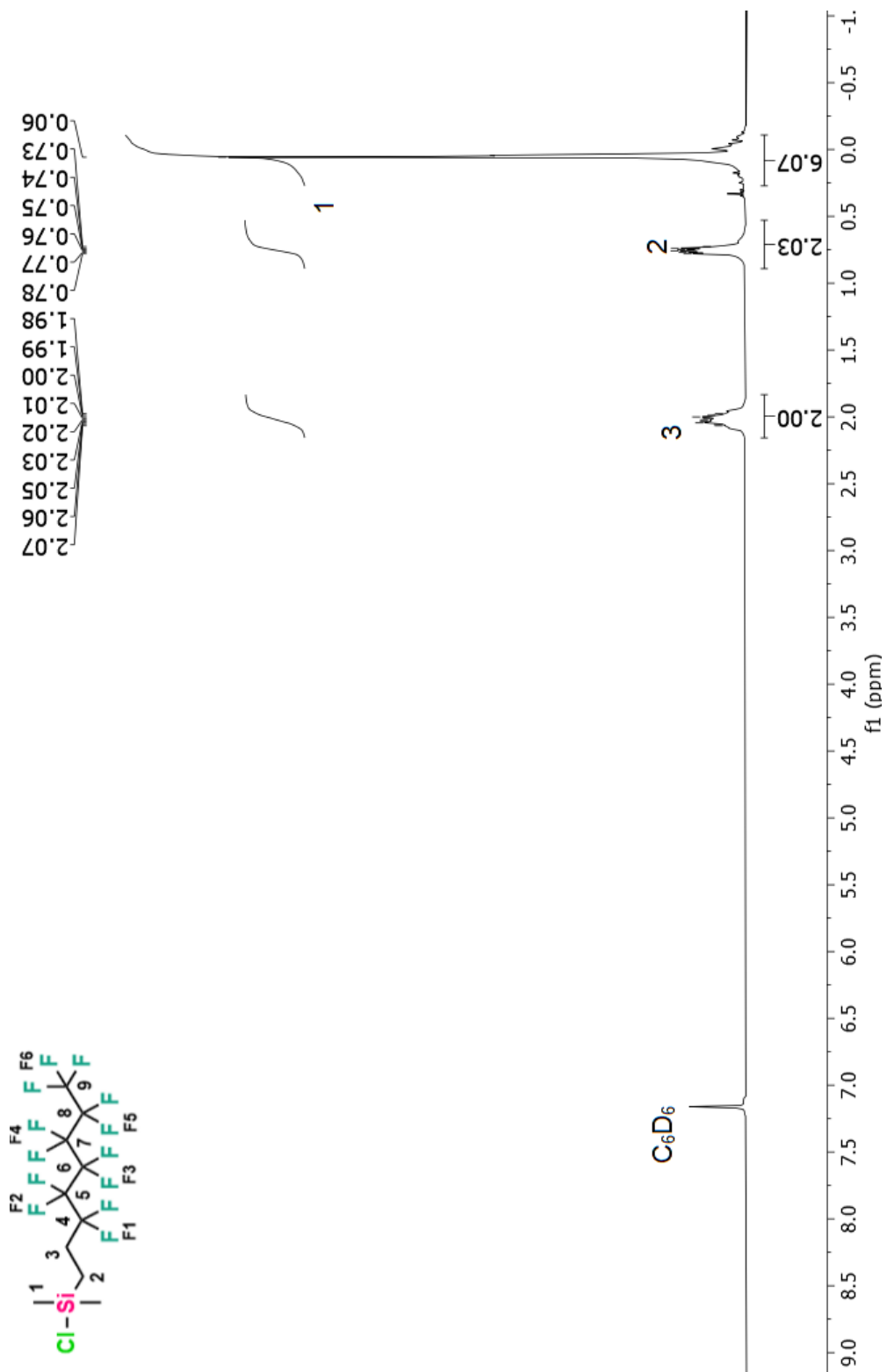
Figure A 36. ^{1}H NMR (C_6D_6) spectrum of **vi.**

126
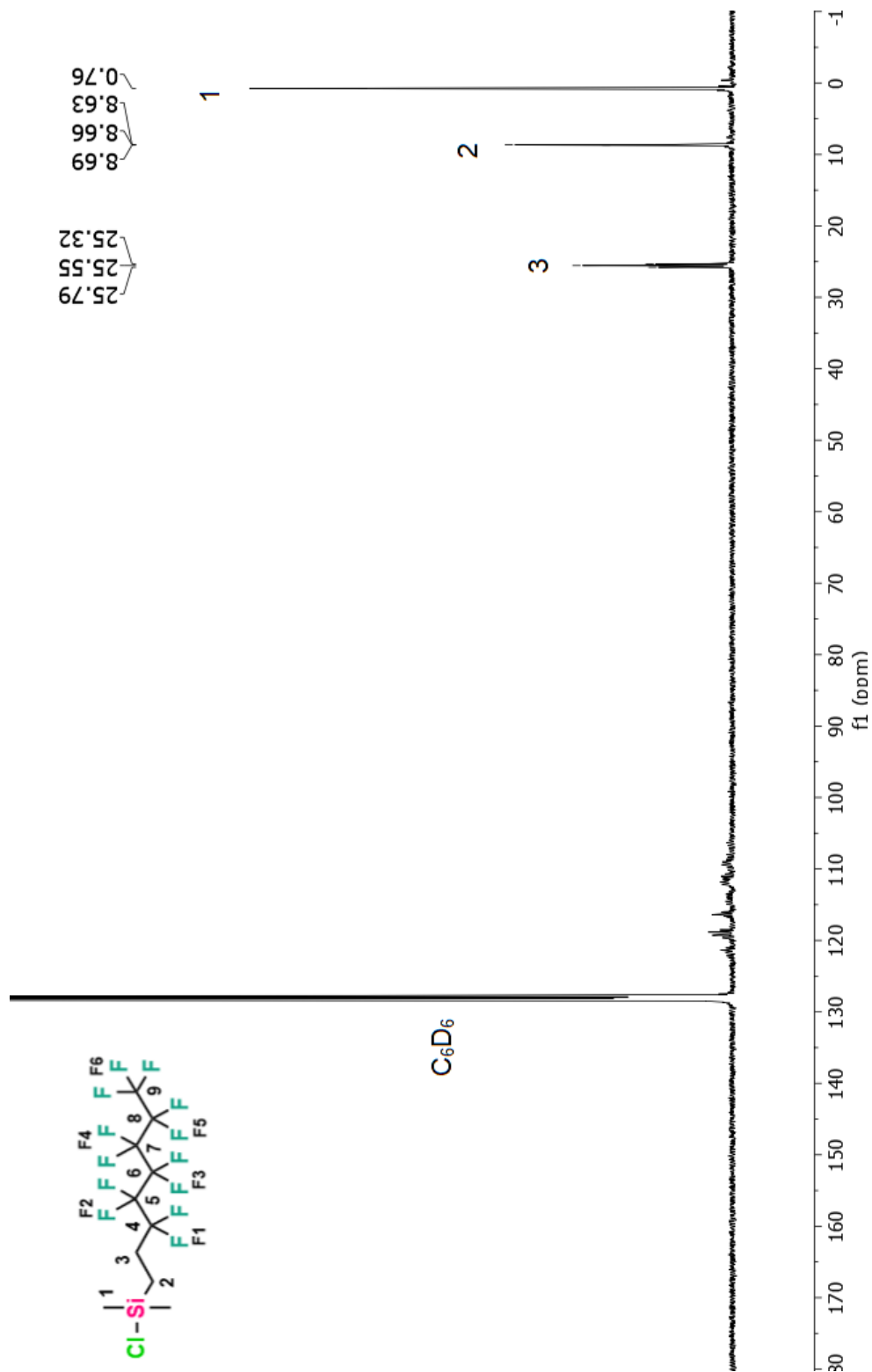
Figure A 37. ^{13}C {^{1}H} NMR (C_6D_6) spectrum of **vi.**
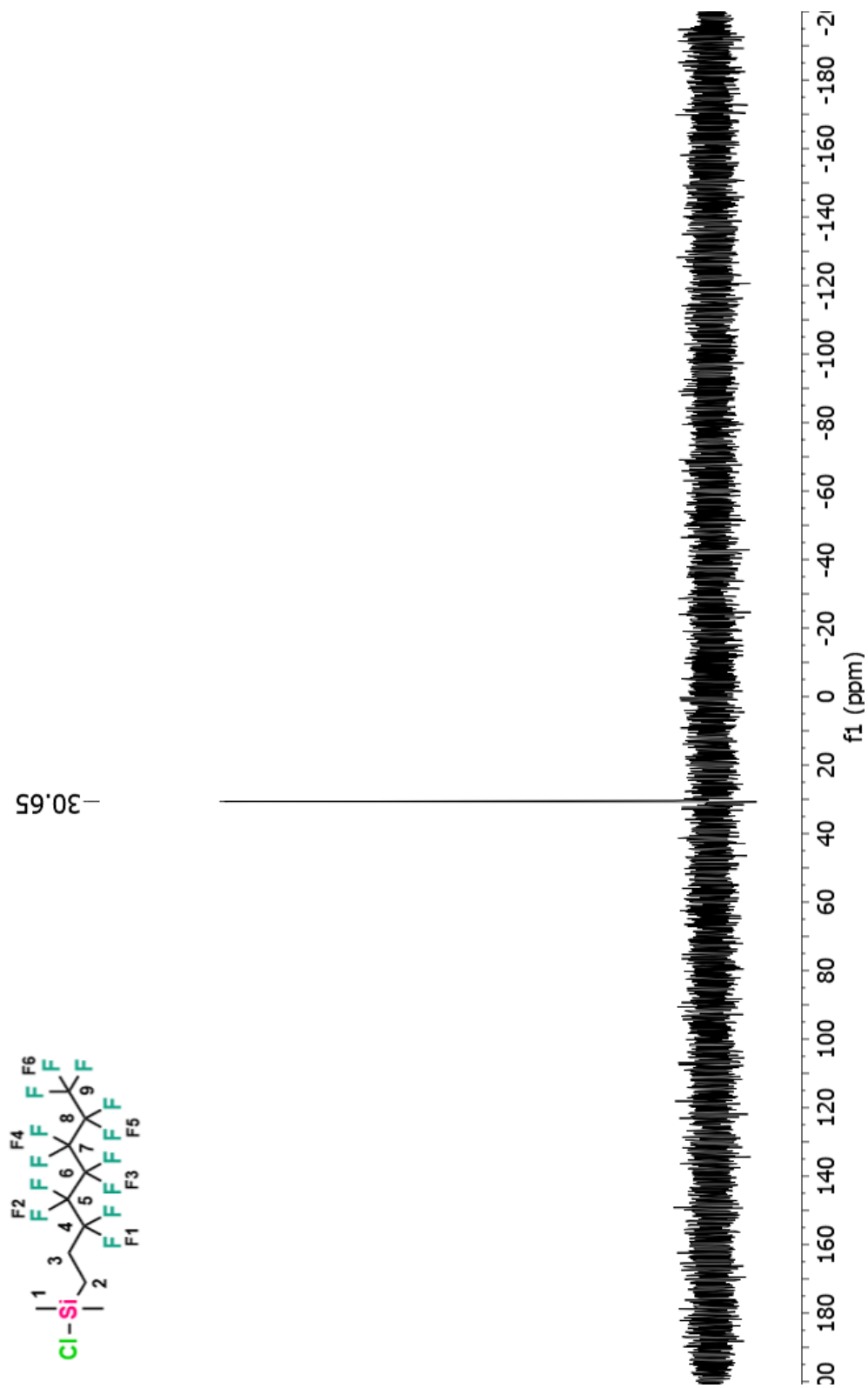
Figure A 38. ^{29}Si {^{1}H} NMR (C_6D_6) spectrum of **vi**.
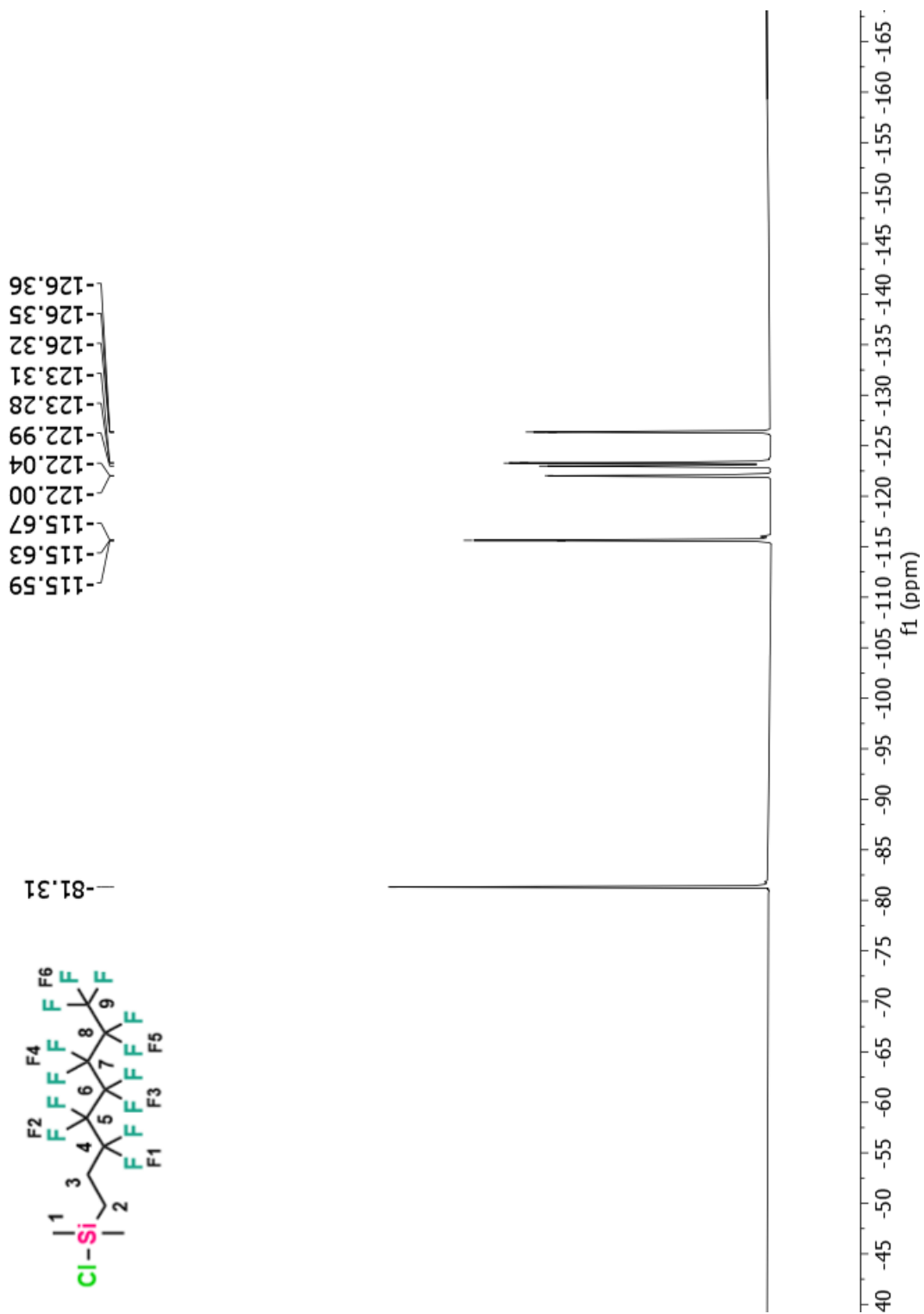
Figure A 39. ^{19}F {^1H} NMR (C$_6$D$_6$) spectrum of **vi**.

Peak labels:
- −126.36
- −126.35
- −126.32
- −123.31
- −123.28
- −122.99
- −122.04
- −122.00
- −115.67
- −115.63
- −115.59
- −81.31

Figure A 40. ^{1}H NMR (C$_6$D$_6$) spectrum of **vii.**
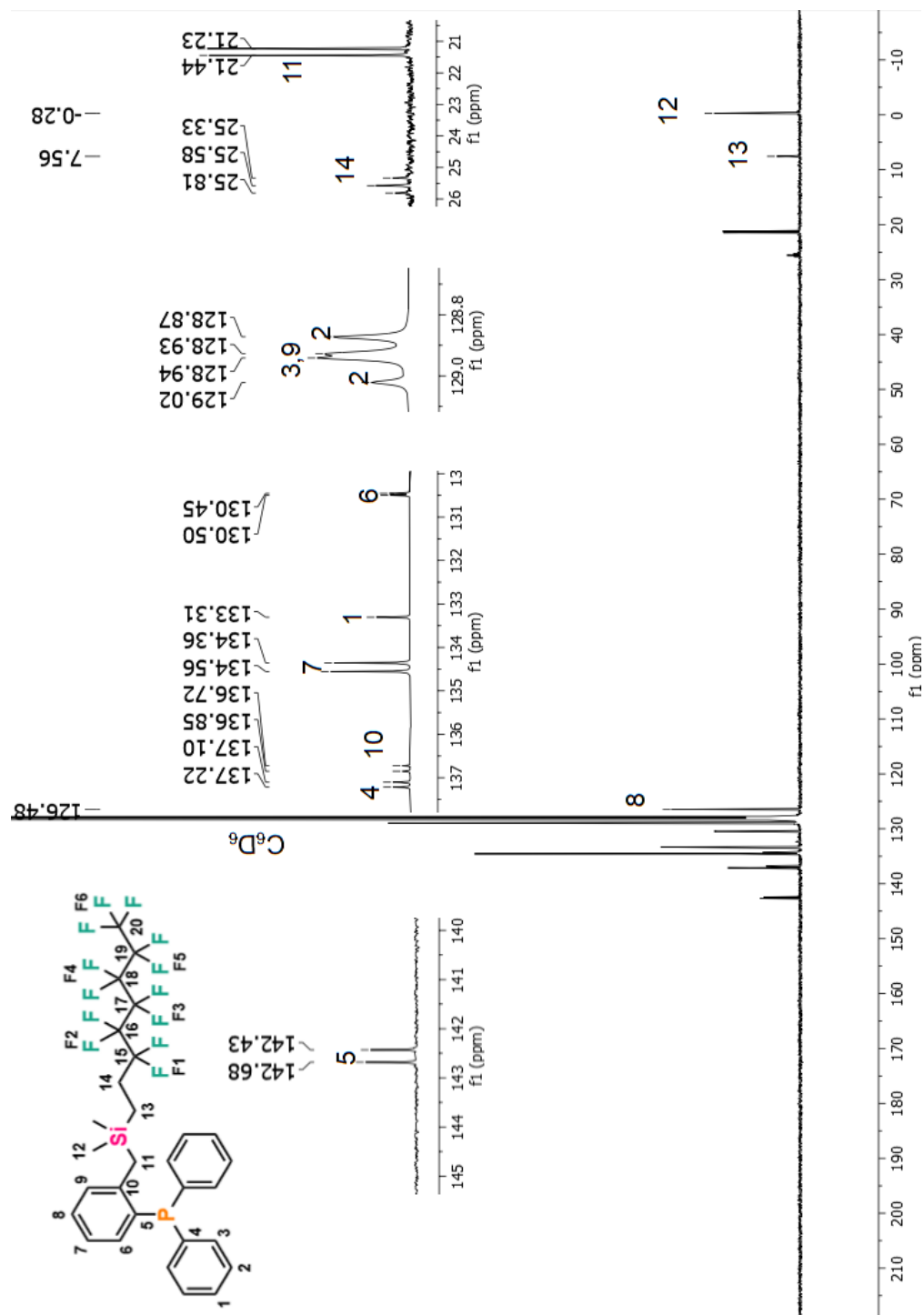
Figure A 41. ^{13}C {^{1}H} NMR (C_6D_6) spectrum of **vii.**

131
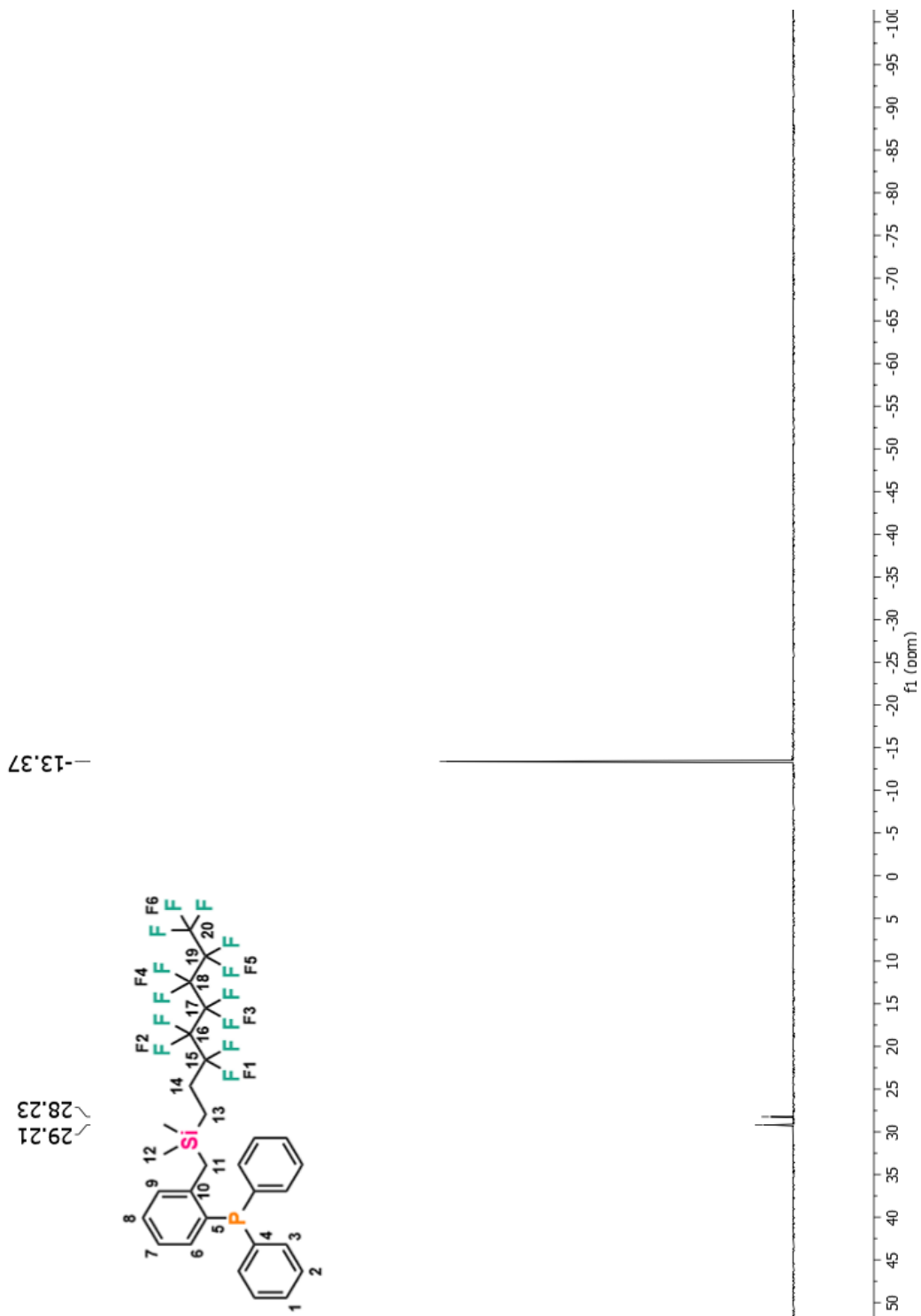
Figure A 42. ^{31}P {^{1}H} NMR (C$_6$D$_6$) spectrum of **vii**.
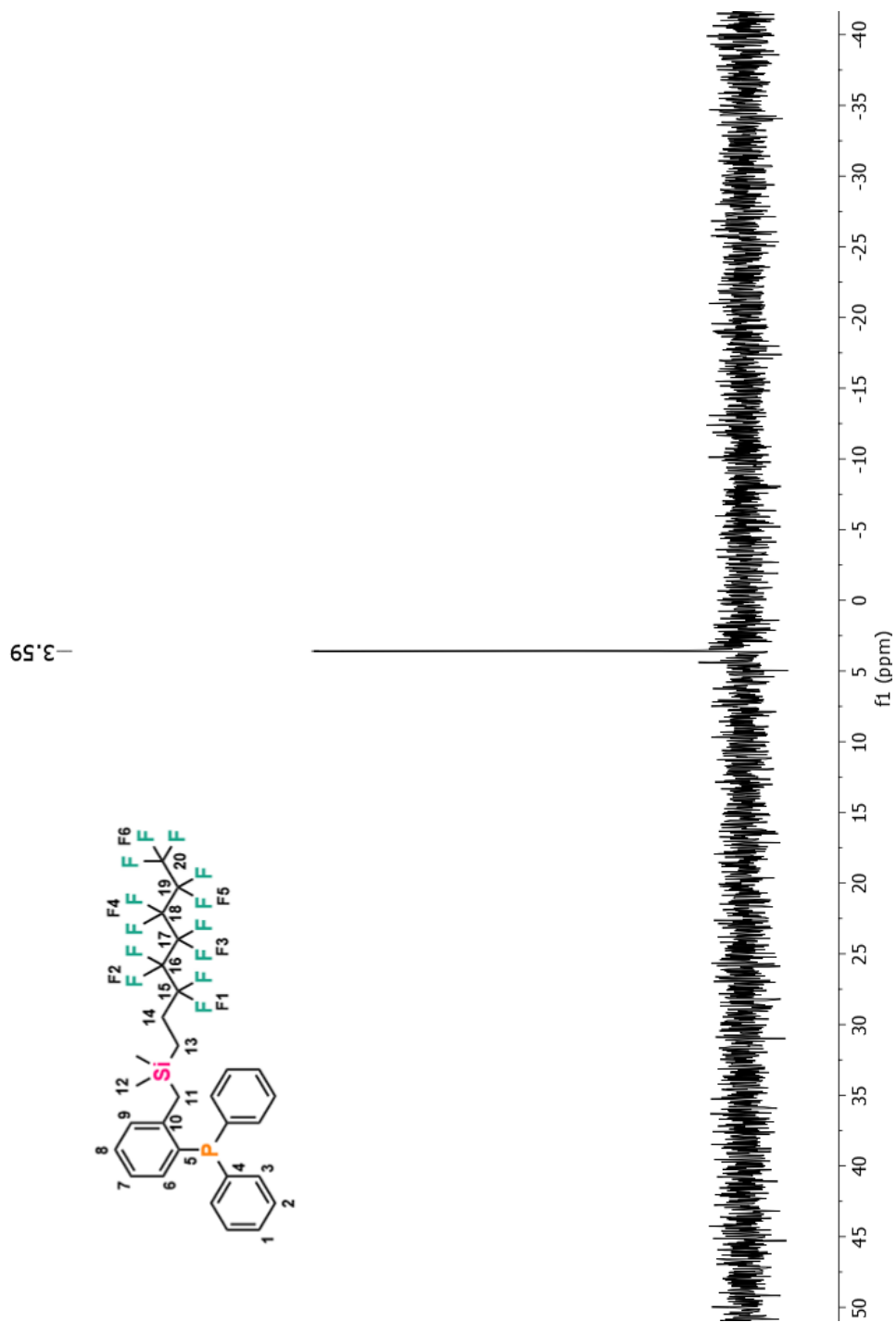
Figure A 43. ^{29}Si {^{1}H} NMR (C$_6$D$_6$) spectrum of **vii.**
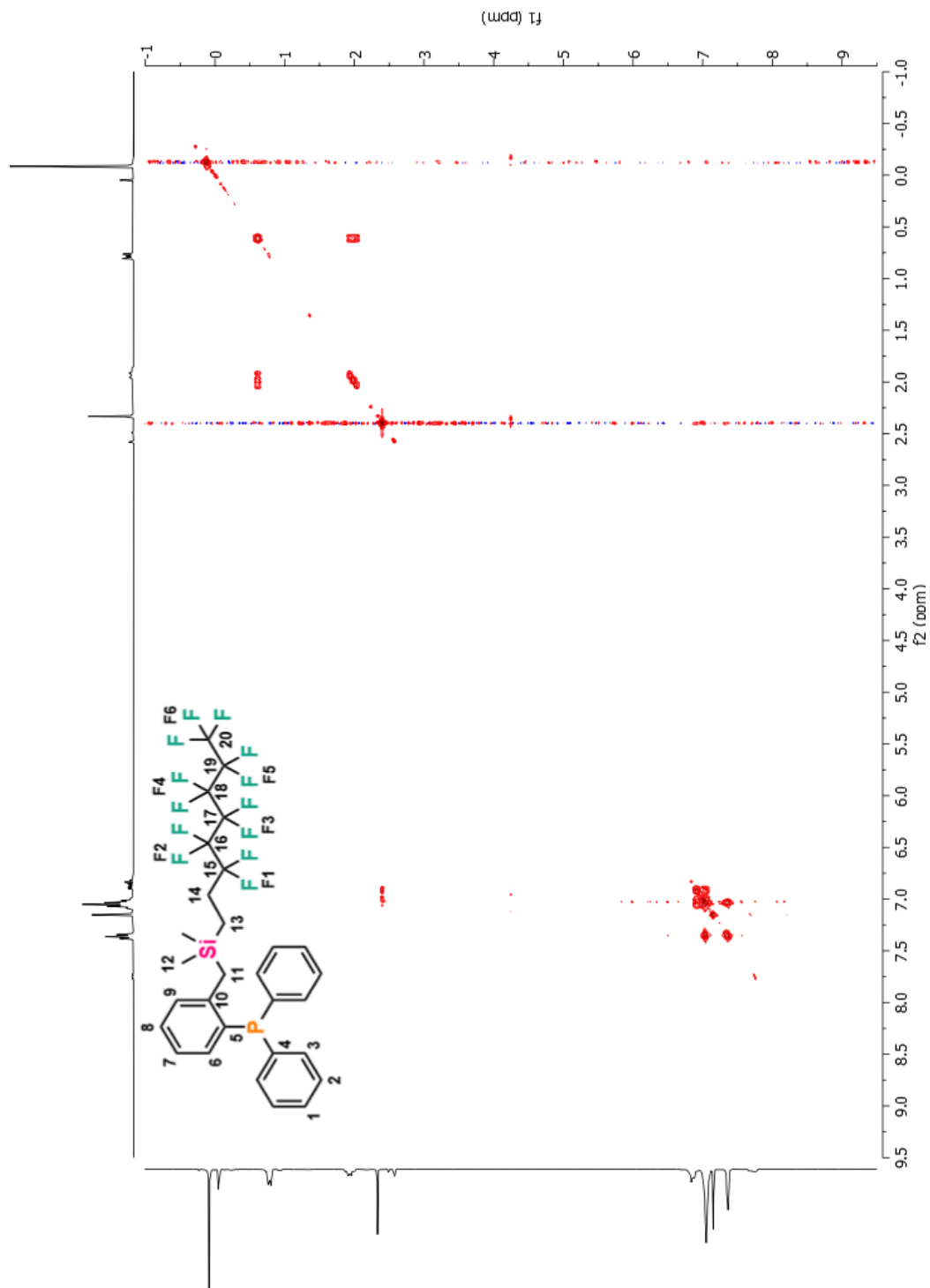
Figure A 44. 2D COSY NMR (C$_6$D$_6$) spectrum of **vii.**
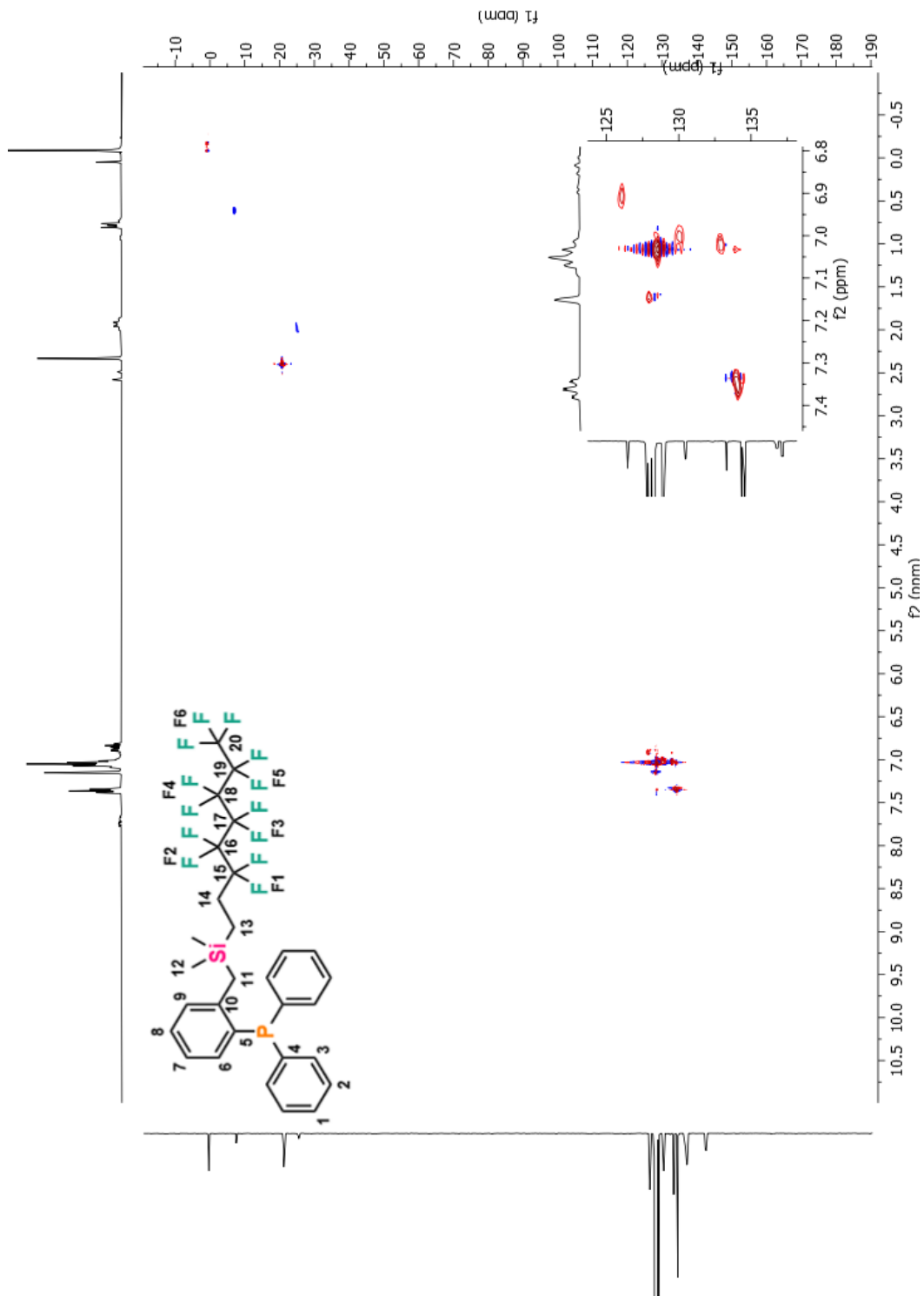
Figure A 45. 2D HSQC NMR (C$_6$D$_6$) spectrum of **vii.**
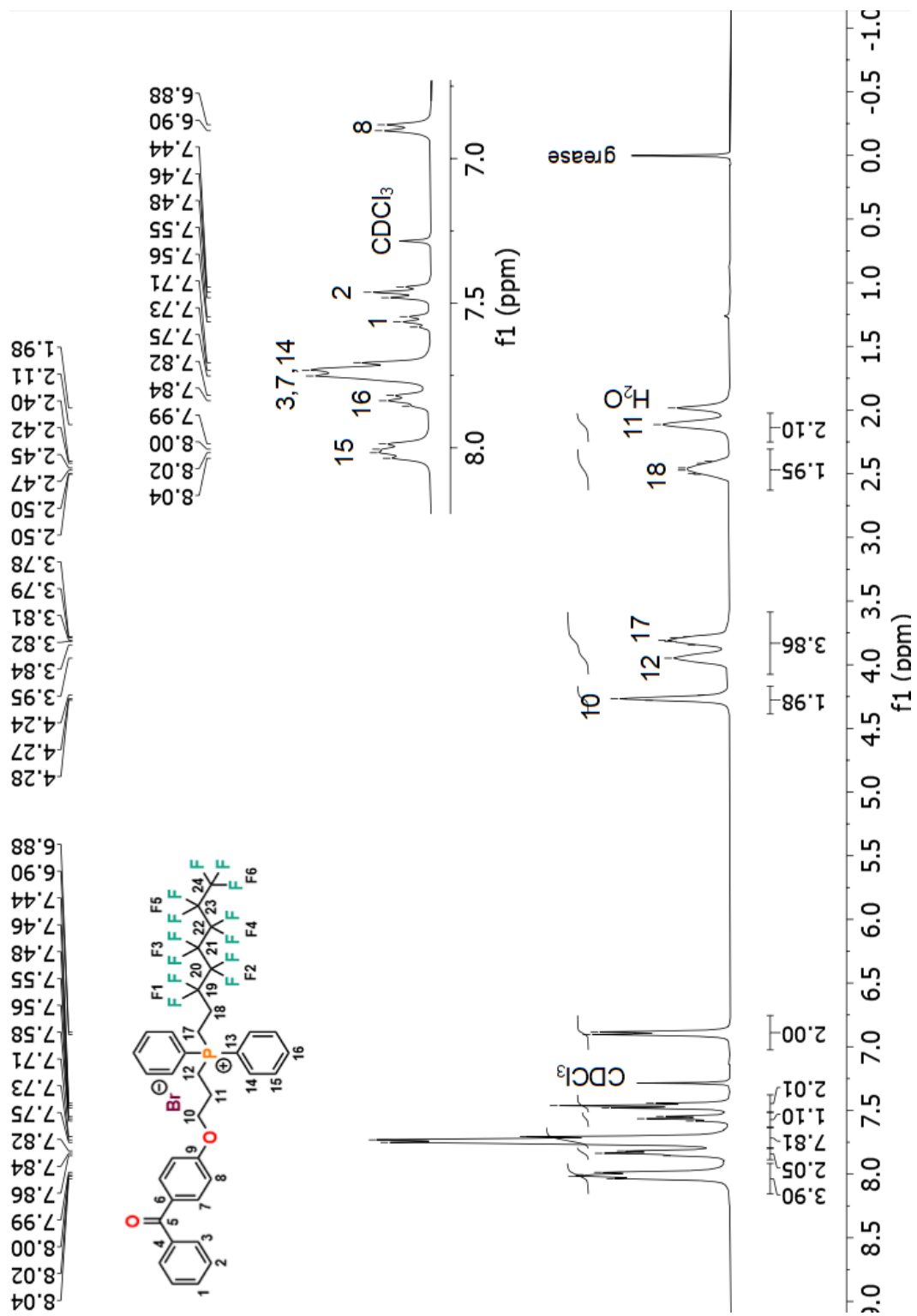
Figure A 46. ^{1}H NMR (CDCl$_3$) spectrum of **4.**

136
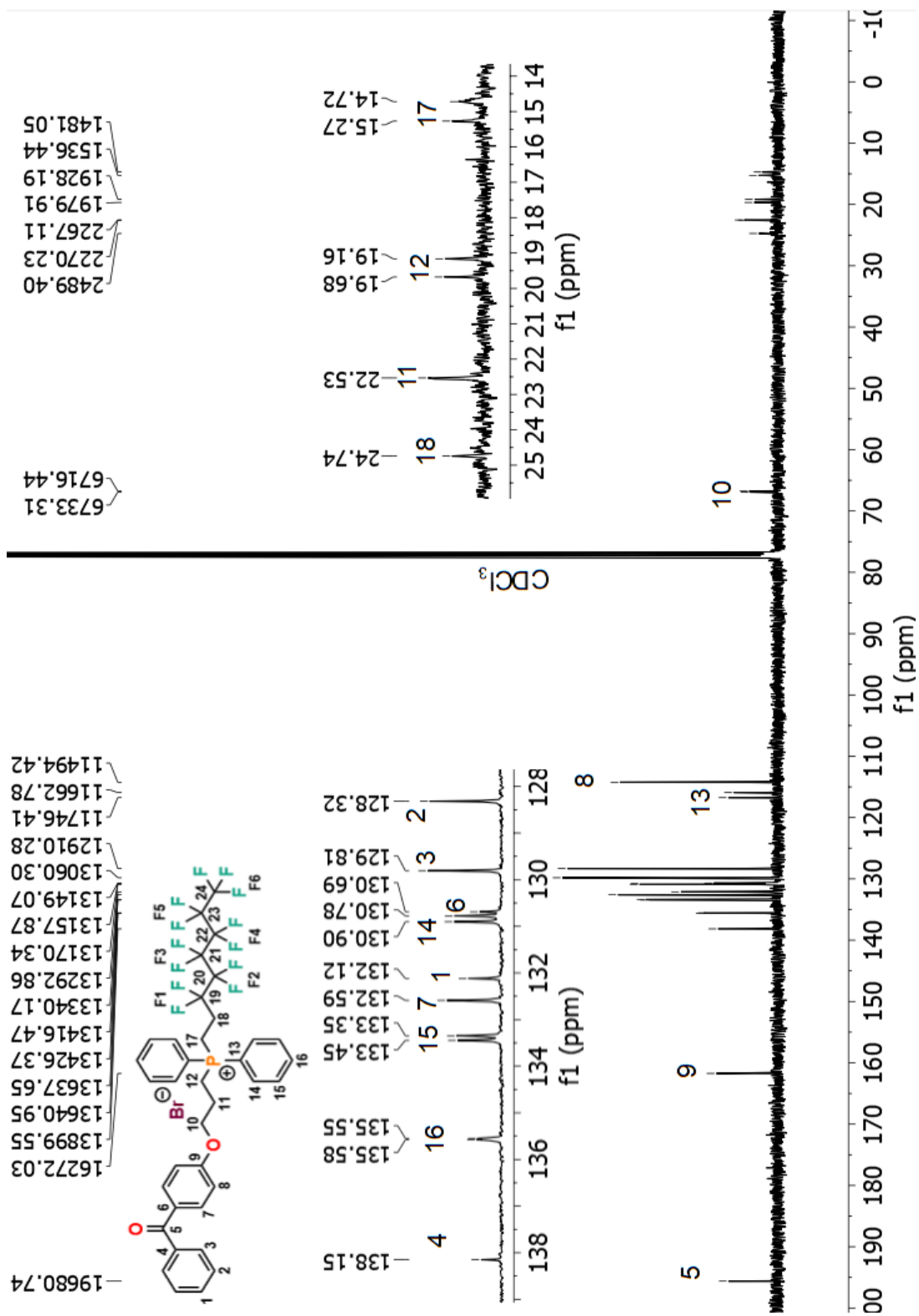
Figure A 47. $^{13}C\{^1H\}$ NMR (CDCl$_3$) spectrum of **4.**
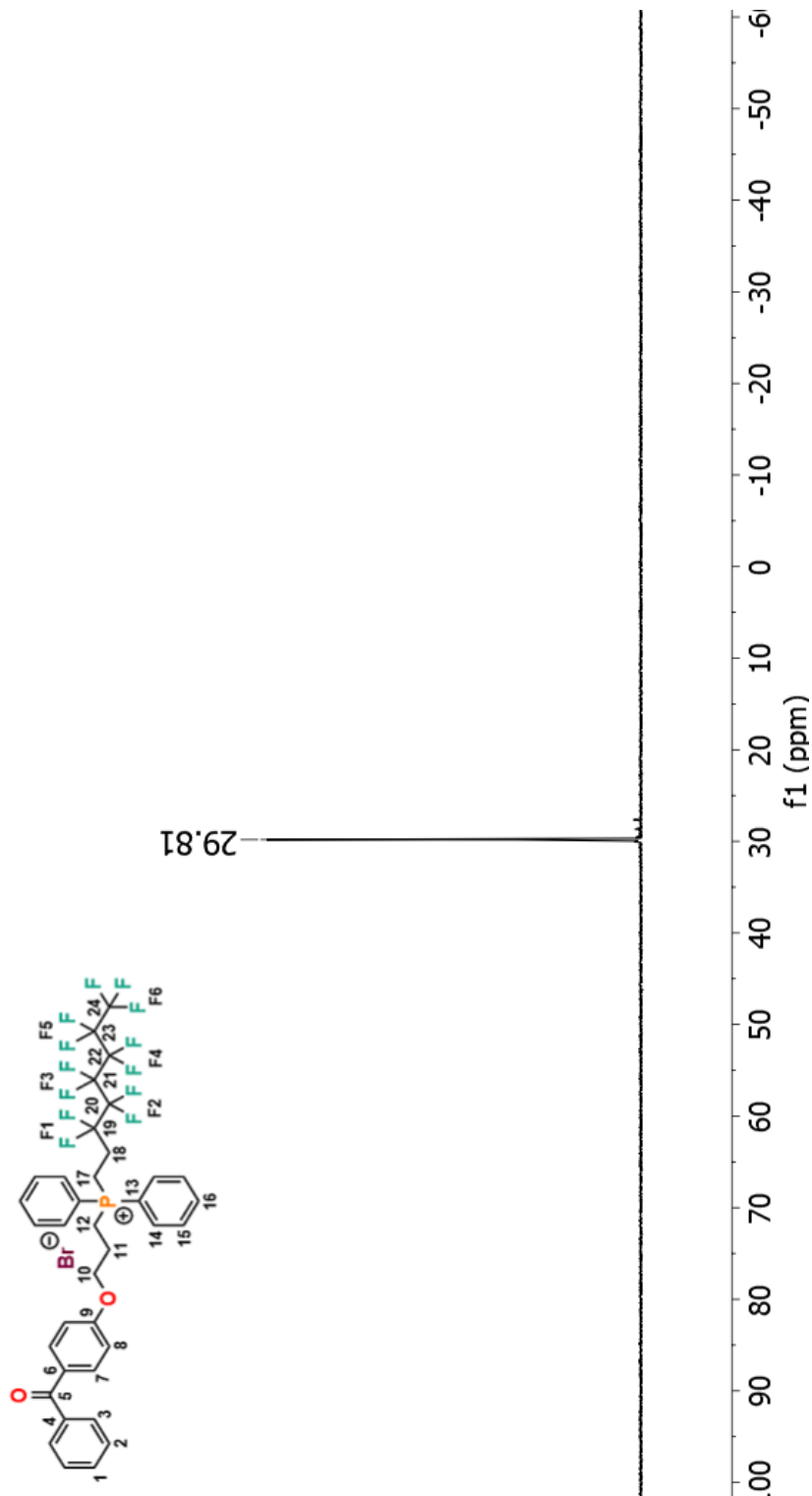
Figure A 48. ^{31}P {^{1}H} NMR (CDCl$_3$) spectrum of **4.**
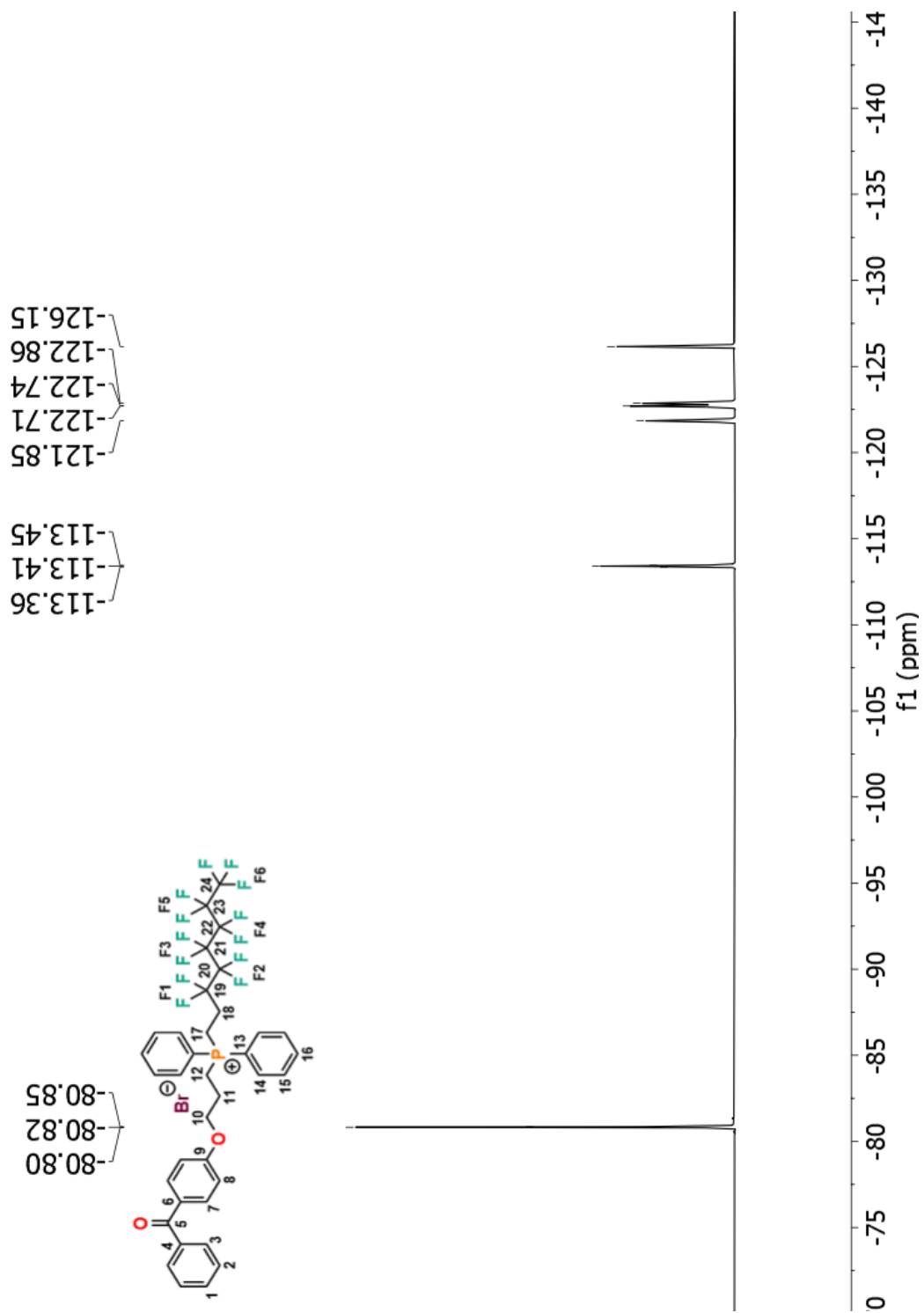
Figure A 49. ^{19}F {^1H} NMR (CDCl$_3$) spectrum of **4.**
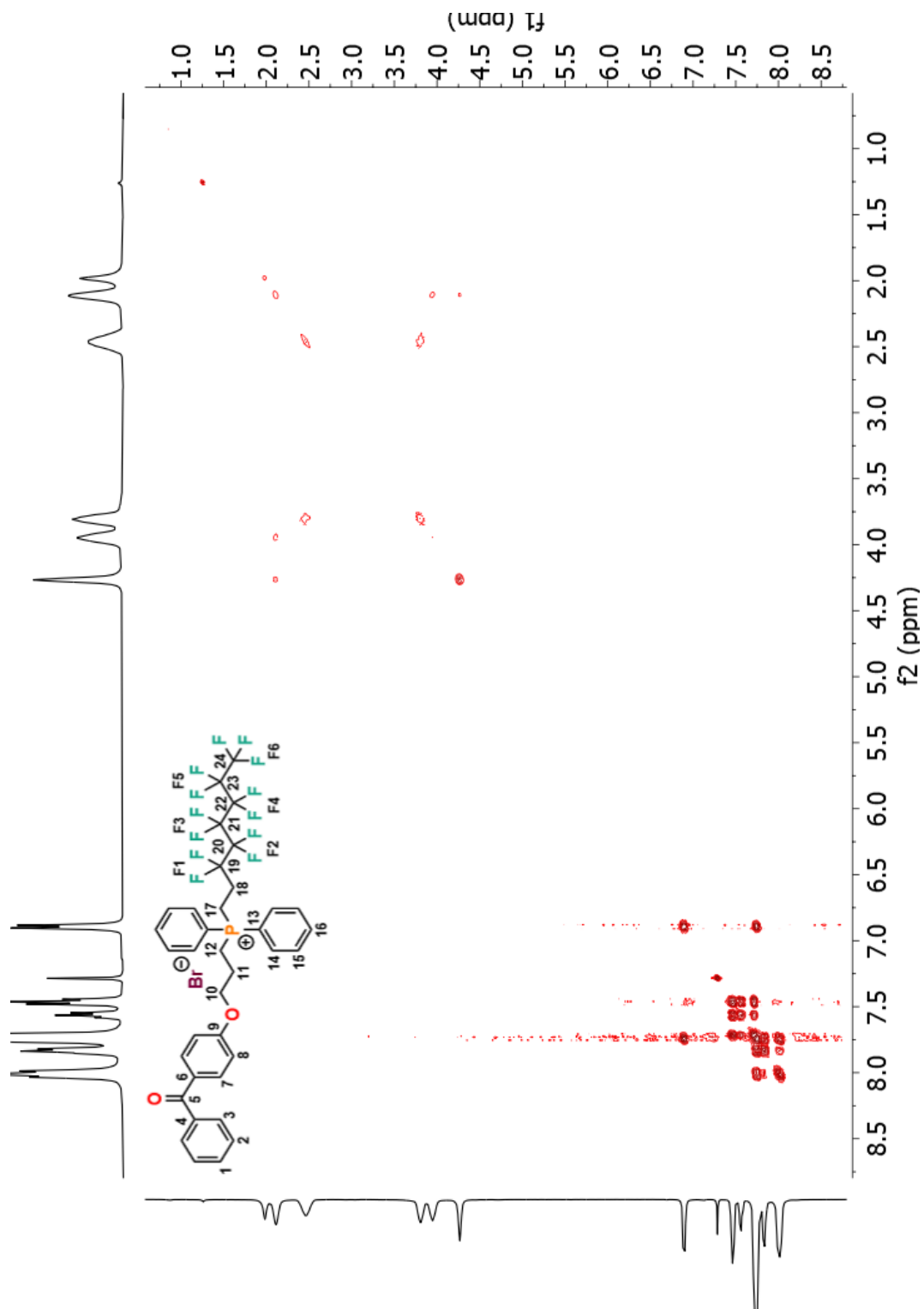
Figure A 50. 2D COSY NMR (CDCl₃) spectrum of **4**.
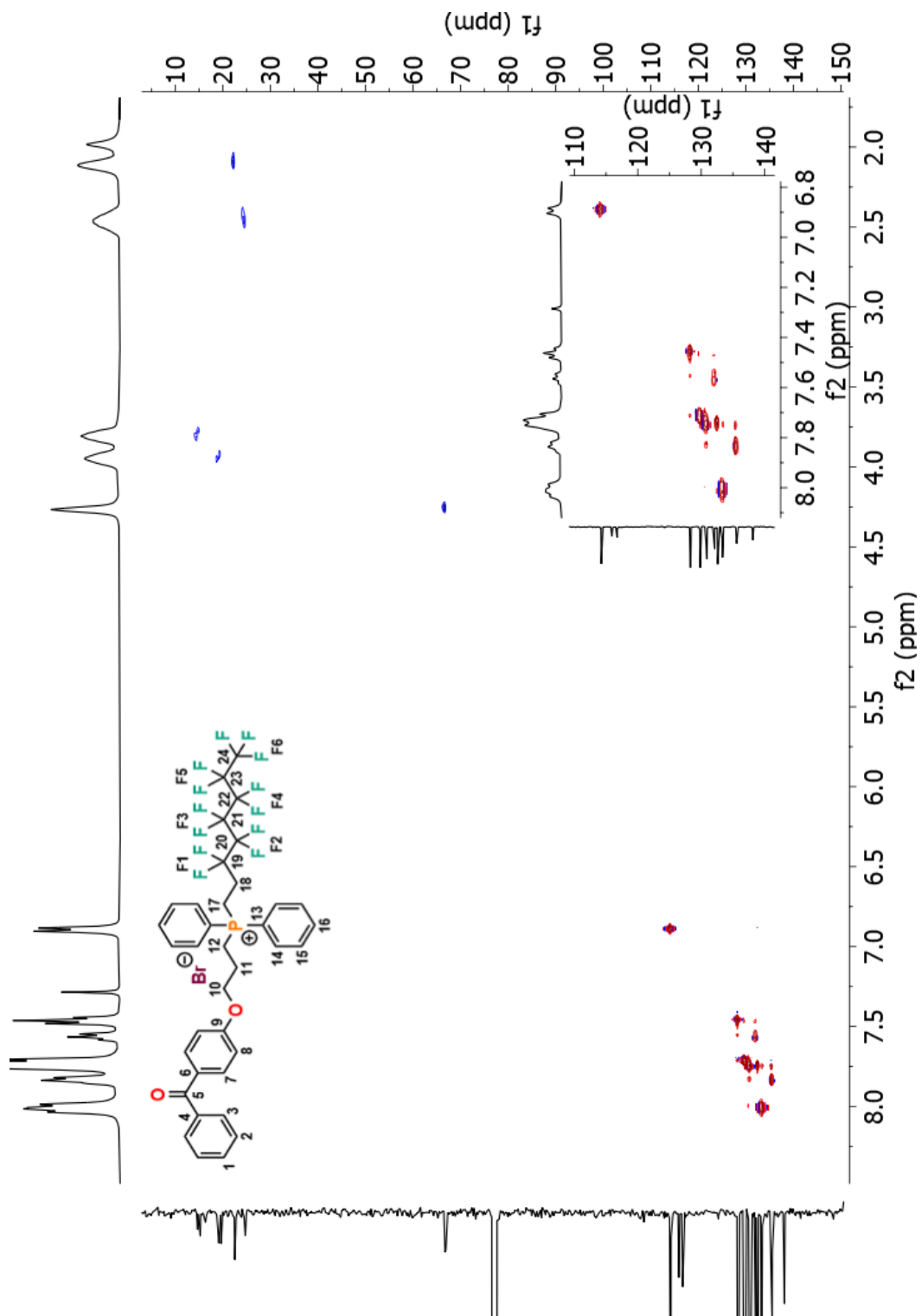
Figure A 51. 2D HSQC NMR (CDCl₃) spectrum of **4**.
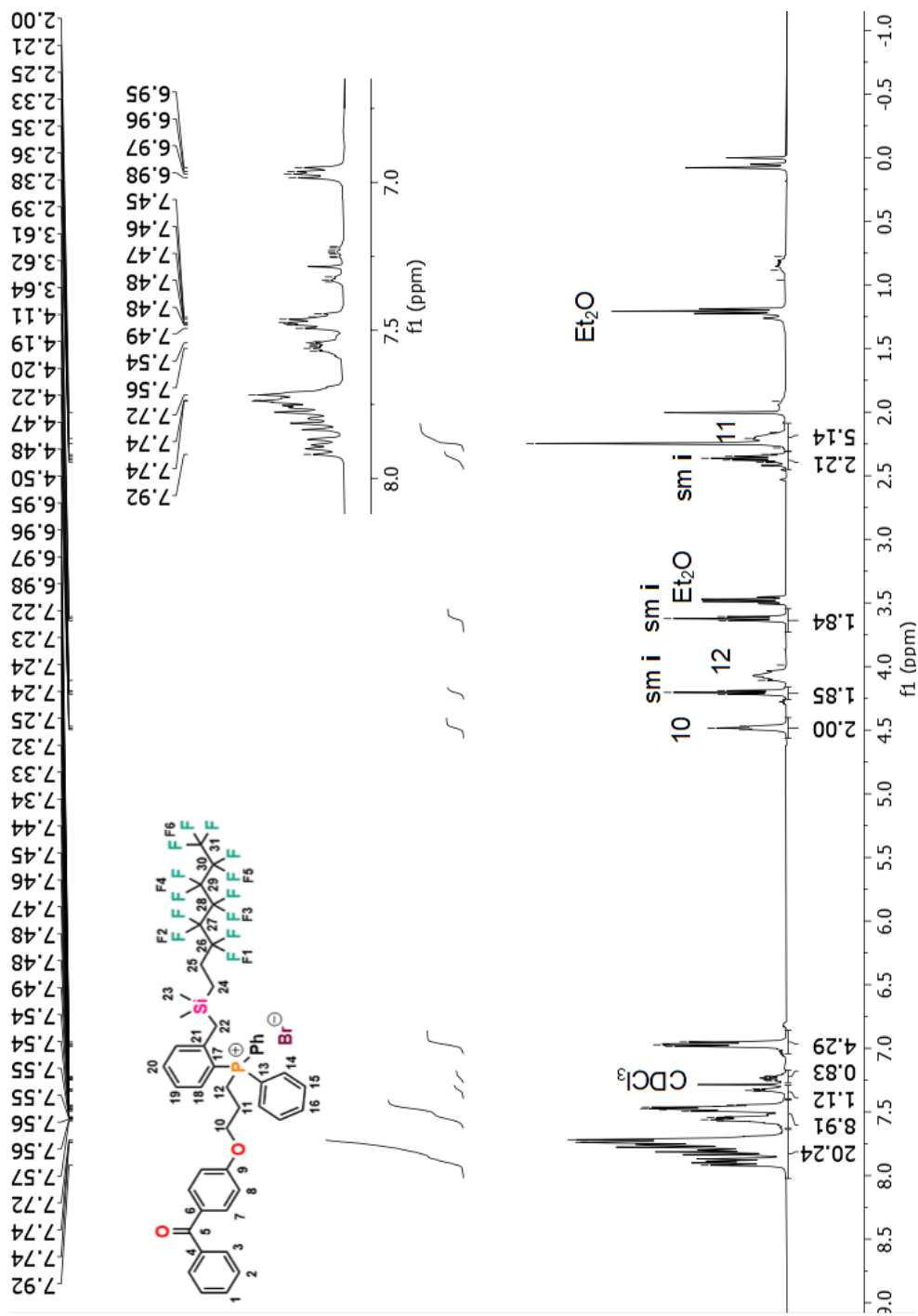
Figure A 52. ^{1}H NMR (CDCl$_3$) spectrum of **5.** Peak assignments and impurities are labelled where possible.
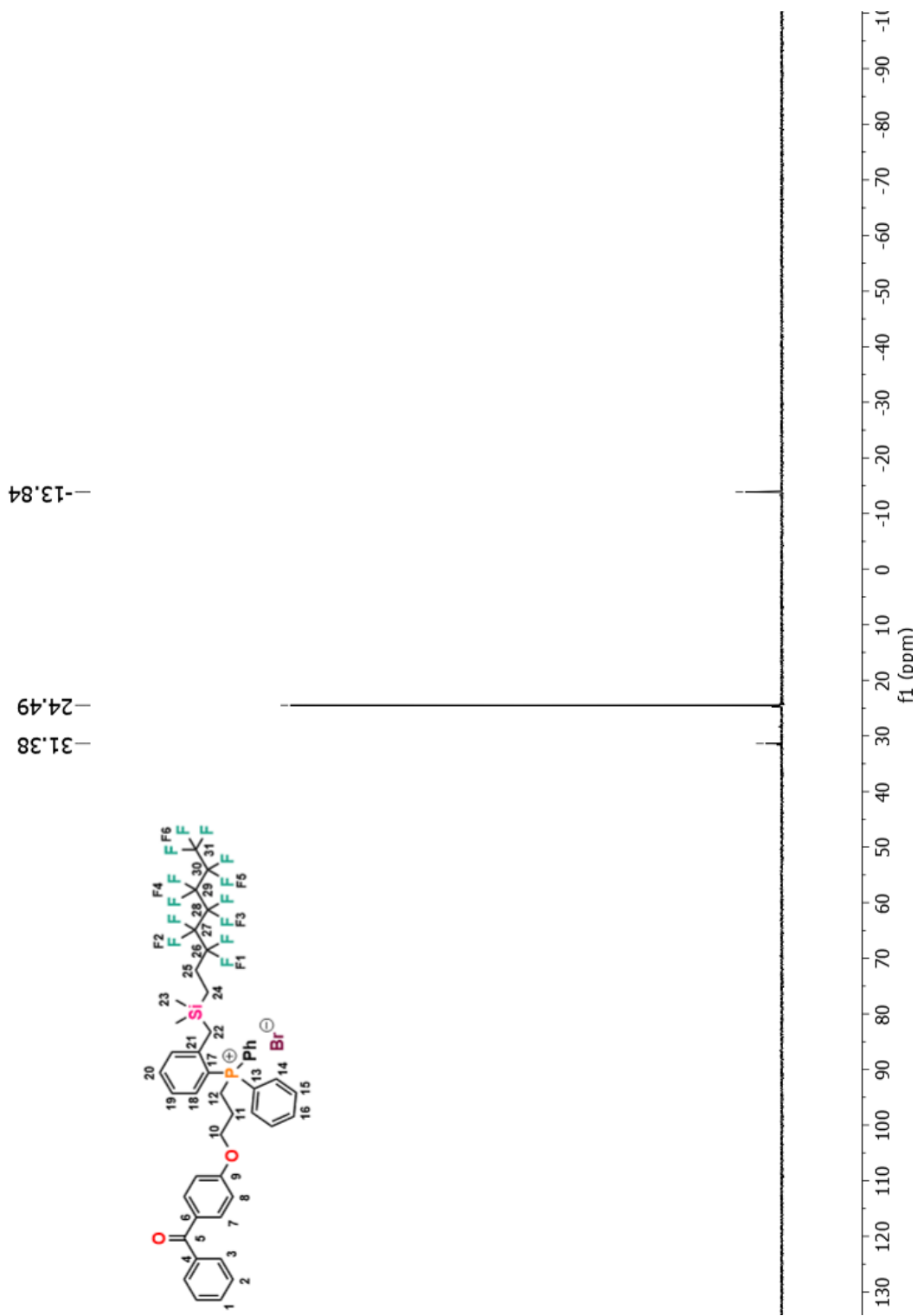
Figure A 53. ^{31}P {^{1}H} NMR (CDCl$_3$) spectrum of **5.**
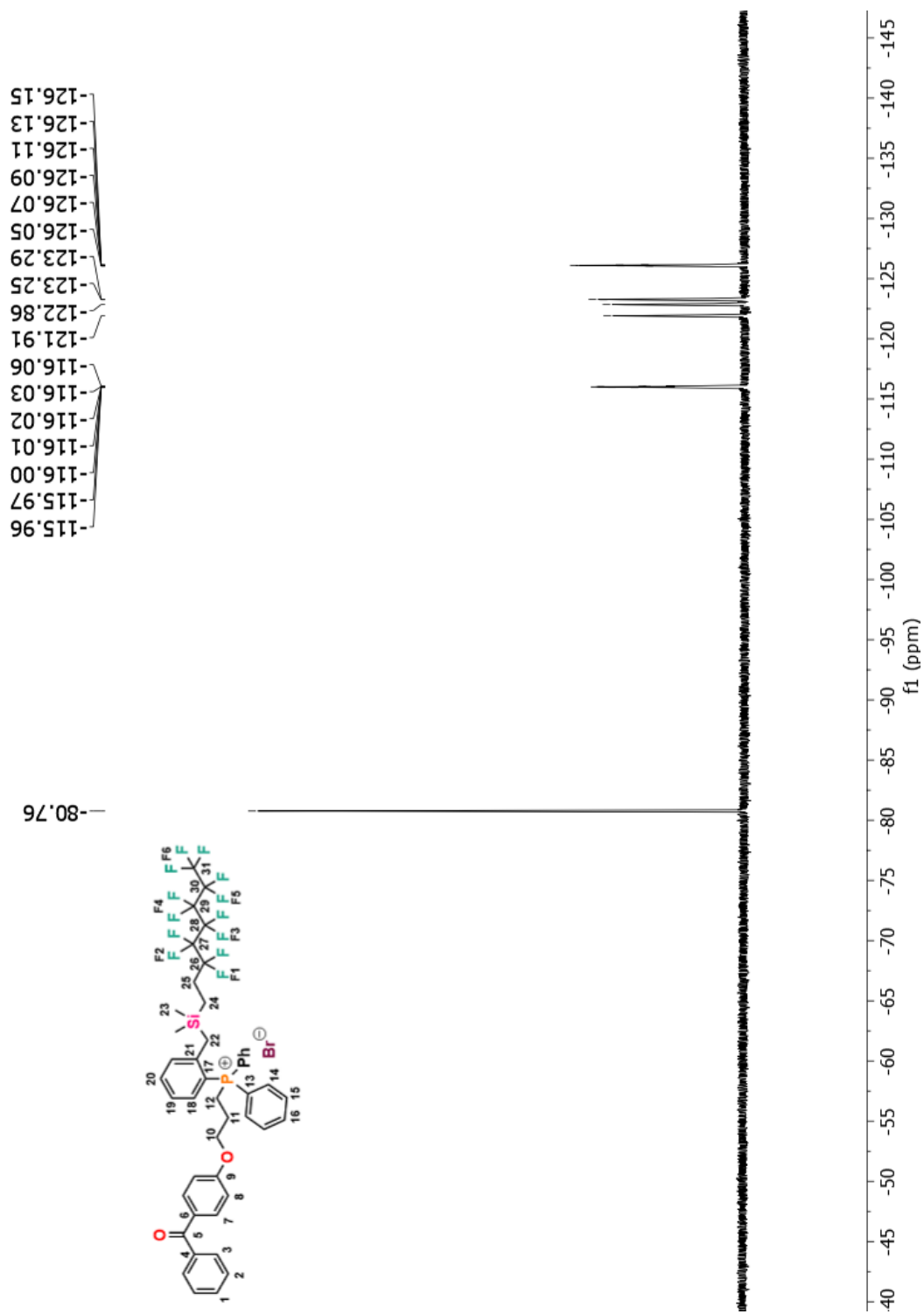
Figure A 54. ^{19}F {^{1}H} NMR (CDCl$_3$) spectrum of **5.**
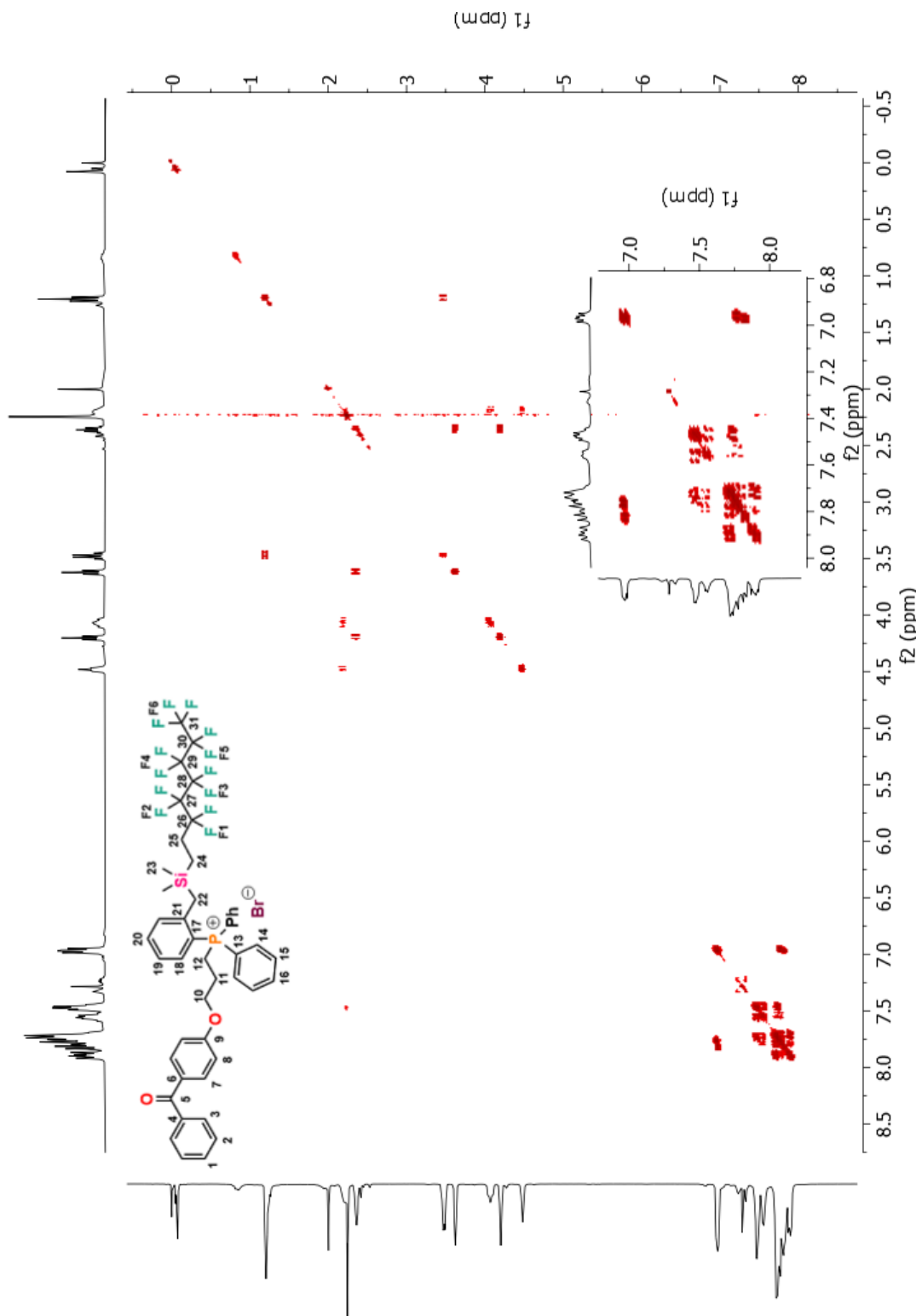
Figure A 55. 2D COSY NMR (CDCl₃) spectrum of **5**.
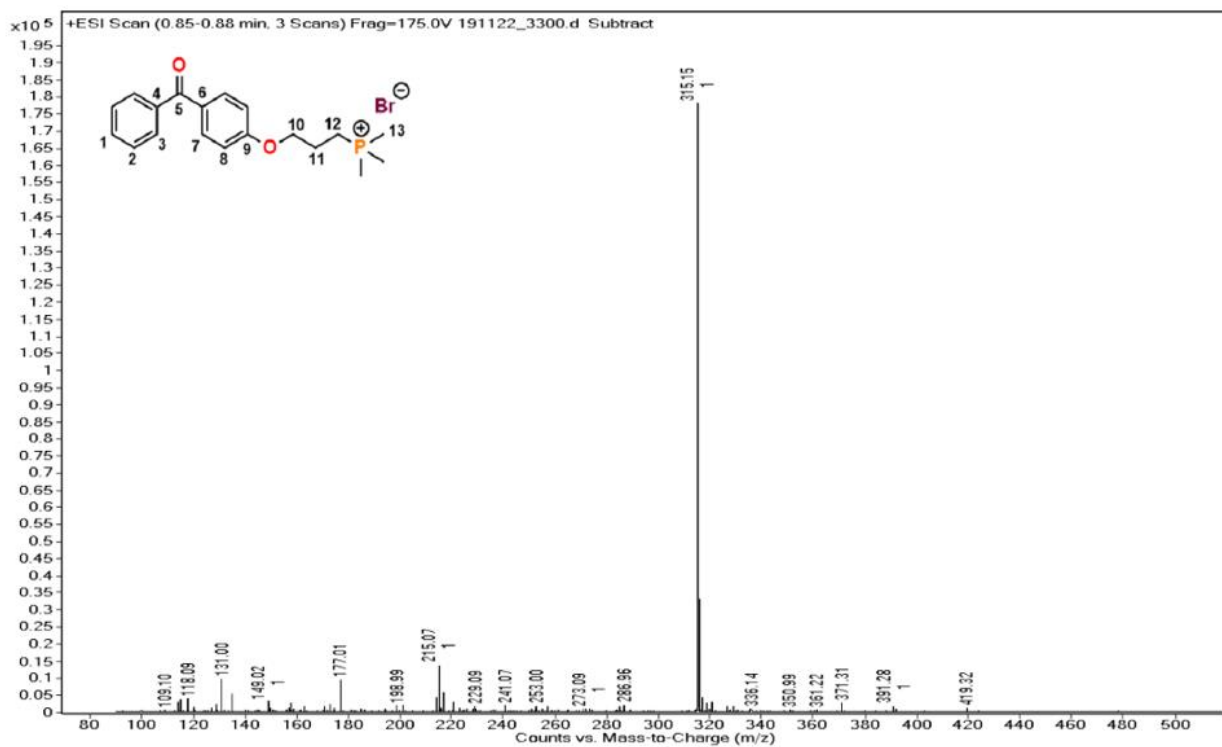
Figure B 1. HRMS (ESI-TOF) of **1**.

146
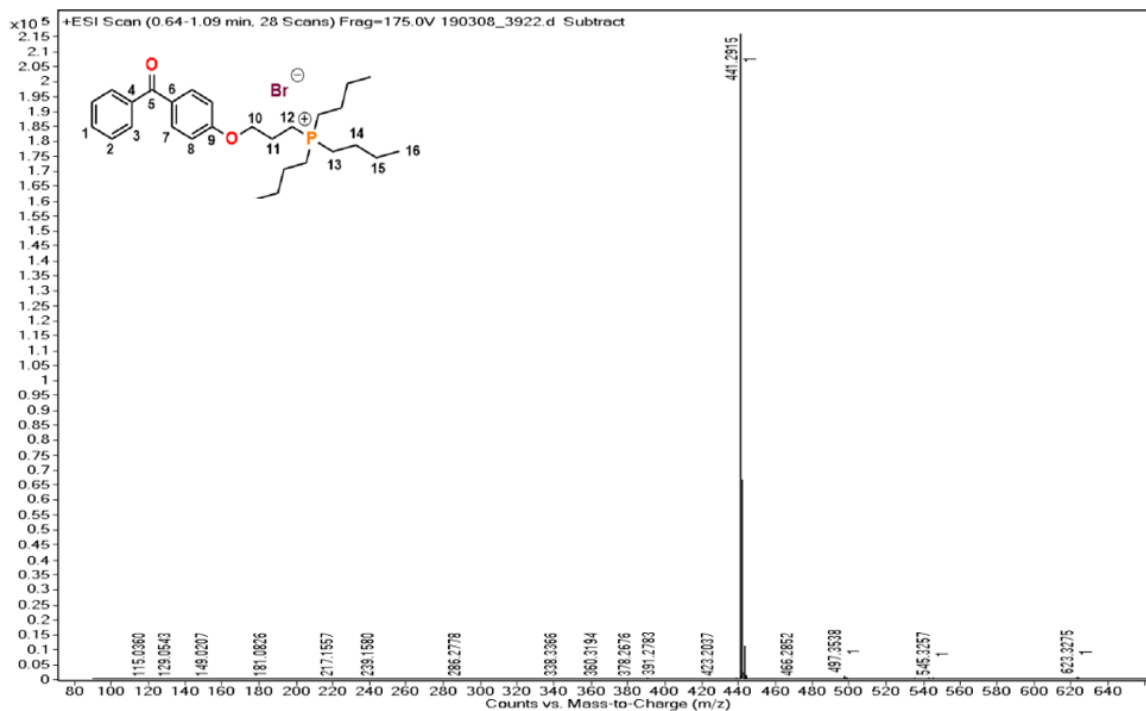
Figure B 2. HRMS (ESI-TOF) of **2**.
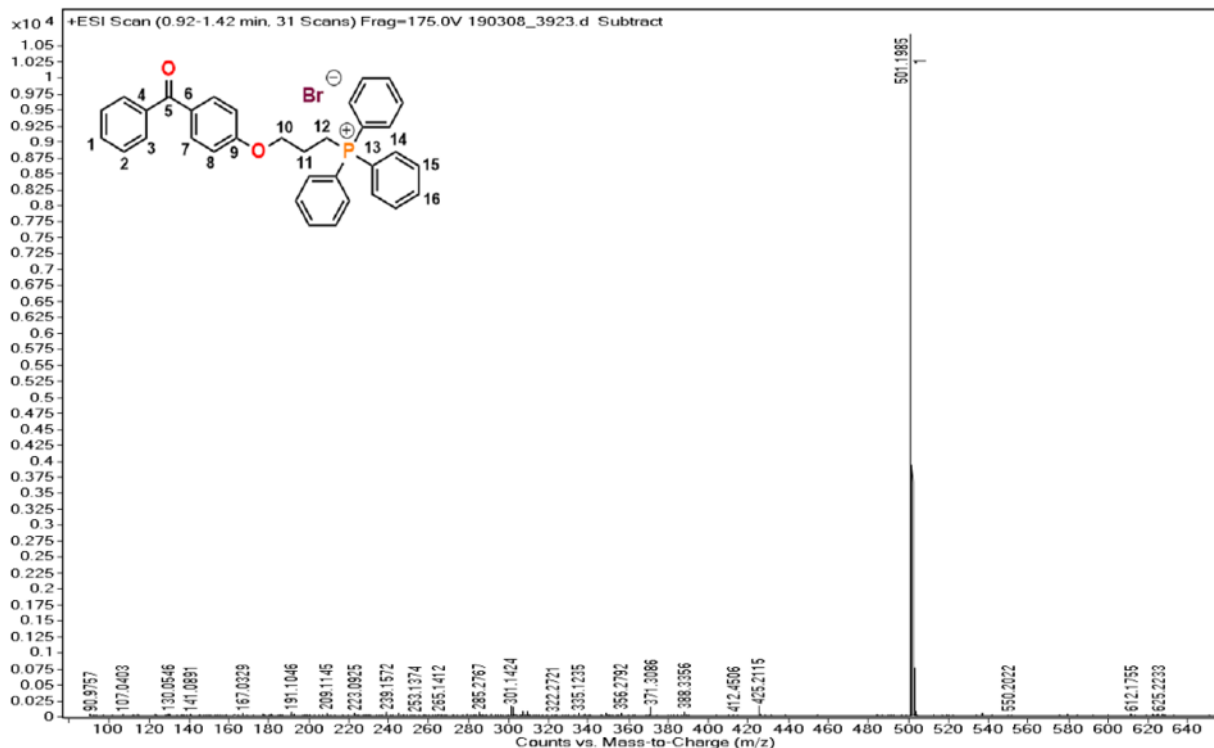
Figure B 3. HRMS (ESI-TOF) of **3**.
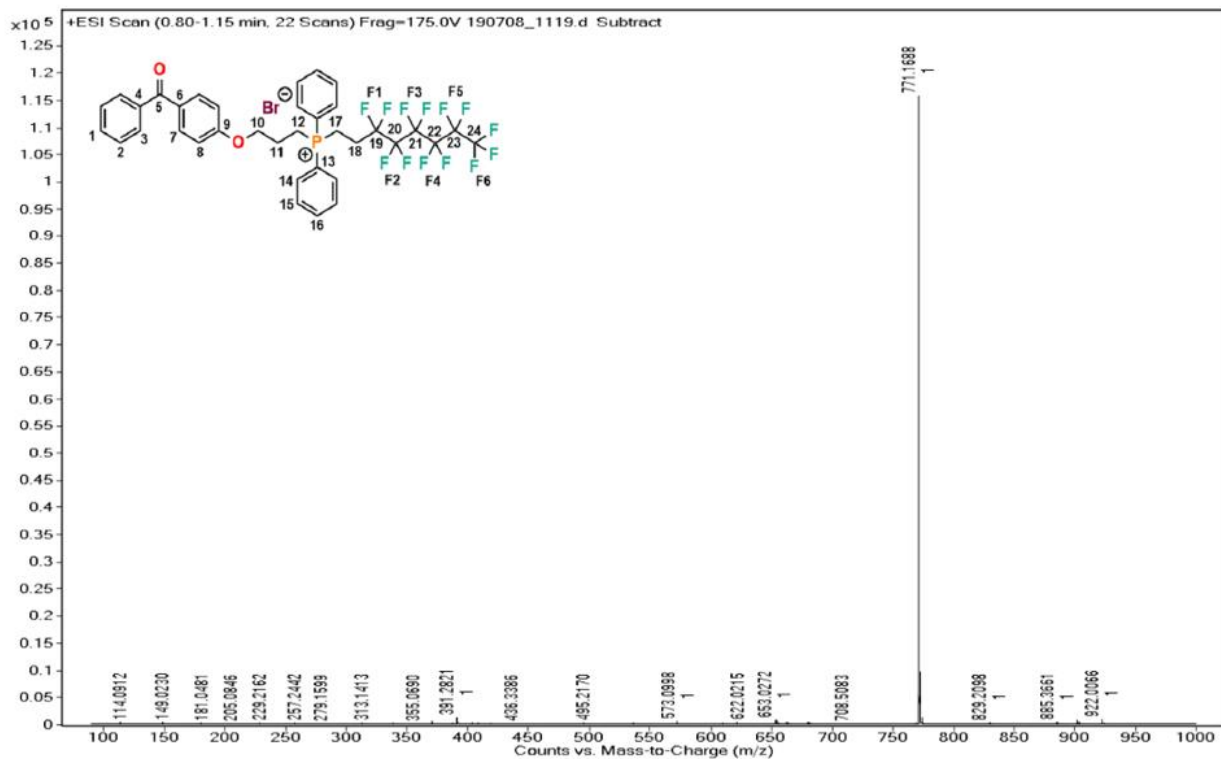
Figure B 4. HRMS (ESI-TOF) of **4**.
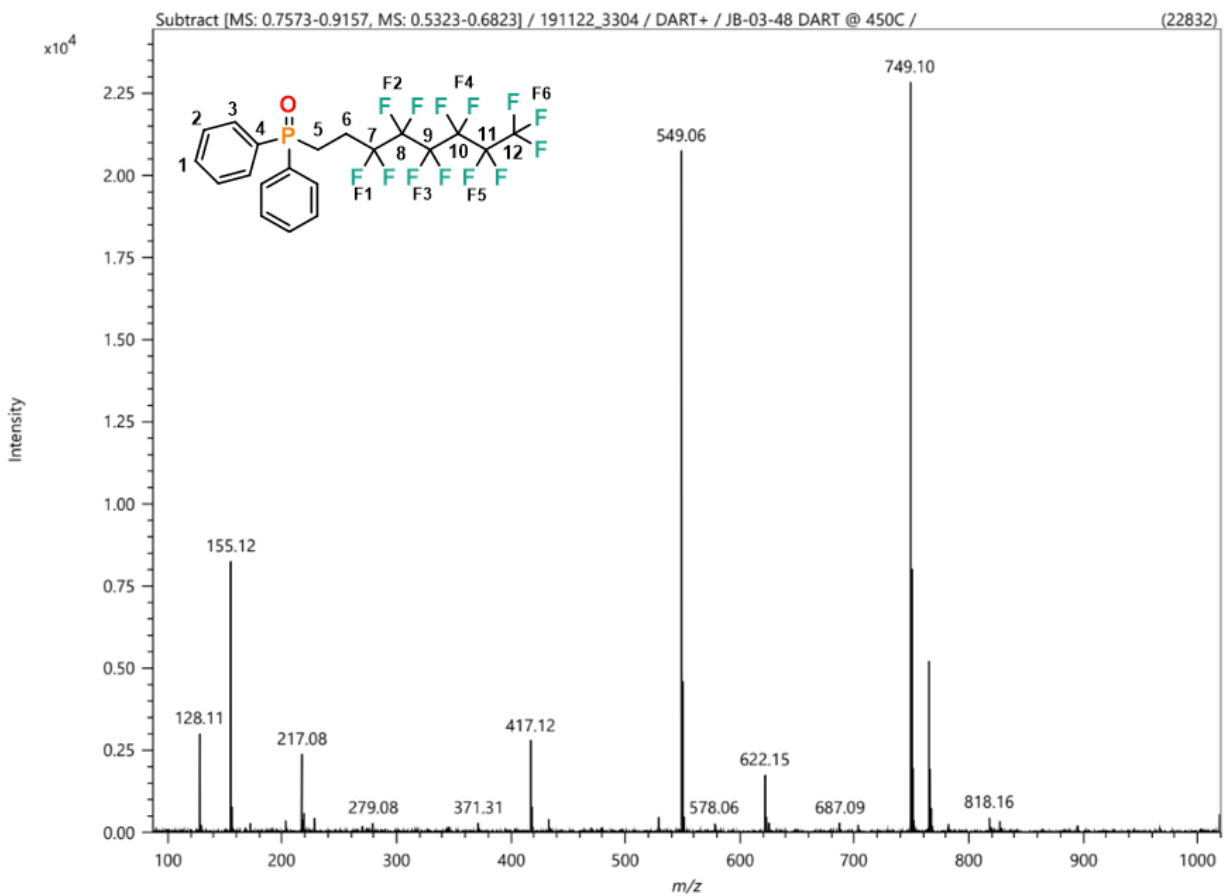
Figure B 5. HRMS (DART) of **iii**.
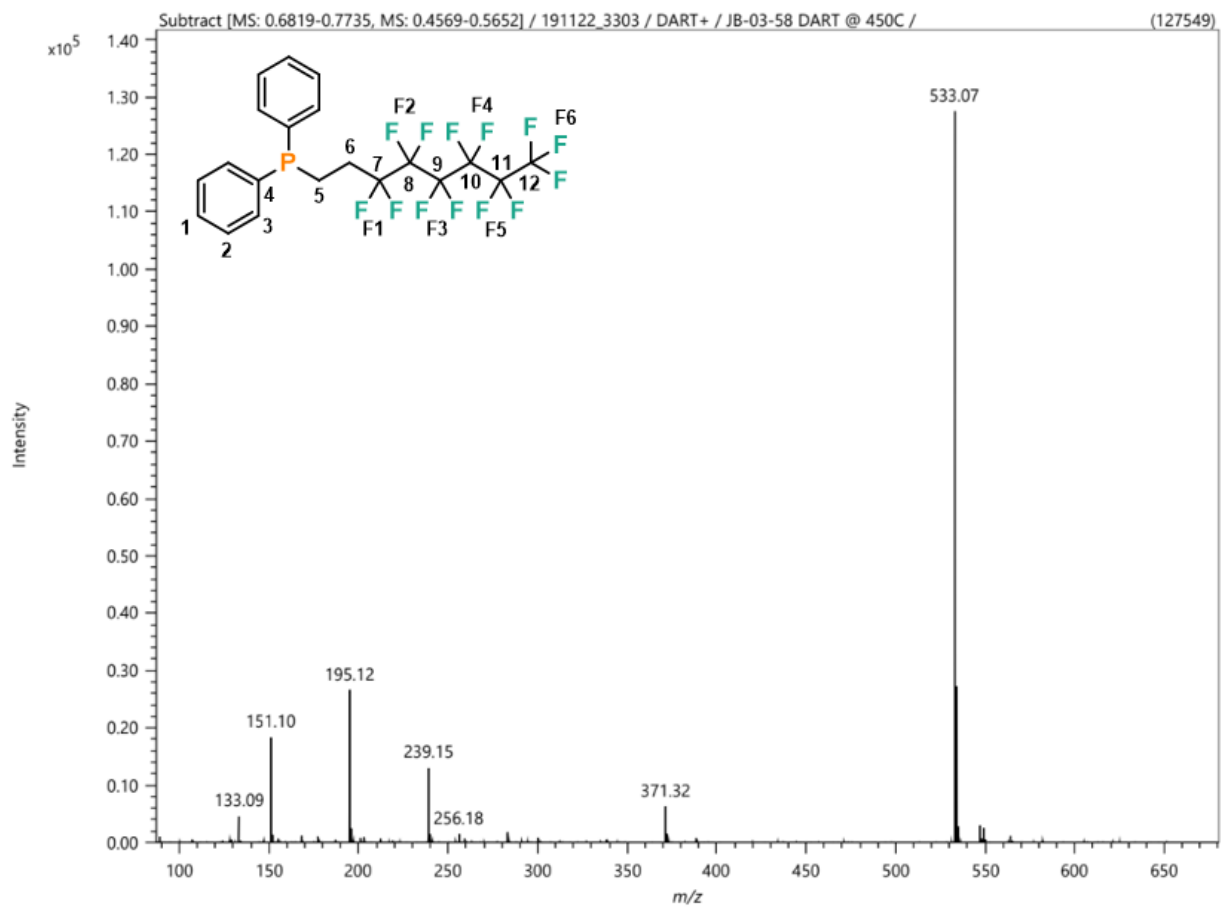
Figure B 6. HRMS (DART) of **iv**.
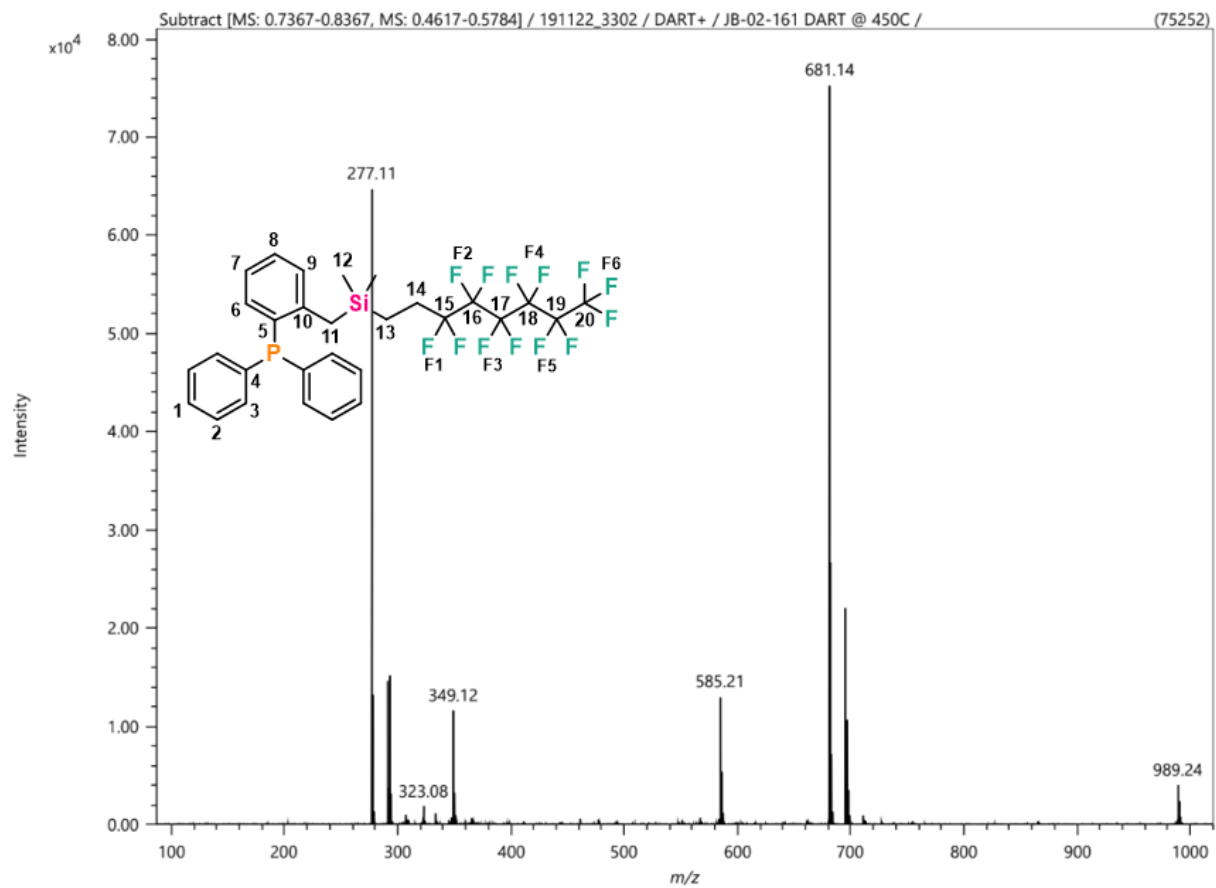
Figure B 7. HRMS (DART) of **vii.**

Appendix C – Surface Characterization

Table C 1. Raw contact angle data for PS coated with phosphoniums.

PS Pieces Coated with Phosphoniums					
Compound	Contact Angle (°)			Average Contact Angle (°)	Deviation
PMe$_3$ (**1**)	77	67.1	71.6	71.9	4.96
PBu$_3$ (**2**)	26.1	35	48	36.4	11.0
PPh$_3$ (**3**)	67.1	66.6	56.9	63.5	5.75
PEtC$_6$F$_{13}$ (**4**)	68.4	65.8	69.7	68.0	1.99

Table C 2. Raw contact angle data for PP coextruded with 1 % (w/w) phosphoniums.

Phosphoniums co-extruded with 1% PP					
Compound	Contact Angle (°)			Average Contact Angle (°)	Deviation
Control	98.3	95.8	96.1	96.7	1.37
PBu$_3$ (**2**)	82.5	78.7	86.1	82.4	3.70
PPh$_3$ (**3**)	85.2	90.5	96.4	90.7	5.6
PEtC$_6$F$_{13}$ (**4**)	79.8	83.2	73.4	78.8	4.98

Table C 3. Raw contact angle data for PP coextruded with 1.5 % (w/w) phosphoniums.

Phosphoniums co-extruded at 1.5% with PP					
Compound	Contact Angle (°)			Average Contact Angle (°)	Deviation
Control	82	90	91.4	87.8	5.07
PBu$_3$ (**2**)	50.8	68.8	74.1	64.6	12.21
PPh$_3$ (**3**)	79	73.3	76.2	76.2	2.9
PEtC$_6$F$_{13}$ (**4**)	73	67.8	73.4	71.4	3.12
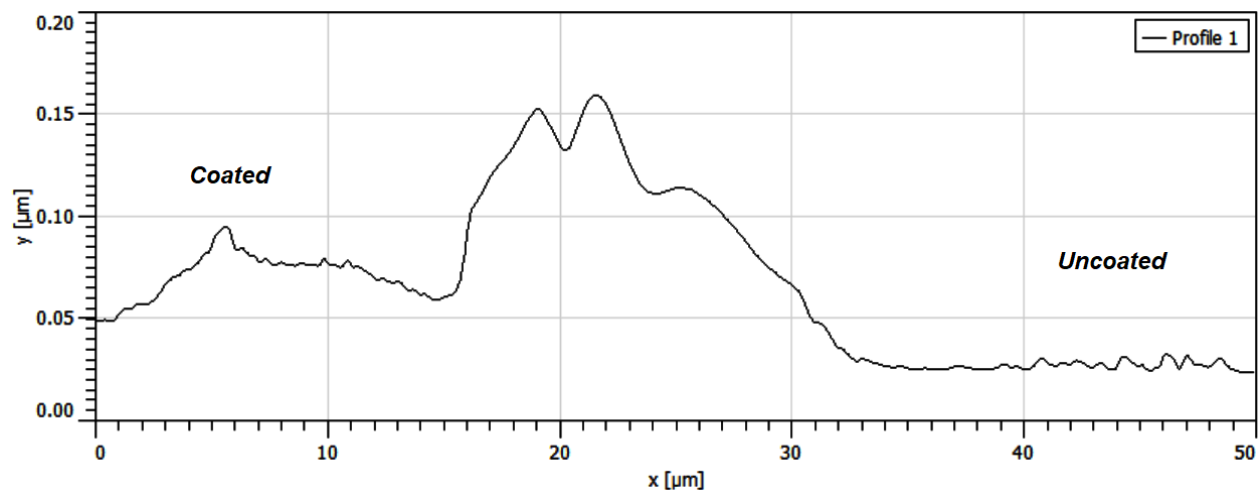
Figure C 1. AFM step height profile 1 for PC coated with **2**.
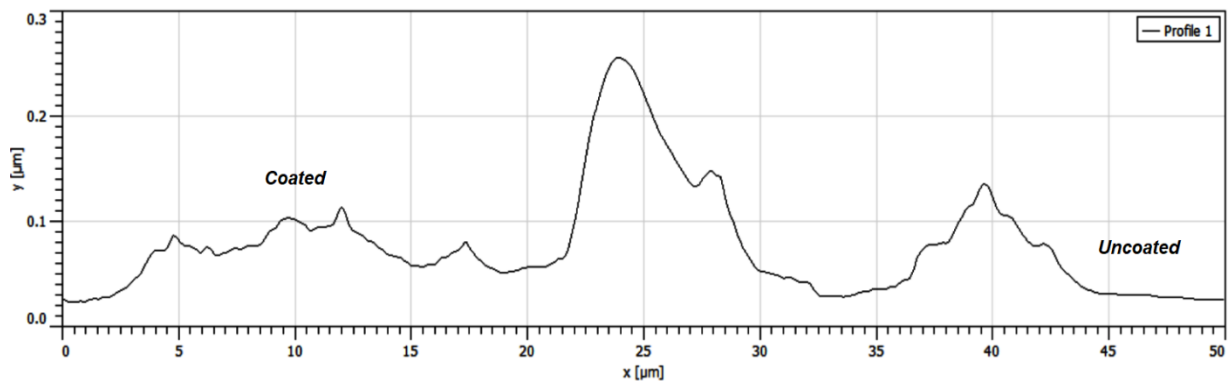
Figure C 2. AFM step height profile 2 for PC coated with **2**.
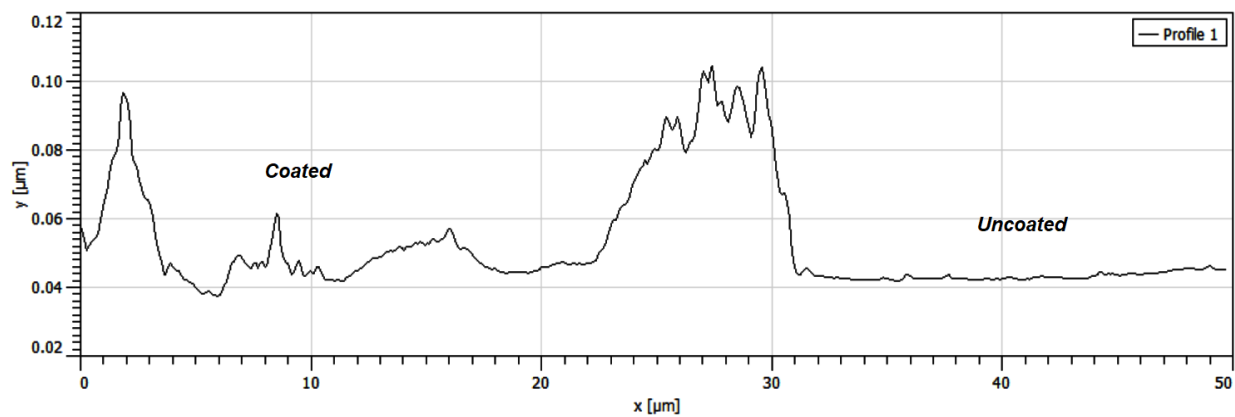
Figure C 3. AFM step height profile 3 for PC coated with **2**.
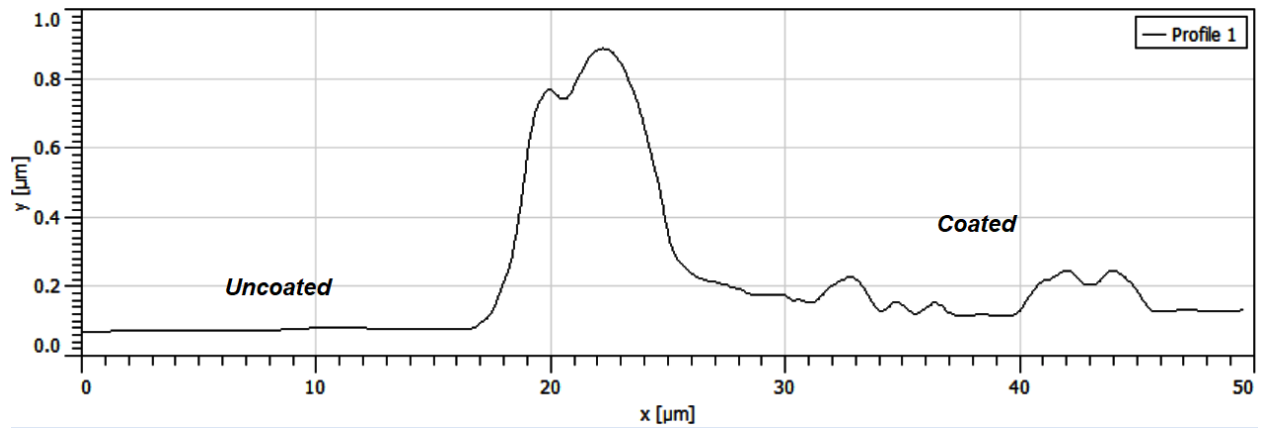
Figure C 4. AFM step height profile 1 for PC coated with **3**.
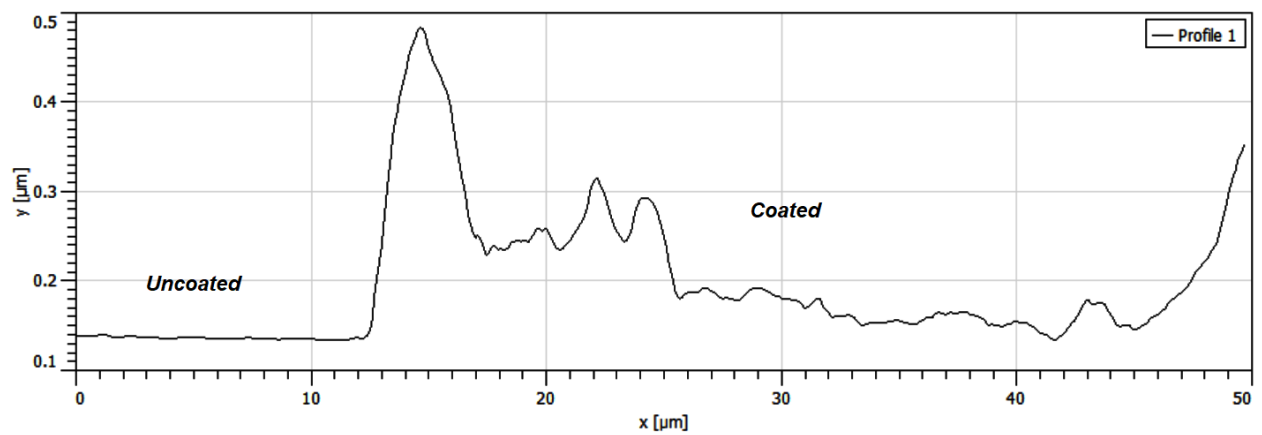
Figure C 5. AFM step height profile 2 for PC coated with **3**.
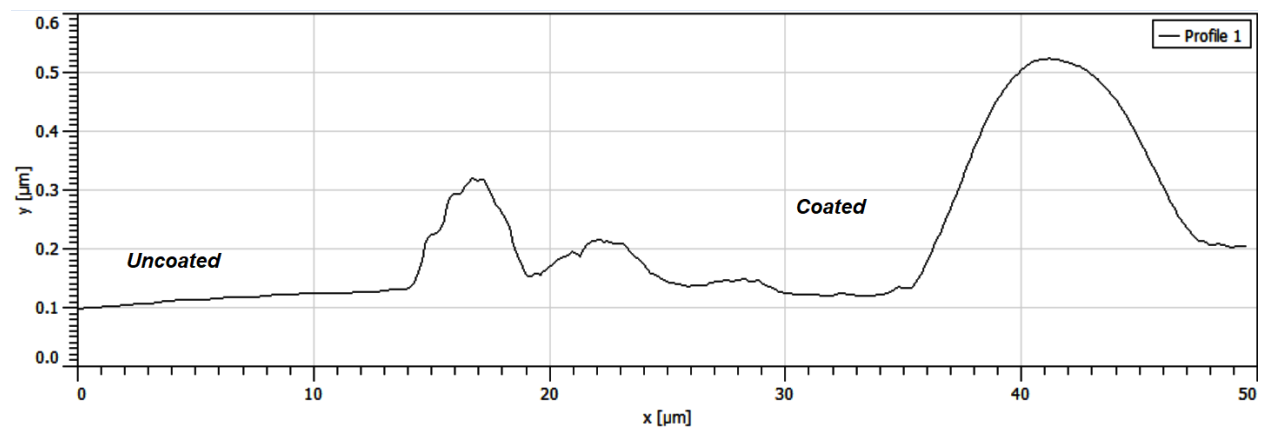
Figure C 6. AFM step height profile 3 for PC coated with **3**.
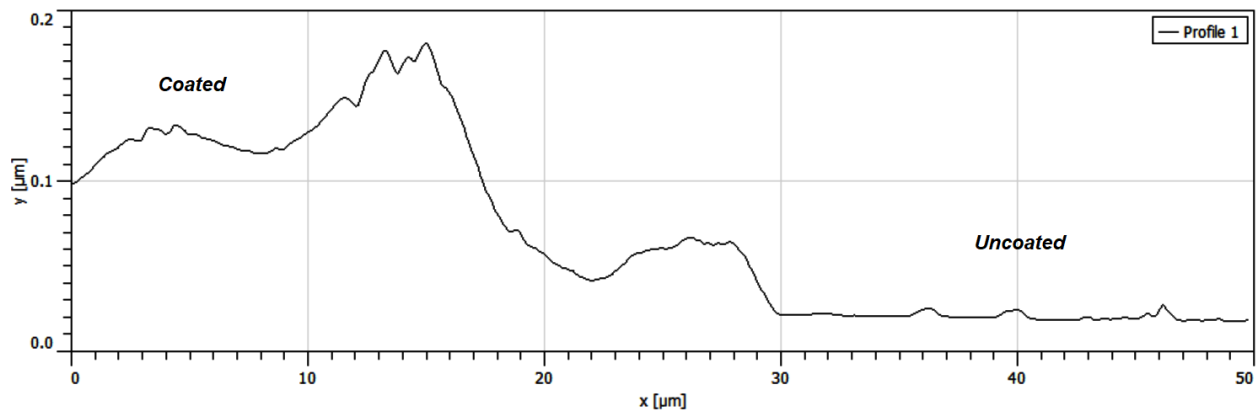
Figure C 7. AFM step height profile 1 for PC coated with **4**.
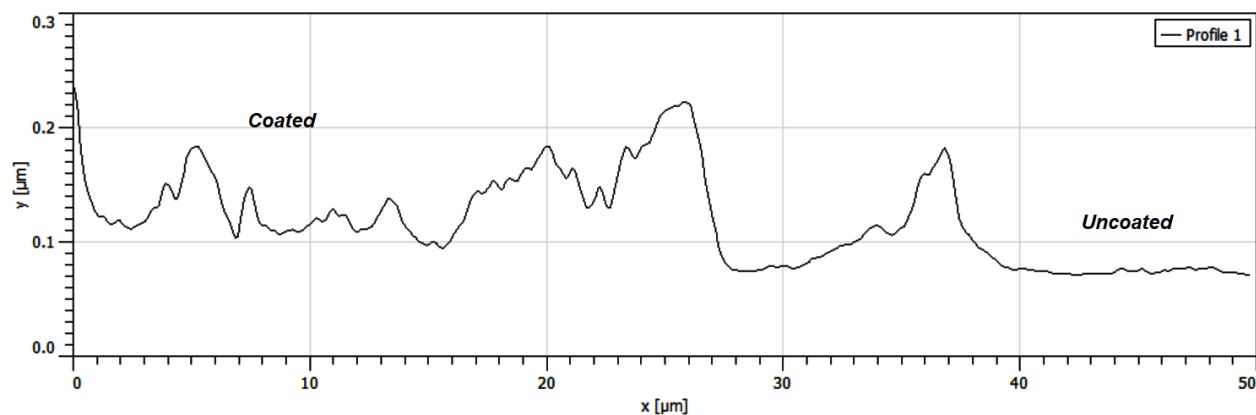
Figure C 8. AFM step height profile 2 for PC coated with **4**.
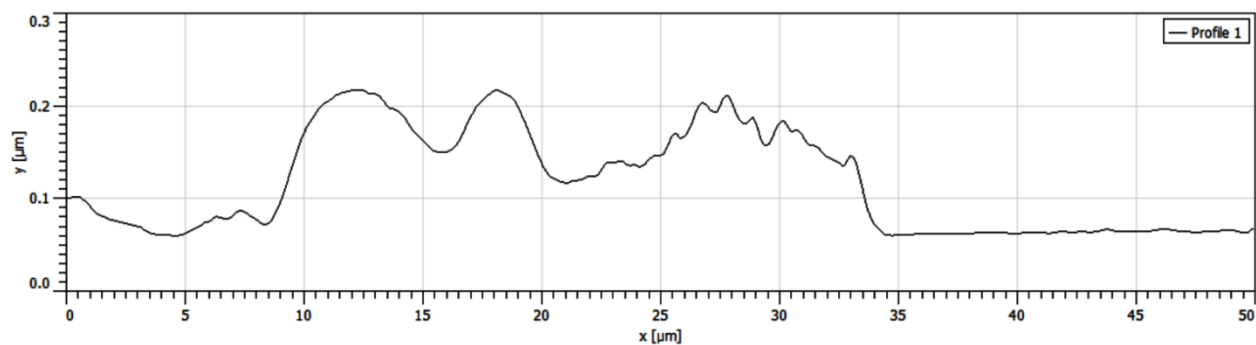
Figure C 9. AFM step height profile 3 for PC coated with **4**.
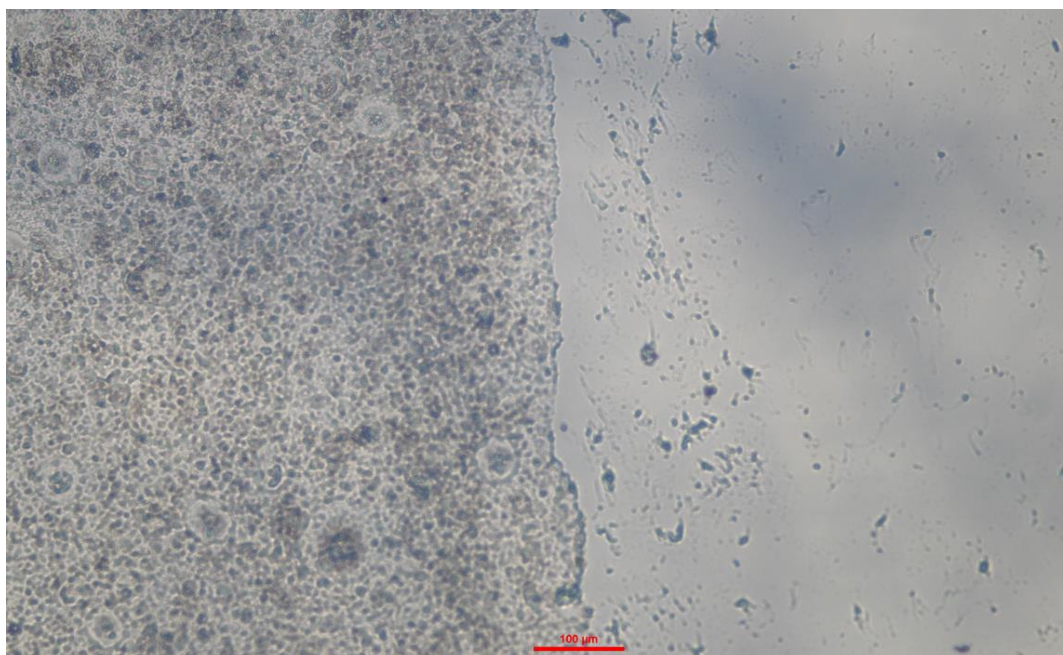
Figure C 10. Optical microscope (10 × magnification) image of **4** coated on PC.

Table C 4. Raw surface charge data of phosphonium coatings.

Phosphonium sample	Avg Abs	Dev	Conc (M)	mol	atoms	charge cm^{-2}
PMe$_3$ (**1**)	0.082	0.0016	1.064×10^{-6}	1.064×10^{-8}	6.405×10^{15}	1.601×10^{15}
PBu$_3$ (**2**)	0.199	0.0247	2.59×10^{-6}	2.590×10^{-8}	1.559×10^{16}	3.899×10^{15}
PPh$_3$ (**3**)	0.148	0.0349	1.926×10^{-6}	1.926×10^{-8}	1.160×10^{16}	2.900×10^{15}
PC$_6$F$_{13}$ (**4**)	0.151	0.0383	1.962×10^{-6}	1.962×10^{-8}	1.181×10^{16}	2.954×10^{15}
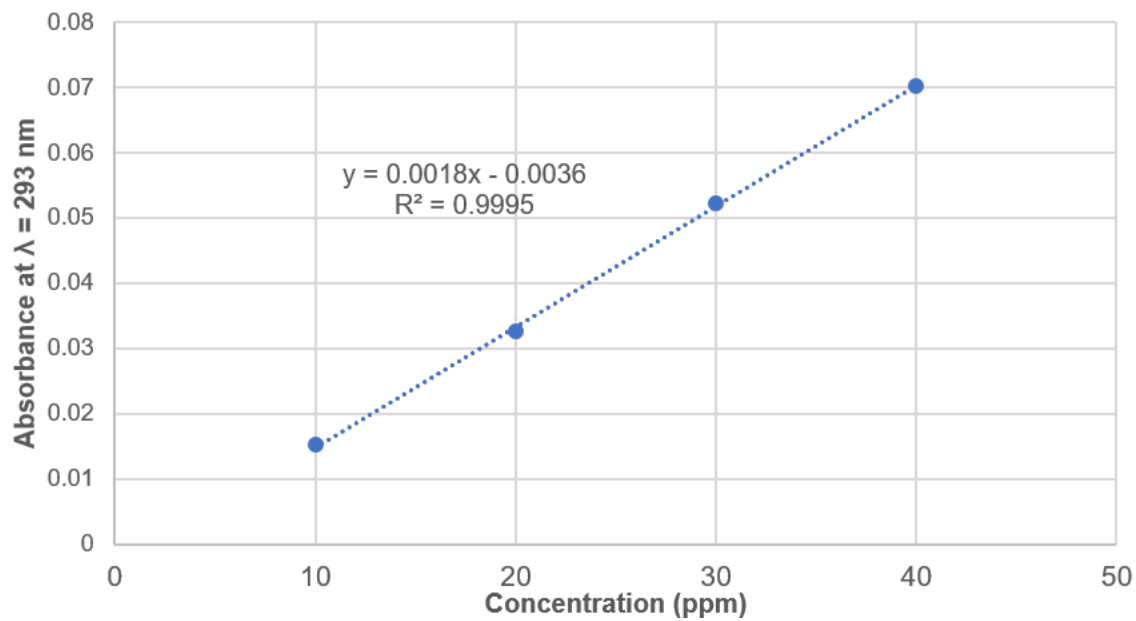
Figure C 12. Calibration curve for **2** in water.
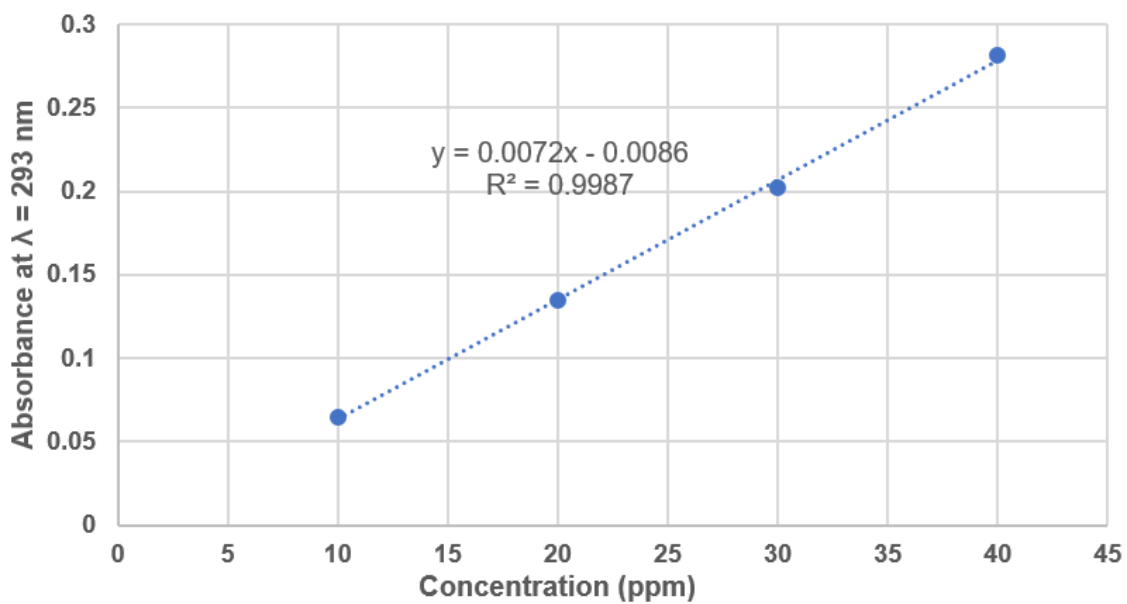
Figure C 11. Calibration curve for **3** in water.

Appendix D – Large droplet inoculum testing data

Table D 1. Raw data from the LDI testing of phosphonium coatings against *Arthrobacter* sp. (IAI-3). Control and treated surfaces were inoculated with a 10 µL droplet of 10^7 CFU in sterile tap water for 3 h.

Coating	Sample	Control		Treated	
		Total CFU	**Log total (log (CFU))**	**Total CFU**	**Log total (log (CFU))**
1	1	1.52×10^7	7.18	1.99×10^7	7.30
	2	1.04×10^7	7.02	1.49×10^7	7.17
	3	1.64×10^7	7.21	1.95×10^7	7.29
	Average	1.40×10^7	**7.15**	1.81×10^7	**7.26**
	STD	3.15×10^6	0.11	2.75×10^6	0.07
2	1	1.52×10^7	7.18	0.00	0.00
	2	1.04×10^7	7.02	0.00	0.00
	3	1.64×10^7	7.21	0.00	0.00
	Average	1.40×10^7	**7.15**	0.00	**0.00**
	STD	3.15×10^6	0.11	-	-
3	1	1.52×10^7	7.18	0.00	0.00
	2	1.04×10^7	7.02	0.00	0.00
	3	1.64×10^7	7.21	0.00	0.00
	Average	1.40×10^7	**7.15**	0.00	**0.00**
	STD	3.15×10^6	0.11	-	-
4	1	3.25×10^5	5.51	0.00	0.00
	2	5.30×10^5	5.72	0.00	0.00
	3	2.20×10^5	5.34	0.00	0.00
	Average	3.58×10^5	**5.53**	0.00	**0.00**
	STD	1.58×10^5	0.19	-	-

Table D 2. Raw data from LDI testing of phosphonium coatings against *E. coli* (ATCC 11229). Control and treated surfaces were inoculated with a 10 µL droplet of 10^7 CFU in sterile tap water for 24 h.

Coating	Sample	Control		Treated	
		Total CFU	Log total (log (CFU))	Total CFU	Log total (log (CFU))
1	1	1.12×10^4	4.05	7.95×10^4	4.90
	2	3.70×10^5	5.57	5.30×10^5	5.72
	3	8.75×10^4	4.94	3.20×10^5	5.51
	Average	1.56×10^5	**5.19**	3.10×10^5	**5.49**
	STD	1.89×10^5	0.76	2.25×10^5	0.43
2	1	1.12×10^4	4.05	0.00	0.00
	2	3.70×10^5	5.57	0.00	0.00
	3	8.75×10^4	4.94	0.00	0.00
	Average	1.56×10^5	**5.19**	0.00	**0.00**
	STD	1.89×10^5	0.76	-	-
3	1	1.12×10^4	4.05	0.00	0.00
	2	3.70×10^5	5.57	0.00	0.00
	3	8.75×10^4	4.94	0.00	0.00
	Average	1.56×10^5	**5.19**	0.00	**0.00**
	STD	1.89×10^5	0.76	-	-
4	1	1.12×10^4	4.05	0.00	0.00
	2	3.70×10^5	5.57	0.00	0.00
	3	8.75×10^4	4.94	0.00	0.00
	Average	1.56×10^5	**5.19**	0.00	**0.00**
	STD	1.89×10^5	0.76	-	-

Table D 3. Raw data from the LDI testing of 1 % phosphonium-containing PP against *Arthrobacter* sp. (IAI-3). Control and treated surfaces were inoculated with a 10 µL droplet of 10^7 CFU in sterile tap water for 3 h.

Material	Sample	Control		Treated	
		Total CFU	Log total (log (CFU))	Total CFU	Log total (log (CFU))
PP-2	1	2.10×10^6	6.32	0.00	0.00
	2	1.20×10^6	6.08	0.00	0.00
	3	2.90×10^6	6.46	0.00	0.00
	Average	2.07×10^6	**6.29**	0.00	**0.00**
	STD	8.53×10^5	0.19	-	-
PP-3	1	2.10×10^6	6.32	0.00	0.00
	2	1.20×10^6	6.08	0.00	0.00
	3	2.90×10^6	6.46	0.00	0.00
	Average	2.07×10^6	**6.29**	0.00	**0.00**
	STD	8.53×10^5	0.19	-	-
PP-4	1	2.10×10^6	6.32	0.00	0.00
	2	1.20×10^6	6.08	0.00	0.00
	3	2.90×10^6	6.46	0.00	0.00
	Average	2.07×10^6	**6.29**	0.00	**0.00**
	STD	8.53×10^5	0.19	-	-

Table D 4. Raw data from the LDI testing of 1 % phosphonium-containing PP against *E. coli* *(*ATCC 11229). Control and treated surfaces were inoculated with a 10 µL droplet of 10^7 CFU in sterile tap water for 24 h.

Material	Sample	Control		Treated	
		Total CFU	Log total (log (CFU))	Total CFU	Log total (log (CFU))
PP-2	1	2.50×10^3	3.40	0.00	0.00
	2	1.03×10^4	4.01	0.00	0.00
	3	4.40×10^3	3.64	0.00	0.00
	Average	5.72×10^3	**3.68**	0.00	**0.00**
	STD	4.04×10^3	0.31	-	-
PP-3	1	2.50×10^3	3.40	0.00	0.00
	2	1.03×10^4	4.01	0.00	0.00
	3	4.40×10^3	3.64	0.00	0.00
	Average	5.72×10^3	**3.68**	0.00	**0.00**
	STD	4.04×10^3	0.31	-	-
PP-4	1	2.50×10^3	3.40	0.00	0.00
	2	1.03×10^4	4.01	0.00	0.00
	3	4.40×10^3	3.64	0.00	0.00
	Average	5.72×10^3	**3.68**	0.00	**0.00**
	STD	4.04×10^3	0.31	-	-

Table D 5. Raw data from the LDI testing of 1 % phosphonium-containing PP against *Arthrobacter* sp. (IAI-3) after 50 solvent double rubs. Control and treated surfaces were inoculated with a 10 µL droplet of 10^7 CFU in sterile tap water for 3 h.

Material	Sample	Control		Treated	
		Total CFU	Log total (log (CFU))	Total CFU	Log total (log (CFU))
PP-2	1	7.80×10^5	5.89	0.00	0.00
	2	8.65×10^5	5.94	2.05×10^4	4.31
	3	1.16×10^6	6.06	6.65×10^4	4.82
	Average	9.33×10^5	**5.96**	2.90×10^4	**3.04**
	STD	1.97×10^5	0.09	-	-
PP-4	1	7.80×10^5	5.89	0.00	0.00
	2	8.65×10^5	5.94	0.00	0.00
	3	1.16×10^6	6.06	0.00	0.00
	Average	9.33×10^5	**5.96**	0.00	0.00
	STD	1.97×10^5	0.09	0.00	0.00

Table D 6. Raw data from the LDI testing of 1 % phosphonium-containing PP against *Arthrobacter* sp. (IAI-3) after 100 solvent double rubs. Control and treated surfaces were inoculated with a 10 µL droplet of 10^7 CFU in sterile tap water for 3 h.

Material	Sample	Control		Treated	
		Total CFU	**Log total (log (CFU))**	**Total CFU**	**Log total (log (CFU))**
PP-2	1	4.60×10^6	6.66	N/A	N/A
	2	6.90×10^6	6.84	2.10×10^6	6.32
	3	1.00×10^7	7.00	5.70×10^6	6.76
	Average	7.17×10^6	**6.83**	3.90×10^6	**6.65**
	STD	2.71×10^6	0.17	2.88×10^6	0.31
PP-4	1	4.60×10^6	6.66	N/A	N/A
	2	6.90×10^6	6.84	3.15×10^4	4.50
	3	1.00×10^7	7.00	1.36×10^5	5.13
	Average	7.17×10^6	**6.83**	8.35×10^4	**4.82**
	STD	2.71×10^6	0.17	7.09×10^4	0.00

Table D 7. Raw data from the LDI testing of 1.5 % phosphonium-containing PP against *Arthrobacter* sp. (IAI-3) after 100 solvent double rubs. Control and treated surfaces were inoculated with a 10 µL droplet of 10^7 CFU in sterile tap water for 3 h.

Material	Sample	Control		Treated	
		Total CFU	Log total (log (CFU))	Total CFU	Log total (log (CFU))
PP-2	1	4.40×10^6	6.64	8.80×10^5	6.64
	2	3.70×10^6	6.57	0.00	0.00
	3	5.30×10^6	6.72	9.60×10^5	6.68
	Average	4.47×10^6	**6.65**	2.40×10^5	**3.34**
	STD	8.02×10^5	0.08	2.66×10^6	3.85
PP-3	1	4.40×10^6	6.64	2.30×10^6	6.36
	2	3.70×10^6	6.57	2.70×10^6	6.43
	3	5.30×10^6	6.72	0.00	0.00
	Average	4.47×10^6	**6.65**	1.35×10^6	**3.22**
	STD	8.02×10^5	0.08	1.46×10^6	4.55
PP-4	1	4.40×10^6	6.64	0.00	0.00
	2	3.70×10^6	6.57	0.00	0.00
	3	5.30×10^6	6.72	0.00	0.00
	Average	4.47×10^6	**6.65**	0.00	**0.00**
	STD	8.02×10^5	0.08	-	-

Table D 8. Raw data from the LDI testing of 1.5 % phosphonium-containing PP against *E. coli* (ATCC 11229) after 100 solvent double rubs. Control and treated surfaces were inoculated with a 10 µL droplet of 10^7 CFU in sterile tap water for 24 h.

Material	Sample	Control		Treated	
		Total CFU	Log total (log (CFU))	Total CFU	Log total (log (CFU))
PP-2	1	3.45×10^3	3.54	2.55×10^3	3.41
	2	2.20×10^4	4.34	1.30×10^3	3.11
	3	2.25×10^3	3.35	5.10×10^2	2.74
	Average	9.23×10^3	**3.74**	1.47×10^3	**2.93**
	STD	1.11×10^4	0.53	1.30×10^3	0.33
PP-3	1	3.45×10^3	3.54	0.00	0.00
	2	2.20×10^4	4.34	0.00	0.00
	3	2.25×10^3	3.35	0.00	0.00
	Average	9.23×10^3	**3.74**	0.00	**0.00**
	STD	1.11×10^4	0.53	-	-
PP-4	1	3.45×10^3	3.54	0.00	0.00
	2	2.20×10^4	4.34	0.00	0.00
	3	2.25×10^3	3.35	0.00	0.00
	Average	9.23×10^3	**3.74**	0.00	**0.00**
	STD	1.11×10^4	0.53	-	-

Table D 9. Raw data from the LDI testing of 1 % phosphonium-containing PS against *E. coli* *(*ATCC 11229). Control and treated surfaces were inoculated with a 10 µL droplet of 10^7 CFU in sterile tap water for 24 h.

Material	Sample	Control		Treated	
		Total CFU	**Log total (log (CFU))**	**Total CFU**	**Log total (log (CFU))**
PS-2	1	4.75×10^6	6.68	0.00	0.00
	2	3.95×10^6	6.60	0.00	0.00
	3	7.35×10^6	6.87	0.00	0.00
	Average	5.35×10^6	**6.71**	0.00	**0.00**
	STD	1.78×10^6	0.14	-	-
PS-3	1	4.75×10^6	6.68	7.40×10^4	4.87
	2	3.95×10^6	6.60	4.85×10^4	4.69
	3	7.35×10^6	6.87	5.40×10^4	4.73
	Average	5.35×10^6	**6.71**	5.88×10^4	**4.77**
	STD	1.78×10^6	0.14	1.34×10^4	0.10

REFERENCES

(1)   Magill, S. S.; Edwards, J. R.; Bamberg, W.; Beldavs, Z. G.; Dumyati, G.; Kainer, M. A.; Lynfield, R.; Maloney, M.; McAllister-Hollod, L.; Nadle, J.; Ray, S. M.; Thompson, D. L.; Wilson, L. E.; Fridkin, S. K. Multistate Point-Prevalence Survey of Health Care–Associated Infections. *N. Engl. J. Med.* **2014**, *370*, 1198–1208.

(2)   Huslage, K.; Rutala, W. A.; Sickbert-Bennet, E.; Weber, D. J. A Quantitative Approach to Defining " High-Touch " Surfaces in Hospitals. *Infect. Control Hosp. Epidemiol.* **2016**, *31*, 850–853.

(3)   Percival, S. L.; Suleman, L.; Vuotto, C.; Donelli, G. Healthcare-Associated Infections, Medical Devices and Biofilms: Risk, Tolerance and Control. *J. Med. Microbiol.* **2015**, *64*, 323–334.

(4)   Dancer, S. J. Importance of the Environment in Meticillin-Resistant Staphylococcus Aureus Acquisition: The Case for Hospital Cleaning. *Lancet Infect. Dis.* **2008**, *8*, 101–113.

(5)   Zimlichman, E.; Henderson, D.; Tamir, O.; Franz, C.; Song, P.; Yamin, C. K.; Keohane, C.; Denham, C. R.; Bates, D. W. Health Care-Associated Infections: A Meta-Analysis of Costs and Financial Impact on the US Health Care System. *JAMA Intern. Med.* **2016**, *173*, 2039–2046.

(6)   Andersson, D. I.; Hughes, D. Evolution of Antibiotic Resistance at Non-Lethal Drug Concentrations. *Drug Resist. Updat.* **2012**, *15*, 162–172.

(7)   Flemming, H.; Wingender, J. The Biofilm Matrix. *Nat. Rev. Microbiol.* **2010**, *8*, 623–633.

(8)   Hoffman, L. R.; D'Argenio, D. A.; MacCoss, M. J.; Zhang, Z.; Jones, R. A.; Miller, S. I. Aminoglycoside Antibiotics Induce Bacterial Biofilm Formation. *Nature* **2005**, *436*, 1171–1175.

(9)   Olsen, I. Biofilm-Specific Antibiotic Tolerance and Resistance. *Eur. J. Clin. Microbiol. Infect. Dis.* **2015**, *34*, 877–886.

(10)   Bandeira, M.; Carvalho, P. A.; Duarte, A.; Jordao, L. Bacterial Biofilms, Antibiotic Resistance and Healthcare-Associated Infections: A Dangerous Connection. *Microsc. Microanal.* **2015**, *21*, 38–39.

(11)   Donlan, R. M. Role of Biofilms in Antimicrobial Resistance. *ASAIO J.* **2000**, *47*, S47–S52.

(12)   Stewart, P. S. Mechanisms of Antibiotic Resistance in Bacterial Biofilms. *Int. J. Med. Microbiol.* **2002**, *292*, 107–113.

(13)   Hausner, M.; Wuertz, S. High Rates of Conjugation in Bacterial Biofilms as Determined by Quantitative in Situ Analysis. *Appl. Environ. Microbiol.* **1999**, *65*, 3710–3713.

(14)   Wessner, D.; Dupont, C.; Charles, T.; Neufeld, J. Microbiology, 2nd ed.; John Wiley & Sons: New York, 2017.

(15)   Klibanov, A. M. Permanently Microbicidal Materials Coatings. *J. Mater. Chem.* **2007**, *17*, 2479–2482.

(16)   Ferreira, L.; Zumbuehl, A. Non-Leaching Surfaces Capable of Killing Microorganisms on Contact. *J. Mater. Chem.* **2009**, *19*, 7796–7806.

(17)   Porosa, L.; Caschera, A.; Bedard, J.; Mocella, A.; Ronan, E.; Lough, A. J.; Wolfaardt, G.; Foucher, D. A. UV-Curable Contact Active Benzophenone Terminated Quaternary Ammonium Antimicrobials for Applications in Polymer Plastics and Related Devices. *ACS Appl. Mater. Interfaces* **2017**, *9*, 27491–27503.

(18)   Siedenbiedel, F.; Tiller, J. C. Antimicrobial Polymers in Solution and on Surfaces: Overview and Functional Principles. *Polymers* **2012**, *4*, 46–71.

(19)   Lewis, K.; Klibanov, A. M. Surpassing Nature: Rational Design of Sterile-Surface Materials. *Trends Biotechnol.* **2005**, *23*, 343–348.

(20)   Chouirfa, H.; Bouloussa, H.; Migonney, V.; Falentin-Daudré, C. Review of Titanium Surface Modification Techniques and Coatings for Antibacterial Applications. *Acta Biomater.* **2019**, *83*, 37–54.

(21)   Gupta, D. Antimicrobial Treatments for Textiles. *Indian J. Fibre Text. Res.* **2007**, *32*, 254–263.

(22)   Salwiczek, M.; Qu, Y.; Gardiner, J.; Strugnell, R. A.; Lithgow, T.; McLean, K. M.; Thissen, H. Emerging Rules for Effective Antimicrobial Coatings. *Trends Biotechnol.* **2014**, *32*, 82–90.

(23)   Kristinsson, K. G. Antimicrobial Activity of Polymers Coated with Iodine-Complexed Polyvinylpyrrolidone. *J. Biomater. Appl.* **1991**, *5*, 173–184.

(24)   Smith, A. W. Biofilms and Antibiotic Therapy: Is There a Role for Combating Bacterial Resistance by the Use of Novel Drug Delivery Systems? *Adv. Drug Deliv. Rev.* **2005**, *57*,

1539–1550.

(25)   Yu, S.; Yin, Y.; Liu, J. Silver Nanoparticles in the Environment. *Environ. Sci. Process. Impacts* **2013**, *15*, 78–92.

(26)   Hegde, K.; Brar, S. K.; Verma, M.; Surampalli, R. Y. Current Understandings of Toxicity, Risks and Regulations of Engineered Nanoparticles with Respect to Environmental Microorganisms. *Nanotechnol. Environ. Eng.* **2016**, *1*, 1–12.

(27)   McGillicuddy, E.; Murray, I.; Kavanagh, S.; Morrison, L.; Fogarty, A.; Cormican, M.; Dockery, P.; Prendergast, M.; Rowan, N.; Morris, D. Silver Nanoparticles in the Environment: Sources, Detection and Ecotoxicology. *Sci. Total Environ.* **2017**, *575*, 231–246.

(28)   Jennings, M. C.; Minbiole, K. P. C.; Wuest, W. M. Quaternary Ammonium Compounds: An Antimicrobial Mainstay and Platform for Innovation to Address Bacterial Resistance. *ACS Infect. Dis.* **2016**, *1*, 288–303.

(29)   Jaeger, W.; Bohrisch, J.; Laschewsky, A. Synthetic Polymers with Quaternary Nitrogen Atoms-Synthesis and Structure of the Most Used Type of Cationic Polyelectrolytes. *Prog. Polym. Sci.* **2010**, *35*, 511–577.

(30)   Mi, L.; Jiang, S. Integrated Antimicrobial and Nonfouling Zwitterionic Polymers. *Angew. Chem. Int. Ed. Engl.* **2014**, *53*, 1746–1754.

(31)   Liu, S. Q.; Venkataraman, S.; Ong, Z. Y.; Chan, J. M. W.; Yang, C.; Hedrick, J. L.; Yang, Y. Y. Overcoming Multidrug Resistance in Microbials Using Nanostructures Self-Assembled from Cationic Bent-Core Oligomers. *Small* **2014**, *10*, 4130–4135.

(32)   Xie, Y.; Liu, Y.; Yang, J.; Liu, Y.; Hu, F.; Zhu, K.; Jiang, X. Gold Nanoclusters for Targeting Methicillin-Resistant Staphylococcus Aureus In Vivo. *Angew. Chemie - Int. Ed.* **2018**, *57*, 3958–3962.

(33)   Liu, L.; Huang, Y.; Riduan, S. N.; Gao, S.; Yang, Y.; Fan, W.; Zhang, Y. Main-Chain Imidazolium Oligomer Material as a Selective Biomimetic Antimicrobial Agent. *Biomaterials* **2012**, *33*, 8625–8631.

(34)   Bieser, A. M.; Thomann, Y.; Tiller, J. C. Contact-Active Antimicrobial and Potentially Self-Polishing Coatings Based on Cellulose. *Macromol. Biosci.* **2011**, *11*, 111–121.

(35)   Zhao, J.; Ma, L.; Millians, W.; Wu, T.; Ming, W. Dual-Functional

Antifogging/Antimicrobial Polymer Coating. *ACS Appl. Mater. Interfaces* **2016**, *8*, 8737–8742.

(36) Isquith, A.; Abbott, E.; Walters, P. Surface-Bonded Antimicrobial Activity of an Organosilicon Quaternary Ammonium Chloride. *Appl. Microbiol.* **1972**, *24*, 859–863.

(37) Park, D.; Wang, J.; Klibanov, A. M. One-Step, Painting-like Coating Procedures to Make Surfaces Highly and Permanently Bactericidal. *Biotechnol. Prog.* **2006**, *22*, 584–589.

(38) Kugel, A.; Stafslien, S.; Chisholm, B. J. Antimicrobial Coatings Produced by "Tethering" Biocides to the Coating Matrix: A Comprehensive Review. *Prog. Org. Coatings* **2011**, *72*, 222–252.

(39) Zoppe, J. O.; Ataman, N. C.; Mocny, P.; Wang, J.; Moraes, J.; Klok, H. A. Surface-Initiated Controlled Radical Polymerization: State-of-the-Art, Opportunities, and Challenges in Surface and Interface Engineering with Polymer Brushes. *Chem. Rev.* **2017**, *117*, 1105–1318.

(40) Higaki, Y.; Kobayashi, M.; Hirai, T.; Takahara, A. Direct Polymer Brush Grafting to Polymer Fibers and Films by Surface-Initiated Polymerization. *Polym. J.* **2018**, *50*, 101–108.

(41) Barbey, R.; Lavanant, L.; Paripovic, D.; Schüwer, N.; Sugnaux, C.; Tugulu, S.; Klok, H. A. Polymer Brushes via Surface-Initiated Controlled Radical Polymerization: Synthesis, Characterization, Properties, and Applications. *Chem. Rev.* **2009**, *109*, 5437–5527.

(42) Iha, R. K.; Wooley, K. L.; Nystro, A. M.; Burke, D. J.; Kade, M. J.; Hawker, C. J. Applications of Orthogonal "Click" Chemistries in the Synthesis of Functional Soft Materials. *Chem. Rev.* **2009**, *109*, 5620–5686.

(43) Huang, J.; Koepsel, R. R.; Murata, H.; Wu, W.; Lee, S. B.; Kowalewski, T.; Russell, A. J.; Matyjaszewski, K. Nonleaching Antibacterial Glass Surfaces via "Grafting Onto": The Effect of the Number of Quaternary Ammonium Groups on Biocidal Activity. *Lagmuir* **2008**, *24*, 6785–6795.

(44) Su, Y.; Zhi, Z.; Gao, Q.; Xie, M.; Yu, M.; Lei, B.; Li, P.; Ma, P. X. Autoclaving-Derived Surface Coating with In Vitro and In Vivo Antimicrobial and Antibiofilm Efficacies. *Adv. Healthc. Mater.* **2017**, *6*, 1–15.

(45) Gao, J.; Huddleston, N. E.; White, E. M.; Pant, J.; Handa, H.; Locklin, J. Surface Grafted

Antimicrobial Polymer Networks with High Abrasion Resistance. *ACS Biomater. Sci. Eng.* **2016**, *2*, 1169–1179.

(46) Ma, H.; Davis, R.; Bowman, C. A Novel Sequential Photoinduced Living Graft Polymerization. *Macromolecules* **2000**, *365*, 331–335.

(47) Carey, D. E.; McNamara, P. J. The Impact of Triclosan on the Spread of Antibiotic Resistance in the Environment. *Front. Microbiol.* **2014**, *5*, 1-11.

(48) Harney, M. B.; Pant, R. R.; Fulmer, P. A.; Wynne, J. H. Surface Self-Concentrating Amphiphilic Quaternary Ammonium Biocides as Coating Additives. *ACS Appl. Mater. Interfaces* **2009**, *1*, 39–41.

(49) Robertson, J.; Gizdavic-Nikolaidis, M.; Swift, S. Investigation of Polyaniline and a Functionalised Derivative as Antimicrobial Additives to Create Contamination Resistant Surfaces. *Materials* **2018**, *11*, 436–461.

(50) Arza, C. R.; Ilk, S.; Demircan, D.; Zhang, B. New Biobased Non-Ionic Hyperbranched Polymers as Environmentally Friendly Antibacterial Additives for Biopolymers. *Green Chem.* **2018**, *20*, 1238–1249.

(51) Gilbert, P.; Moore, L. E. Cationic Antiseptics: Diversity of Action under a Common Epithet. *J. Appl. Microbiol.* **2005**, *99*, 703–715.

(52) Ioannou, C. J.; Hanlon, G. W.; Denyer, S. P. Action of Disinfectant Quaternary Ammonium Compounds against Staphylococcus Aureus. *Antimicrob. Agents Chemother.* **2007**, *51*, 296–306.

(53) Vieira, D. B.; Carmona-Ribeiro, A. M. Cationic Lipids and Surfactants as Antifungal Agents: Mode of Action. *J. Antimicrob. Chemother.* **2006**, *58*, 760–767.

(54) Holdsworth, S. R.; Law, C. J. The Major Facilitator Superfamily Transporter Mdtm Contributes to the Intrinsic Resistance of Escherichia Coli to Quaternary Ammonium Compounds. *J. Antimicrob. Chemother.* **2013**, *68*, 831–839.

(55) Tabata, A.; Nagamune, H.; Maeda, T.; Murakami, K.; Miyake, Y.; Kourai, H. Correlation between Resistance of Pseudomonas Aeruginosa to Quaternary Ammonium Compounds and Expression of Outer Membrane Protein OprR. *Antimicrob. Agents Chemother.* **2003**, *47*, 2093–2099.

(56) Tiller, J. C.; Liao, C. J.; Lewis, K.; Klibanov, A. M. Designing Surfaces That Kill Bacteria

on Contact. *Proc. Natl. Acad. Sci. U. S. A.* **2001**, *98*, 5981–5985.

(57)   Cao, B.; Tang, Q.; Li, L.; Humble, J.; Wu, H.; Liu, L.; Cheng, G. Switchable Antimicrobial and Antifouling Hydrogels with Enhanced Mechanical Properties. *Adv. Healthc. Mater.* **2013**, *2*, 1096–1102.

(58)   Li, P.; Poon, Y. F.; Li, W.; Zhu, H.; Yeap, S. H.; Cao, Y.; Qi, X.; Zhou, C.; Lamrani, M.; Beuerman, R. W.; et al. A Polycationic Antimicrobial and Biocompatible Hydrogel with Microbe Membrane Suctioning Ability. *Nat. Mater.* **2010**, *10*, 2–9.

(59)   Bieser, A. M.; Tiller, J. C. Mechanistic Considerations on Contact-Active Antimicrobial Surfaces with Controlled Functional Group Densities. *Macromol. Biosci.* **2011**, *11*, 526–534.

(60)   Silhavy, T.; Kahne, D.; Walker, S. The Bacterial Cell Envelope. *Cold Spring Harb. Perspect. Biol.* **2010**, *5*, 1–16.

(61)   Yatvin, J.; Gao, J.; Locklin, J. Durable Defense: Robust and Varied Attachment of Non-Leaching Poly"-Onium" Bactericidal Coatings to Reactive and Inert Surfaces. *Chem. Commun.* **2014**, *50*, 9433–9442.

(62)   Asri, L. A. T. W.; Crismaru, M.; Roest, S.; Chen, Y.; Ivashenko, O.; Rudolf, P.; Tiller, J. C.; Van Der Mei, H. C.; Loontjens, T. J. A.; Busscher, H. J. A Shape-Adaptive, Antibacterial-Coating of Immobilized Quaternary-Ammonium Compounds Tethered on Hyperbranched Polyurea and Its Mechanism of Action. *Adv. Funct. Mater.* **2014**, *24*, 346–355.

(63)   Gao, J.; White, E. M.; Liu, Q.; Locklin, J. Evidence for the Phospholipid Sponge Effect as the Biocidal Mechanism in Surface-Bound Polyquaternary Ammonium Coatings with Variable Cross-Linking Density. *ACS Appl. Mater. Interfaces* **2017**, *9*, 7745–7751.

(64)   Guterman, R.; Berven, B. M.; Chris Corkery, T.; Nie, H. Y.; Idacavage, M.; Gillies, E. R.; Ragogna, P. J. Fluorinated Polymerizable Phosphonium Salts from PH3: Surface Properties of Photopolymerized Films. *J. Polym. Sci. Part A Polym. Chem.* **2013**, *51*, 2782–2792.

(65)   Cuthbert, T. J.; Harrison, T. D.; Ragogna, P. J.; Gillies, E. R. Synthesis, Properties, and Antibacterial Activity of Polyphosphonium Semi-Interpenetrating Networks. *J. Mater. Chem. B* **2016**, *4*, 4872–4883.

(66)   Cuthbert, T. J.; Hisey, B.; Harrison, T. D.; Trant, J. F.; Gillies, E. R.; Ragogna, P. J.

Surprising Antibacterial Activity and Selectivity of Hydrophilic Polyphosphoniums Featuring Sugar and Hydroxy Substituents. *Angew. Chemie - Int. Ed.* **2018**, *57*, 12707–12710.

(67) Stewart, B.; Harriman, A.; Higham, L. J. Predicting the Air Stability of Phosphines. *Organometallics* **2011**, *30*, 5338–5343.

(68) Kanazawa, A.; Ikeda, T.; Endo, T. Novel Polycationic Biocides: Synthesis and Antibacterial Activity of Polymeric Phosphonium Salts. *J. Polym. Sci. Part A Polym. Chem.* **1993**, *31*, 335–343.

(69) Kanazawa, A.; Ikeda, T.; Endo, T. Polymeric Phosphonium Salts as a Novel Class of Cationic Biocides. II. Effects of Counter Anion and Molecular Weight on Antibacterial Activity of Polymeric Phosphonium Salts. *J. Polym. Sci. Part A Polym. Chem.* **1993**, *31*, 1441–1447.

(70) Kanazawa, A.; Ikeda, T.; Endo, T. Polymeric Phosphonium Salts as a Novel Class of Cationic Biocides. III. Immobilization of Phosphonium Salts by Surface Photografting and Antibacterial Activity of the Surface-treated Polymer Films. *J. Polym. Sci. Part A Polym. Chem.* **1993**, *31*, 1467–1472.

(71) Kanazawa, A.; Ikeda, T.; Endo, T. Polymeric Phosphonium Salts as a Novel Class of Cationic Biocides. IV. Synthesis and Antibacterial Activity of Polymers with Phosphonium Salts in the Main Chain. *J. Polym. Sci. Part A Polym. Chem.* **1993**, *31*, 3031–3038.

(72) Kanazawa, A.; Ikeda, T.; Endo, T. Polymeric Phosphonium Salts as a Novel Class of Cationic Biocides. V. Synthesis and Antibacterial Activity of Polyesters Releasing Phosphonium Biocides. *J. Appl. Polym. Sci.* **1993**, *31*, 3003–3011.

(73) Kanazawa, A.; Ikeda, T.; Endo, T. Polymeric Phosphonium Salts as a Novel Class of Cationic Biocides. VI. Antibacterial Activity of Fibers Surface-treated with Phosphonium Salts Containing Trimethoxysilane Groups. *J. Appl. Polym. Sci.* **1994**, *52*, 641–647.

(74) Kanazawa, A.; Ikeda, T.; Endo, T. Polymeric Phosphonium Salts as a Novel Class of Cationic Biocides. VII. Synthesis and Antibacterial Activity of Polymeric Phosphonium Salts and Their Model Compounds Containing Long Alkyl Chains. *J. Appl. Polym. Sci.* **1994**, *53*, 1237–1244.

(75) Speier, J. L.; Malek, J. R. Destruction of Microorganisms by Contact with Solid Surfaces.

J. Colloid Interface Sci. **1982**, *89*, 68–76.

(76)   Kenawy, E. R.; Abdel-Hay, F. I.; El-Shanshoury, A. E. R. R.; El-Newehy, M. H. Biologically Active Polymers. V. Synthesis and Antimicrobial Activity of Modified Poly(Glycidyl Methacrylate-Co-2-Hydroxyethyl Methacrylate) Derivatives with Quaternary Ammonium and Phosphonium Salts. *J. Polym. Sci. Part A Polym. Chem.* **2002**, *40*, 2384–2393.

(77)   Cieniecka-Rosłonkiewicz, A.; Pernak, J.; Kubis-Feder, J.; Ramani, A.; Robertson, A. J.; Seddon, K. R. Synthesis, Anti-Microbial Activities and Anti-Electrostatic Properties of Phosphonium-Based Ionic Liquids. *Green Chem.* **2005**, *7*, 855–862.

(78)   Chitwood, L. A. Tube Dilution Antimicrobial Susceptibility Testing: Efficacy of a Microtechnique Applicable to Diagnostic Laboratories. *Appl. Environ. Microbiol.* **1969**, *17*, 707–709.

(79)   Pernak, J.; Sobaszkiewicz, K.; Mirska, I. Anti-Microbial Activities of Ionic Liquids. *Green Chem.* **2003**, *5*, 52–56.

(80)   Tindale, J. J.; Ragogna, P. J. Highly Fluorinated Phosphonium Ionic Liquids: Novel Media for the Generation of Superhydrophobic Coatings. *Chem. Commun.* **2009**, 1831–1833.

(81)   Cuthbert, T. J.; Guterman, R.; Ragogna, P. J.; Gillies, E. R. Contact Active Antibacterial Phosphonium Coatings Cured with UV Light. *J. Mater. Chem. B* **2015**, *3*, 1474–1478.

(82)   Corbridge, D. E. C. Phosphorus: An Outline of Its Chemistry, Biochemistry, and Technology, 4th ed.; Elsevier: New York, 1990.

(83)   Erre, G.; Enthaler, S.; Junge, K.; Gladiali, S.; Beller, M. Synthesis and Application of Chiral Monodentate Phosphines in Asymmetric Hydrogenation. *Coord. Chem. Rev.* **2008**, *252*, 471–491.

(84)   Shaughnessy, K. H. Hydrophilic Ligands and Their Application in Aqueous-Phase Metal-Catalyzed Reactions. *Chem. Rev.* **2009**, *109*, 643–710.

(85)   Meijboom, R.; Bowen, R. J.; Berners-Price, S. J. Coordination Complexes of Silver (I) with Tertiary Phosphine and Related Ligands. *Coord. Chem. Rev.* **2009**, *253*, 325–342.

(86)   Brynda, M. Towards "User-Friendly" Heavier Primary Pnictanes: Recent Developments in the Chemistry of Primary Phosphines, Arsines and Stibines. *Coord. Chem. Rev.* **2013**, *249*, 2013–2034.

(87)   Kenaree, A. R.; Cuthbert, T. J.; Barbon, S. M.; Boyle, P. D.; Gillies, E. R.; Ragogna, P. J.; Gilroy, J. B. Synthesis and Characterization of a Family of Air-Stable Ferrocene- and Ruthenocene-Containing Primary, Secondary, and Tertiary Phosphines. *Organometallics* **2015**, *34*, 4272–4280.

(88)   Beland, V. A.; Wang, Z.; Sham, T.; Ragogna, P. J. Antimony-Functionalized Phosphine-Based Photopolymer Networks. *Angew. Chemie - Int. Ed.* **2018**, *57*, 13252–13256.

(89)   Wauters, I.; Debrouwer, W.; Stevens, C. V. Preparation of Phosphines through C–P Bond Formation. *Beilstein J. Org. Chem.* **2014**, *10*, 1064–1096.

(90)   Franks, S.; Hartley, F. R.; McCaffery, D. J. A. The Preparation and Properties of Tertiary Phosphines and Tertiary Phosphine Oxides with Long Alkyl Chains. *J. Chem. Soc. Perkins Trans. 1* **1979**, 3029-3033.

(91)   Gilman, H.; Van Ess, P. R. The Preparation of Ketones by the Carbonation of Organolithium Compounds. *J. Am. Chem. Soc.* **1933**, *55*, 1258–1261.

(92)   Huang, T.; Wu, X.; Yu, Y.; An, L.; Yin, X. A Convenient Synthesis of 2-Acyl Benzothiazoles/Thiazoles from Benzothiazole/Thiazole and N,N'-Carbonyldiimidazole Activated Carboxylic Acids. *Tetrahedron Lett.* **2019**, *60*, 1667–1670.

(93)   Amigues, E. J.; Hardacre, C.; Keane, G.; Migaud, M. E. Solvent-Modulated Reactivity of PCl3 with Amines. *Green Chem.* **2008**, *10*, 660–669.

(94)   Dyer, P. W.; Fawcett, J.; Hanton, M. J.; Kemmitt, R. D. W.; Padda, R.; Singh, N. Exploring the Coordination Chemistry and Reactivity of Dialkylamino- and Bis (Dialkylamino)-Phosphines in the Coordination Sphere of Metals. *Dalton Trans.* **2003**, *103*, 104–113.

(95)   Singh, S.; Nicholas, K. M. A Novel Synthesis of Unsymmetrical Tertiary Phosphines: Selective Nucleophilic Substitution on Phosphorus (III). *Chem. Commun.* **1998**, *1*, 149–150.

(96)   Greenberg, S.; Stephan, D. W. Stoichiometric and Catalytic Activation of P–H and P–P Bonds. *Chem. Soc. Rev.* **2008**, *37*, 1482–1489.

(97)   Mann, F. G.; Millar, I. T. The Cyanoethylation of Aryl Phosphines. *J. Chem. Soc.* **1952**, 4453–4457.

(98)   Hinton, R. C.; Mann, F. G.; Todd, D. The Abnormal Hydrolysis of Certain β-(Diarylphosphino)-Propionic Esters. Part I. *J. Chem. Soc.* **1952**, 5454–5470.

(99)   Rauhut, M. M.; Hechenbleikner, I.; Currier, H. A.; Schaefer, F. C.; Wystrach, V. P. The Cyanoethylation of Phosphine and Phenylphosphine. *J. Am. Chem. Soc.* **1959**, *81*, 1103–1107.

(100)   Hoff, M. C.; Hill, P. Acid-Catalyzed Addition of Phosphine to Olefins. *J. Org. Chem.* **1959**, *24*, 356–359.

(101)   Rauhut, M. M.; Hechenbleikner, I.; Currier, H. A.; Schaefer, F. C.; Wystrach, V. P. The Free Radical Addition of Phosphines. *J. Org. Chem.* **1961**, *26*, 5138–5146.

(102)   Alonso, F.; Moglie, Y.; Radivoy, G.; Yus, M. Solvent- and Catalyst-Free Regioselective Hydrophosphanation of Alkenes. *Green Chem.* **2012**, *14*, 2699–2702.

(103)   Moglie, Y.; González-Soria, M. J.; Martín-García, I.; Radivoy, G.; Alonso, F. Catalyst- and Solvent-Free Hydrophosphination and Multicomponent Hydrothiophosphination of Alkenes and Alkynes. *Green Chem.* **2016**, *18*, 4896–4907.

(104)   Fan, Y. C.; Kwon, O. Advances in Nucleophilic Phosphine Catalysis of Alkenes, Allenes, Alkynes, and MBHADs. *Chem. Commun.* **2013**, *49*, 11588–11619.

(105)   Menshutkin, N. Ueber Die Einwirkung Des Chloroacetyls Auf Phosphorige Saure. *Ann. der Chemie und Pharm.* **1865**, *133*, 317–320.

(106)   Sola, M.; Lledos, A.; Duran, M. Analysis of Solvent Effects on the Menshutkin Reaction. *J. Am. Chem. Soc.* **1991**, *113*, 2873–2879.

(107)   Acevedo, O.; Jorgensen, W. L. Exploring Solvent Effects upon the Menshutkin Reaction Using a Polarizable Force Field. *J. Phys. Chem. B* **2010**, *114*, 8425–8430.

(108)   Komen, C. M. D. Phosphonium Salts, Ylides, and Phosphoranes; Hartley, F. R., Ed.; Chichester, 1994.

(109)   Thom, K. A.; Standiford, H. C.; Johnson, K. J.; Furuno, J. P. Contamination of Environmental Surfaces in the Clinical Setting. *Infect. Control Hosp. Epidemiol.* **2015**, *35*, 1060–1062.

(110)   Murata, H.; Koepsel, R. R.; Matyjaszewski, K.; Russell, A. J. Permanent, Non-Leaching Antibacterial Surfaces-2: How High Density Cationic Surfaces Kill Bacterial Cells. *Biomaterials* **2007**, *28*, 4870–4879.

(111)   ASTM E2149 - 13a Standard Test Method for Determining the Antimicrobial Activity of Antimicrobial Agents Under Dynamic Contact Conditions. 2013.

(112) ISO 22196:2011 Measurement of Antibacterial Activity on Plastics and Other Non-Porous Surfaces. 2016.

(113) Campos, M. D.; Zucchi, P. C.; Phung, A.; Leonard, S. N.; Hirsch, E. B. The Activity of Antimicrobial Surfaces Varies by Testing Protocol Utilized. *PLoS One* **2016**, *11*, 1–11.

(114) Ronan, E.; Yeung, C. W.; Hausner, M.; Wolfaardt, G. M. Interspecies Interaction Extends Bacterial Survival at Solid – Air Interfaces. *Biofouling* **2013**, *29*, 1087–1096.

(115) Saettone, M. F.; Alderigi, C.; Giannaccini, B.; Anselmi, C.; Rossetti, M. G.; Scotton, M.; Cerini, R. Substantivity of Sunscreens-Preparation and Evaluation of Some Quaternary Ammonium Benzophenone Derivatives. *Int. J. Cosmet. Sci.* **1988**, *109*, 99–109.

(116) Pena-Pereira, F.; Kloskowski, A.; Namieśnik, J. Perspectives on the Replacement of Harmful Organic Solvents in Analytical Methodologies: A Framework toward the Implementation of a Generation of Eco-Friendly Alternatives. *Green Chem.* **2015**, *17*, 3687–3705.

(117) Caschera, A. UV Radical Initiated Antimicrobial Polymer Coatings, Ryerson University, 2014, MSc. Thesis.

(118) Lygo, B.; Andrews, B. I. Asymmetric Phase-Transfer Catalysis Utilizing Chiral Quaternary Ammonium Salts: Asymmetric Alkylation of Glycine Imines. *Acc. Chem. Res.* **2004**, *37*, 518–525.

(119) Landini, D.; Maia, A.; Montanari, F. Mechanism of Phase-Transfer Catalysis. *J. Chem. Soc. Chem. Commun.* **1977**, 112–113.

(120) Landini, D.; Maia, A.; Montanari, O. Phase-Transfer Catalysis. Nucleophilicity of Anions in Aqueous Organic Two-Phase Reactions Catalyzed by Onium Salts. A Comparison with Homogeneous Organic Systems. *J. Am. Chem. Soc.* **1978**, *100*, 2796–2801.

(121) Solà, M.; Lledós, A.; Duran, M.; Bertrán, J.; Abboud, J. L. M. Analysis of Solvent Effects on the Menshutkin Reaction. *J. Am. Chem. Soc.* **1991**, *113*, 2873–2879.

(122) Caschera, A.; Mistry, K. B.; Bedard, J.; Ronan, E.; Syed, M. A.; Khan, A. U.; Lough, A. J.; Wolfaardt, G.; Foucher, D. A. Surface-Attached Sulfonamide Containing Quaternary Ammonium Antimicrobials for Textiles and Plastics. *RSC Adv.* **2019**, *9*, 3140–3150.

(123) Alpers, T.; Muesmann, T. W. T.; Temme, O.; Christoffers, J. Perfluorinated Ammonium and Phosphonium Ionic Liquids. *Synthesis* **2018**, *50*, 3531–3539.

(124) Monçalves, M.; Rampon, D. D. S.; Schneider, P. H.; Rodembusch, F. S.; Silveira, C. D. C. Divinyl Sulfides/Sulfones-Based D-π-A-π-D Dyes as Efficient Non-Aromatic Bridges for π-Conjugated Compounds. *Dyes Pigm.* **2014**, *102*, 71–78.

(125) Alvey, L. J.; Rutherford, D.; Juliette, J. J. J.; Gladysz, J. A. Additions of PH3 to Monosubstituted Alkenes of the Formula H2C=CH(CH2)x(CF2)YCF3: Convenient, Multigram Syntheses of a Family of Partially Fluorinated Trialkylphosphines with Modulated Electronic Properties and Fluorous Phase Affinities. *J. Org. Chem.* **1998**, *63*, 6302–6308.

(126) Krenske, E. H. Theoretical Investigation of the Mechanisms and Stereoselectivities of Reductions of Acyclic Phosphine Oxides and Sulfides by Chlorosilanes. *J. Org. Chem.* **2012**, *77*, 3969–3977.

(127) Xue, M.; Li, J.; Peng, J.; Bai, Y.; Zhang, G.; Xiao, W.; Lai, G. Effect of Triarylphosphane Ligands on the Rhodium-Catalyzed Hydrosilylation of Alkene. *Appl. Organomet. Chem.* **2014**, *28*, 120–126.

(128) De Pater, J. J. M.; Maljaars, C. E. P.; De Wolf, E.; Lutz, M.; Spek, A. L.; Deelman, B. J.; Elsevier, C. J.; Van Koten, G. (Perfluoro)Alkylsilyl-Substituted 2-[Bis(4-Aryl)Phosphino]Pyridines: Synthesis and Comparison of Their Palladium Complexes in Methoxycarbonylation of Phenylacetylene in Regular Solvents and Supercritical CO 2. *Organometallics* **2005**, *24*, 5299–5310.

(129) Kügler, R.; Bouloussa, O.; Rondelez, F. Evidence of a Charge-Density Threshold for Optimum Efficiency of Biocidal Cationic Surfaces. *Microbiology* **2005**, *151*, 1341–1348.

(130) McDonnell, A. M. P.; Beving, D.; Wang, A.; Chen, W.; Yan, Y. Hydrophilic and Antimicrobial Zeolite Coatings for Gravity-Independent Water Separation. *Adv. Funct. Mater.* **2005**, *15*, 336–340.

(131) Francolini, I.; Vuotto, C.; Piozzi, A.; Donelli, G. Antifouling and Antimicrobial Biomaterials: An Overview. *APMIS* **2017**, *125*, 392–417.

(132) Borgs, C.; De Coninck, J.; Kotecký, R.; Zinque, M. Does the Roughness of the Substrate Enhance Wetting? *Phys. Rev. Lett.* **1995**, *74*, 2292–2294.

(133) Herminghaus, S. Roughness-Induced Non-Wetting. *Europhys. Lett.* **2000**, *52*, 165–170.

(134) Cao, L.; Hu, H. A.; Gao, D. Design and Fabrication of Micro-Textures for Inducing a

Superhydrophobic Behavior on Hydrophilic Materials. *Langmuir* **2007**, *23*, 4310–4314.

(135) Ronan, E.; Yeung, C. W.; Hausner, M.; Wolfaardt, G. M. Interspecies Interaction Extends Bacterial Survival at Solid-Air Interfaces. *Biofouling* **2013**, *29*, 1087–1096.

(136) Stone, W.; Kroukamp, O.; Korber, D. R.; McKelvie, J.; Wolfaardt, G. M. Microbes at Surface-Air Interfaces: The Metabolic Harnessing of Relative Humidity, Surface Hygroscopicity, and Oligotrophy for Resilience. *Front. Microbiol.* **2016**, *7*, 1–15.

(137) Hartleb, W.; Saar, J. S.; Zou, P.; Lienkamp, K. Just Antimicrobial Is Not Enough: Toward Bifunctional Polymer Surfaces with Dual Antimicrobial and Protein-Repellent Functionality. *Marcomolecular Chem. Phys.* **2016**, *217*, 225–231.

(138) Blundell, R. K.; Licence, P. Quaternary Ammonium and Phosphonium Based Ionic Liquids: A Comparison of Common Anions. *Phys. Chem. Chem. Phys.* **2014**, *16*, 15278–15288.

(139) Hazut, O.; Agarwala, A.; Amit, I.; Subramani, T.; Zaidiner, S.; Rosenwaks, Y.; Yerushalmi, R. Contact Doping of Silicon Wafers and Nanostructures with Phosphine Oxide Monolayers. *ACS Nano* **2012**, *6*, 10311–10318.

(140) Ye, L.; Pujari, S. P.; Zuilhof, H.; Kudernac, T.; De Jong, M. P.; Van Der Wiel, W. G.; Huskens, J. Controlling the Dopant Dose in Silicon by Mixed-Monolayer Doping. *ACS Appl. Mater. Interfaces* **2015**, *7*, 3231–3236.

(141) Reddy, G. S.; Nadagouda, M. N.; Sekhar, J. A. Nanostructured Surfaces That Show Antimicrobial, Anticorrosive, and Antibiofilm Properties. *Key Eng. Mater.* **2012**, *521*, 1–33.

(142) Connelly, M. C.; Reddy, G. S.; Nadagouda, M. N.; Sekhar, J. A. Antimicrobial and Anticorrosive Efficacy of Inorganic Nanoporous Surfaces. *Clean Technol. Environ. Policy* **2017**, *19*, 845–857.

(143) ASTM D5402 - 19 Standard Practice for Assessing the Solvent Resistance of Organic Coatings Using Solvent Rubs. 2019.

(144) Tung, S. H.; Kalarickal, N. C.; Mays, J. W.; Xu, T. Hierarchical Assemblies of Block-Copolymer-Based Supramolecules in Thin Films. *Macromolecules* **2008**, *41*, 6453–6462.

(145) De Wolf, E.; Riccomagno, E.; De Pater, J. J. M.; Deelman, B. J.; Van Koten, G. Parallel Synthesis and Study of Fluorous Biphasic Partition Coefficients of 1H,1H,2H,2H-Perfluoroalkylsilyl Derivatives of Triphenylphosphine: A Statistical Approach. *J. Comb.*

Chem. **2004**, *6*, 363–374.